

# **L-Amino acid Based Amphiphilic Polymers for Drug Delivery Application**

**Thesis Submitted to**

**IISER PUNE**

**For the Degree of**

**DOCTOR OF PHILOSOPHY**

**By**

**DHEERAJ CHANDRA JOSHI**

**Reg. No. 20153400**



Department of Chemistry

**INDIAN INSTITUTE OF SCIENCE EDUCATION AND RESEARCH,  
PUNE**

Pune 411008, Maharashtra, India

**February 2022**

Dedicated to....

*My Parents*



भारतीय विज्ञान शिक्षा एवं अनुसंधान संस्थान पुणे  
INDIAN INSTITUTE OF SCIENCE EDUCATION AND RESEARCH PUNE  
(An Autonomous Institution of Ministry of Human Resource Development, Govt. of India)  
Dr. Homi Bhabha Road, Pune - 411 008.

**Prof. M. Jayakannan**

Professor

Department of Chemistry

## **CERTIFICATE**

Certified that the work incorporated in the thesis entitled "*L-Amino acid Based Amphiphilic Polymers for Drug Delivery Application*" Submitted by **Mr. Dheeraj Chandra Joshi** was Carried out by the candidate under my supervision the work presented here or any part of it has not been included in any other thesis submitted previously or the award of any degree or diploma from any other University or Institution.

Date: 11<sup>th</sup> February

Pune (MH) India

A handwritten signature in blue ink, appearing to read "M. Jayakannan".

**Prof. M. Jayakannan**

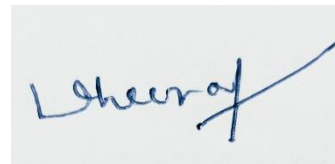
(Thesis supervisor)

## **Declaration**

I declare that this written submission represents my ideas in my own words and where others' ideas have been included; I have adequately cited and referenced the original sources. I also declare that I have adhered to all principles of scientific honesty and integrity and have not misrepresented or fabricated or falsified any idea/data/fact/source in my submission. I understand the violation of above will cause for disciplinary action by the institute and can also evoke penal action from the sources which have thus not been properly cited or from whom proper permission has not been taken when needed.

**Date: 11<sup>th</sup> February 2022**

**Pune (MH) India**

A rectangular box containing a handwritten signature in blue ink. The signature is written in a cursive style and appears to read 'Dheeraj'.

**Dheeraj Chandra Joshi**

**Roll No. 20153400**

# Acknowledgments

Firstly, I would like to acknowledge my Ph.D. thesis supervisor Prof. M. Jayakannan for his constant guidance, encouragement and valuable suggestions throughout my research. The numerous discussions with him have inspired me to push my limits and achieve the toughest goal. I am extremely thankful to him for teaching me all the basic skills in chemistry, providing me the opportunity to work freely, to explore and learn many things. He has always inspired me to become a better researcher.

I would like to thank my research advisory committee (RAC) members Dr. S. Britto and Dr. J. Nithyanandhan for the valuable suggestions and ideas during RAC meetings. The discussions with the RAC members have helped me to shape my project in the best possible way. Apart from RAC meetings, they were always available for intellectual inputs regarding my research work.

I would like to extend my sincere thanks to Prof. K. N. Ganesh, Former Director, IISER-Pune for providing world-class research facility for the research scholars. I would further like to thank Prof. J. Udgaonkar, current director for maintaining a healthy and efficient research environment at IISER-Pune.

I will be forever grateful to Dr. Asha, S.K (NCL-Pune) for providing me an opportunity to access the research facilities for my research work and fruitful scientific discussions.

I would like to extend my sincere thanks to all the faculty members at IISER-Pune for feeding me the scientific understanding, which was helpful throughout my research tenure at IISER-Pune.

I would like to thank Dr. Rajendra for teaching me the basics of instrumentation and synthetic methods required for my research work.

I would like to specially acknowledge my lab members, Dr. Nilesh U. Deshpande, Dr. Sonashree Saxena, and Ms. Mishika Virmani for helping me in biological experiments.

I would also like to thank all my current and former lab mates for their unconditional support and motivation during my entire tenure of Ph.D. at IISER Pune especially, Dr. Ananthraj, Dr. Narsimha Karnati, Dr. Bhagyashree Kulkarni, Dr. Mehak Malhotra, Ruma Ghosh, Utreshwar Gavane, Mohammed Khuddus, Parshuram Kamble, Pranav U., Shahidkhan Pathan, Rahul Nisal, Akash A., Bhatta Chandrashekar, Kajal Singh, Sharaffudin, Anu, Swetha Aditi,

Keerthana, Devesh, Lipi, Khusboo, Sharda, Nithish, Shraddha, Hemlata, Rasika. Prajitha, Sandeep Saibal, Moumita, Sarabhjot, Shrikant, Ganesh, Shivam, Navnath, and. Pooja.

The research environment created by all the lab members was one of the driving force for my successful Ph.D.

I like to express my wholehearted thanks to all the instruments' technicians of IISER Pune for their timely support during the Ph.D. tenure: Sandeep Mishra, Nitin Dalvi (NMR), Suresh Chandra Prajapati (MALDI), Sandeep Kanade (HRMS), Megha (AFM), Anil, Yatish, Mahesh (FE-SEM), Mayuresh.

I would like to thank my friends for helping and encouraging me during the Ph.D. journey at IISER Pune: Manu, Uday, Satish, Mohit, Rishabh.

Words are not sufficient to express my deep gratitude and profound reverence to my most precious and loving parents, Mr. Mahesh Chandra Joshi and Mrs. Prabha Joshi for their unwavering love, support and motivation. The blessings from them have installed a deep sense of belief in me. I like to express my wholehearted thanks to my brother, Lalit Mohan Joshi, and my sister-in-law Radha Joshi for giving me emotional support and who have been the pillars of my strength. I would like to thank my niece Manshi Joshi who joined our family during my Ph.D. final year, for giving me ultimate happiness.

I would like to acknowledge IISER Pune, UGC, and DST SERB for their financial support.

# **Synopsis**

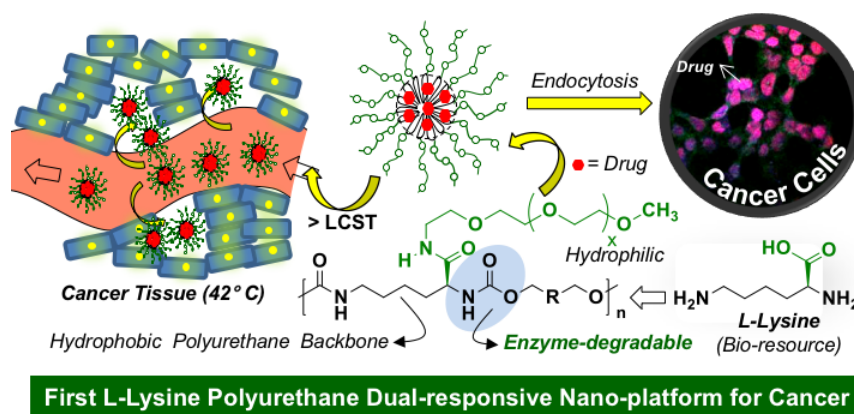
**Name of the Candidate:** Dheeraj Chandra Joshi

**Title of the Thesis:** L-Amino acid Based Amphiphilic Polymers for Drug Delivery Application.

L-Amino acids are biologically active molecules and play vital role in many biological processes. Synthetic polymers based on L-amino acids have attracted much attention because of their excellent biocompatibility and diverse functionality which provides them improved hydrophilicity and an opportunity for further modifications with bioactive molecules. Our laboratory has developed melt polycondensation approach for L-amino acid bioresources and successfully introduced wide ranges of polyesters, poly(ester-urethane)s and their amphiphilic nano assemblies for drug delivery in biomedical field. The aim of this thesis work is design and develop new melt polycondensation approach synthesis of L-amino acid-based polyurethanes by solvent free green synthetic route and demonstrate their drug delivery applications in cancer cells, Further, the methodology is also expanded to make new classes of amino acid and sugar based fully biodegradable hybrid polymers as next generation green polymers for both thermoplastic and biomedical applications. The thesis has been divided into four chapters:

1. First chapter is devoted to give very good literature account of polymer drug delivery systems, requirement and update on sustainable polymers in biomedical field, detail report on the synthetic methodologies reported for polypeptides and non-peptide polymers based on the L-amino acids, etc.
2. Second chapter describes the development of melt trans urethane polycondensation approach for L-lysine bioresources and develop amphiphilic polyurethanes as stimuli-responsive nanocarriers for drug delivery.
3. Third chapter describes the development of phenol-containing polymers based on L-tyrosine and L-DOPA and explore their strong aromatic  $\pi$ -core in the nanoparticle for substantial enhancement of drug loading content and deliver the drugs by intracellular lysosomal enzyme responsiveness in cancer cells.
4. Fourth chapter describes the development of new classes of sugar-amino acid hybrid polymers by solvent free melt polycondensation process in accomplishing the fully biobased and biodegradable thermoplastic polymers.

Briefly, the chapter 2 reports the development of new classes of L-lysine based polyurethanes by solvent and isocyanate free melt trans urethane polycondensation approach. Multifunctional L-lysine monomers were tailor-made by suitably converting the amine functionalities into urethanes (or carbamates) while masking the carboxylic acid functional unit as amide pendants. The L-lysine monomers underwent melt trans urethane polymerization with diols at 150 °C in the presence of catalyst to produce high molecular weight linear polyurethanes. Further, a new amphiphilic L-lysine monomer was designed with PEG-350 chain as a pendant and this monomer upon polymerization yielded well-defined amphiphilic aliphatic polyurethanes (APU). The APU was found to undergo core-shell type self-assembly in aqueous medium to produce nanoparticles of size < 175 nm and exhibited excellent

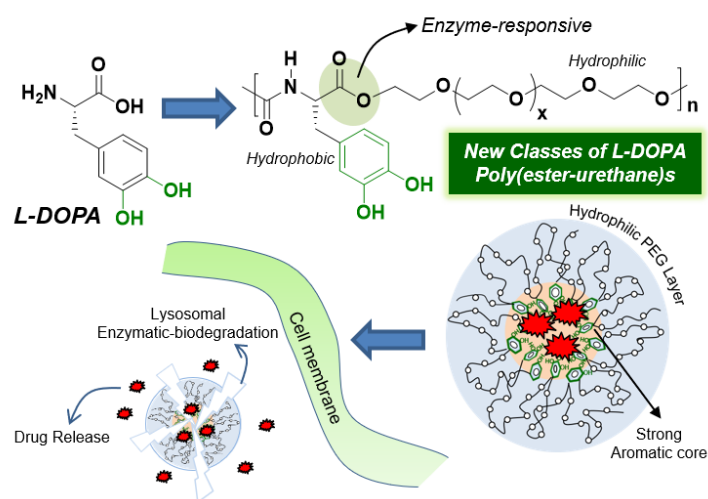


encapsulation capabilities for anticancer drug such as doxorubicin (DOX). The APU nano-carriers showed thermo-responsiveness from clear to turbid solution above the lower critical solution temperature (LCST) at 41-43 °C corresponding to cancer tissue temperature. At extracellular level, the thermal-stimuli responsiveness (*stimuli-1*) in the APU nano-carrier was employed as trigger to deliver the DOX at cancer tissue temperature. At the intracellular level, the aliphatic urethane linkages in the APU backbone underwent lysosomal enzymatic-biodegradation (*stimuli-2*) to deliver DOX. Cytotoxicity studies revealed that the APU nanoparticles were not toxic to cells up to 80.0 µg/mL whereas their DOX-loaded nanoparticles accomplished more than 90 % cell death in breast cancer (MCF 7) cells. Confocal microscopy and flow cytometry analysis confirmed that the L-lysine based polymer nanoparticles were readily taken up and internalized in the cancer cells. Live cell imaging using Lyso-trackers was done to prove the intracellular bio-degradation of the APU nano-carriers.

The chapter 3 report a new class of enzymatically biodegradable L-amino acid based poly(ester-urethane)s and their drug delivery applications in cancer cells. For that L-tyrosine and L-DOPA resources were suitably modified into dual ester urethane monomer in which the –OH groups were protected as silyl ether. The newly designed monomers were subjected for solvent free melt polymerization with hydrophilic polyethylene glycol to get the poly(ester-

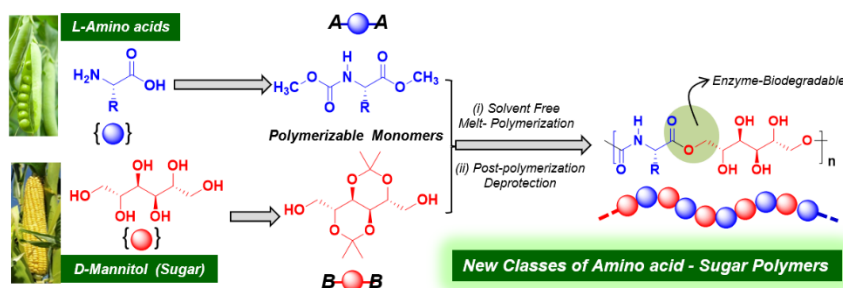


urethane)s. The post polymerisation deprotection of silyl ether yielded a new classes of enzyme-responsive phenol and catechol functionalized poly(ester-urethane)s in which the backbone of polymer contains polyethylene glycol and the side chain contains a pendent aromatic unit. The amphiphilic nature of polymer and hydrophobic interactions between aromatic units facilitates the formation of core shell type nanoparticle in aqueous medium having size around  $100 \pm 10$  nm. The electron rich aromatic nature of L-DOPA was explored for the encapsulation of drug molecules inside the hydrophobic core. The aromatic electron rich nature of polymeric backbone promotes the encapsulation of electron deficient drug molecules by aromatic  $\pi$ - $\pi$  stacking interactions. The aromatic interactions between L-DOPA and drug molecule was confirmed



by decrease in the fluorescent intensity of drug and L-DOPA by fluorescence spectroscopy. The backbone of polymer contains the ester linkages which underwent enzymatic biodegradation in presence of lysosomal enzymes, resulting the disassembly of nanoparticle and release of loaded cargo. Cytotoxicity studies in the breast cancer (MCF-7) and normal WT-MEFs cell lines revealed that the nascent nanoparticles were nontoxic, whereas the DOX and TPT drug-loaded polymer nanoparticles exhibited excellent cell killing in cancer cells. Confocal microscopic imaging confirmed the cellular internalization of drug-loaded nanoparticles.

In chapter 4 completely biomass-based amino acid sugar hybrid polyester(urethane)s synthesis from eco-friendly solvent free melt condensation approach. D-mannitol was converted into two different bicyclic diacetalized monomers leaving the two primary hydroxyl group free for polymerization reaction.



The structure of both the diols was confirmed by their single crystal structure analysis. The

second reacting partner was selected from amino acid resources and converted into dual ester-urethane monomer by suitable modifications. Both, amino acid monomer and diacetalized sugar diol was subjected for melt polymerisation at 150 °C to synthesise completely renewable resource-based polyester(urethane)s. The dual ester-urethane condensation was successfully demonstrated for variety of amino acids including glycine, L-alanine, L-valine, L-leucine, L-isoleucine and L-phenylalanine. The occurrence of melt polymerisation and structure of polymers was confirmed by NMR technique. The end group analysis by MALDI-TOF-MS confirmed the stability of both the monomers under melt condition. The amino acid sugar hybrid polyester(urethane)s were showing relatively high glass transition temperature ( $T_g \geq 80$  °C) compare to their aliphatic diol based polyester(urethane)s counterparts. Further the acetal unit in the polymer was deprotected to get amphiphilic amino acid sugar hybrid polyester(urethane)s which was forming  $200 \pm 10$  nm size nanoparticle in aqueous solvent. The biocompatibility of these sugar based diols were checked in normal (WT-MEFs) cell line and it was found that polymers were highly biocompatible.

The last chapter summarizes the overall outcome of the thesis work with future perspectives.

# **TABLE OF CONTENTS**

## **Chapter 1: Introduction**

- 1.1. Introduction to Cancer Drug Delivery**
- 1.2. Polymer Drug Delivery**
- 1.3. Effect of Physicochemical Properties of Polymer on Drug Delivery Systems (DDSs)**
- 1.4. Sustainable Polymers in Drug Delivery**
- 1.5. Melt Polycondensation approach for L-amino acid**
- 1.6. Aim of thesis**

## **Chapter 2: Development of L-Lysine Based Biodegradable Polyurethanes and Their Dual-Responsive Amphiphilic Nanocarriers for Drug Delivery to Cancer Cells**

- 2.1. Introduction**
- 2.2. Experimental Section**
- 2.3. Result and Discussion**
- 2.4 Conclusion**

## **Chapter 3: L-Amino acid Based Aromatic $\pi$ - $\pi$ Interaction Driven Polymeric Drug Delivery System in Cancer Research**

- 3.1. Introduction**
- 3.2. Experimental Section**
- 3.3. Result and Discussion**
- 3.4 Conclusion**

## **Chapter 4: *Development of Melt Polycondensation Strategy for L-Amino acids and Sugar Based Hybrid Polymers***

- 4.1. Introduction**
- 4.2. Experimental Section**
- 4.3. Result and Discussion**
- 4.4 Conclusion**

*Summery and Future direction*

## *List of Publications*

# *Chapter 1*

---

## *Introduction*

## **1.1. Introduction to Cancer Drug Delivery**

Most of the advanced countries throughout the world still rank cancer as a leading cause of death. Surgical removal of early-stage tumors that have not metastasized to a nearby organ is most effective for treating malignancies such as colonic, gastric, and cervical cancers. As a last resort, chemotherapy has been used to treat cancer from the past few decades. Chemotherapy has a crucial role in the treatment of cancer, though most chemotherapeutic drugs are hydrophobic and cannot be used *in vivo*. Due to their small molecular weight, most chemotherapeutic drugs lack tumor selectivity and can be easily excreted from the body. In order to reduce drug toxicity and improve the therapeutic effectiveness of chemotherapy, it is essential to develop drugs with high tumor selectivity. Over the years, the development of technology and the astonishing growth of biotechnology industry is revolutionizing the development of drug delivery systems. In recent decades, great advances have been made in understanding biology and the mechanisms behind the administration of cancer drugs. The world is now moving into the era of precision and personalized medicines where the selective implementation of therapeutic agents into solid tumors is considered one of the most important barriers to long-term recovery from the disease. Tumor selectivity of therapeutic drug has been the main aim of a major research body in medication delivery which is based on the assumption that higher levels of drugs in tumor tissue result in improved therapeutic efficiency. Recently, with growing advances in nanotechnology, a large number of drug delivery systems are reported annually. Improved drug efficacy against different kinds of tumors have been demonstrated in different types of animal models and patients. Multiple delivery systems tested in clinical trials and some have been approved clinically. However, the progress made in the delivery of medicines has not led to curative therapies in a majority of cases, especially patients with aggressive solid tumors. A lot of cancer drug delivery knowledge and experience has been accumulated within the community, with an ongoing discussion regarding the limitations of existing theories and methods in cancer therapy.

## **1.2. Polymer Drug Delivery**

In 1975, Helmut Ringsdorf proposed a theoretical model for pharmacologically active polymers. This concept of covalently bound polymer-drug conjugates still forms the basis for much work in this field today. The Ringsdorf model consists of a polymer backbone bound to three components: (a) Solubilizer, the solubilizer's role is to impart hydrophilicity to the product, thereby ensuring the water solubility (b) Drug, which is usually bound to the polymer

backbone through a linker and (c) a targeting moiety designed to transport the drug to targeted location or bind to a specific target.<sup>1</sup>

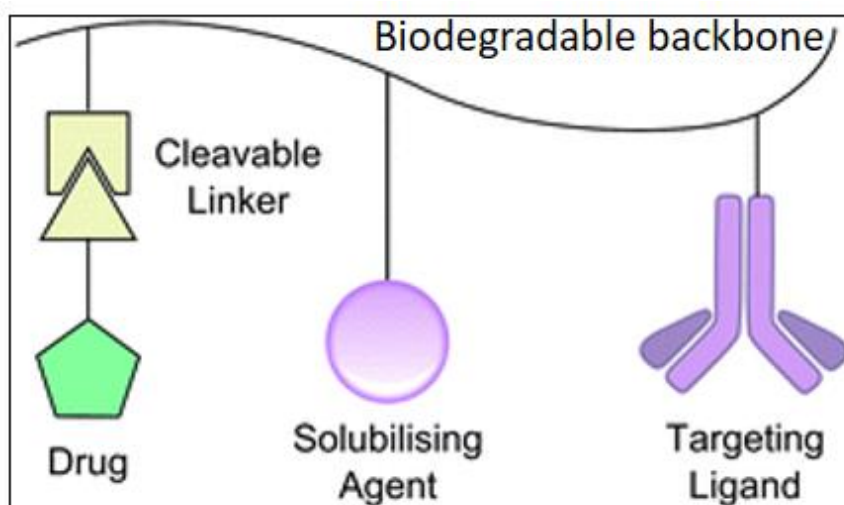


**Figure 1.1.** Ringsdorf model for drug delivery via polymer–drug conjugates. (Adopted from Ringsdorf, H. J. *Polym. Sci. Polym. Symp.* **1975**, 51, 135.)

Ringsdorf model is of particular interest to drug delivery community, whose aim is to deliver therapeutic agents to their site of action in order to improve efficacy and reduce toxicity. In comparison with traditional small molecule therapeutics, polymer-drug conjugates offer several significant advantages. Firstly, a water-soluble polymer can dramatically improve a drug's aqueous solubility. In addition, polymer-drug conjugates provide the possibility of controlled drug delivery, where the release of the drug occurs over a defined period of time. Therefore, delivery rate and duration can be tailored to meet the desired therapeutic concentration. Consequently, large fluctuations in systemic drug concentrations may not occur, which could lead to unwanted side effects or organ damage. The therapeutic index of a drug is an important factor and given by the ratio between its toxic and therapeutic dose of that drug. For scientists the primary goal is increase the drug concentration at cancer tissue. Unfortunately, toxicity to other vital organs limits the maximum dose administered at tumour tissue. For cancer patient's slight improvement in the therapeutic index of such drugs may result in higher drug concentration at tumour tissue while minimizing potentially life-threatening side effects. So to increase the therapeutic index of a drug Maeda et al in 1986 has purposed a theory known as enhanced permeability and retention (EPR) effect.<sup>2</sup> Most solid tumors are found to have blood vessels with a defective architecture, and they often produce excessive amounts of vascular endothelial growth factor. Because of this most solid tumor have

high vascular density, which ensures that they receive adequate oxygen and nutrition for uncontrolled growth. Because of this leaky vasculature nature of endothelial cells tumor tissue shows selective accumulation of macromolecular drugs over normal cells.<sup>3</sup> Moreover, the poor lymphatic drainage of tumor environments permits the leaked nanoparticles to remain in tumor tissue for longer periods of time.<sup>4,5</sup> The leaky vasculature nature of tumor endothelial cells and poor lymphatic drainage of solid tumor accounts for the 20 to 30 % more nanoparticles localisation in tumor tissue than in healthy tissue.<sup>6-8</sup> Nanocarriers size and molecular weight of polymer play an influential role in the EPR effect. Polymer nanocarriers with a molecular weight of less than 40,000 and a size of 100-250 nm are preferred for their better EPR effects.<sup>2,4</sup>

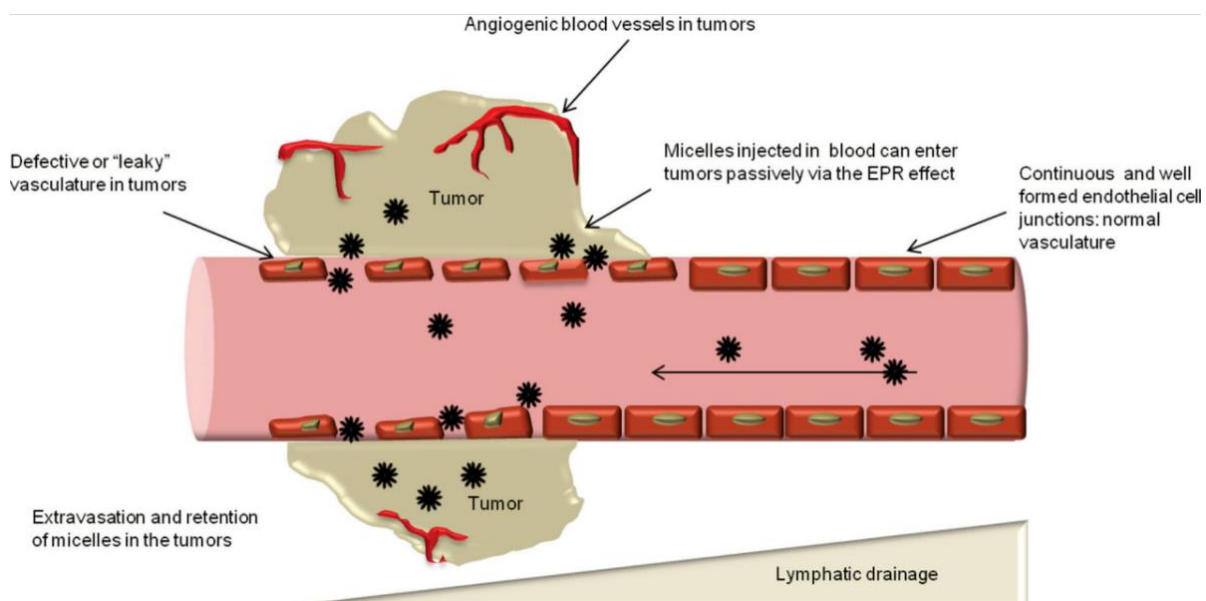


**Figure 1.2.** *Origin of polymer drug delivery and enhanced permeability and retention effect.* (Adopted from *Adv. Drug Deliv. Rev.* **2011**, 63, 136.)

In addition to their size, the charge, surface properties, and shape of nanoparticles play a crucial role in determining the overall efficacy of nanoparticles.<sup>9-12</sup> For systemic treatment of solid tumors, nanoparticles should go through a five-step cascade [i.e., circulation, accumulation, penetration, internalization, and release (CAPIR)] for delivering the drug into cancer cells and to show their therapeutic effect.<sup>13,14</sup> After injection the interactions of nanoparticles with local environment generated by the combination of their size and surface properties, determines the ultimate fate of nanoparticles within the body. The surface of cell membranes is generally negatively charged, so it is expected that positively charged nanoparticles will penetrate the cellular interior more easily than negatively charged ones. Liu et al. synthesized curcumin-loaded chitosan/poly(caprolactone) (chitosan/PCL) nanoparticles that showed enhanced cellular uptake of curcumin after curcumin was encapsulated into cationic chitosan/PCL nanoparticles.<sup>15</sup> The surface charge plays a major role in cellular uptake,



but as the surface charge increases, macrophage scavenging becomes more active, resulting in a greater amount of clearance by the reticuloendothelial system.<sup>16</sup> To avoid nonspecific adsorption on cell membranes of proteins, neutral ligand coated nanoparticles gradually gained attention. Studies has shown that the PEGylation of NPs reduces the formation of protein corona thus the nonspecific interactions with serum proteins can be avoided.<sup>17-19</sup> Various studies have been carried out to check the effect of PEGylated density and molecular weight of PEG chains on protein adsorption which showed that PEG-chain surface density has a direct effect on the efficacy of nanoparticle.<sup>19</sup> This method has been widely used to reduce immune clearance of nanoparticles. Xu and coworkers have shown that the Mucin binding of nanoparticle surfaces is decreasing and transport rates of nanoparticle increased in human CVM *ex vivo* as the density of PEG is increased on the nanoparticle surface as shown in figure 1.3.<sup>20</sup>

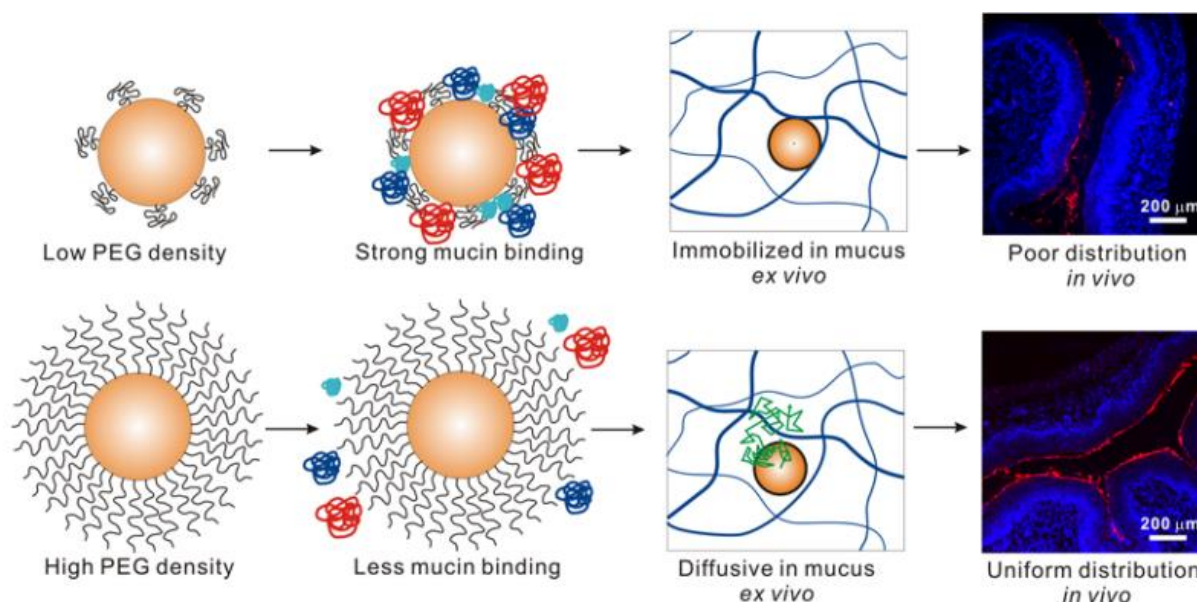


**Figure 1.3.** PEG surface density effects on mucus interaction and uniform coverage of the vaginal surface by nanoparticles with high PEG surface density. (Adapted from *ACS Nano* **2015**, 9, 9217–9227)

The morphology of nanoparticles, such as spherical, cubic, rod-like, or worm-like, impacts cellular uptake. Studies have shown that sphere-shaped and rod-shaped NPs are more readily absorbed by cells compare to others.<sup>21,22</sup> The cellular uptake of cubic, spherical, and rod-shaped gold nanoparticles was compared by Niikura et al. who found that spherical particles had the greatest uptake by weight, but rod-shaped particles had the greatest uptake by quantity.<sup>23</sup> The side effects associated with anticancer drugs could be minimized as well as their efficacy could be enhanced by optimizing the combination of these features in nanoparticle design. The growing interest in nanoparticle drug delivery is reflected in clinical

trials that show promising results. Various liposomal or polymer-based compounds are now in clinical trials and the patient usage of Doxil, Abraxane, DaunoXome, and Genexol-PM has already been approved.<sup>24</sup>

In addition to modify these fundamental properties, nanoparticles can also be conjugated with several targeting ligands to enhance the therapeutic efficacy. One of the major challenge in developing an effective and safe cancer therapy is the poor distribution of nanocarriers at tumor sites and the insufficient penetration of drugs. EPR effect (passive targeting) can provides a little tumour specificity (20-30%) when compared with normal organs. The active targeting can even increase the drug efficiency after accumulation in the tumour region.

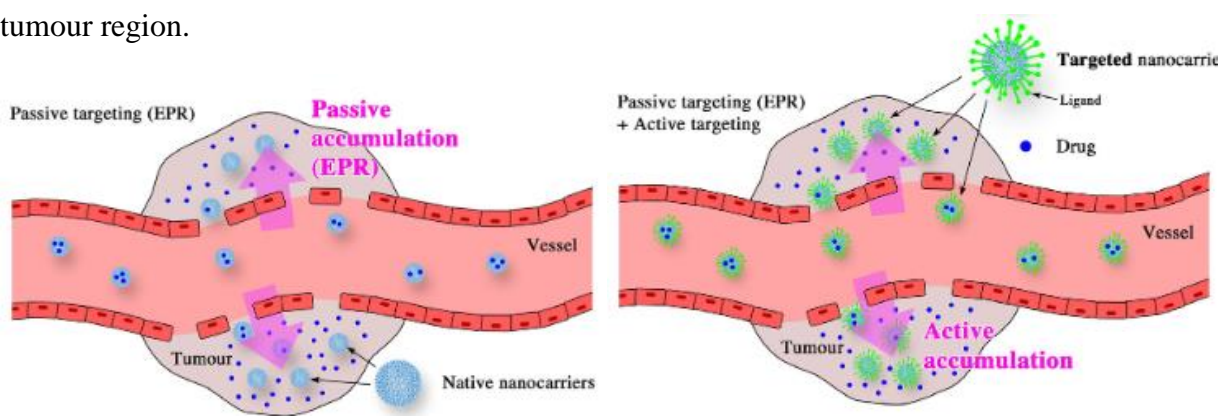


**Figure 1.4.** Scheme showing the passive targeting (EPR) and the active targeting into a tumour tissue. (Adopted from *J. Pharm. Pharmacol.* **2019**, 71, 1185–1198)

An active targeting strategy involves applying affinity ligands that direct the binding of nanoparticles to antigens that are overexpressed on the plasma membrane of diseased cells.<sup>25</sup> So far, several receptors have been identified and antibodies have been synthesized and tested both *in vitro* and *in vivo* conditions. Peptide based receptors like Arg-Gly-Asp (**RGD**) and Asn-Gly-Arg (**NGR**) peptides are well studied peptide receptors. RGD peptide known to bind with  $\alpha_v\beta_3$  integrin overexpressed in glioma cells while NGR peptide known to bind with aminopeptidase N (CD13) overexpressed in HUVEC and HT-1080 cell line.<sup>26</sup> A classic example of a ligand is folic acid (FA), which binds specifically to the folate receptor (FAR), which is often overexpressed in different tumors such as breast, lung, kidney, and brain.<sup>27</sup> The folate receptors consist of a family of four homologous proteins that have a high affinity for folic acid. Because FR- $\alpha$  and FR- $\beta$  have limited expression in healthy human tissues, they have been used for targeted delivery to cancerous tissues.<sup>28</sup> In comparison to normal cells, cancer cells have a high affinity for carbohydrates due to their need for nutrients for rapid proliferation

that's why many tumor cells overexpress mannose receptors and mannose-6-phosphate receptors.<sup>29</sup> Due to this distinct property of tumor cells various mannose receptor based drug delivery systems have been reported in literature.<sup>30</sup> Biotin (vitamin B7) receptors are overexpressed in various cancer cells, such as cervical, breast, lung, and ovarian cell lines, which has higher affinity for streptavidin-type membrane proteins Recently Jayakannan et al. Developed biotin-tagged multistimuli responsive dextran vesicles for doxorubicin delivery. Biotin-tagged dextran vesicles and normal dextran vesicles were exposed to HeLa cells. Fluorescence intensities were calculated at different time intervals which revealed a higher uptake of biotin-tagged Dextran vesicles compare to normal dextran vesicles.<sup>31</sup> By choosing proper targeting ligands active targeting can be used to target specific sites within the target cells. For example, the negative membrane potential of mitochondria facilitates the uptake of positively charged nanocarriers even against the concentration gradient. Phosphonium ion is one of the most well explored cationic ligand for targeting mitochondria.<sup>32</sup> Active targeting is a potential method for site-specific delivery and to enrich the drug concentration in selectively in tumor tissue, the strategy has some disadvantages, such as low blood circulation time of nanoparticles due to nonspecific binding with proteins, compromised tumor penetration, and high susceptibility for lysosomal degradation.<sup>33</sup>

### **1.3. Effect of Physicochemical Properties of Polymer on Drug Delivery Systems (DDSs)**

The synthetic biodegradable polymers are important class of polymers have been mainly used for drug delivery and tissue engineering applications.<sup>34-36</sup> The physical properties of polymer like solubility (hydrophilicity/hydrophobicity) <sup>37</sup>crystallinity,<sup>38,39</sup>glass transition and temperature, molecular weight of polymer<sup>40</sup> can influence degradation and drug release kinetics from a polymer nanoparticle which ultimately affects the therapeutic efficacy of nanocarrier. Other than physical properties the chemical nature of monomers from which polymer has synthesised also play a crucial role because final biodegradation of polymer will give the monomeric units which will ultimately decides the biocompatibility of polymer.

Solubility of polymer is a key parameter for designing a drug delivery system. The solubility of polymer depends upon chemical structure of monomers and degree of crystallinity of polymer which ultimately effects the drug release kinetics.<sup>41</sup> The drug release from a polymer matrix can be achieved by following three methods. (i) surface erosion, (ii) bulk erosion and (iii) diffusion of drug molecules from polymer nanocarrier. In case of hydrophobic polymers, the drug release is mainly governed by surface erosion while in case of hydrophilic

polymer the drug release mainly controlled by bulk erosion.<sup>42</sup> Various studies have been carried out to check the effect of polymer hydrophilicity on drug release kinetics and it was observed that the drug release kinetics was faster for hydrophilic polymers. The Incorporation of the less hydrophobic glycolide comonomer in block copolymer led to in vitro degradation of up to 2 times greater mass loss, release of up to ~7 folds.

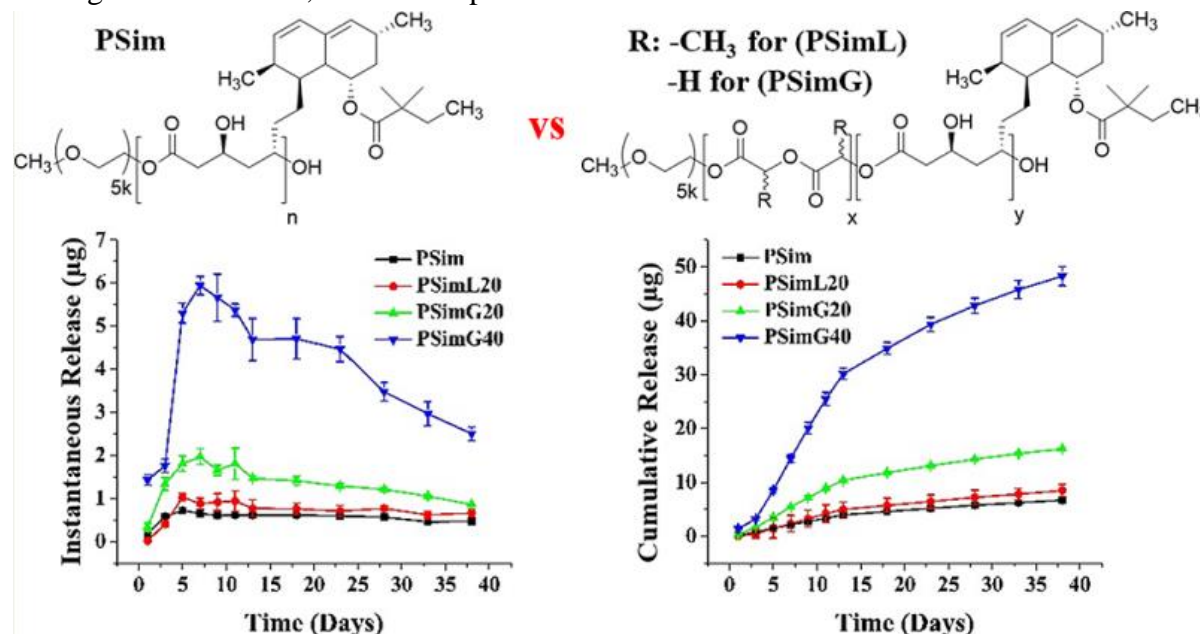


**Figure 1.5.** Effect of polymer hydrophilicity on in vitro drug release. (Adopted from *ACS Biomater. Sci. Eng.* **2018**, *4*, 4193–4199)

Liyanage and coworkers have shown that the drug release from polymer nanoparticle can be varied by changing the ratio of glycolide and lactide comonomers in block copolymer as shown in figure 1.5.<sup>43</sup> Crystallinity of the polymer is another important parameter that affects DDs. The partially aligned polymer molecular chains participate in polymer crystallization, which impacts the polymer's physical and chemical properties. An important concept in drug delivery is the degree of crystallinity of a polymer sample versus the degree of amorphous regions. Because Only amorphous regions are permeable, so they are available to water molecules.<sup>44</sup> The degree of crystallinity of polymers affects their mechanical strength, swelling, hydrolysis, and biodegradation rates. It has been demonstrated that polymers with a low degree of crystallinity release drugs at a higher rate since they have a greater degree of chain mobility.<sup>38</sup> Karavelidis et al. synthesized Four different polyesters from 1,3-propanediol with different chain length aliphatic dicarboxylic acids (Adipic acid, glutaric acid, pimelic acid, and azelaic acid) by polycondensation method. They have found that as the chain length of carboxylic acid was increasing crystallinity of polymer was increasing. To check the effect of crystallinity *in vitro* drug release and degradation was carried out and they found that as the crystallinity of

polymer was increasing the degradation and drug release kinetics was decreasing.<sup>38</sup> Another Important parameter for designing polymer based DDs is glass transition temperature of polymer, depending upon temperature the amorphous domain of a polymer can have either in glassy state or in rubbery state. The temperature at which a polymer transforms into rubbery state from a glassy state and vice versa is called glass transition temperature of polymer. In glassy state the polymer chains have very low mobility compare to the rubbery state which directly facilitate the higher mass mobility of water and other molecules which affects the degradation and drug release from polymer nanoparticle.<sup>45</sup>

The molecular weight of polymer has a significant effect on DDs because the physical properties of polymer like Solubility, glass transition temperature, crystallinity and mechanical properties are directly related to polymer molecular weight so on polymer degradation and drug release. In general, lower molecular weight polymers have higher degradation kinetics compare to high molecular weight polymers. To check the effect of molecular weight on degradation and drug release kinetics Braunecker et al. has synthesised a series of polyglycolide based biodegradable polymer.<sup>46</sup> The results showed a decrease in molecular weight results increase in porosity and increased drugs release as shown in figure 1.6.

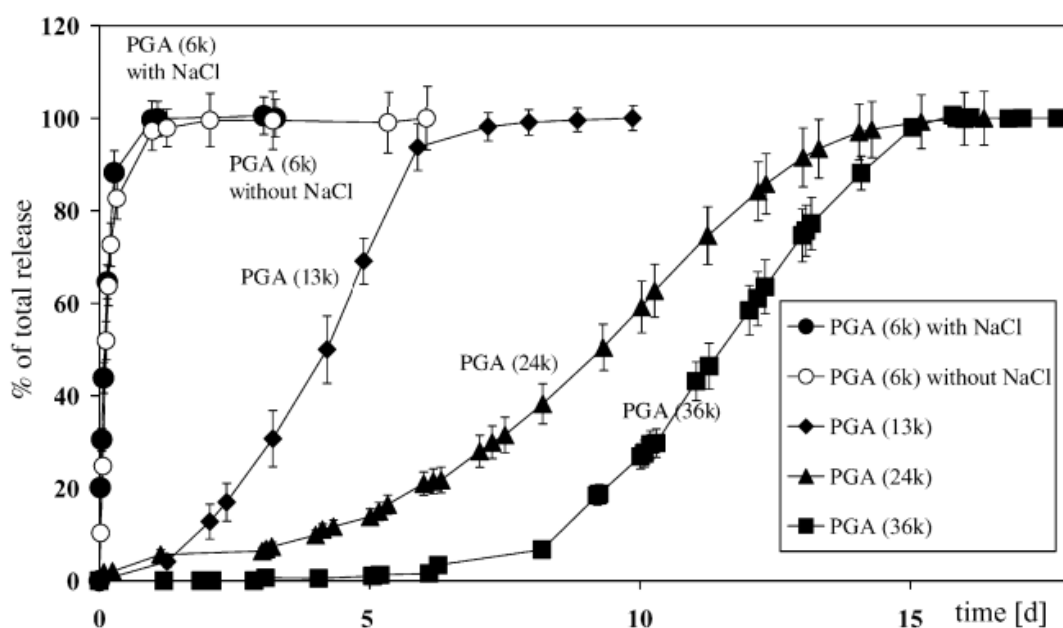


**Figure 1.6.** Effect of molecular weight on in vitro drug release kinetics. (Adopted from *Int. J. Pharm.* **2004**, 282, 19–34)

## 1.4. Sustainable Polymers in Drug Delivery

A sustainable polymer can be classified into two major groups: Natural polymers and synthetic biobased polymers. Different Natural polymers such as cellulose starch and protein have been widely utilized for preparing bioplastics and for other purposes.<sup>47</sup> Synthetic biobased polymers can be derived from a variety of molecular biomass such as plant oils, fatty acids, furans, amino acids and carbohydrates.<sup>48,49</sup> In recent years, there have been growing concerns over the sustainability of materials and chemicals produced using petrochemical-based resources due to the threats they pose to welfare, health, and the environment. There is an enduring requirement to replace polymers from fossil fuels with renewable materials that are more environmentally friendly. The development of modern polymers produced from renewable resources with better properties and possibly lower costs has stimulated enthusiasm about replacing traditional petrochemical based polymers. Recently, synthetic polymers derived from biobased monomers have gained much more attention due to their inherent biocompatibility and biodegradability.<sup>50</sup> Some representative examples of biodegradable polymers synthesised from natural resources are discussed below.

### 1.4.1. Sugar derived polymers:

Among all naturally occurring resources carbohydrate based monomers are most important because of their high abundance, low cost and easy availability. Synthetic polymers from carbohydrate monomers are superior to polymers derived from petroleum based monomers in terms of biocompatibility and biodegradability moreover the hydroxyl groups in polymer chain gives higher water solubility and enhanced hydrolytic degradation.<sup>51,52</sup> The primary concern to use carbohydrate based building blocks is presence of multiple hydroxyl groups which can lead to various side reactions during polymerisation reaction.<sup>53-57</sup> So to prevent these unwanted side reactions mainly bicyclic sugar based diols and diacids in which exceeding functional groups are protected has been mainly reported in literature. Polymer synthesis from acyclic carbohydrate based diols and diacids are also known in which the secondary hydroxyl groups were protected as methyl, silyl and benzyl ether.<sup>58-60</sup> Stereoisomers of 1,4:3,6-Dianhydrohexitol known as isosorbide, isoidide and isomannide synthesized by dehydration of corresponding hexitol are well explored building blocks in condensation polymerisation for the synthesis of various classes of polymers like polyester,<sup>61,62</sup> polyamides,<sup>63</sup> polyurethanes<sup>64</sup> etc. Chemical modifications of polyester like PET and PBT with these isohexides has been also reported to enhance the thermal properties of polymers.<sup>65</sup> The cyclic structure of these building blocks gives high glass transition temperature to the polymer

but the secondary nature and spatial arrangement of hydroxyl groups seriously hampers the polycondensation reaction resulting low molecular weight polymers.<sup>66</sup>

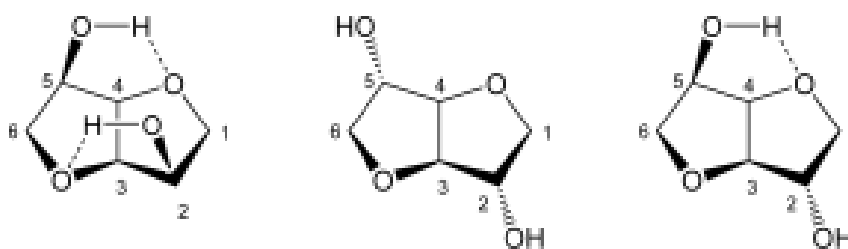


**Figure 1.7.** The spatial arrangement of hydroxyl groups in isohexides. (Adopted from *Biomacromolecules* **2012**, *13*, 4138–4145)

Wu et al reported fully isohexide based polymers where Isoidide Dimethyl Dicarboxylate was reacted with isomannide to get the fully carbohydrate based polymers.<sup>62</sup> Jingying Chen and coworkers have synthesised a series of polyester by incorporating isohexide into PBT (poly(butylene terephthalate)) and they have found that as the mole ratio of isohexide was increasing in the polyester the rate of hydrolytic degradation was also increasing.<sup>67</sup> Radical polymerisation of isosorbide based (meth)acrylate is also known.<sup>68,69</sup> However, in this case the isosorbide was employed as a pendent group in (meth)acrylic backbone which is nonbiodegradable. Very recently Derek J. Saxon and coworkers have developed a method to incorporate the isosorbide into polymer backbone by ring opening polymerisation.<sup>70</sup>

The another class of sugar based building blocks which are well explored are bicyclic diacetalized diols and diacids synthesized from of C-6 alditols like mannitol, glucitol, galactitol. The intramolecular diacetalization of hexitol gives 1,6 diol having better reactivity than 1,4:3,6-Dianhydrohexitols and retaining the high glass transition temperature. A detailed reactivity analysis regarding isosorbide and diacetalized hexitols monomers for the synthesis of sugar-based aromatic copolyesters revealed that diacetalized diols had a greater reactivity than isosorbide under similar reaction conditions.<sup>56</sup>

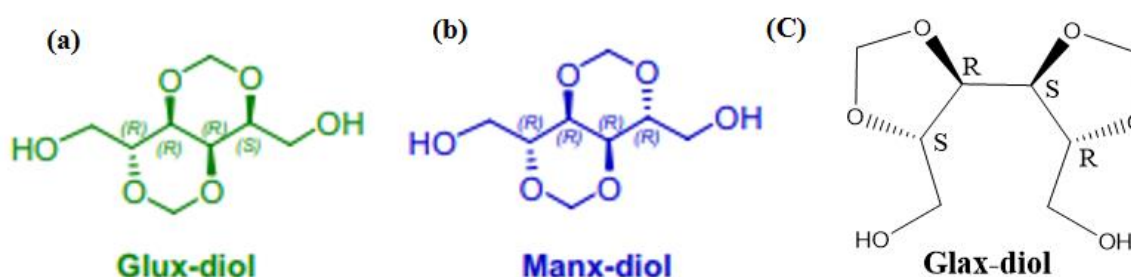


**Figure 1.8.** Molecular structures of glucitol, mannitol and galactitol based diacetalized diols.

Muñoz-Guerra and co-workers prepared different bicyclic diacetalized hexitols from galactitol, mannitol and glucitol, and widely explored these diacetalized sugar based diols with various aliphatic and aromatic ester building blocks for polyester synthesis which were more susceptible for enzymatic and hydrolytic degradation.<sup>71-75</sup> Polyurethanes from these bicyclic sugar based diols are also known where hexamethylene diisocyanate (HMDI) and 4,4'-methylene-bis(phenyl isocyanate) (MDI) was polymerised with these sugar diols to synthesise linear polyurethanes. Further, deacetalization of these polyurethanes yielded polyhydroxylated polyurethanes with better hydrophilicity and enhanced degradability.<sup>76</sup> The 1,2 hydroxyl groups of sugar molecule are known to form dynamic covalent bonds with boronic acid depending upon the pH of medium.<sup>77</sup> This dynamic covalent bonding has been used for the crosslinking reaction between D-mannitol and boronic acid to make hydrogels.<sup>78</sup>

Carbohydrates are biomolecules found in the body, they have great potential to be excellent drug delivery vehicles due to their inherent biocompatibility and can be excreted naturally from the body.<sup>79-82</sup> Stebbins and coworkers have reported D-mannitol based poly(anhydride-ester) in which each repeating unit contains four chemically conjugated Ibuprofen molecules by an ester bond as shown in figure 1.9.<sup>83</sup> The polymer was showing controlled hydrolytic degradation to release the ibuprofen for anti-inflammatory activity. The released ibuprofen was collected to perform the cyclooxygenase-2 (COX-2) assay, which showed that the released ibuprofen was retaining its anti-inflammatory activity.

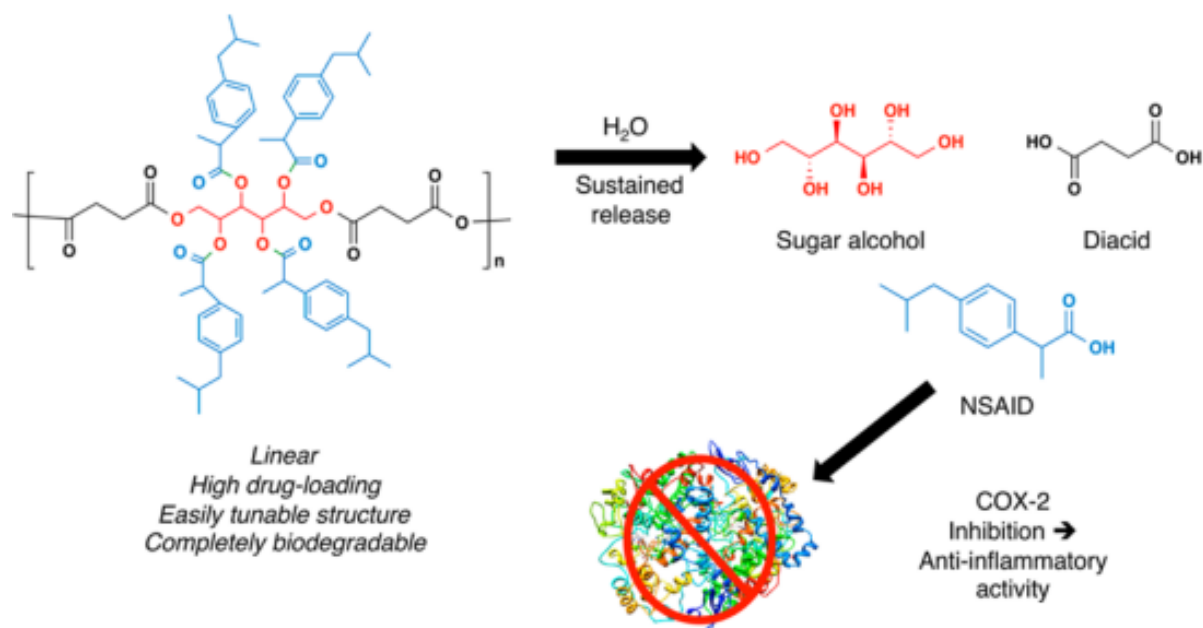


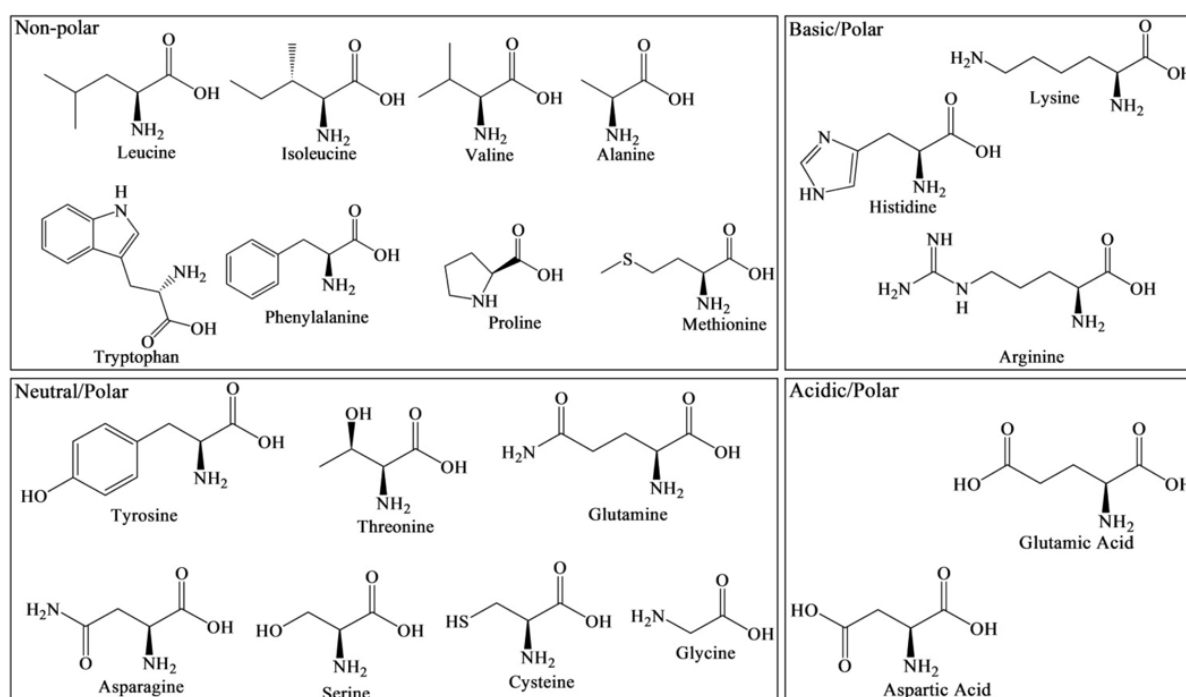
**Figure 1.9.** Synthesis of D-Mannitol-Based prodrug for anti-inflammatory activity. (Adopted from *Biomacromolecules* **2015**, *16*, 3632–3639).



Several sugar-based amphiphilic nanocarriers with extremely low CMC values and excellent physiological stability and bioactivity have been reported by Urich and coworkers. These sugar based amphiphiles was explored for chemical conjugations or physical encapsulation of various anticancer hydrophilic and hydrophobic anticancer drugs.<sup>84</sup>

#### 1.4.2. Amino acids and oligopeptides:

Amino acids are biologically important molecules and play a crucial role in many special physiological functions like protein synthesis, metabolism, neurotransmission, body development<sup>85</sup> etc. The amino acids contain both amine ( $-NH_2$ ) and carboxylic acid ( $-COOH$ ) groups and a side chain which is responsible for the unique property of each amino acid.<sup>86</sup> Amino acids in which the carboxylic group and amine groups are separated by one carbon are known as alpha amino acid. There are 20 naturally occurring alpha amino acids which are found in proteins. Except glycine all the naturally amino acids are chiral and exist as enantiomeric pair and have L-configuration (Relative Configuration). Depending upon the nature of side chain amino acid can be classified into different categories like aliphatic, aromatic, acidic, basic, amidic, alcohol and thiol.



**Scheme 1.1.** Chemical structure of  $\alpha$ -amino acids.

As amino acids contains both acidic and basic group so they exists as zwitterions or dipolar ions depending upon the pH of medium. Change in pH cause amino acids to go through

a state at which there are equal numbers of positive and negative charges which is a specific value for each amino acid and known as isoelectric point of that amino acid and represented as  $P_i$ . At isoelectric point the amino acid carries no net charge and charge on amino acid is purely dependent on pH of medium. A variety of methods are available for producing amino acids, including chemical synthesis, extraction, fermentation, and enzymatic catalysis.<sup>87</sup> Most of the chemical synthetic methods gives racemic mixture<sup>88</sup> which needs further purification to get optically pure amino acid. In chemical synthesis, the Stracker synthesis is one of the most popular chemical synthetic method to synthesise  $\alpha$ -amino acids. The extraction method involves breaking down proteins to produce amino acids where protein rich materials are used to get the amino acids. An enzyme or combination of enzymes can catalyse the production of amino acids using the enzymatic process which gives optically pure amino acids. Different enzymes like hydrolytic enzymes etc. have been used for the synthesis of amino acids. The fermentation process is used in most industrial amino acid production where the sugar present in a substrate is converted into a wide range of amino acids by microorganisms like *C. glutamicum* and *E. coli*.<sup>89</sup> A wide range of applications for amino acids are found in foods, cosmetics, polymers, pharmaceuticals, and other areas of everyday life.<sup>90</sup> Due to diverse functionality, bioactivity and biocompatibility amino acids have been used to synthesise different classes of polymers via different methodologies.

Synthetic Peptides are highly versatile materials, the high structural versatility is result of diversity archived by 20 different natural amino acids in peptide sequence and the functional diversity is result of a wide range of chemical functionality present in natural amino acids. There are mainly two methods for the synthesis of oligopeptides. First method is solution phase synthesis in which the amine and carboxylic groups of amino acids couples together in presence of a couple agent to give peptide bond.<sup>91</sup> The solution phase peptide synthesis needs multiple protection deprotection steps and purification in each step which make it tedious process for longer chain peptide synthesis. The second method is solid phase peptide synthesis,<sup>92</sup> discovered by Robert Bruce Merrifield in 1962. In solid phase peptide synthesis, a C-terminal resin protected amino acid is reacted with N-terminus protected amino acids and each step involves washing to remove the unreacted amino acid and by-products. Other than the hydrogens bonding between peptide unit there are various interactions exist in peptide chain which can directly affect the confirmation and self-assembly of peptide. For example, the  $-R$  group in hydrophobic amino acids can involve in various hydrophobic interactions, aromatic amino acid can engage in aromatic  $\pi - \pi$  interactions,<sup>93</sup> hydrophilic amino acids can involve

in hydrogen bonding<sup>94,95</sup> and charged amino acids can participate in charge-charge interactions based upon the pH of medium.<sup>96</sup> The combination of specific amino acids and directional self-assemblies in peptide molecules is critical for morphologies of nanostructures, such as  $\alpha$ -helices,  $\beta$ -sheets,  $\beta$ -turns, and random coils.<sup>97-100</sup>

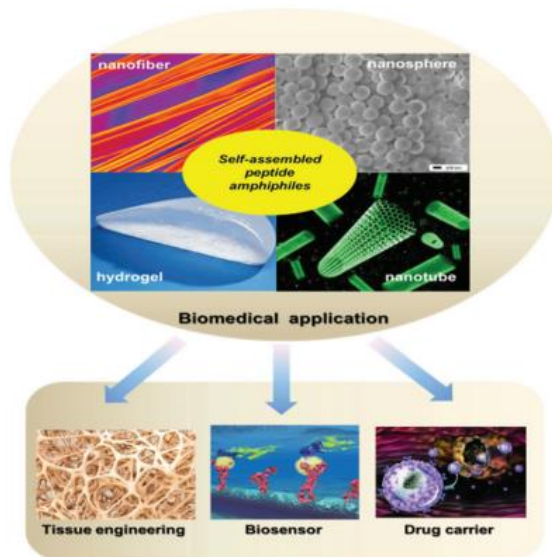


**Figure 1.10.** Self-assembled structures from amphiphilic peptides (peptide amphiphiles) and their use in biomedical application (Adopted from *Biomater. Sci.* **2017**, 5, 2369–2380)

Tuttle and coworkers have shown that how the nature and sequence of amino acid in peptide chain can directly affect the gelation property of tripeptide.<sup>101</sup> In other study have found that how a minor alteration in amino acid sequence can influence the self-assembly of pentapeptide.<sup>102</sup> Peptide chain having proper amphiphilicity are known as peptide amphiphiles which can self-assemble into various nanostructures.<sup>103</sup> Like micelle, vesicle, fibres, hydrogels, tubes<sup>104-106</sup> etc. Peptide amphiphiles can be synthesised by three different route<sup>103</sup> as shown in figure 1.11 amphiphilic peptides: are made up of a combination of hydrophilic and hydrophobic amino acids. (2) lipidated peptide amphiphiles: Mainly the C-

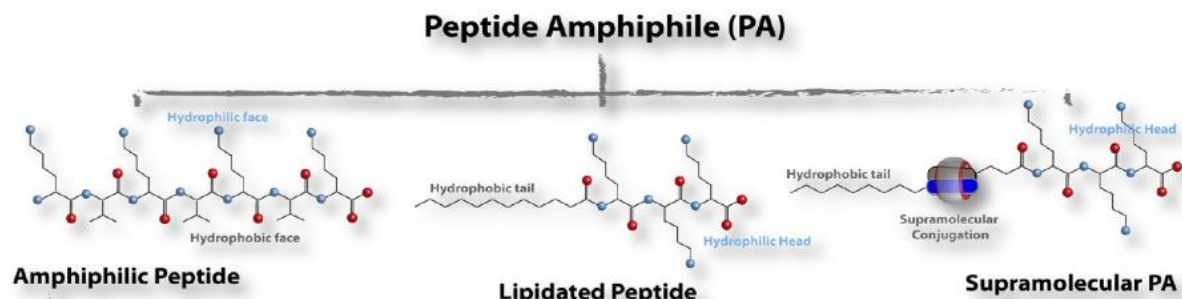


**Figure 1.11.** Different methods to synthesise peptide amphiphiles. (Adopted from *Langmuir* **2019**, 35, 10704–10724)

terminal a hydrophilic peptide is attached with a lipid chain, and (3) supramolecular peptide amphiphile conjugates: Two different molecules are combined to form an amphiphilic structure through dynamic covalent bonds or supramolecular interactions. Inherent biocompatibility and biodegradability of peptides makes them a prominent candidate in biomedical field.<sup>107</sup> Usually, the secondary structure of peptide amphiphiles is altered to respond to different environment conditions, followed by the configuration of the self-assembling systems. For example, Jacoby et al. reported peptide amphiphiles which underwent a pH-induced phase transition from spherical micelles to elongated worm-like micelles.<sup>108</sup>

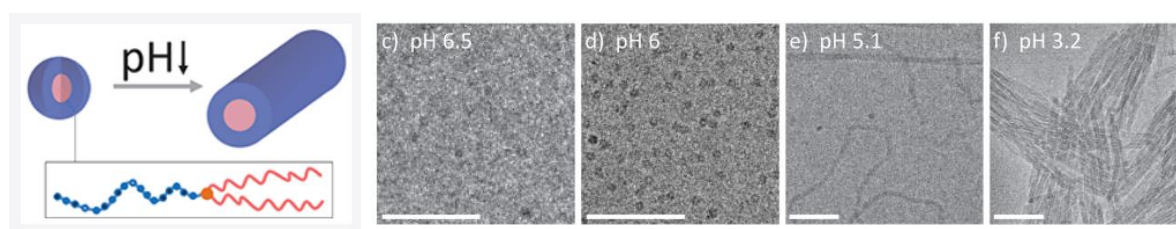


**Figure 1.12.** *pH induced transition of peptide amphiphiles from spherical to worm like micelles. (Adopted from J. Am. Chem. Soc. 2021, 143, 11879–11888.)*

Jeena et al. developed a mitochondria-accumulating amphiphilic peptide (Mito-FF) from diphenylalanine, triphenyl phosphonium (TPP) a mitochondria-targeting moiety and pyrene. Due to the negative membrane potential of mitochondria, the monomolecular (Mito-FF) are able to enter tumor cells and self-assemble in mitochondria to form nanofibers of 9-11 nm in size. By destroying the mitochondrial membrane, these nanofibers are capable of activating the apoptotic response in tumor cells resulting in self-delivery of toxic assemblies.<sup>32</sup>



**Figure 1.13.** *Chemical structure of Mito-FF and its self-assembly. (B) Leakage of mitochondrial protein to the cytosol monitored using APEX labelling showing membrane disruption induced by Mito-FF. (Adopted from Jeena et al. Nat. Commun. 2017, 8, 26).*

Nandi et al. reported a phenyl alanine based peptide amphiphiles in which C-terminal free amine was covalently attached with a fatty acyl chain and N terminal was attached with

various alkyl amine. These peptide amphiphiles were forming hydrogels at higher temperature and showing excellent antimicrobial activity against Gram-positive bacteria (*Staphylococcus aureus*, *Bacillus subtilis*) and Gram-negative bacteria (*Escherichia coli*).<sup>109</sup>

By mixing various bipyridine derivatives with N-terminally capped diphenylalanine, Ji Wie and coworkers investigated the morphology manipulation of assemblies through intermolecular hydrogen bonds. Multifunctional bipyridine molecules are incorporated into two-component supramolecular gels to produce multiple-responsive gels and they were studied with various biophysical and protected diphenylalanine (ZFF), Boc-protected diphenylalanine (Boc-FF), and acetyl-protected diphenylalanine.

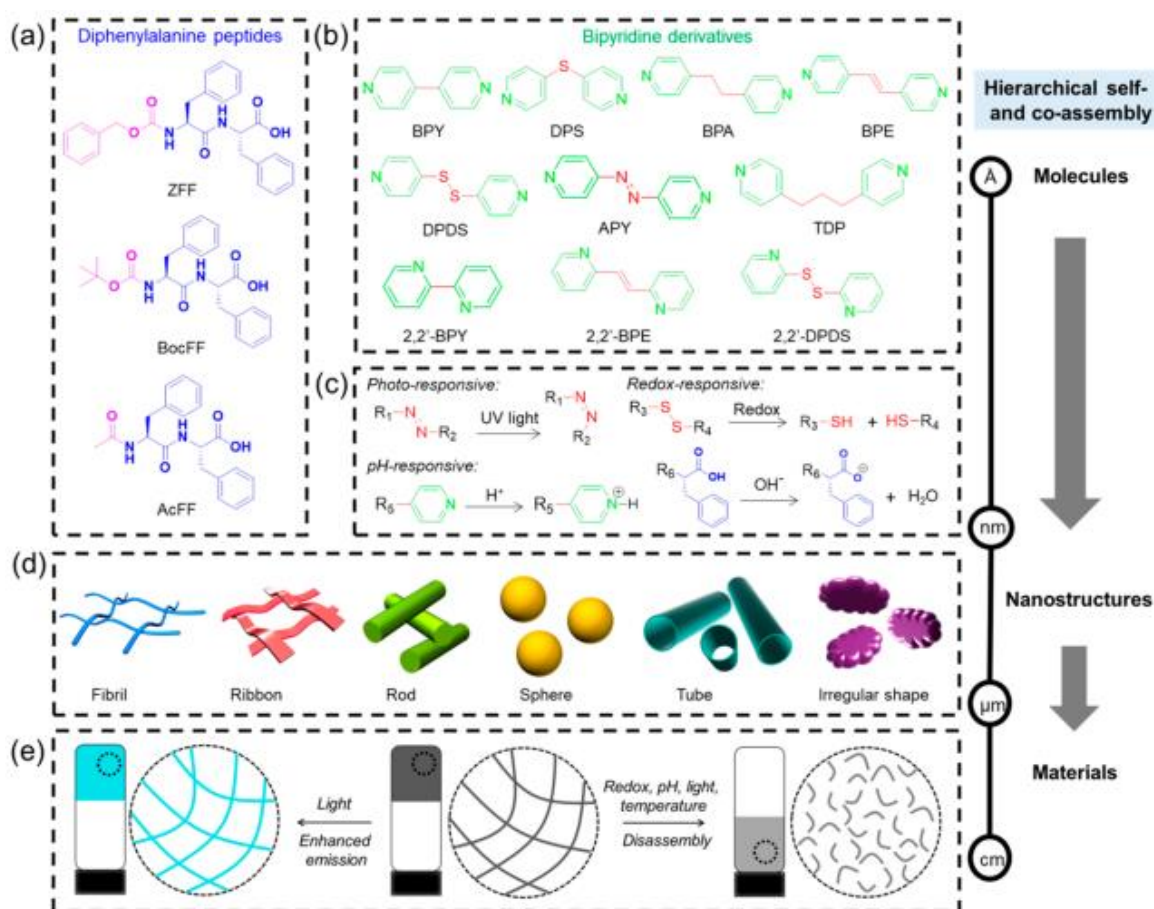


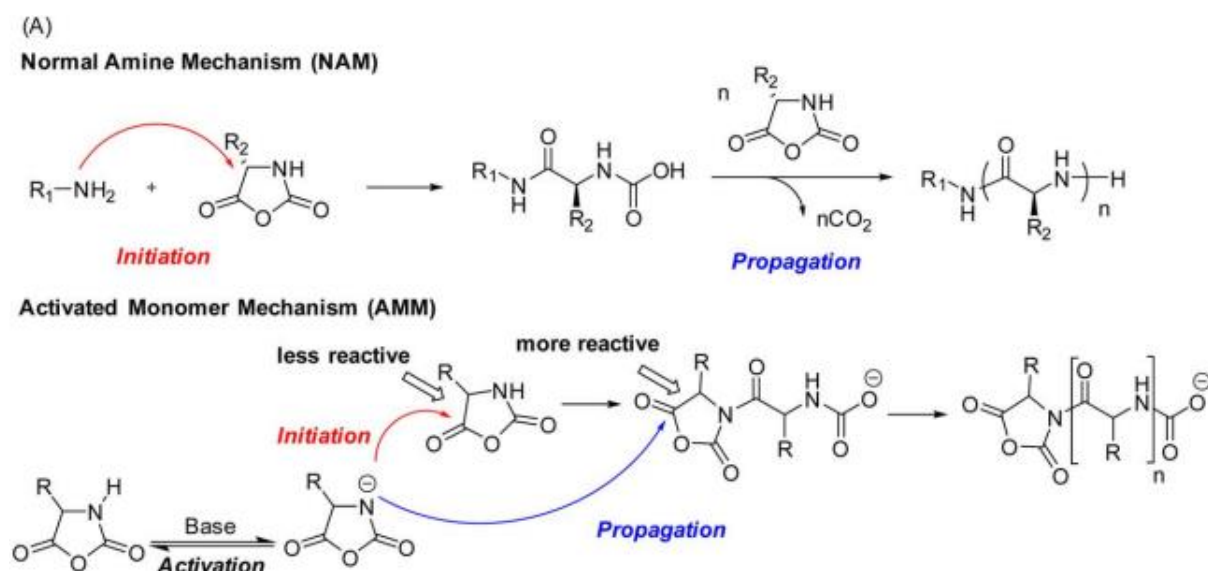
**Figure 1.14.** Schematic presentation of a structure-based assembly that generates multiple-responsive gel materials by co-assembly modulated structural diversity. (a–c) Chemical structures of (a) Three different FF peptides, (b) bipyridine derivatives, and (c) stimulus-responsiveness different bipyridine derivatives. (d) morphologies obtained from hierarchical self- and coassembly of FF peptides. (e) Multiple responsive gels obtained from FF-based peptides and functional bipyridine derivatives. (Adopted from *J. Am. Chem. Soc.* **2021**, *143*, 17633–17645).

(AcFF) were mixed with 10 different bipyridine derivatives. These dipeptides underwent crossassembly due to strong hydrogen bonding between free carboxylic acid and

pyridine moiety. Using bipyridine/dipeptide components, the morphological diversity was controlled to obtain different nanostructures like nanofibrils, nanoribbons, nanorods, nanospheres, nanotubes, and irregular shapes. Due to different molecular functionality in bipyridine, multiple hydrogels were obtained which were showing responsiveness to various external stimuli like, pH, light, redox, and temperature.<sup>110</sup>

### 1.4.3. Synthetic polypeptides in biomedical applications:

Poly(amino acid) or polypeptides special class of polymers consists of amino acid repeating unit connected together by an amide bond. Low molecular weight polypeptides can be synthesised by polycondensation method in which the acid group of amino acid can be converted into acid chloride or activated ester group so that the amine group of amino acid can undergo polycondensation reaction to give polypeptide.<sup>111</sup> High molecular weight polypeptides can be obtained by ring opening polymerisation of  $\alpha$ -N-Carboxyanhydride (NCA) monomer.<sup>112</sup> The reaction between amino acid and triphosgene gives optically pure amino acid based NCA monomer which can undergo ring opening polymerisation by two different mechanisms. (i) Activated amine mechanism (AAM) involve deprotection of NCA monomer by a non-nucleophilic base to give a NCA anion which subsequently attacks on the another NCA monomer to propagate the ring opening polymerisation. Various catalyst like transition metal catalysts,<sup>113</sup> hexamethylsilazane,<sup>114</sup> ammonium salt<sup>115</sup> etc. have been used to avoid the side reactions.



**Scheme 1.2.** Ring opening polymerisation of  $\alpha$ -N-Carboxyanhydride (NCA) monomer *J. Polym. Sci. A: Polym. Chem.* **2016**, *54*, 311–315.

(ii) The second method for NCA polymerisation is normal amine mechanism (NAM) in which nucleophilic amine or alcohols are commonly used for nucleophilic attack on NCA monomer to give polypeptide. In polypeptide synthesis ring opening polymerisation method has several advantage over condensation method like control over the molecular weight by varying the M/I (monomer to initiator ratio), low polydispersity and synthesis of block copolymers etc. Poly(Cbz- L-Cys) oligomers have the strongest tendency to form secondary structures like  $\beta$ -sheets, which results the precipitation of oligomers in reaction medium although, the addition of hydrogen-bond breaking agents like urea to the reaction mixture breaks the  $\beta$ -sheets assembly which keeps the polymer chain alive by providing proper solubility in reaction medium. Recently the side chain modified functional polypeptides are gaining much more attention in biomedical field because the polypeptide main chain can mimic the protein structure while the side chain can be tagged with various bioactive, stimuli responsive, fluorophore etc molecules which enriches the bioactive properties in polypeptide. There are two general methods for the synthesis of chain modified functional polypeptide. (i) Functional monomer route: In this method the side chain modified NCA monomer are polymerised to get the functional polymer. (ii) Post polymerisation modification (PPM): in this method the reactive group in polypeptide chain are reacted with desired functional groups to get the modified polypeptide. Each method has its advantages and disadvantages like the functional monomer route needs high precautions in the synthesis and purification of monomer but it gives 100 % substitution while the post polymerisation method is insufficient to give 100 % substitution on side chain.<sup>116</sup>

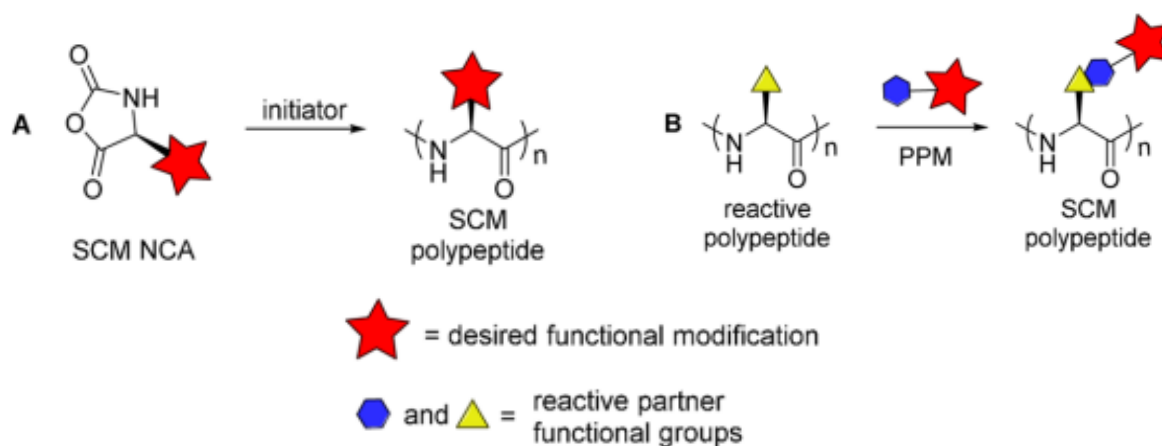


**Figure 1.15.** Synthetic routes for synthesis of side-chain modified polypeptides (Adopted from *Chem. Rev.* **2016**, 116, 786–808)

Using synthetic diblock copolypeptides, Deming and co-workers have created sheet-structured hydrogel assemblies through the polyion complexation of positively and negatively charged ionic segments in aqueous solutions. For that two different polypeptides having opposite charge were synthesised by NCA polymerisation. A diblock copolypeptide containing poly(L-methionine-stat-L-alanine), MA, segments joined to side-chain-protected segments of K or E. Oxidation methionine (M) followed by deprotection of side chain in lysine (K) and glutamic acid (E) gave the oppositely charged polypeptides which upon mixing in water undergoing polyion complexation to give hydrogels.<sup>117</sup> Further these hydrogels were used as 3D matrix for cell culture.



**Figure 1.16.** Schematic representation of two oppositely charged diblock copolymer followed by their polyion complexation. (Adopted from Deming and coworkers. *J. Am. Chem. Soc.* **2017**, *139*, 15114–15121)

Using post polymerisation modification approach recently Shixian Lv and coworkers have reported a high drug loading polypeptide where mPEG-b-poly( $\gamma$ -benzyl-L-aspartate) was reacted with ethanol amine to get methoxy poly(ethylene glycol)-b-poly- [(N-2-hydroxyethyl)-aspartamide] which was further reacted with phenylboronic acid pinacol carbonylimidazole to get the final amphiphilic polypeptide in which the electro acceptor boronic acid was hanging as a pendent group. Doxorubicin was loaded as a model drug and it was found that the  $-\text{NH}_2$  group of doxorubicin was making a complex with boronic acid which was confirmed by  $^{11}\text{B}$  NMR. Due to strong electronic interactions between doxorubicin and boronic acid high drug loading (DLC = 49%) was obtained.<sup>118</sup> Similarly, by post polymerisation modification Hang



Liu and coworkers reported a cholesterol modified poly(L-cysteine) copolymer in which post polymerisation oxidation of thioether groups in the side chains induces a change in packing characteristics of the peptide backbone resulting in a  $\beta$ -sheet to  $\alpha$ -helix transition, along with a fascinating morphological change from micelle like structures to vesicles. As the secondary structures and morphologies change, the polymer assemblies gain a high degree of specificity for controlled release of the payload and improved cell interaction in response to reactive oxygen species.<sup>119</sup>

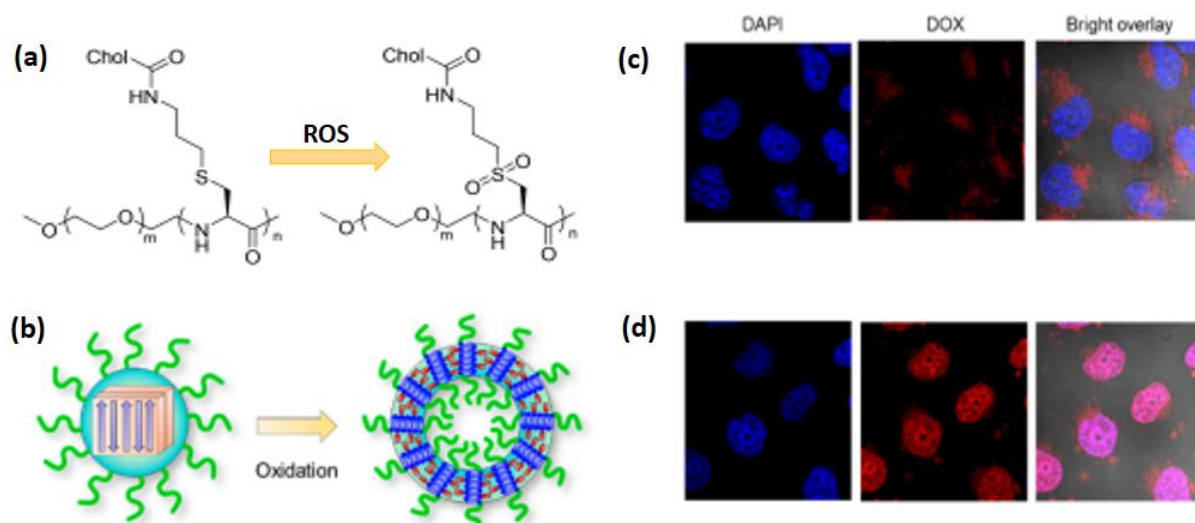


**Figure 1.17.** (a) Structure of PEG-PCys-Chol Before and PEG-PCys-Chol-O<sub>2</sub> after oxidation. (B) Schematic representation of the self-assembled amphiphilic polypeptides before and after oxidation. (c) CLSM images of DOX@PEG-PCys-Chol (d) DOX@PEG-PCys-Chol-O<sub>2</sub> after 4h incubation. (Adopted from Liu and coworkers *J. Am. Chem. Soc.* **2018**, 140, 6604.)

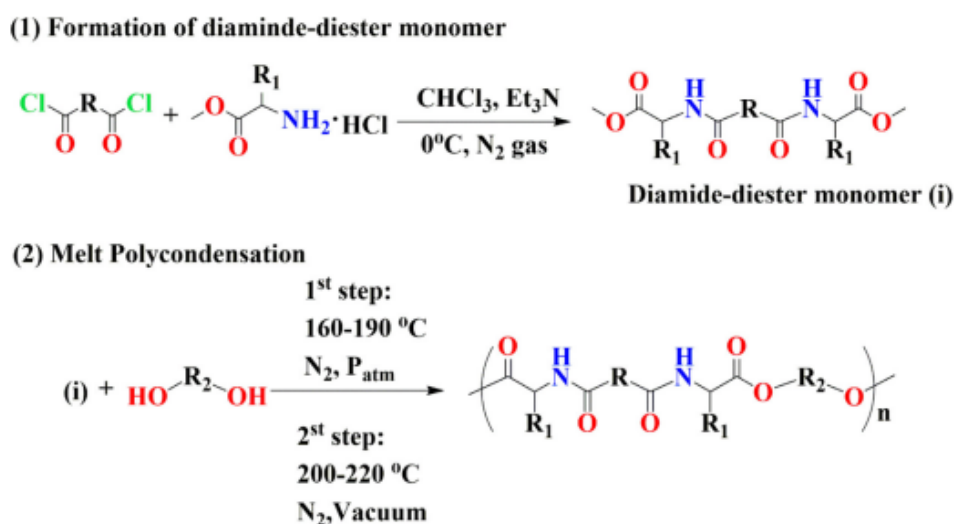
#### 1.4.4. Non-peptide polymer analogues from amino acids:

Polymers derived from L-amino acids are key components for engineering nanoscaffolds for various applications in biomedical field like, drug delivery, tissue engineering, gene delivery etc. Ring opening polymerization of NCA monomers from L-amino acids is a well-known procedure for the synthesis of well-defined di- and triblock synthetic polypeptides. Polypeptides self-assemble into nanostructures such as fibrillar networks, micelles, and vesicles, which have been found to have applications in the material science and biomedical fields. Despite their remarkable biocompatibility, biodegradability of high molecular weight polypeptides by intracellular enzymes is one of the main concerns for long-term applications of synthetic polypeptides in biomedical applications. In the last decade, significant efforts have

been to develop alternative strategy for synthesizing biodegradable polymeric nanomaterials from amino acids using different polymerisation techniques. A number of nonpeptide polymers derived from amino acids including poly(ester amide)s, polyurethanes poly(disulfide-urea-urethane), and polycarbonates etc. have found diverse application in biomedical field.

**Poly(ester amide)s:** Poly(ester amide)s are immerging group of polymer having excellent mechanical properties combined with good biocompatibility and biodegradability. Because of these combined properties they have been used as biodegradable plastics for consumable as well as in medical fields. Amino acid based poly(ester amide)s can be synthesised by two methods. (A) Polycondensation method and (b) Ring opening polymerisation of morpholino-2,5-diones. The polycondensation method can be further classified into three subclasses (i) melt polycondensation (MP method) (ii) solution polycondensation (SP method) (iii) interfacial polymerization (IP method)<sup>120</sup>

Amino acid based poly(ester amide)s can be synthesised by melt condensation method in two steps. First step involve the reaction of amino acid methyl ester with diacyl chloride to get diamide – diester monomer. This monomer can subsequently undrgo polymerisation with diol under melt condition to give oligomers which further subjected under vaccum to give high molecular weight poly(ester amide)s.

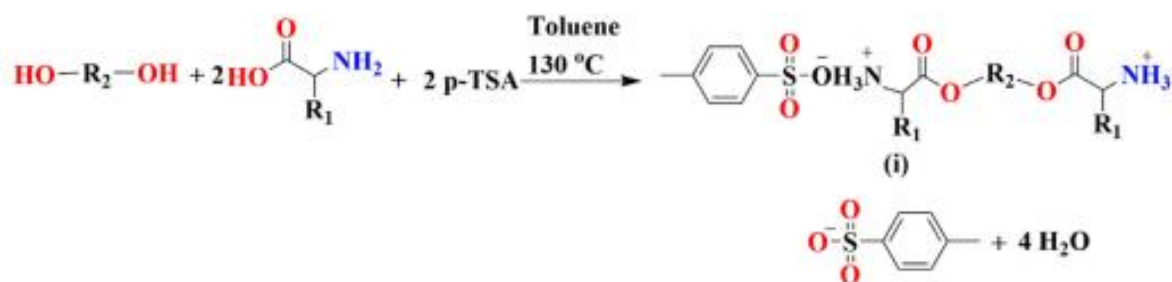


**Scheme 1.3.** Synthesis of poly(ester amide)s comprising amino acid from a diamide-diester and diol by melt polycondensation method. (*Polym. Degrad. Stab.* **2020**, 181, 109323.)

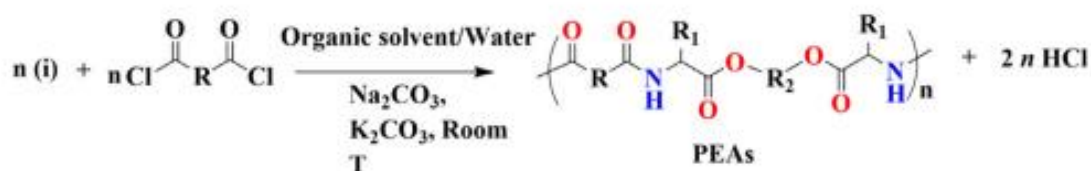
Asin et al. has synthesised various glycine based polyester amides using sebacid or terephthalic acid with different chain length aliphatic diols. The degradation studies of these polyester amides were carried out with different protease enzymes and they have found that the hydrophilicity of polymer was playing a crucial role in enzymatic degradation.<sup>121</sup> Jongh et al.

has synthesised a series of polymers using citric acid (CA), D-glucono- $\delta$ -lactone (GL) and different amino acids (AAs) and they found that incorporation of amino acid into polymer is significantly increasing the glass transition temperature of polymers.<sup>122</sup>

Interfacial polymerisation is carried out at the interface of two immiscible (Organic/water) solvents and synthetic route of PEAs by IP method



## (2) Interfacial polycondensation synthesis of PEAs



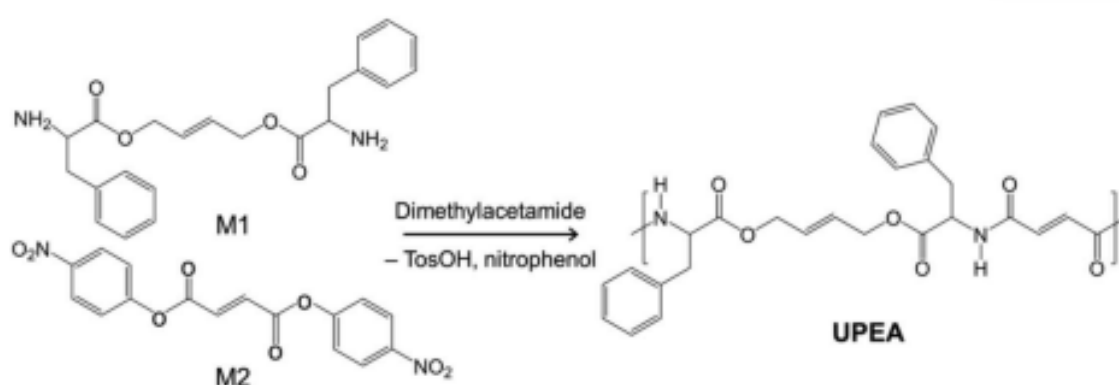
**Scheme 1.4.** Synthesis of amino acid polyester amides by interfacial polymerisation. (Adopted from *Polym. Degrad. Stab.* **2020**, *181*, 109323.)

can be classified into two different steps (i) preparation of di-toluene sulfonic acid salts of bis- $\alpha$ -(L-amino acid)- $\alpha,\omega$  alkylene diesters by Fischer esterification reaction in presence of PTSA between alcohols and amino acids (ii) Reaction of diacyl chlorides with in presence of a proton receptor (inorganic base). The hydrolysis of diacyl chloride can slow down the kinetics of polymerisation so use of hydrophobic diacyl chloride can solve the problem. Knight et al. has synthesised series of biodegradable PEAs from the amino acids L-alanine, L-lysine and L-phenylalanine using IP and these biodegradable polymers and Human coronary artery smooth muscle cells (HCASMCs) cultured on polymer films.<sup>123</sup> Recently Cao et al. has synthesised of a L-lysine-containing PEAs functionalization with maleic anhydride to introduce cross-linkable alkenes and carboxylic acid conjugation sites. these scaffolds supported were used for adhesion and proliferation of mouse embryonic multipotent mesenchymal progenitor cells.<sup>124</sup>

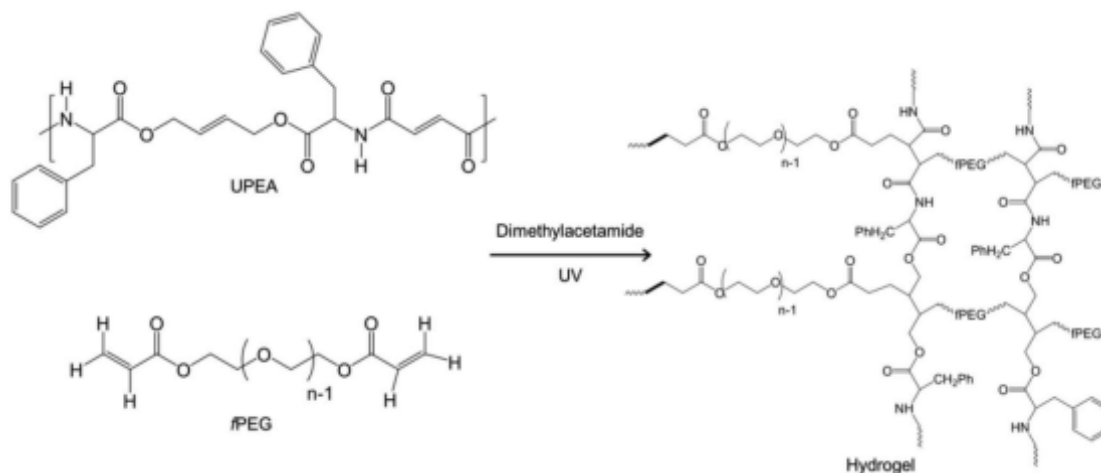
The solution polycondensation for polyester amide synthesis was first reported by Katarawara et al. in 1980s. solution condensation is most used polycondensation technique for polyester amide synthesis due to its high polymerisation rate and mild reaction conditions. The synthetic procedure involves polycondensation between di-toluene sulfonic acid salts of bis- $\alpha$ -(L-amino

acid)- $\alpha,\omega$  alkylene diesters and a activated carboxylic acid. Okada and coworkers have reported renewable resource based polyester amides using glucitol and amino acids. Biodegradability of these polymer was tested by Soil burial degradation test and enzyme degradation test which showed all these poly(ester amide)s were biodegradable in nature. An unsaturated polyester amide consisting of phenylalanine, butenediol, and fumarate was synthesized by Ruano et al. which was photo-crosslinked to produce a hydrogel. These hydrogels were further used for cell proliferation assays, performed by measuring the viability of the samples after seven days showed a significant improvement in the cellular colonization.<sup>125</sup>

(a)



(b)

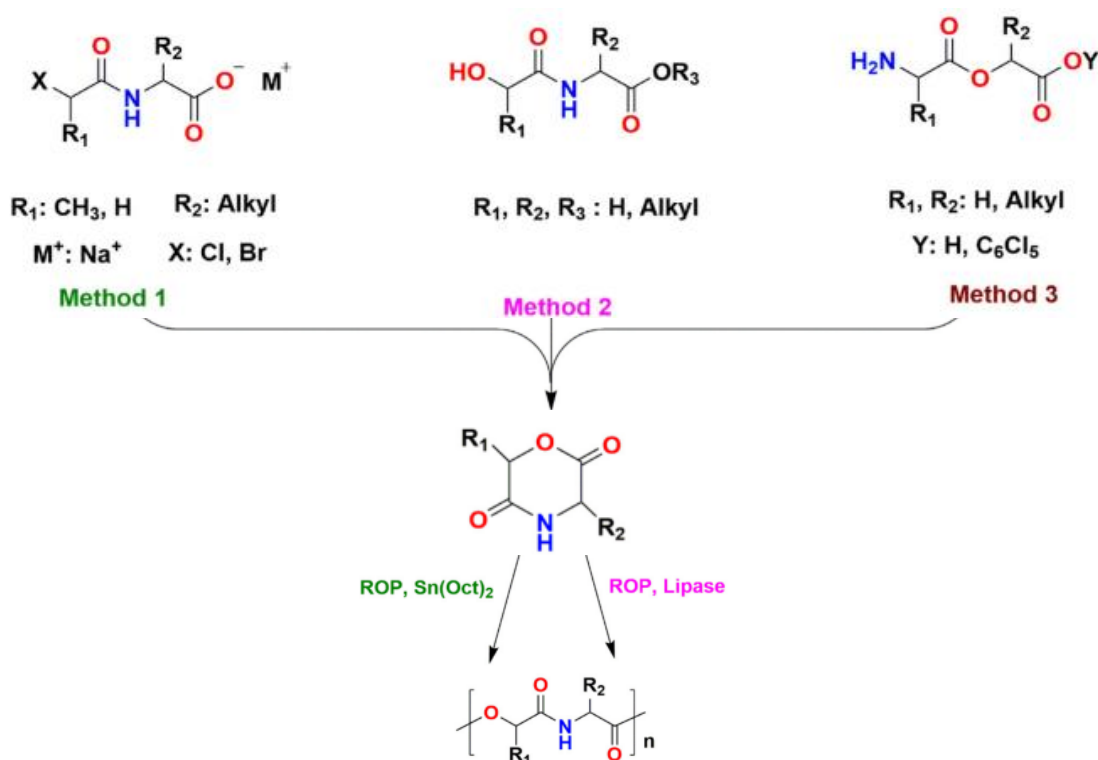


**Scheme 1.5.** (a) Synthesis of AAs based unsaturated polyester amides UPEA via solution polycondensation method. (b) UV crosslinking of UPEA to produce hydrogels. (Adopted from *Polym. Test.* **2020**, 82, 106300.)

Sun et al. reported amino acids based poly (ester amides) by solution polycondensation of di-*p*-toluenesulfonic acid salts of bis-L-phenylalanine diesters (SS-Phe- 2TsOH) with di-*p*-nitrophenyl adipate to give enzymatically and reductively degradable poly (ester amides). SS-PEA films were shown to have excellent adhesion and proliferation properties by preliminary cell culture studies, indicating exceptional cell compatibility with SS-PEA films. Degradation

studies of SSPEA films revealed fast surface degradation by  $\alpha$ -chymotrypsin, and bulk degradation under a reductive environment. Further the cytotoxicity of DOX loaded SS-PEA nanoparticles were checked in drug-sensitive and drug-resistant MCF-7 cells which showed the potent cytotoxicity of these nanoparticles.<sup>126</sup>

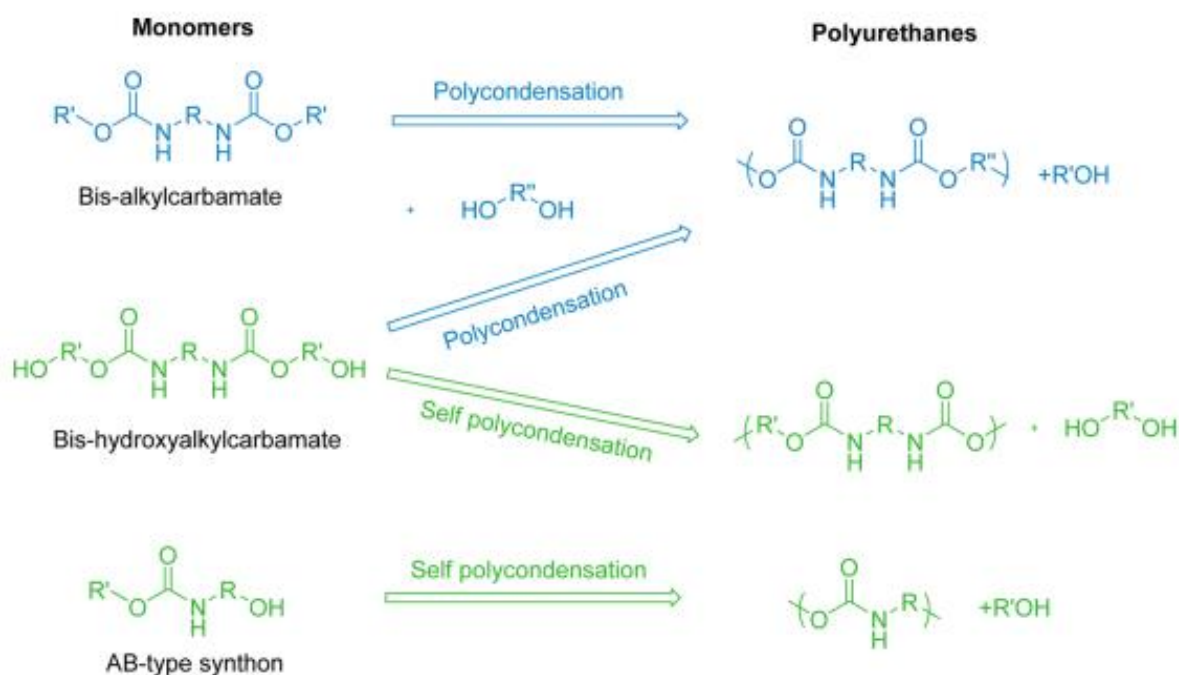
**Ring opening polymerisation:** Poly(depsipeptide)s (PDPs) can be explained as alternating copolymers of an  $\alpha$ - amino acid with an  $\alpha$ -OH acid. In 1985 Helder and coworkers have synthesised (PDPs) first time by ring opening polymerisation of morpholine-2,5-dione (MDs). The 6-membered derivatives of MDs can be prepared by three methods. (i) intramolecular transesterification of N-( $\alpha$ -hydroxyacyl)- $\alpha$ -amino acid esters (ii) cyclization of N-( $\alpha$ -haloacyl)- $\alpha$ -amino acid salts and (iii) O-( $\alpha$ -aminoacyl)- $\alpha$ -hydroxycarboxylic acids. The ring opening polymerisation of MDs generally carried out at high temperature under melt condition using tin based catalyst stannous octoate ( $\text{Sn}(\text{Oct})_2$ ). Another effective method for PDPs Is lipase catalysed ring opening of MDs. Chang-Xia Shi and group have synthesised a series Different MDs from amino acids like glycine, phenylalanine and leucine. The ring opening polymerisation of these MDs resulted into PDPs which were showing acid catalysed degradation to give the monomers.<sup>127</sup> The copolymerisation of MDs with caprolactone, glycolide, and lactide is also known where the properties of polymer can be tuned by varying the monomer ratio.



**Scheme 1.6.** Preparation of morpholine-2,5-dione (MDs) derivatives via the ROP method. (Adopted from *Polym. Degrad. Stab.* **2020**, *181*, 109323).

**L-Lysine based polyurethanes:** Among synthetic polymers, polyurethanes are an essential class with important applications in industry. These materials include thermoplastic elastomers, foams, adhesives, and surface coatings. Polyurethanes were synthesized by Otto Bayer in 1937 using the polyaddition reaction between di-isocyanates and diols.<sup>128</sup> Isocyanates are highly toxic compounds so alternative methods for polyurethane synthesis are more attractive specially for biomedical applications. Scheme represent some of the important non isocyanate routes for polyurethane synthesis.

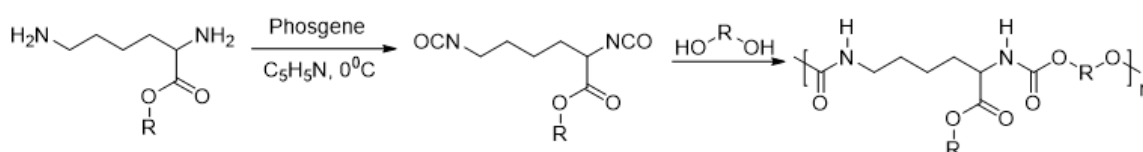
**Polycondensation route for polyurethane synthesis:** In polycondensation route the amine group was first converted into carbamate linkage by reacting with s dimethyl carbonate (DMC) or methyl chloroformate which can further undergo polycondensation or self polycondensation depending upon the nature of monomer.<sup>129</sup> Deepa et al. has synthesized different aliphatic polyurethanes from aliphatic diamines using melt polycondensation.<sup>130</sup>



**Scheme 1.7.** Polycondensation route for polyurethane synthesis via a transurethane polymerization. (Adopted from Cramail et al. *Chem. Rev.* **2015**, *115*, 12407–12439)

Other than polycondensation route other non-isocyanate routes are also known for polyurethane synthesis.<sup>129</sup>

Lysine based polyurethanes were mainly synthesised from L-lysine diisocyanate where first L-lysine was converted into diisocyanate monomer which can undergo polyaddition reaction with alcohols to give polyurethanes.<sup>131,132</sup>



**Scheme 1.8.** Lysine diisocyanate based polyurethanes (*React. Funct. Polym.* **2007**, *67*, 1338–1345)

Various medical devices, such as heart valves, catheters, and vascular grafts use polyurethane as one of the most common synthetic biomaterials. Because of their excellent biocompatibility polyurethanes have been used for tissue engineering and drug delivery applications.<sup>133,134</sup> Zhong and coworkers have reported L-lysine based biodegradable polyurethanes for drug delivery applications where L-lysine diisocyanate was reacted with a diacetal containing diol terephthalilidene-bis(trimethylolethane) to give pH responsive polyurethanes.<sup>135</sup> Same group has reported reductively biodegradable polyurethanes for intracellular drug delivery applications.<sup>136</sup>

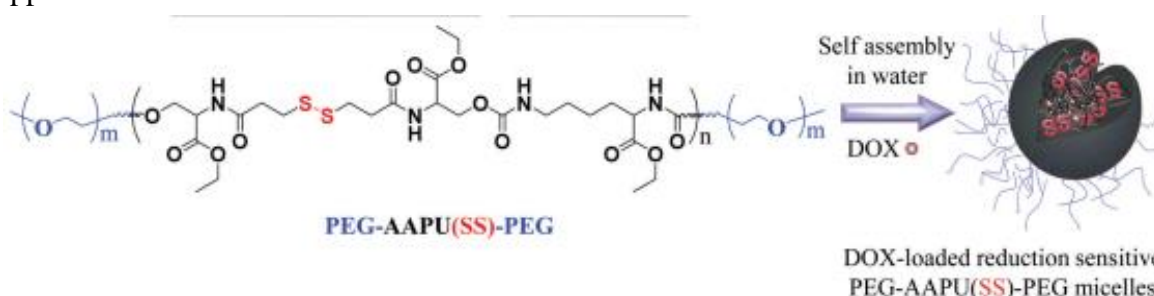


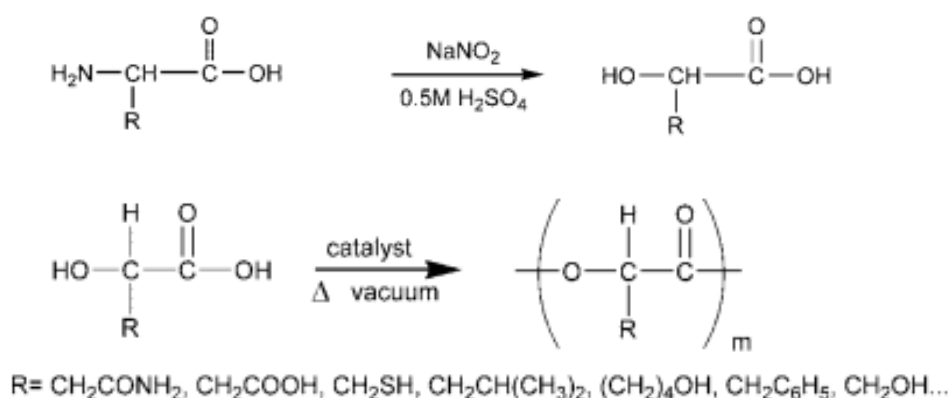
**Figure 1.18.** L-lysine based triblock copolymers for intracellular drug delivery. (adopted from *Polym. Chem.* **2015**, *6*, 6001–6010).

Kihara et al. reported L-lysine based optically active Polyhydroxy urethanes from a 5-membered cyclic carbonate and L-lysine hydrochloride. The polymerisation was carried out at 100 °C in presence of a bulky base (DBU) to obtain high molecular weight Polyhydroxy urethanes.<sup>137</sup>

**Poly ( $\alpha$ -hydroxy acids):** PAHAs (Poly( $\alpha$ -hydroxy acids)) are a class of biocompatible and biodegradable polymers that include poly(lactide), poly(glycolide), and poly(lactide-co-glycolide). Poly( $\alpha$ -hydroxy acids) (PAHAs) are biodegradable and biocompatible polymers, which have been widely used in biomedical and pharmaceutical applications, such as restorable

sutures, implantable gadgets, drug delivery, and tissue engineering. PAHAs can be readily obtained by ring-opening polymerizing of lactide (LA), glycolide (GA), and a combination of LA and GA from inexpensive, renewable sources. Various attempts have been made to develop methodologies that make it possible to prepare PAHAs for a variety of utilities.<sup>138,139</sup> The preparation of PAHAs usually involves two synthetic approaches. The polycondensation reaction of lactic acid at high temperatures and ring-opening polymerization of the dilactone of lactic acid to synthesize high molecular weight polylactide (molecular weight above 100 kDa). Several catalyst/initiator systems have been developed over the past few years for this purpose.<sup>140-142</sup> Traditional PAHAs are deficient in side-chain functionalities, preventing conjugation of actives to them or altering their physical properties through side-chain modification.

Functional polyesters are typically synthesized from  $\alpha$ -amino acids through polycondensation or ring opening polymerization. In polycondensation method the amino group of  $\alpha$ - amino acid was converted into hydroxyl by diazotization to develop polyesters.<sup>143</sup>

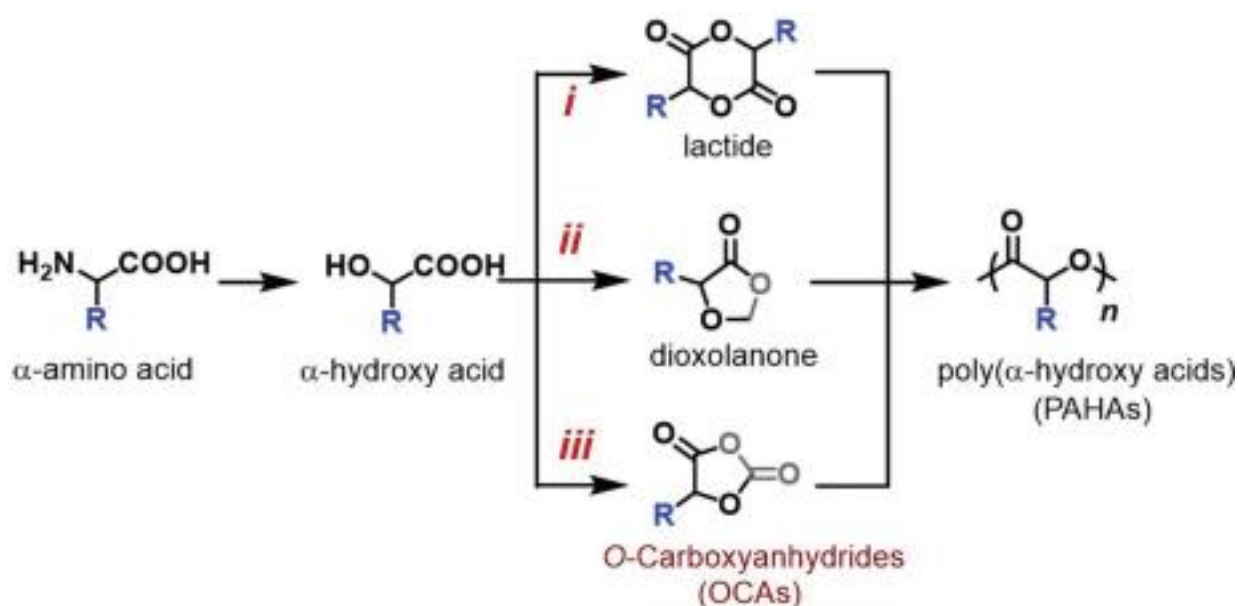


**Scheme 1.9.** Synthesis of  $\alpha$ - hydroxy acids from  $\alpha$ - amino acid and polycondensation of  $\alpha$ -hydroxy acids (Adopted from *Macromolecules* **2008**, 41, 7259.)

Direct polycondensation usually produces low molecular weight polymers with poor dispersity. Michal Kolitz and coworkers have synthesised a series polyester from hydroxy acids of the amino acids like isoleucine, leucine, phenylalanine, valine, methionine, arginine, histidine, asparagine, and glutamine using p-toluenesulfonic acid as catalyst.<sup>143</sup> Alternative strategies have been developed to synthesise PAHAs with better control and under milder reaction condition through the cyclic dimerization of  $\alpha$ -hydroxy acids, subsequent ring opening



polymerisation produces PAHAs with predictable molecular weights and precise chain structures.<sup>144</sup>



**Scheme 1.10.** Synthesis of functionalised (PAHAs) from α-hydroxy acids via ring opening polymerisation of different cyclic monomers. (Adopted from *Organic Materials* **2021**, 3, 41–50)

Typically, PAHAs are prepared from functionalized cyclic diesters (or LAs), however their multistep synthesis is challenging; monomers are obtained in low yields and their polymerization reactivity significantly decreases after pendant groups are introduced.<sup>145</sup> A series of catalyst have been developed for ring opening polymerisation of dilactide monomer.<sup>142</sup> Over the last decade, O-carboxyanhydrides (OCAs) have attracted a great deal of attention as another promising cyclic monomer. Studies have shown that LacOCA has higher reaction kinetics (ROP) than lactide because carbon dioxide molecule is released during OCA polymerization process.<sup>146</sup> Cheng et al have used ring opening polymerisation of (OCAs) to synthesise water soluble L-serine based polylactide,<sup>147</sup> redox responsive core crosslinked nanoparticles<sup>148,149</sup> for drug delivery and gene delivery applications.<sup>150</sup> Same group have reported ring opening of (OCAs) with various hydroxyl containing drugs to synthesise polymer

drug conjugates.<sup>151</sup> Block copolymer based on ring opening of (OCAs) are also known. Khuphe et al. has synthesised a pH responsive block copolymer based on lysine and glutamic acid.<sup>152</sup>

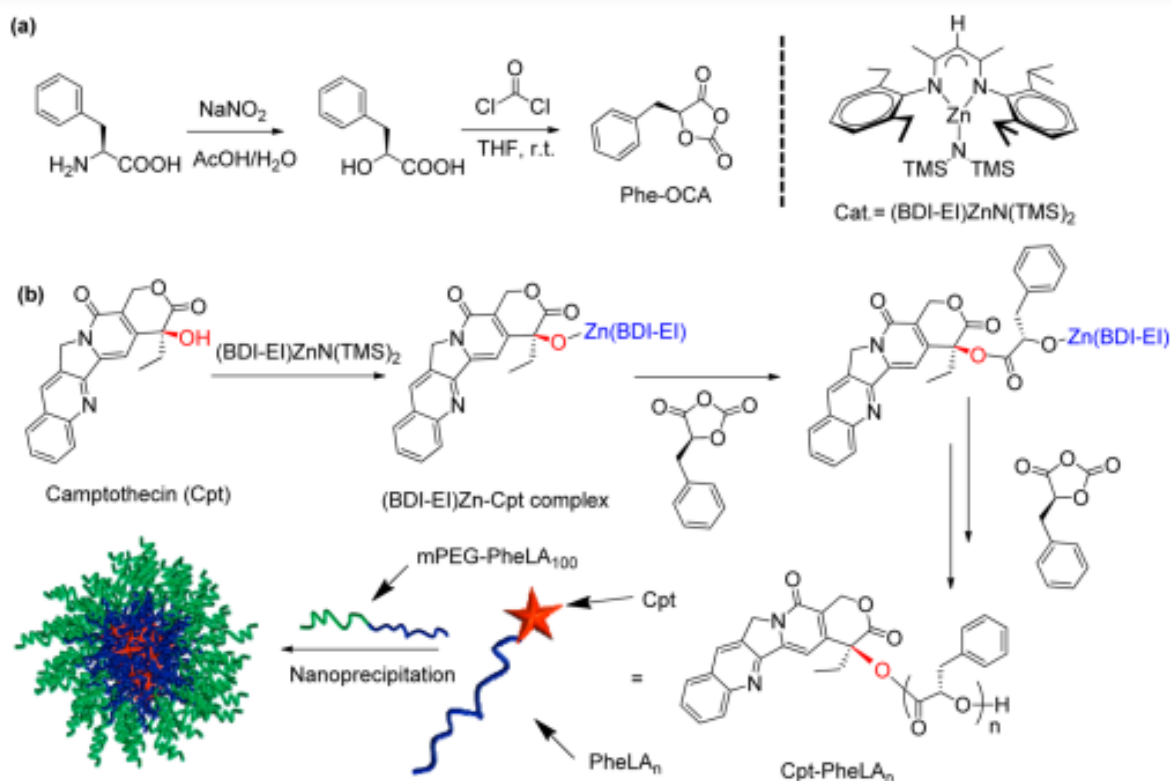


**Figure 1.19.** (a) Synthetic scheme of Phe-OCA monomer and the structure of (BDI-EI)ZnN(TMS)<sub>2</sub> catalyst. (b) Schematic illustration of (BDI-EI)ZnN(TMS)<sub>2</sub>/Cpt-mediated ROP of Phe-OCA followed by formulation of Cpt-PheLA<sub>n</sub> nanoconjugates (NCs,  $n$  = the feed ratio of Phe-OCA/ Cpt) using nanoprecipitation. (Adopted from *Biomacromolecules* **2013**, *14*, 920–929).

An ester- and acetal-containing 1,3-dioxolan-4-one heterocycle has been recently developed for ring opening polymerisation.<sup>153,154</sup> This monomer enables the preparation of PAHAs at an affordable cost through the delimitation of formaldehyde. Nevertheless, further optimization is necessary for 1,3-dioxolan-4-one ROP because the obtained polymers have low molecular weights (MWs; less than 20 kDa) as a result of side reactions; and formaldehyde has to be removed from the reaction mixture for ROP to proceed.<sup>154,155</sup>

### 1.5 Melt Polycondensation approach for L-amino acid

From our laboratory Deepa et al. has developed a non-isocyanate solvent free melt trans urethane polycondensation chemistry to synthesise aliphatic polyurethanes.<sup>130</sup> The commercially available diamines were converted into diurethane monomers which subsequently used for melt polycondensation with various diols in presence Ti catalyst to

produce high molecular weight polyurethanes. This Polycondensation approach was further extended to amino acids by Ananthraj et al. to synthesise polyester urethanes by solvent free melt polycondensation where amino acid monomers were converted into dual ester urethane monomers.<sup>156,157</sup> For this amino acid was reacted with thionyl chloride and methanol to get amino acid methyl ester hydrochloride salt which was further reacted with methyl chloroformate to get amino acid based dual ester urethane monomer. Equimolar amount of amino acid monomer and commercially available diol were subjected for two step melt polymerisation. In first step monomers were allowed to react at 150<sup>0</sup>C under nitrogen condition using 1 mol % of catalyst. In final step the oligomeric melt was subjected for high vacuum (0.01 mm of Hg) to get the polyester urethane. The polymers were further purified by precipitating in methanol to get white coloured fibrous polyester urethanes. The occurrence of polycondensation reaction was confirmed by NMR by comparing the integration of end groups with newly formed ester and urethane peaks. The reactivity of amino acid monomer was tested by varying the substitution at carbonyl carbon. The R group at carbonyl carbon was varied as methyl, ethyl, and t-butyl and it was found that as the steric hindrance at carbonyl carbon was increasing the reactivity was decreasing resulting in low molecular weight polymers.

The nature of both the carbonyl carbon is different in amino acid monomer so to check the effect of temperature on the reactivity of these carbonyl carbon polycondensation reaction was carried out at different temperature and it was found that the ester linkage was undergoing exchange reaction at 120<sup>0</sup>C while the urethane linkage was inert at this temperature. However, at 150<sup>0</sup>C both ester and carbamate bonds underwent the exchange reaction.<sup>158</sup>

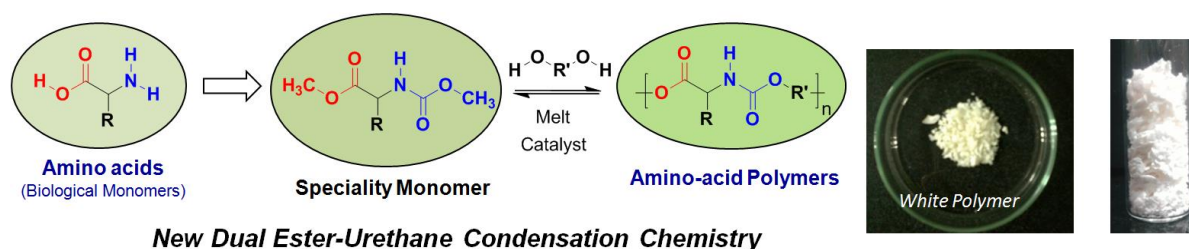


**Figure 1.20.** Schematic representation of one-pot high temperature melt condensation chemistry for amino acid based monomers. (Adopted from Anantharaj et al. *Biomacromolecules*, **2012**, *13*, 2446-2455).

The mechanism for this thermoselective reaction has been shown in figure 2. Under melt condition the hydroxyl group of R-OH reacts with Ti(OBu)<sub>4</sub> to give an active complex Ti-OR which finally attack on the carbonyl carbon via four membered transition state during the

exchange reaction. In case of urethane linkage, the lone pair on the p orbital of nitrogen atom interact more effectively with  $\pi^*$  orbital of carbonyl carbon making it less electrophilic which was further proved from DFT calculations which shows that the electron density on urethane carbonyl carbon was more compare to ester carbonyl carbon. At higher temperature due to active rotation between N-C=O bond the interaction between the filled p orbital and empty  $\pi^*$  orbital was not possible which makes it reactive and exchange reaction possible at higher temperature.<sup>158</sup>

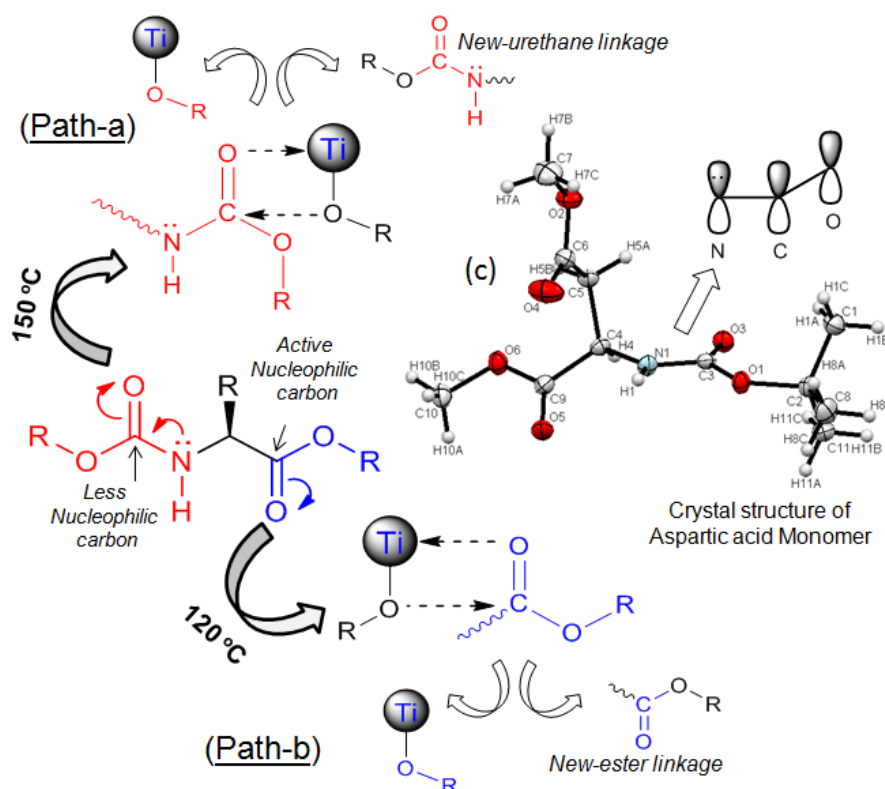


**Figure 1.21.** Mechanism of ester (a) and urethane (b) melt condensation. Single crystal structure of aspartic acid monomer (c). (adopted from Anantharaj et al. *J. Polym. Sci. Part A: Polym. Chem.* **2016**, 54, 1065-1077).

To check the effect of catalyst on polycondensation reaction a wide range of catalysts were scanned. Metal catalyst like alkali, alkali earth metal, transition metals various lanthanide chloride, nitrates oxides, alkoxides, acetates and acetylacetonate were tested and their reactivity towards ester and urethane functional group was also investigated.<sup>158</sup> To check the optical purity after polycondensation reaction polymers from L- and D-amino acids were synthesised and subjected for circular dichroism (CD) analysis. poly(ester-urethane) synthesised from L-alanine and L-valine showed a positive CD band at 217 nm and a negative band at 237 nm while, poly(ester-urethane) synthesised from D-alanine and D-valine based showed a negative

CD band at 217 nm and a positive CD band at 237 nm. The CD signals were attributed to the right and left handed  $\beta$ -sheet conformation.

Similarly, L- and D-phenyl alanine based poly (ester-urethane) were showing CD band at 230 nm with respect to right and left-handed polyproline type-II secondary structures. These results confirm that the amino acids are retaining their optical purity during the high temperature melt polycondensation.<sup>156</sup>

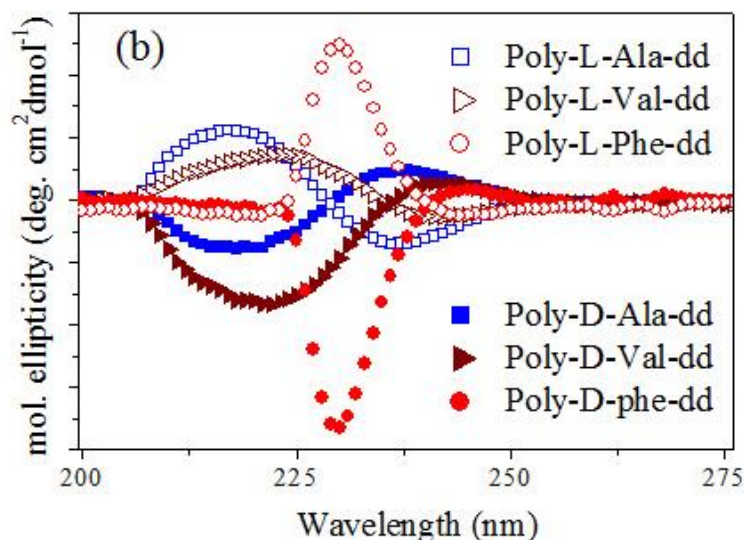
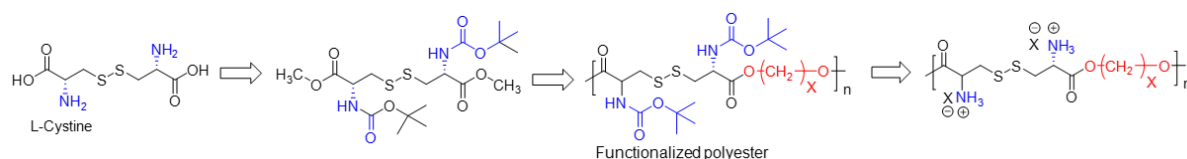


**Figure 1.22.** CD spectra of linear poly(ester-urethane)s made from D and L-amino acid monomers. (adopted from Anantharaj et al. *Biomacromolecules*, **2012**, 13, 2246-2455).

The melt polycondensation chemistry was further explored to synthesise redox responsive polyester from L-cysteine. The acid groups were converted into methyl ester and amine group was concealed as Boc urethane. The thermoselectivity between ester and urethane group was exploited to synthesise linear polyesters.



**Scheme 1.11.** Synthesis of L-cysteine based reduction responsive poly(ester urethane)s. (Adopted from Anantharaj et al. *J. Polym. Sci. A: Polym. Chem.* **2016**, 54, 2864.)

At 120<sup>0</sup>C only ester functionality underwent the exchange reaction leaving the Boc urethane unreacted to give the disulphide containing leaner polyester.<sup>159</sup> The post polymerisation deprotection of Boc urethane resulted in a cationic polymer which was getting self-assembled

in aqueous solvent to give a charged nanoparticle. To check the reduction responsiveness, the degradation studies of polymer was carried out in presence of DTT. The aliquots were collected at different time interval and subjected for GPC and NMR analysis. The GPC and NMR analysis showed that the disulphide bond in polymer was completely chopped out to give the monomeric units.

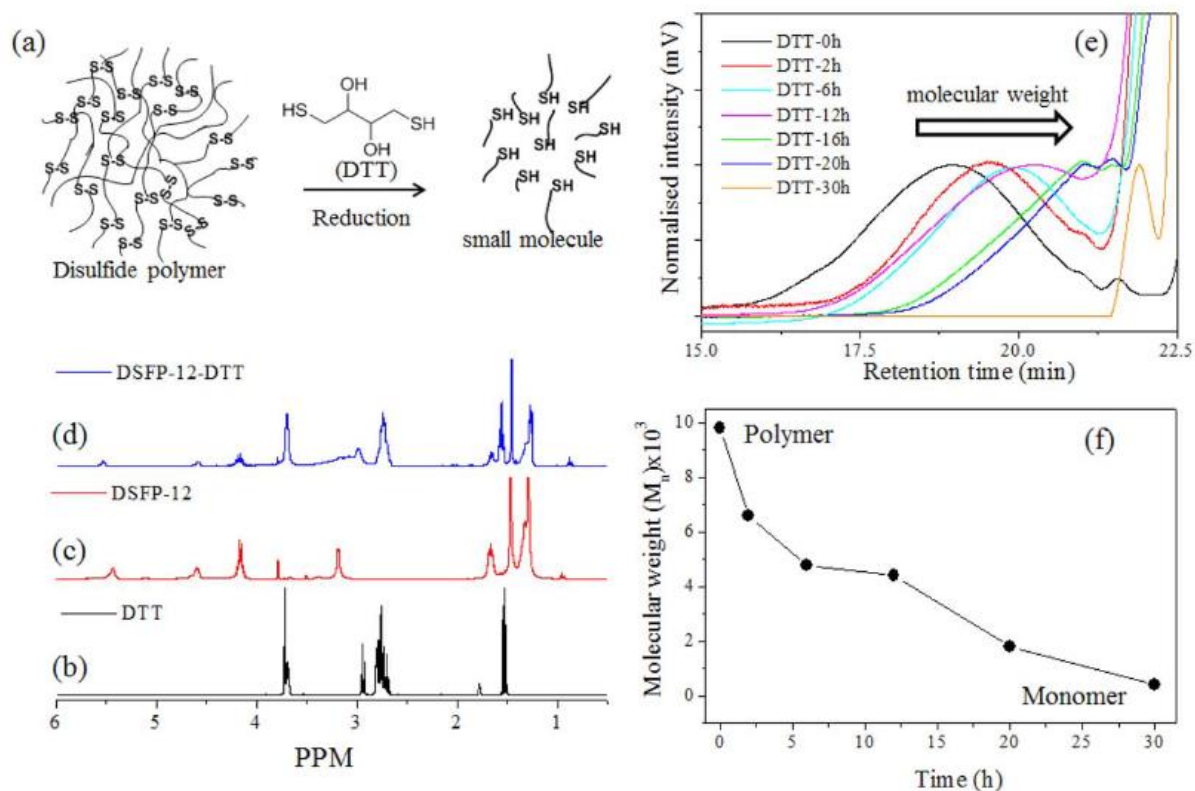


**Figure 1.23.** Representation of disulphide polymer degradation by DTT (a). <sup>1</sup>H NMR stack plot for DTT (b), disulphide polymer (c), and DTT degraded disulphide polymer (d). GPC chromatograms of degradation product aliquots (e). Plot of  $M_n$  versus degradation reaction time (f). (Adopted from Anantharaj et al. *J. Polym. Sci. A: Polym. Chem.* **2016**, 54, 2864.)

The melt polycondensation was translated into multifunction amino acids like D and L-Serin, L-Threonine and L-tyrosine by Dr. Rajendra to synthesise various linear and hyperbranched polyester and polyesterurethanes.<sup>160</sup> The reactivity difference between ester and urethane group was exploited to synthesise linear and hyperbranched polymers from serine and threonine in single pot. Serin and threonine was converted into ABB' type ester urethane monomer (where A = hydroxy group, B = ester group and B' = urethane group) and subjected for melt polymerisation at 120°C so that only ester group could react with -OH group to give linear polyesters. Upon increasing the temperature there was no reactivity difference between ester and urethane group so it gives the hyperbranched polyester urethanes. The secondary structure

and their morphological features were investigated by circular dichroism spectroscopy and electron and atomic microscopy. Interestingly, these linear and hyperbranched polymers were showing different confirmation and morphologies. The linear polyesters synthesised from L and D-serine adopted a  $\beta$ -sheet conformation and showed a helical nano-fibrous morphology while the hyperbranched polymers underwent a globular coil-like conformation to give spherical nano-particular assemblies.

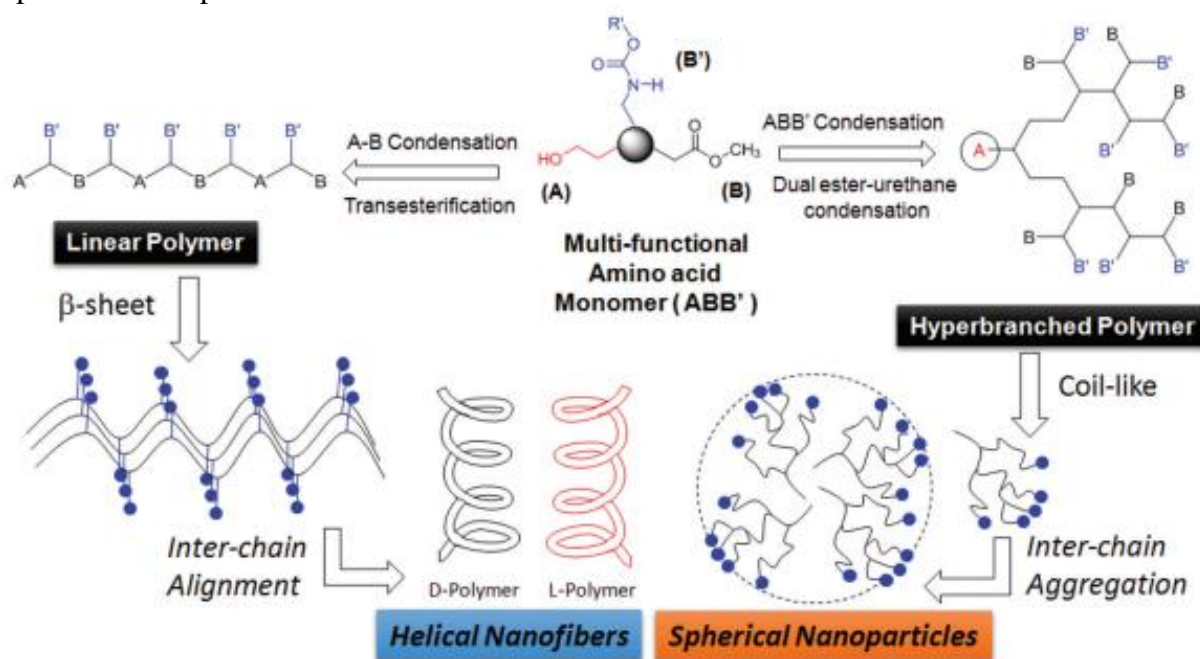


**Figure 1.24.** Thermoselective polycondensation approach for the synthesis of linear and hyperbranched polymers from L-amino acids and their self-assembled nano-structures. (adopted from Rajendra et al. *polym. Chem.* **2015**, 6, 4641- 4649.)

Two different classes of Biodegradable amphiphilic polymers were synthesised using L-tyrosine as shown in figure 1.25.<sup>161,162</sup>

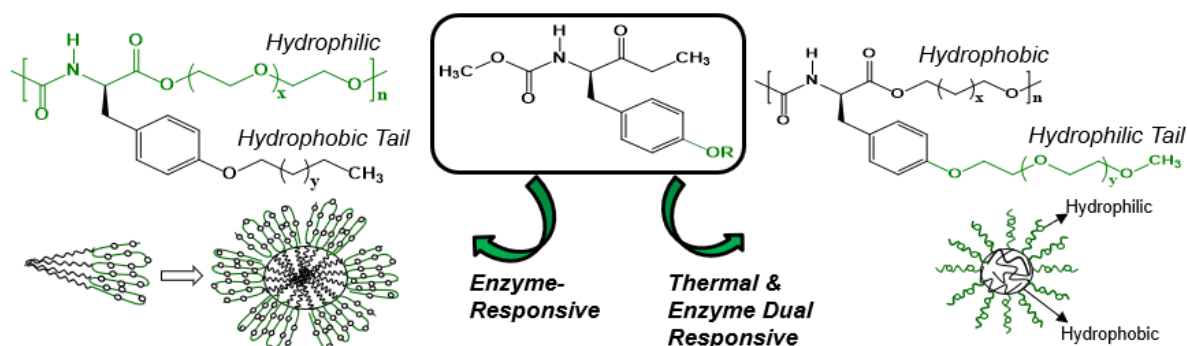
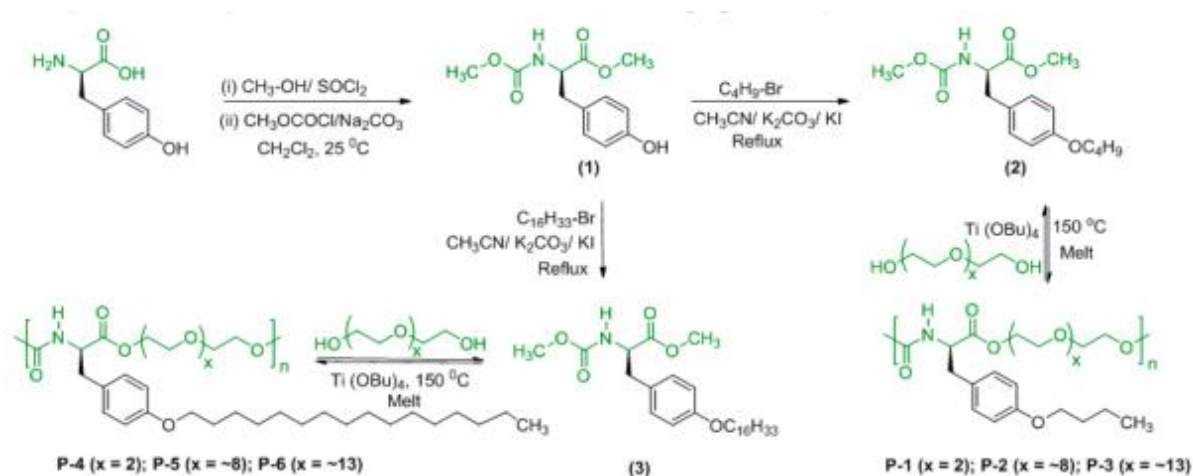


**Figure 1.25.** Development of two different types of amphiphilic polyester urethane nanocarrier for drug delivery applications in cancer cells.

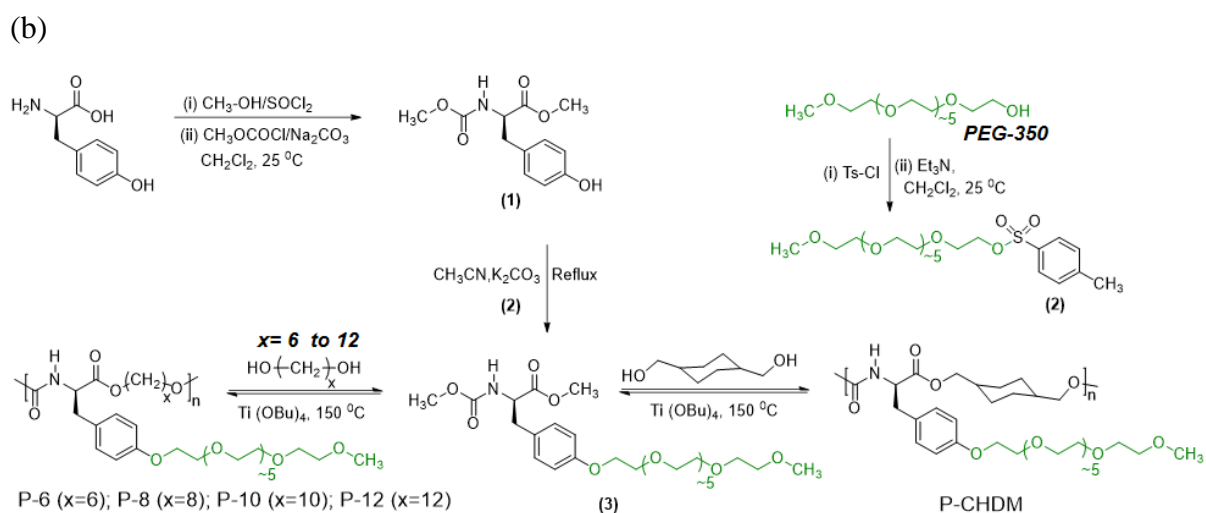
(i) L- tyrosine based Enzyme responsive amphiphilic Poly(ester-urethane) nanocarriers were designed and developed for multiple Drug Delivery to cancer cells. For that Phenolic –OH group of L-tyrosine ester urethane monomer was coupled with different chain length alkyl halides and these monomers was polymerised with polyethylene glycol diols (PEG 400, PEG 600) to get L-tyrosine based amphiphilic polyester urethanes in which the aliphatic side chain was acting as hydrophobic unit and main chain polyethylene glycol was acting as hydrophilic unit. The synthetic design for monomer and polymer synthesis is shown in scheme 1.12.a. Depending upon the length of alkyl chain the polymer having C16 alkyl side chain and PEG 400 in main chain was showing proper amphiphilicity and getting self-assembled aqueous solvent to give a core shell type of nanoparticle having size around 200 nm.

(ii) In second case multiple-responsive amphiphilic poly(ester-urethane) nanoassemblies were designed for Drug Delivery applications in Cancer Cells. The phenolic –OH group of L-tyrosine polyester urethane was anchored with PEG 350 monomethyl ether and polymerised with various aliphatic and cyclic aliphatic diols to get different polymers. Diols varying from 1,4- cyclohexanedimethanol 1,6 hexane diol, 1,8 octane diol, 1,10 decan diol, and 1,12 dodecanediol were used for polycondensation reaction to optimise the hydrophilic and hydrophobic balance as shown in scheme 1.12.b. It was observed that polymer synthesised from 1,12 dodecan diol was giving proper amphiphilicity and showing thermoresponsive behaviour at a concentration of 3 mg/ml. To check the lower solution critical temperature (LCST) transmittance studies was carried out and it was found the LCST temperature of polymer was varying from 32 °C- 50 °C depending upon the length of diol.

(a)







**Scheme 1.12.** Synthesis of *L*-tyrosine based monomers and polymers.

The *L*-tyrosine based multistimuli responsive nanocarriers were designed by optimising proper amphiphilicity. The newly designed Poly(ester urethane)s self-assembled in aqueous solvent to form nanoparticles of 200 nm size which were able to load two different anticancer drugs, doxorubicin and camptothicine. The thermoresponsive behaviour of these nanoparticles was examined by conducting variable temperature transmittance studies which revealed that the aqueous solutions of polymers were changing from transparent to turbid solutions at LCST = 40–42 °C as showed in figure 1.26.

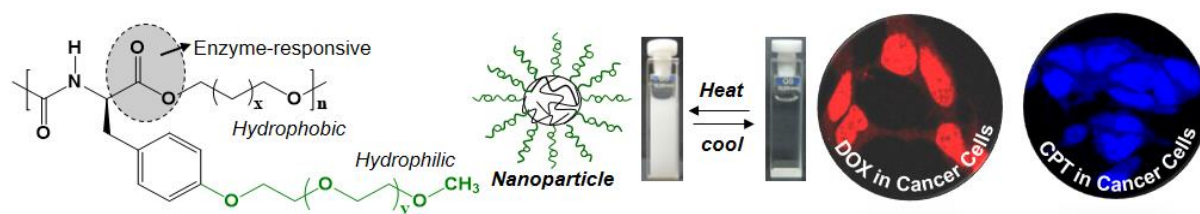


**Figure 1.26.** *L*-tyrosine based multistimuli responsive poly(ester urethane)s for drug delivery applications in cancer cells.

The thermoresponsive release behaviour of drug-loaded nanoparticles was investigated at two different temperatures, 37<sup>0</sup>C (physiological temperature) and 42<sup>0</sup>C (near to cancer tissue temperature). The drug release profile revealed that nanocarriers were stable at physiological temperature and showing a control drug release at 42<sup>0</sup>C. Further, the cellular uptake of nanoparticles was confirmed by confocal laser scanning microscopy and flow cytometry test which revealed the higher uptake of drug loaded nanocarriers compare to free drug. The cytotoxicity tests were performed in healthy wild-type mouse embryonic fibroblast (WT-MEF) cell line, (MCF7) breast cancer cell line, and (HeLa) cervical cancer cell line and result showed that nanocarriers were showing potent cytotoxicity effect.<sup>162</sup>

Recently, Sonashree et al. has developed enzyme and pH responsive polyester nanocarriers from L- aspartic acid using melt polycondensation chemistry. L-aspartic acid was transformed into multifunctional monomer by converting acid and amine groups into methyl ester and Boc urethane respectively. The multifunctional monomer was subjected for themoselective copolymerisation with triethylene glycol and dodecan diol to synthesise a series of amphiphilic copolymers.<sup>163</sup> These amphiphilic polymers were forming a core shell type nanoparticle in aqueous solvent and capable of loading multiple anticancer drugs like Topotecan, Doxorubicin and Curcumin. The enzymatic and pH biodegradability of these polymer nanoparticles was facilitated by their polyester backbone and BOC urethane pendant. Further polymer nanoparticles were examined for their cellular uptake and cytotoxicity test in cervical cancer cell lines (HeLa) and breast cancer cell lines (MCF-7) and the results showed that they could deliver the drugs into intracellular environment and exhibited potent cytotoxicity.

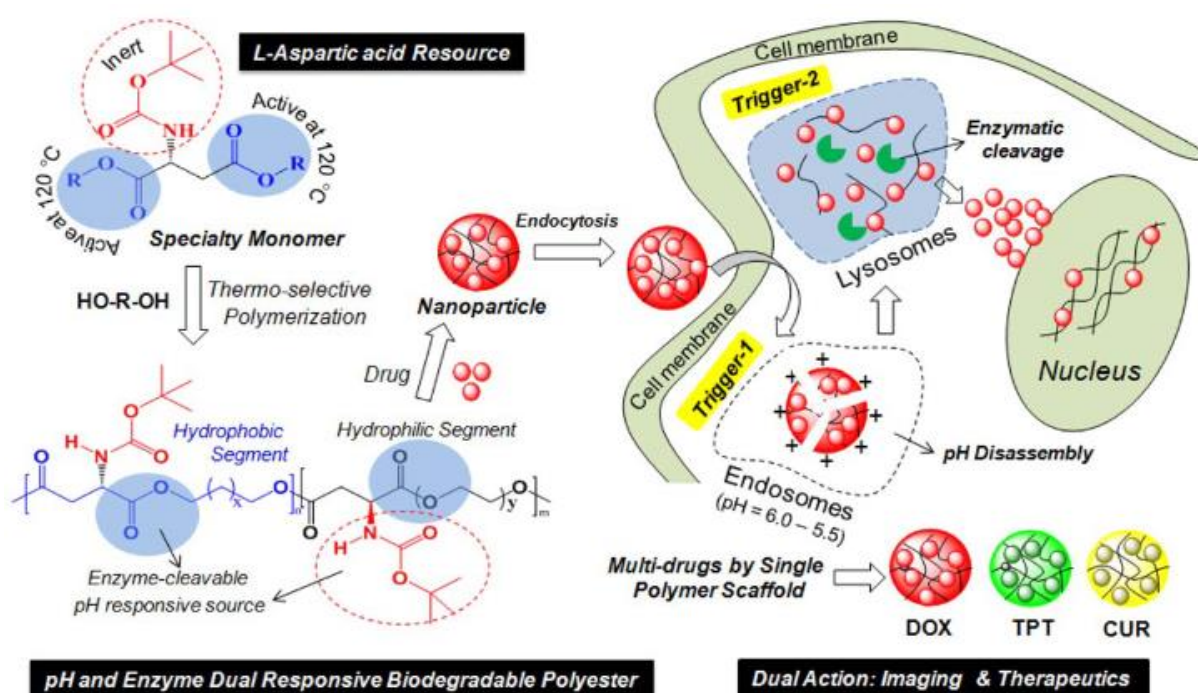


**Figure 1.27.** Schematic representation of pH and enzyme responsive polymer nano-assemblies from L-aspartic acid (adopted from Sonashree et al. *J. Polym. Sci. Part A: Polym. Chem.* **2016**, *54*, 3279-3296)

Hydroxyl functionalised polyesters were synthesized using L-aspartic acid, a novel L-aspartic acid based multifunctional monomer was synthesized with an acetal protecting group and dicarboxylic esters. Aspartic acid monomer underwent transesterification with various aliphatic commercial diols to give acetal-functionalized polyesters under the melt condition.

The acid catalysed deprotection of acetal polymer gave a hydroxyl polymer having a bishydroxy functionality in each repeating unit.<sup>164</sup> These polymers were amphiphilic in nature because both the hydrophilic hydroxyl groups in side chain and hydrophobic aliphatic backbones allowed them to self-assemble into spherical nanoparticles in water. Hydroxyl functionalized polyester nanoparticles were encapsulated with various hydrophilic and hydrophobic anticancer drugs such as doxorubicin (DOX), camptothecin (CPT), and curcumin (CUR), as well as fluorophores such as Nile red (NR), Rose Bengal (RB), and Congo red (CR). The luminescent nature of fluorophore loaded nanoparticle was used for colour tuneable bio imaging in cancer cells. The cellular uptake and biodegradation of these nanoparticle was confirmed by Live cell imaging. *in vitro* cytotoxicity tests of these nascent polymers showed no cytotoxicity, while their anticancer drug-loaded nanoparticles showed excellent killing of cervical cancer (HeLa) cells in.

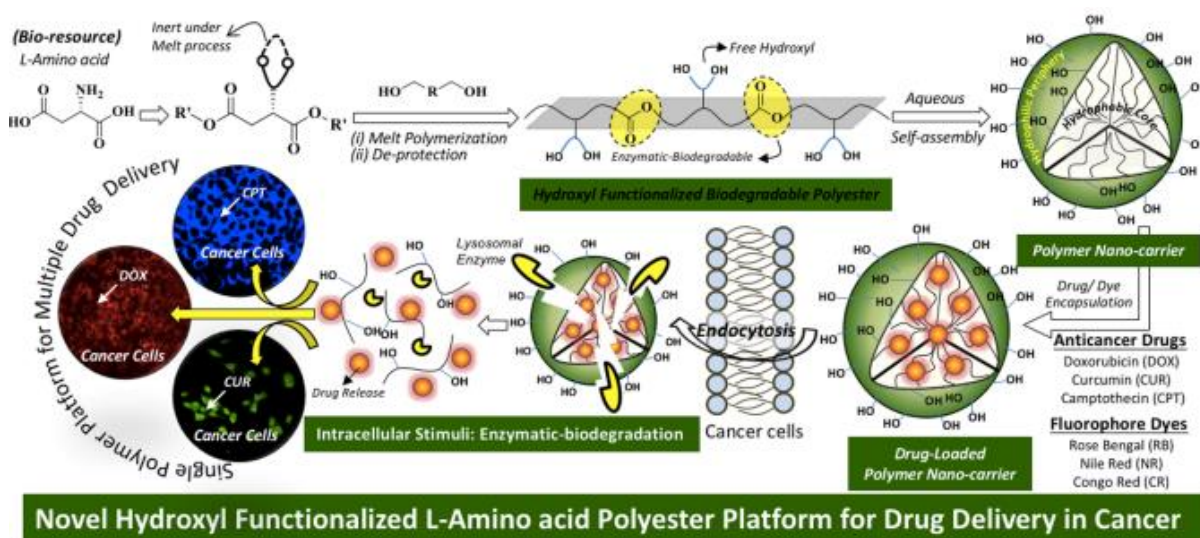


**Figure 1.28.** Schematic representation of novel hydroxyl functionalized L-aspartic acid based enzyme responsive polymer nanoassemblies for anticancer drug delivery. (Adopted from Sonashree et al. *Biomacromolecules* **2020**, *21*, 171–187)

Subsequently, L-aspartic acid polymer nanoassemblies were used to create two types of enzyme-degradable fluorescence resonance energy transfer (FRET) probes and these nanoassemblies were used for anticancer drug delivery and bioimaging purpose in cancer cells. The FRET probes were designed by chemical conjugation or physical encapsulation of suitable fluorophore molecules. In first case the L-aspartic acid based monomer was copolymerised with triethylene glycol, dodecane diol and oligo-phenylenevinylene (OPV) diol via melt polymerisation to get a fluorophore tagged amphiphilic polymer. The amphiphilic polymer

underwent a  $\pi$ - $\pi$  stacking assisted self-assembly in aqueous solvent to give a 200 nm size blue luminescent nanoparticles. A fluorescent drug nile red was physically encapsulated in these OPV tagged nanoparticle to get a FRET pair in which OPV fluorophore was serving as a FRET donor and nile red was serving as a FRET acceptor.<sup>165</sup>

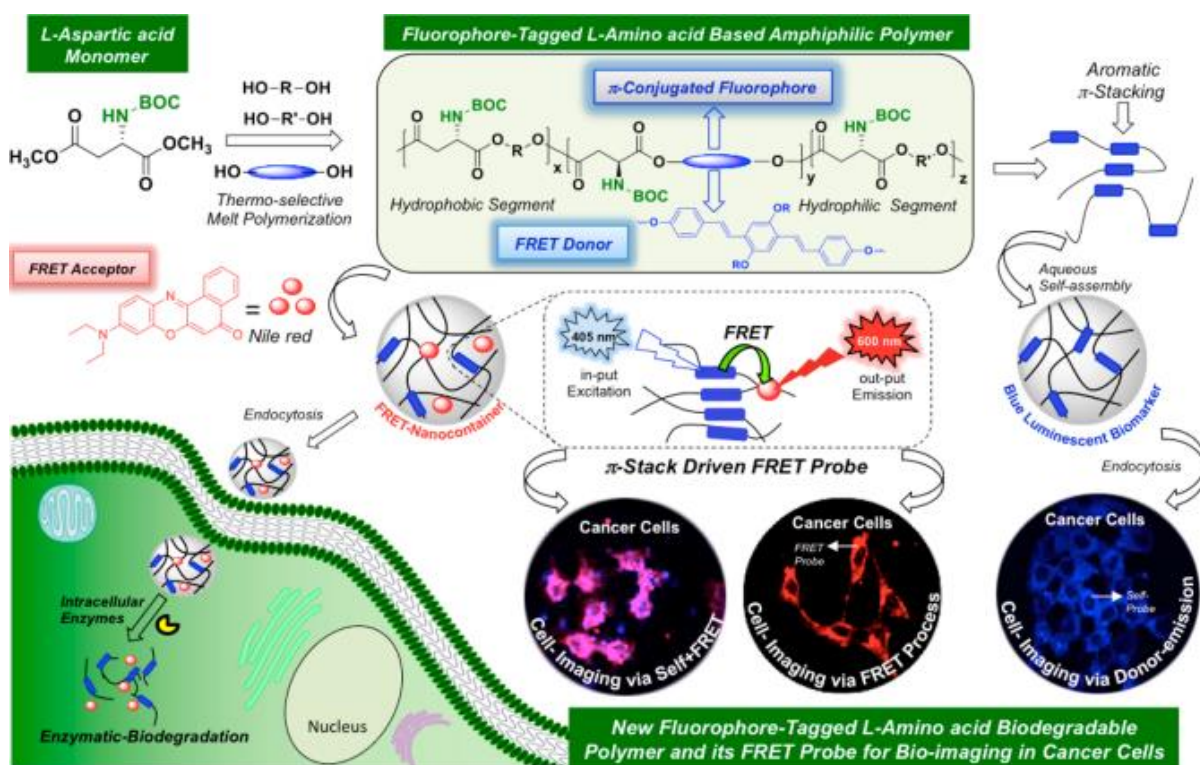
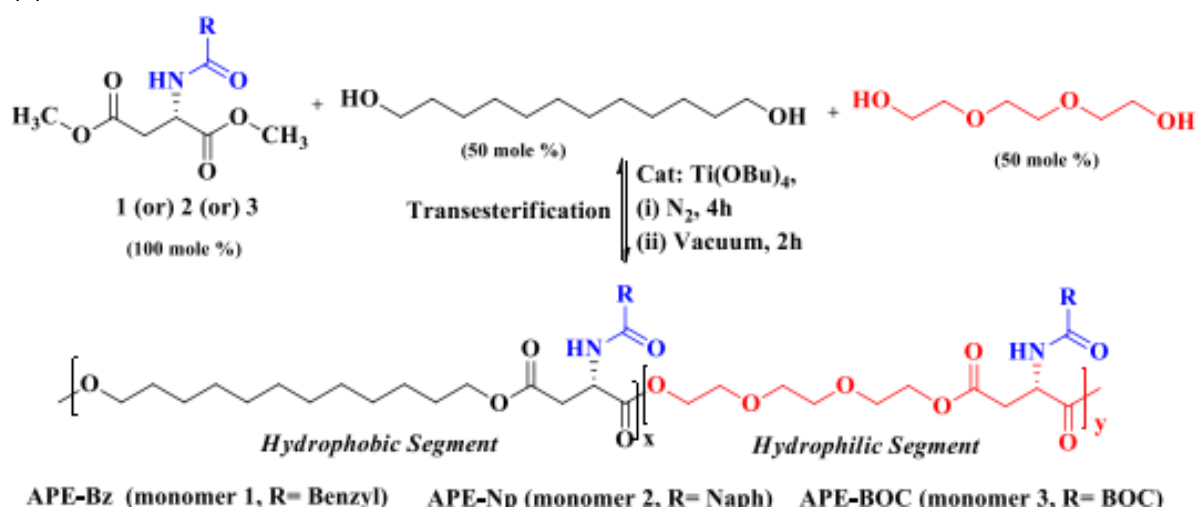


**Figure 1.29.** Enzyme-responsive  $\pi$ -conjugated fluorophore-tagged L-aspartic acid polyester and its FRET probe for bioimaging at the intracellular level. (Adopted from Sonashree et al. *Biomacromolecules* **2017**, 18, 2594–2609)

A detailed in vitro photophysical study was carried out to study the FRET phenomenon between OPV and nile red and FRET overlap integral between donor (OPV) and acceptor (nile red) was estimated more than 75 %. The FRET phenomenon was further used for cellular imaging in breast cancer (MCF 7) and cervical cancer (HeLa) cell lines. The cells were incubated with these nanoparticles for four hours and selectively excited at 405 nm corresponding to OPV excitation which results a strong emission from OPV (blue channel) and nile red (red channel) confirming the FRET phenomenon at cellular level. The enzymatic biodegradation of these nanoparticle was monitored by the effect of different enzymes on the FRET process of these nanoparticle. The polymer nanoparticles were incubated with four different enzymes, esterase, chymotrypsin, trypsin, and a time dependent study was carried out to monitor the FRET process and it was observed that the self-emission from OPV and FRET

emission from Nile red was decreased with time which confirms the biodegradation of these nanoparticle by the effect of these enzymes.<sup>165</sup>

(a)



**Scheme** Synthesis of L-aspartic acid based biodegradable polymers via melt polycondensation.

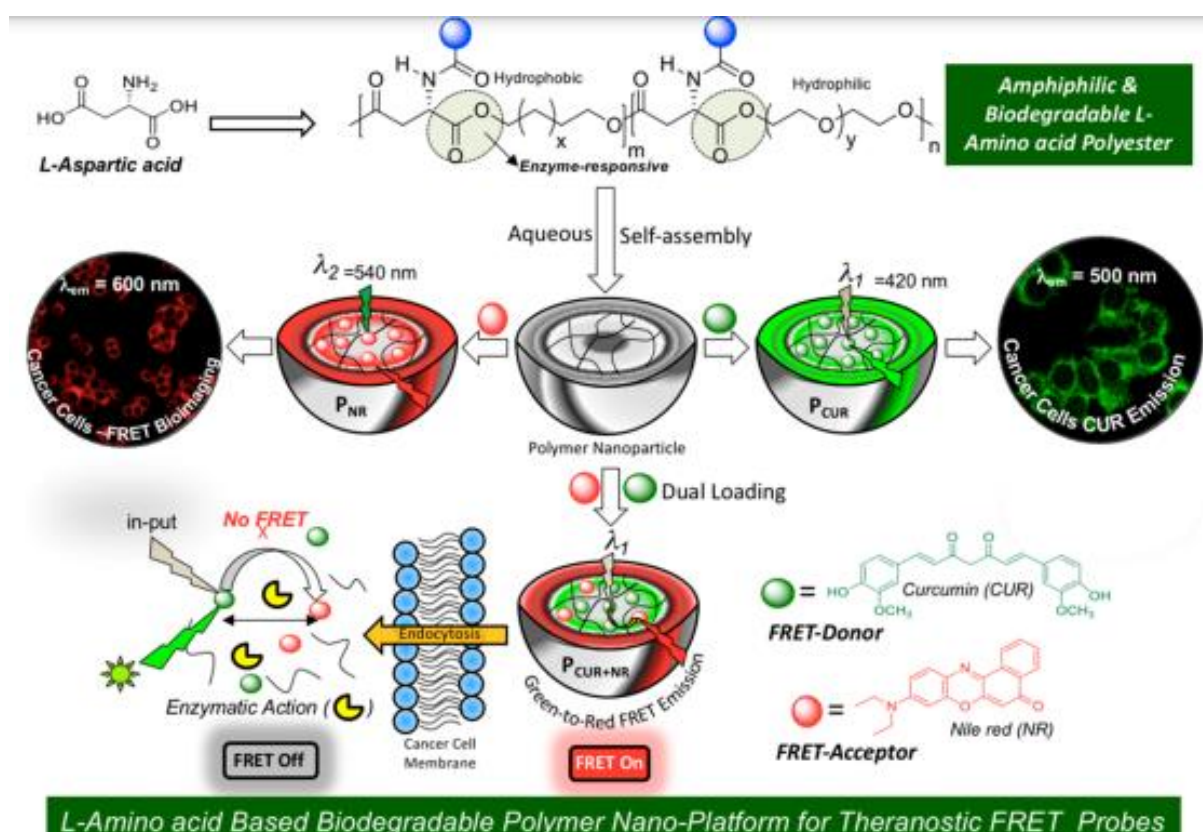


**Figure 1.30.** FRET bioimaging probes based on L-aspartic acid based biodegradable polyester nanoassemblies for cancer cells on the basis of a curcumin drug donor and Nile red acceptor. (Adopted from Sonashree et al. *ACS Appl. Bio Mater.* **2019**, 2, 5245–5262)

A FRET pair (curcumin and nile red) was physically encapsulated into L-aspartic acid based polyesters to design a theranostic FRET probe. The amine group of L-aspartic acid diester was covalently attached with three different pendent to synthesise (benzoyl and naphthoyl) amide and BOC urethane monomers. All three monomers were copolymerised with dodecanediol and triethylene glycol to synthesize a series of polyesters. The polyester having Boc as a pendent group was found to have proper amphiphilicity for the encapsulation of curcumin and nile red. The FRET between curcumin and nile red was successfully demonstrated at cellular level and dual loaded nanoparticles were studied for their theranostic applications in MCF7 cells.<sup>166</sup>

## **1.6 Aim of Thesis**

From previous discussion it is clear that L-amino acid based nano-assemblies are emerging as a potential candidate in the biomedical field. L-Amino acid based synthetic polypeptides and their well-defined di- and tri-block copolymers were extensively explored for the above applications. In the last one decade, significant effort has been taken to design non-peptide polymer analogues for biomedical application owing to their structural diversity, biocompatibility and biodegradability. The aim of this thesis work is development of a green synthetic route for the synthesis of L-amino acid-based polyurethanes and poly ester-urethanes for drug delivery applications in cancer cells. The second chapter describes the synthesis of L-Lysine based dual responsive polyurethane nanocarriers by non-isocyanate route using solvent free melt polycondensation. In chapter 3 the aromatic amino acids (L-Tyrosine and L-DOPA) resources were suitably modified with masked-monomer approach and subjected for melt polymerization with various aliphatic diols to make new classes of enzyme-responsive poly(ester-urethane)s. The aromatic electron rich nature of polymeric backbone was designed to promote the encapsulation of electron deficient drug molecules by aromatic pi-pi stacking interactions. Further moving one step ahead completely biobased polymers was derived by combining to most abundant natural resources i.e sugar and amino acids. The naturally abundant D- mannitol was modified into diol using multistep organic reactions and detailed analysis was done to study the structural and thermal properties. The sugar diol was used for the melt polycondensation with different amino acid based monomers to give poly(ester urethane)s.

## References

- (1) Ringsdorf, H. *j. polym. sci. polym. symp* **2007**, *51*, 135.
- (2) Matsumura, Y.; Maeda, H. *Cancer Res.* **1986**, *46*, 6387.
- (3) Fang, J.; Nakamura, H.; Maeda, H. *Adv Drug Deliv Rev.* **2011**, *63*, 136.
- (4) Maeda, H.; Nakamura, H.; Fang, J. *Adv. Drug Deliv. Rev.* **2013**, *65*, 71.
- (5) Nakamura, Y.; Mochida, A.; Choyke, P. L.; Kobayashi, H. *Bioconjugate Chem.* **2016**, *27*, 2225.
- (6) Maeda, H. *Bioconjug Chem.* **2010**, *21*, 797.
- (7) Haag, R.; Kratz, F. *Angew. Chem. Int. Ed.* **2006**, *45*, 1198.
- (8) Stylianopoulos, T. *Ther. Deliv.* **2013**, *4*, 421.
- (9) Ma, N.; Ma, C.; Li, C.; Wang, T.; Tang, Y.; Wang, H.; Moul, X.; Chen, Z.; Hel, N. *J. Nanosci. Nanotechnol.* **2013**, *13*, 6485.
- (10) Gratton, S. E.; Ropp, P. A.; Pohlhaus, P. D.; Luft, J. C.; Madden, V. J.; Napier, M. E.; DeSimone, J. M. *Proc Natl Acad Sci U S A.*, **2008**, *105*, 11613.
- (11) Mahmoud, K. A.; Mena, J. A.; Male, K. B.; Hrapovic, S.; Kamen, A.; Luong, J. H. T. *Appl. Mater. Interfaces* **2010**, *2*, 2924.
- (12) Fröhlich, E. *Int. J. Nanomedicine* **2012**, *7*, 5577.
- (13) Dong, H.; Pang, L.; Cong, H.; Shen, Y.; Yu, B. *Drug Deliv.* **2019**, *26*, 416.
- (14) Wang, J.; Mao, W.; Lock, L. L.; Tang, J.; Sui, M.; Sun, W.; Cui, H.; Xu, D.; Shen, Y. *ACS Nano* **2015**, *9*, 7195.
- (15) Liu, J.; Xu, L.; Liu, C.; Zhang, D.; Wang, S.; Deng, Z.; Lou, W.; Xu, H.; Bai, Q.; Ma, J. *Carbohydr. Polym.* **2012**, *90*, 16.
- (16) Göppert, T. M.; Müller, R. H. *Int J Pharm.* **2005**, *302*, 172.
- (17) Suk, J. S.; Xu, Q.; Kim, N.; Hanes, J.; Ensign, L. M. *Adv. Drug Deliv. Rev.* **2016**, *99*, 28.
- (18) Dai, Q.; Walkey, C.; Chan, W. *Angew. Chem. Int. Ed.* **2014**, *53*.
- (19) Pelaz, B.; del Pino, P.; Maffre, P.; Hartmann, R.; Gallego, M.; Rivera-Fernández, S.; de la Fuente, J. M.; Nienhaus, G. U.; Parak, W. J. *ACS Nano* **2015**, *9*, 6996.
- (20) Xu, Q.; Ensign, L. M.; Boylan, N. J.; Schön, A.; Gong, X.; Yang, J.-C.; Lamb, N. W.; Cai, S.; Yu, T.; Freire, E.; Hanes, J. *ACS Nano* **2015**, *9*, 9217.
- (21) Kolhar, P.; Anselmo, A.; Gupta, V.; Pant, K.; Prabhakarandian, B.; Ruoslahti, E.; Mitragotri, S. *Proc. Natl. Acad. Sci. U.S.A.* **2013**, *110*.

- (22) Karagoz, B.; Esser, L.; Duong, H. T.; Basuki, J. S.; Boyer, C.; Davis, T. P. *Polym. Chem.*, **2014**, *5*, 350.
- (23) Niikura, K.; Matsunaga, T.; Suzuki, T.; Kobayashi, S.; Yamaguchi, H.; Orba, Y.; Kawaguchi, A.; Hasegawa, H.; Kajino, K.; Ninomiya, T.; Ijio, K.; Sawa, H. *ACS Nano* **2013**, *7*, 3926.
- (24) Davis, M. E.; Chen, Z.; Shin, D. M. *Nat. Rev. Drug Discov.* **2008**, *7*, 771.
- (25) Kumar Khanna, V. *ISRN Pharmacol.* **2012**, *2012*, 571394.
- (26) Zhen, Z.; Tang, W.; Chen, H.; Lin, X.; Todd, T.; Wang, G.; Cowger, T.; Chen, X.; Xie, J. *ACS Nano* **2013**, *7*, 4830.
- (27) Weitman, S. D.; Weinberg, A. G.; Coney, L. R.; Zurawski, V. R.; Jennings, D. S.; Kamen, B. A. *Cancer Res.* **1992**, *52*, 6708.
- (28) Elnakat, H.; Ratnam, M. *Adv. Drug Deliv. Rev.* **2004**, *56*, 1067.
- (29) Phan, L. M.; Yeung, S.-C. J.; Lee, M.-H. *Cancer Biol. Med.* **2014**, *11*, 1.
- (30) Irache, J. M.; Salman, H. H.; Gamazo, C.; Espuelas, S. *Expert Opin Drug Deliv.* **2008**, *5*, 703.
- (31) Toma, C. C.; Aloisi, A.; Bordoni, V.; Di Corato, R.; Rauner, M.; Cuniberti, G.; Delogu, L. G.; Rinaldi, R. *Biomacromolecules* **2018**, *19*, 3560.
- (32) Jeena, M. T.; Palanikumar, L.; Go, E. M.; Kim, I.; Kang, M. G.; Lee, S.; Park, S.; Choi, H.; Kim, C.; Jin, S.-M.; Bae, S. C.; Rhee, H. W.; Lee, E.; Kwak, S. K.; Ryu, J.-H. *Nat. Commun.* **2017**, *8*, 26.
- (33) Chen, W.; Zhang, A.; Li, S.-D. *Eur. J. Nanomed.* **2012**, *4*.
- (34) Prajapati, S. K.; Jain, A.; Jain, A.; Jain, S. *Eur. Polym. J.* **2019**, *120*, 109191.
- (35) Tibbitt, M. W.; Dahlman, J. E.; Langer, R. *J. Am. Chem. Soc.* **2016**, *138*, 704.
- (36) Kirillova, A.; Yeazel, T. R.; Asheghali, D.; Petersen, S. R.; Dort, S.; Gall, K.; Becker, M. L. *Chem. Rev.* **2021**, *121*, 11238.
- (37) Makadia, H. K.; Siegel, S. J. *Polymers* **2011**, *3*, 1377.
- (38) Karavelidis, V.; Karavas, E.; Giliopoulos, D.; Papadimitriou, S.; Bikiaris, D. *International journal of nanomedicine* **2011**, *6*, 3021.
- (39) Zilberman, M. *Acta Biomater.* **2005**, *1*, 615.
- (40) Steendam, R.; van Steenberg, M. J.; Hennink, W. E.; Frijlink, H. W.; Lerk, C. F. *J. Control. Release* **2001**, *70*, 71.
- (41) Lu, L.; Peter, S. J.; Lyman, M. D.; Lai, H. L.; Leite, S. M.; Tamada, J. A.; Uyama, S.; Vacanti, J. P.; Langer, R.; Mikos, A. G. *Biomaterials* **2000**, *21*, 1837.
- (42) Langer, R. S.; Peppas, N. A. *Biomaterials* **1981**, *2*, 201.



- (43) Liyanage, A. D. T.; Chen, A. J.; Puleo, D. A. *ACS Biomater. Sci. Eng.* **2018**, *4*, 4193.
- (44) Jeong, J. C.; Lee, J.; Cho, K. *Journal of controlled release : official journal of the Controlled Release Society* **2003**, *92*, 249.
- (45) Liechty, W. B.; Kryscio, D. R.; Slaughter, B. V.; Peppas, N. A. *Annu. Rev. Chem. Biomol. Eng.* **2010**, *1*, 149.
- (46) Braunecker, J.; Baba, M.; Milroy, G. E.; Cameron, R. E. *Int. J. Pharm.* **2004**, *282*, 19.
- (47) Yao, K.; Tang, C. *Macromolecules* **2013**, *46*, 1689.
- (48) Zhu, Y.; Romain, C.; Williams, C. K. *Nature* **2016**, *540*, 354.
- (49) Wang, Z.; Ganewatta, M. S.; Tang, C. *Prog. Polym. Sci.* **2020**, *101*, 101197.
- (50) Vilela, C.; Sousa, A. F.; Fonseca, A. C.; Serra, A. C.; Coelho, J. F. J.; Freire, C. S. R.; Silvestre, A. J. D. *Polym. Chem.* **2014**, *5*, 3119.
- (51) Göpferich, A. *Biomaterials* **1996**, *17*, 103.
- (52) García-Martín, M. G.; Hernández, E. B.; Pérez, R. R.; Galbis, J. A. *Polym. Degrad. Stab.* **2008**, *93*, 1370.
- (53) Wu, J.; Eduard, P.; Thiyagarajan, S.; Jasinska-Walc, L.; Rozanski, A.; Guerra, C. F.; Noordover, B. A. J.; van Haveren, J.; van Es, D. S.; Koning, C. E. *Macromolecules* **2012**, *45*, 5069.
- (54) Galbis, J. A.; García-Martín, M. d. G.; de Paz, M. V.; Galbis, E. *Chem. Rev.* **2016**, *116*, 1600.
- (55) Gregory, G. L.; Jenisch, L. M.; Charles, B.; Kociok-Köhn, G.; Buchard, A. *Macromolecules* **2016**, *49*, 7165.
- (56) Lavilla, C.; Muñoz-Guerra, S. *Green Chem.* **2013**, *15*, 144.
- (57) Zakharova, E.; Martínez de Ilarduya, A.; León, S.; Muñoz-Guerra, S. *Des. Monomers Polym.* **2017**, *20*, 157.
- (58) Zamora, F.; Bueno, M.; Molina, I.; Iribarren, J. I.; Muñoz-Guerra, S.; Galbis, J. A. *Macromolecules* **2000**, *33*, 2030.
- (59) de Paz, M. V.; Zamora, F.; Begines, B.; Ferris, C.; Galbis, J. A. *Biomacromolecules* **2010**, *11*, 269.
- (60) Mancera, M.; Roffe, I.; Al-Kass, S. S. J.; Rivas, M.; Muñoz, S. *Macromolecules* **2003**, *36*, 1089.
- (61) Gustini, L.; Lavilla, C.; de Ilarduya, A. M.; Muñoz-Guerra, S.; Koning, C. E. *Biomacromolecules* **2016**, *17*, 3404.
- (62) Wu, J.; Eduard, P.; Jasinska, L.; Rozanski, A.; Noordover, B.; Van Es, D.; Koning, C. *Macromolecules* **2013**, *46*, 384.

- (63) Jasinska, L.; Villani, M.; Wu, J.; van Es, D.; Klop, E.; Rastogi, S.; Koning, C. E. *Macromolecules* **2011**, *44*, 3458.
- (64) Bachmann, F.; Reimer, J.; Ruppenstein, M.; Thiem, J. *Macromol. Chem. Phys.* **2001**, *202*, 3410.
- (65) Lavilla, C.; Alla, A.; Martínez de Ilarduya, A.; Benito, E.; García-Martín, M. G.; Galbis, J. A.; Muñoz-Guerra, S. *Polymer* **2012**, *53*, 3432.
- (66) Fenouillot, F.; Rousseau, A.; Colomines, G.; Saint-Loup, R.; Pascault, J. P. *Prog. Polym. Sci.* **2010**, *35*, 578.
- (67) Chen, J.; Wu, J.; Qi, J.; Wang, H. *ACS Sustainable Chem. Eng.* **2019**, *7*, 1061.
- (68) Laanesoo, S.; Bonjour, O.; Parve, J.; Parve, O.; Matt, L.; Vares, L.; Jannasch, P. *Biomacromolecules* **2021**, *22*, 640.
- (69) Beghdadi, S.; Abdelhedi Miladi, I.; Ben Romdhane, H.; Bernard, J.; Drockenmuller, E. *Biomacromolecules* **2012**, *13*, 4138.
- (70) Saxon, D. J.; Nasiri, M.; Mandal, M.; Maduskar, S.; Dauenhauer, P. J.; Cramer, C. J.; LaPointe, A. M.; Reineke, T. M. *J. Am. Chem. Soc.* **2019**, *141*, 5107.
- (71) Lavilla, C.; Alla, A.; Martínez de Ilarduya, A.; Muñoz-Guerra, S. *Biomacromolecules* **2013**, *14*, 781.
- (72) Lavilla, C.; de Ilarduya, A. M.; Alla, A.; García-Martín, M. G.; Galbis, J. A.; Muñoz-Guerra, S. *Macromolecules* **2012**, *45*, 8257.
- (73) Japu, C.; Martínez de Ilarduya, A.; Alla, A.; García-Martín, M. G.; Galbis, J. A.; Muñoz-Guerra, S. *Polym. Chem.* **2014**, *5*, 3190.
- (74) Muñoz-Guerra, S.; Lavilla, C.; Japu, C.; Martínez de Ilarduya, A. *Green Chem.* **2014**, *16*, 1716.
- (75) Japu, C.; Martínez de Ilarduya, A.; Alla, A.; Jiang, Y.; Loos, K.; Muñoz-Guerra, S. *Biomacromolecules* **2015**, *16*, 868.
- (76) Begines, B.; Zamora, F.; Benito, E.; García-Martín, M. d. G.; Galbis, J. A. *J. Polym. Sci., Part A: Polym. Chem.* **2012**, *50*, 4638.
- (77) Lopalco, A.; Marinaro, W. A.; Day, V. W.; Stella, V. J. *J. Pharm. Sci.* **2017**, *106*, 601.
- (78) Marco-Dufort, B.; Willi, J.; Vielba-Gomez, F.; Gatti, F.; Tibbitt, M. W. *Biomacromolecules* **2021**, *22*, 146.
- (79) Djordjevic, J.; Barch, M.; Uhrich, K. E. *Pharm. Res.* **2005**, *22*, 24.
- (80) Harmon, A. M.; Lash, M. H.; Sparks, S. M.; Uhrich, K. E. *J. Control. Release* **2011**, *153*, 233.

- (81) Rushworth, J. L.; Montgomery, K. S.; Cao, B.; Brown, R.; Dibb, N. J.; Nilsson, S. K.; Chiefari, J.; Fuchter, M. J. *ACS Appl. Bio Mater.* **2020**, *3*, 5775.
- (82) Bhatia, S.; Mohr, A.; Mathur, D.; Parmar, V. S.; Haag, R.; Prasad, A. K. *Biomacromolecules* **2011**, *12*, 3487.
- (83) Stebbins, N. D.; Yu, W.; Uhrich, K. E. *Biomacromolecules* **2015**, *16*, 3632.
- (84) Gu, L.; Faig, A.; Abdelhamid, D.; Uhrich, K. *Acc. Chem. Res.* **2014**, *47*, 2867.
- (85) Wu, G. *Adv. Nutr.* **2010**, *1*, 31.
- (86) Yang, J.; An, H.-W.; Wang, H. *ACS Appl. Bio Mater.* **2021**, *4*, 24.
- (87) Ivanov, K.; Stoimenova, A.; Obreshkova, D.; Saso, L. *Biotechnol. Biotechnol. Equip.* **2013**, *27*, 3620.
- (88) Smith, G. G.; Sivakua, T. *J. Org. Chem.* **1983**, *48*, 627.
- (89) Izumi, Y.; Chibata, I.; Itoh, T. *Angew. Chem. Int. Ed.* **1978**, *17*, 176.
- (90) Ikeda, M. *Adv. Biochem. Eng. Biotechnol.* **2003**, *79*, 1.
- (91) De Marco, R.; Spinella, M.; De Lorenzo, A.; Leggio, A.; Liguori, A. *Org. Biomol. Chem.* **2013**, *11*, 3786.
- (92) Fields, G. B. *Curr. Protoc. Protein Sci.* **2001**, *26*, 18.1.1.
- (93) Dyson, H. J.; Wright, P. E.; Scheraga, H. A. *Proc. Natl. Acad. Sci.* **2006**, *103*, 13057.
- (94) Scheiner, S.; Kar, T.; Pattanayak, J. *J. Am. Chem. Soc.* **2002**, *124*, 13257.
- (95) Kim, K.; Friesner, R. A. *J. Am. Chem. Soc.* **1997**, *119*, 12952.
- (96) Vaitheeswaran, S.; Thirumalai, D. *Proc. Natl. Acad. Sci.* **2008**, *105*, 17636.
- (97) Zhang, S.; Rich, A. *Proc. Natl. Acad. Sci.* **1997**, *94*, 23.
- (98) Garner, J.; Harding, M. M. *Org. Biomol. Chem.* **2007**, *5*, 3577.
- (99) Wolfgang, J.; Risser, S. M.; Priyadarshy, S.; Beratan, D. N. *J. Phys. Chem. B* **1997**, *101*, 2986.
- (100) Sinha, N. J.; Langenstein, M. G.; Pochan, D. J.; Kloxin, C. J.; Saven, J. G. *Chem. Rev.* **2021**, *121*, 13915.
- (101) Frederix, P. W. J. M.; Scott, G. G.; Abul-Haija, Y. M.; Kalafatovic, D.; Pappas, C. G.; Javid, N.; Hunt, N. T.; Ulijn, R. V.; Tuttle, T. *Nat. Chem.* **2015**, *7*, 30.
- (102) Clarke, D. E.; Parmenter, C. D. J.; Scherman, O. A. *Angew. Chem. Int. Ed.* **2018**, *57*, 7709.
- (103) Dasgupta, A.; Das, D. *Langmuir* **2019**, *35*, 10704.
- (104) Mikhalevich, V.; Craciun, I.; Kyropoulou, M.; Palivan, C. G.; Meier, W. *Biomacromolecules* **2017**, *18*, 3471.

- (105) Meng, Q.; Kou, Y.; Ma, X.; Liang, Y.; Guo, L.; Ni, C.; Liu, K. *Langmuir* **2012**, *28*, 5017.
- (106) Sheehan, F.; Sementa, D.; Jain, A.; Kumar, M.; Tayarani-Najjaran, M.; Kroiss, D.; Ulijn, R. V. *Chem. Rev.* **2021**, *121*, 13869.
- (107) Rad-Malekshahi, M.; Lempsink, L.; Amidi, M.; Hennink, W. E.; Mastrobattista, E. *Bioconjugate Chem.* **2016**, *27*, 3.
- (108) Jacoby, G.; Segal Asher, M.; Ehm, T.; Abutbul Ionita, I.; Shinar, H.; Azoulay-Ginsburg, S.; Zemach, I.; Koren, G.; Danino, D.; Kozlov, M. M.; Amir, R. J.; Beck, R. *J. Am. Chem. Soc.* **2021**, *143*, 11879.
- (109) Nandi, N.; Gayen, K.; Ghosh, S.; Bhunia, D.; Kirkham, S.; Sen, S. K.; Ghosh, S.; Hamley, I. W.; Banerjee, A. *Biomacromolecules* **2017**, *18*, 3621.
- (110) Ji, W.; Tang, Y.; Makam, P.; Yao, Y.; Jiao, R.; Cai, K.; Wei, G.; Gazit, E. *J. Am. Chem. Soc.* **2021**, *143*, 17633.
- (111) Katchalski, E.; Grossfeld, I.; Frankel, M. *Journal of the American Chemical Society* **1948**, *70*, 2094.
- (112) Hadjichristidis, N.; Iatrou, H.; Pitsikalis, M.; Sakellariou, G. *Chemical Reviews* **2009**, *109*, 5528.
- (113) Cheng, J.; Deming, T. J. *Top. Curr. Chem.* **2012**, *310*, 1.
- (114) Lu, H.; Cheng, J. *Journal of the American Chemical Society* **2007**, *129*, 14114.
- (115) Vacogne, C. D.; Schlaad, H. *Chem. Commun.* **2015**, *51*, 15645.
- (116) Deming, T. J. *Chem. Rev.* **2016**, *116*, 786.
- (117) Sun, Y.; Wollenberg, A. L.; O'Shea, T. M.; Cui, Y.; Zhou, Z. H.; Sofroniew, M. V.; Deming, T. J. *J. Am. Chem. Soc.* **2017**, *139*, 15114.
- (118) Lv, S.; Wu, Y.; Cai, K.; He, H.; Li, Y.; Lan, M.; Chen, X.; Cheng, J.; Yin, L. *J. Am. Chem. Soc.* **2018**, *140*, 1235.
- (119) Liu, H.; Wang, R.; Wei, J.; Cheng, C.; Zheng, Y.; Pan, Y.; He, X.; Ding, M.; Tan, H.; Fu, Q. *J. Am. Chem. Soc.* **2018**, *140*, 6604.
- (120) Ranganathan, P.; Chen, C.-W.; Rwei, S.-P.; Lee, Y.-H.; Ramaraj, S. K. *Polym. Degrad. Stab.* **2020**, *181*, 109323.
- (121) Asín, L.; Armelin, E.; Montané, J.; Rodríguez-Galán, A.; Puiggali, J. *J. Polym. Sci. A: Polym. Chem.* **2001**, *39*, 4283.
- (122) de Jongh, P. A. J. M.; Paul, P. K. C.; Khoshdel, E.; Wilson, P.; Kempe, K.; Haddleton, D. M. *Eur. Polym. J.* **2017**, *94*, 11.
- (123) Knight, D. K.; Gillies, E. R.; Mequanint, K. *Biomacromolecules* **2011**, *12*, 2475.

- (124) Cao, K.; Flegg, D. S.; Lin, S.; Lagurné-Labarthe, F.; Mequanint, K.; Gillies, E. R. *ACS Appl. Polym. Mater.* **2019**, *1*, 2360.
- (125) Ruano, G.; Díaz, A.; Tononi, J.; Torras, J.; Puiggalí, J.; Alemán, C. *Polym. Test.* **2020**, *82*, 106300.
- (126) Sun, H.; Meng, F.; Dias, A. A.; Hendriks, M.; Feijen, J.; Zhong, Z. *Biomacromolecules* **2011**, *12*, 1937.
- (127) Shi, C.-X.; Guo, Y.-T.; Wu, Y.-H.; Li, Z.-Y.; Wang, Y.-Z.; Du, F.-S.; Li, Z.-C. *Macromolecules* **2019**, *52*, 4260.
- (128) Bayer, O. J. A. C. *Angew. Chem. Int. Ed.* **1947**, *59*, 257.z
- (129) Maisonneuve, L.; Lamarzelle, O.; Rix, E.; Grau, E.; Cramail, H. *Chem. Rev.* **2015**, *115*, 12407.
- (130) Deepa, P.; Jayakannan, M. *J. Polym. Sci. A: Polym. Chem* **2008**, *46*, 2445.
- (131) Yamamoto, N.; Nakayama, A.; Oshima, M.; Kawasaki, N.; Aiba, S.-i. *React. Funct. Polym.* **2007**, *67*, 1338.
- (132) Yin, J.; Wildeman, J.; Loontjens, T. *J. Polym. Sci. A: Polym. Chem.* **2015**, *53*.
- (133) Wang, C.; Cao, X.; Zhang, Y. *Oncotarget* **2017**, *8*, 31612.
- (134) He, X.; Ding, M.; Li, J.; Tan, H.; Fu, Q.; Li, L. *RSC Adv.* **2014**, *4*, 24736.
- (135) Huang, F.; Cheng, R.; Meng, F.; Deng, C.; Zhong, Z. *Biomacromolecules* **2015**, *16*, 2228.
- (136) Lu, W.; Wang, X.; Cheng, R.; Deng, C.; Meng, F.; Zhong, Z. *Polym. Chem.* **2015**, *6*, 6001.
- (137) Kihara, N.; Kushida, Y.; Endo. *J. Polym. Sci. A: Polym. Chem* **1996**, *34*, 2173.
- (138) Yamamoto, H.; Kuno, Y.; Sugimoto, S.; Takeuchi, H.; Kawashima, Y. *J. Control. Release* **2005**, *102*, 373.
- (139) Gilding, D. K.; Reed, A. M. *Polymer* **1979**, *20*, 1459.
- (140) Zhong, Z.; Dijkstra, P. J.; Feijen, J. *Angew. Chem. Int. Ed.* **2002**, *41*, 4510.
- (141) McGuinness, D. S.; Marshall, E. L.; Gibson, V. C.; Steed, J. W. *J. Polym. Sci. A: Polym. Chem.* **2003**, *41*, 3798.
- (142) Jérôme, C.; Lecomte, P. *Adv. Drug Deliv. Rev.* **2008**, *60*, 1056.
- (143) Cohen-Arazi, N.; Katzhendler, J.; Kolitz, M.; Domb, A. J. *Macromolecules* **2008**, *41*, 7259.
- (144) Yin, Q.; Yin, L.; Wang, H.; Cheng, J. *Acc. Chem. Res.* **2015**, *48*, 1777.
- (145) Simmons, T. L.; Baker, G. L. *Biomacromolecules* **2001**, *2*, 658.

- (146) Thillaye du Boullay, O.; Marchal, E.; Martin-Vaca, B.; Cossío, F. P.; Bourissou, D. *J. Am. Chem. Soc.* **2006**, *128*, 16442.
- (147) Lu, Y.; Yin, L.; Zhang, Y.; Zhang, Z.; Xu, Y.; Tong, R.; Cheng, J. *ACS Macro Lett.* **2012**, *1*, 441.
- (148) Wang, H.; Tang, L.; Tu, C.; Song, Z.; Yin, Q.; Yin, L.; Zhang, Z.; Cheng, J. *Biomacromolecules* **2013**, *14*, 3706.
- (149) Zhang, Z.; Yin, L.; Tu, C.; Song, Z.; Zhang, Y.; Xu, Y.; Tong, R.; Zhou, Q.; Ren, J.; Cheng, J. *ACS Macro Lett.* **2013**, *2*, 40.
- (150) Zhang, Z.; Yin, L.; Xu, Y.; Tong, R.; Lu, Y.; Ren, J.; Cheng, J. *Biomacromolecules* **2012**, *13*, 3456.
- (151) Yin, Q.; Tong, R.; Xu, Y.; Dobrucki, L. W.; Fan, T. M.; Cheng, J. *Biomacromolecules* **2013**, *14*, 920.
- (152) Khuphe, M.; Ingram, N.; Thornton, P. D. *Nanoscale* **2018**, *10*, 14201.
- (153) Martin, R. T.; Camargo, L. P.; Miller, S. A. *Green Chem.* **2014**, *16*, 1768.
- (154) Xu, Y.; Perry, M. R.; Cairns, S. A.; Shaver, M. P. *Polym. Chem.* **2019**, *10*, 3048.
- (155) Cairns, S. A.; Schultheiss, A.; Shaver, M. P. *Polym. Chem.* **2017**, *8*, 2990.
- (156) Anantharaj, S.; Jayakannan, M. *Biomacromolecules* **2012**, *13*, 2446.
- (157) Anantharaj, S.; Jayakannan, M. *Biomacromolecules* **2015**, *16*, 1009.
- (158) Anantharaj, S.; Jayakannan, M. *J. Polym. Sci. A: Polym. Chem.* **2016**, *54*, 1065.
- (159) Anantharaj, S.; Jayakannan, M. *J. Polym. Sci. A: Polym. Chem.* **2016**, *54*, 2864.
- (160) Aluri, R.; Jayakannan, M. *Polym. Chem.* **2015**, *6*, 4641.
- (161) Aluri, R.; Jayakannan, M. *Biomacromolecules* **2017**, *18*, 189.
- (162) Aluri, R.; Saxena, S.; Joshi, D. C.; Jayakannan, M. *Biomacromolecules* **2018**, *19*, 2166.
- (163) Saxena, S.; Jayakannan, M. *J. Polym. Sci. A: Polym. Chem.* **2016**, *54*, 3279.
- (164) Saxena, S.; Jayakannan, M. *Biomacromolecules* **2020**, *21*, 171.
- (165) Saxena, S.; Jayakannan, M. *Biomacromolecules* **2017**, *18*, 2594.
- (166) Saxena, S.; Pradeep, A.; Jayakannan, M. *ACS Appl. Bio Mater.* **2019**, *2*, 5245.

# **Chapter 2**

---

## **Development of L-Lysine Based Biodegradable Polyurethanes and Their Dual-Responsive Amphiphilic Nanocarriers for Drug Delivery to Cancer Cells**

## Abstract

*The present investigation reports the development of new classes of L-lysine based polyurethanes by solvent and isocyanate free melt transurethane polycondensation approach. New enzyme and thermo-dual responsive amphiphilic polyurethane nano-carriers were developed for the delivery of drugs both at the intracellular level and at cancer tissue temperature. Multifunctional L-lysine monomers were tailor-made by suitably converting the amine functionalities into urethanes (or carbamates) while masking the carboxylic acid functional unit as amide pendants. The L-lysine monomers underwent melt transurethane polymerization with diols at 150 °C in the presence of catalyst to produce moderate to high molecular weight linear polyurethanes. Further, a new amphiphilic L-lysine monomer was designed with PEG-350 chain as a pendant and this monomer upon polymerization yielded well-defined amphiphilic aliphatic polyurethanes (APU). The APU was found to undergo core-shell type self-assembly in aqueous medium to produce nanoparticles of size < 175 nm and exhibited excellent encapsulation capabilities for anticancer drug such as doxorubicin (DOX). The APU nano-carriers showed thermo-responsiveness from clear to turbid solution above the lower critical solution temperature (LCST) at 41-43 °C corresponding to cancer tissue temperature. At extracellular level, the thermal-stimuli responsiveness (stimuli-1) in the APU nano-carrier was employed as trigger to deliver the DOX at cancer tissue temperature. At the intracellular level, the aliphatic urethane linkages in the APU backbone underwent lysosomal enzymatic-biodegradation (stimuli-2) to deliver DOX. Cytotoxicity studies revealed that the APU nanoparticles were not toxic to cells up to 80.0 µg/mL whereas their DOX-loaded nanoparticles accomplished more than 90 % cell death in breast cancer (MCF 7) cells. Confocal microscopy and flow cytometry analysis confirmed that the L-lysine based polymer nanoparticles were readily taken up and internalized in the cancer cells. Live cell imaging using lyso-trackers was done to prove the intracellular bio-degradation of the APU nano-carriers.*



## 2.1. Introduction

Synthetic polymers based on bio-resources are emerging as potential biomaterials in drug and gene delivery in cancer, tissue engineering, bone-repair, and antimicrobial application, etc.<sup>1-2</sup> L-Amino acids are natural building blocks in proteins and important bio-resources in designing diverse polymer architectures such as amphiphilic polypeptides<sup>3</sup> di and tri-block copolymers<sup>4-7</sup> etc for biomedical application. Recently, efforts have also been taken to make non-peptide polymer analogues<sup>8</sup> such as poly(ester-amide)s,<sup>9-12</sup> poly(disulfide-ester-amide),<sup>13</sup> poly(disulfide-urethane)s,<sup>14</sup> poly(acetal-urethane),<sup>15</sup> poly(ester-urea-urethane)<sup>16-17</sup> and polycarbonates,<sup>18-21</sup> etc through polycondensation approaches.

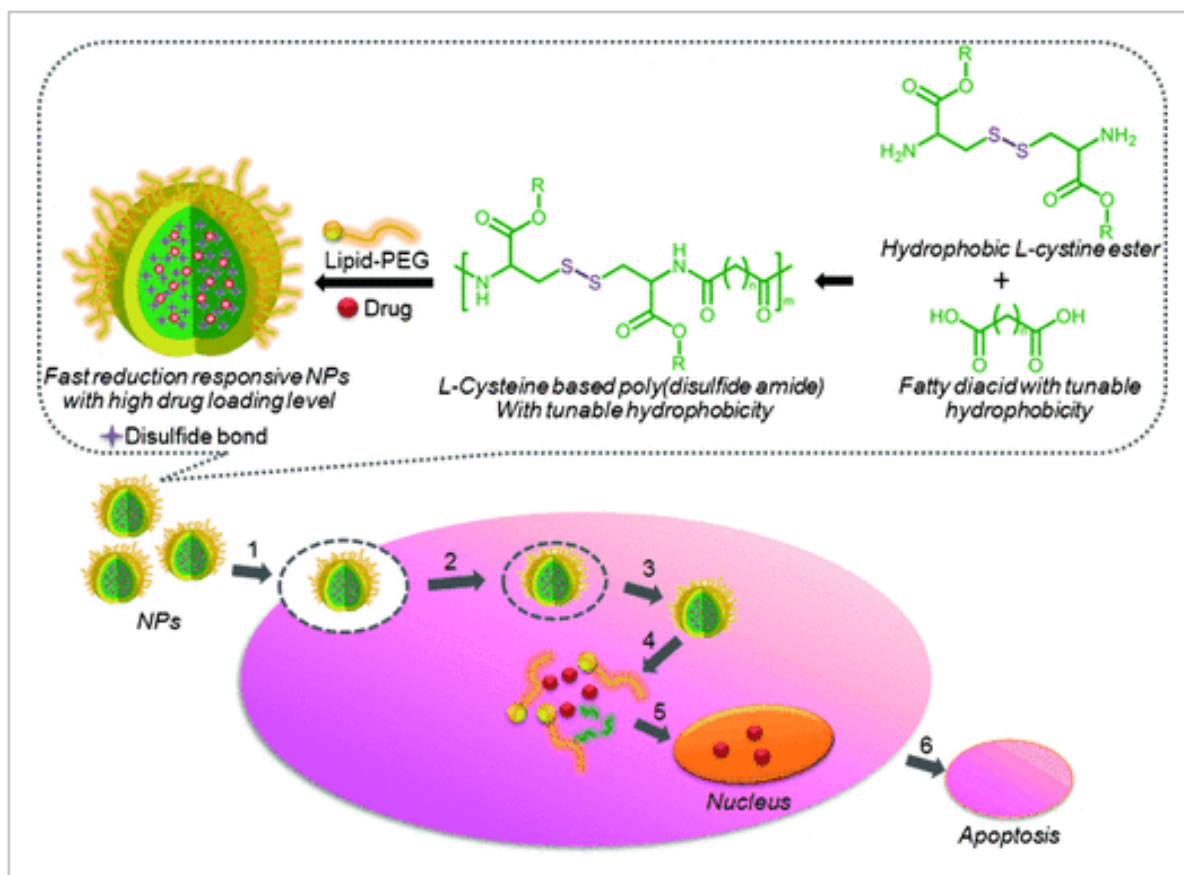


**Figure 2.1.** L-Cysteine based disulfide containing poly(ester-amide)s. (Adopted from Farokhzad et al. *Angew.Chem.* **2015**, 54, 9218–9223.)

From our group we have developed a novel ester-urethane melt polycondensation approach to make poly(ester-urethane)s from amino acid resources. This approach was extended to various multifunctional amino acids to synthesise a new class of linear<sup>22</sup> and hyperbranched poly(ester-urethane)s,<sup>23</sup> functional polyesters<sup>24,25</sup> from simple and multifunctional L-amino acid resources such as L-serine<sup>23</sup>, L-cysteine,<sup>26</sup> and L-tyrosine,<sup>27-28</sup> etc. L-amino acid based polymers were engineered as amphiphilic nano-assemblies for drug (or gene)

delivery,<sup>8</sup> FRET bio-imaging probes,<sup>13,29,30</sup> and tissue fillers, etc.<sup>31,32</sup> These polymer analogues were found to be readily degradable upon exposure to the lysosomal enzymes,<sup>33</sup> thus render the unique opportunity to deliver the desired cargoes at the intracellular compartments.

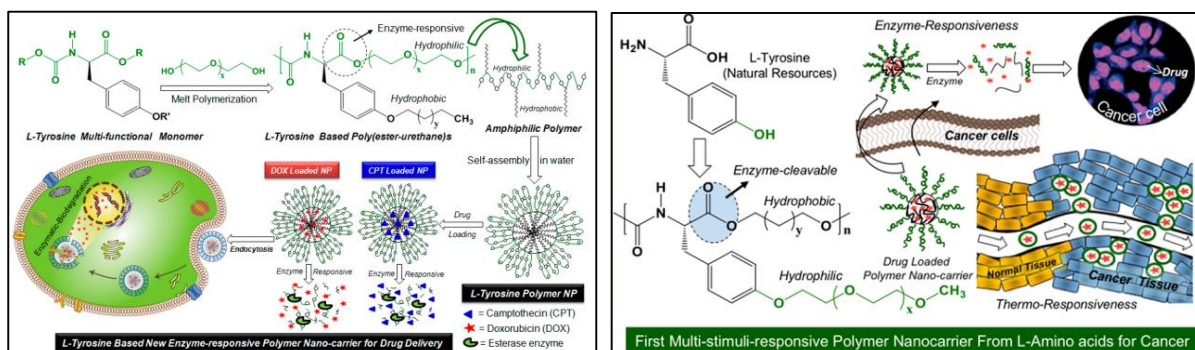


**Figure 2.2.** *L-Tyrosine based stimuli responsive poly(ester urethane)s for drug delivery applications in cancer cells. (Adopted from Rajendra et al. Biomacromolecules 2017, 18, 189–200. and Biomacromolecules 2018, 19, 2166–2181).*

Polyurethanes are unique class of engineering thermoplastic associated with excellent elastomeric and hydrogen bonding properties.<sup>34–37</sup> PEGy-lated polyurethanes have been explored as thermo-responsive materials and also employed as nano-scaffolds for delivering anticancer drug doxorubicin.<sup>38–40</sup> Polyurethanes are typically made using diisocyanate chemistry, a highly toxic process; hence, non-isocyanate synthetic pathways are highly in demand for polyurethanes development in biomedical applications.<sup>41–42</sup> These non-isocyanate methodologies include the thermal polymerization of cyclic or linear carbonates with amines<sup>43–46</sup> and monomer containing azide and hydroxyl functional groups,<sup>47–50</sup> and so on so forth.

A decade ago, Deepa et al. from our group reported a non-isocyanate route for polyurethane synthesis based on melt transurethane polycondensation approach under solvent free eco-friendly process.<sup>51</sup> In this methodology, aliphatic diamines were converted into di-urethane monomer and polymerized with diols in the presence of a catalyst to produce moderate to high molecular weight polyurethanes.<sup>52</sup> Cramail and co-workers have employed the transurethane methodology to make polyurethanes based on oleic and fatty acids.<sup>53,54</sup> There are few attempts also reported in the literature for L-amino acid based polyurethanes.<sup>55–58</sup> L-Tyrosine based polyurethanes were designed by modifying the amine group into isocyanate and then subjected to self-polycondensation with the phenolic functionality.<sup>55–56</sup> A similar approach was employed to produce L-Lysine based polyurethanes in which the amine groups

were converted into diisocyanates and polycondensed with diols or polyols to produce polyurethanes.<sup>57,58</sup>

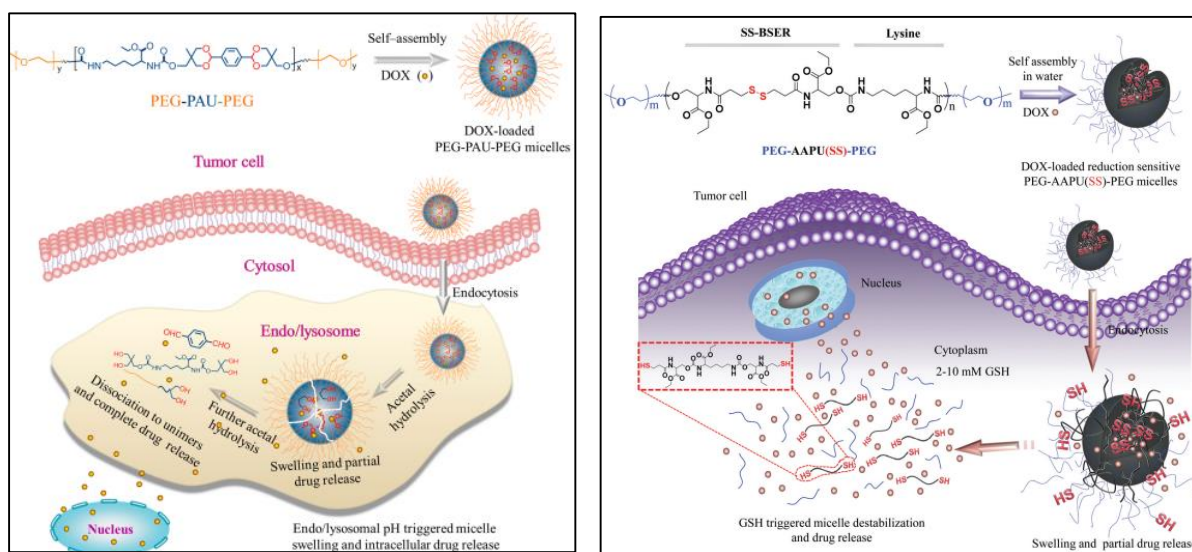


**Figure 2.3.** Development of L-Lysine based stimuli responsive polyurethanes via isocyanate route and their drug delivery applications in cancer cells. (Adopted from Huang et al. *Biomacromolecules* **2015**, *16*, 2228–2236. and *Biomater. Sci.* **2016**, *4*, 1682–1690).

Up to our knowledge, there are no non-isocyanate synthetic methodologies reported to make aliphatic polyurethanes directly from L-amino acid resources for employing them for drug delivery. Aliphatic urethane linkage (carbamate) is a widely-employed chemical linkage for enzymatic-biodegradation in prodrug pharmaceuticals.<sup>59</sup> Thus, the development of new non-isocyanate synthetic methodologies for aliphatic polyurethanes based on L-amino acids could open new avenue of research opportunities in drug delivery research. To accomplish this task, here, melt transurethane polycondensation approach was successfully designed and developed for L-lysine resources. This methodology was employed to make novel *thermo-responsive and enzymatic-biodegradable dual-purpose amphiphilic polyurethane* and demonstrate their drug delivering capability in cancer cells. The new synthetic concept and drug delivery of the nano-carrier is shown in Figure 2.4.

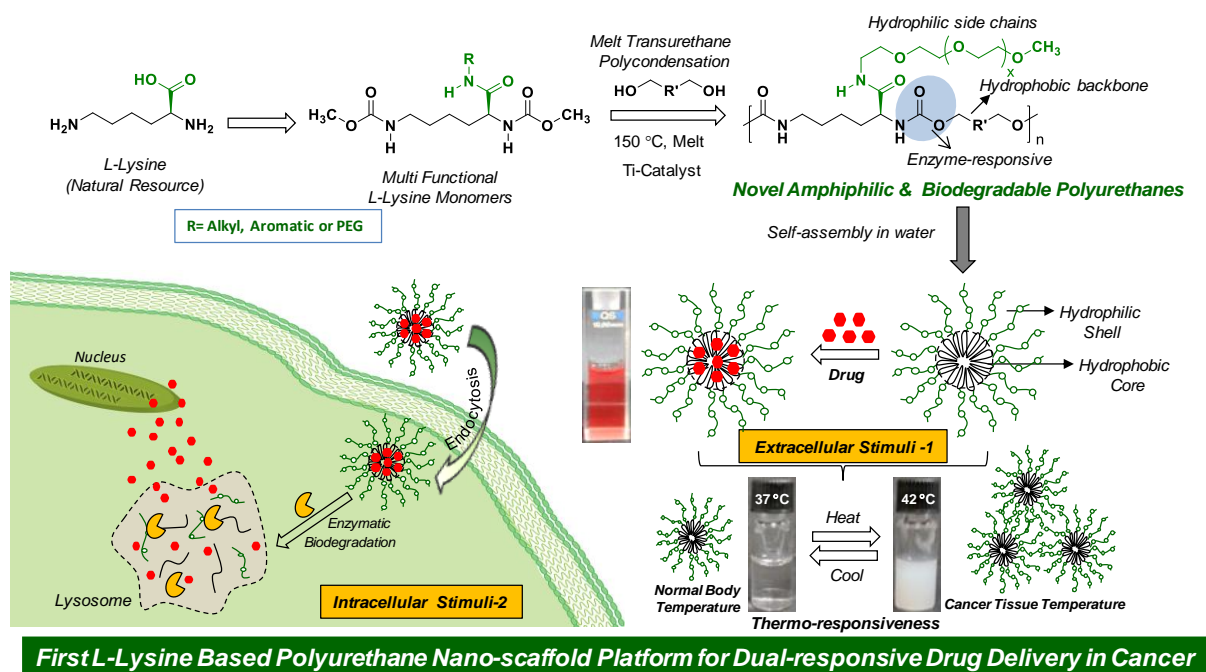


**Figure 2.4.** Development of dual responsive L-lysine based amphiphilic polyurethanes and their drug delivering capabilities in cancer cells.

The present investigation is emphasized to design L-lysine based biodegradable aliphatic polyurethanes through solvent-free melt transurethane polycondensation process and employs them as thermal and enzyme dual-responsive nanocarriers. For this purpose, the multi-functional L-lysine monomers were carefully designed with the following features: (i) the carboxylic acid functionality in the L-lysine was masked as amide chemical linkages so that it does not interfere with the polymerization process, (ii) the diamine functionalities were readily converted into di-urethanes for melt transurethane polycondensation with commercial diols to produce moderate to high molecular weight polyurethanes, (iii) the carboxylic acid unit was also explored as an anchoring point in the hydrophobic polyurethanes backbone for substituting hydrophilic PEG chains so that appropriate amphiphilicity could be attained in the polymer for their aqueous self-assembly, (iv) the PEG-side arm and polyurethane backbone facilitated the polymers to self-assemble into core-shell nano-assemblies which exhibited unique thermo-responsiveness as extracellular trigger (*stimuli-1*) to disassemble nano-carriers for delivering the loaded cargoes, (v) the aliphatic urethane chemical linkages were found to readily biodegrade by lysosomal enzymes which was explored as intracellular trigger (*stimuli-2*) to release the drugs exclusively inside the cancer cells. The thermo-responsiveness of the PEG-substituted amphiphilic polyurethanes showed lower critical solution temperature

(LCST) in the range of 41-43 °C which was closer to cancer tissue temperature (40-42 °C) compared to normal tissues (37 °C). This provided new polyurethane with in-built thermo-responsive trigger to disassemble the polyurethane carrier at cancer tissue temperature. Anticancer drug doxorubicin (DOX) was successfully encapsulated in the polyurethane nano-carrier and *in vitro* release kinetics confirmed the thermo- and enzyme dual responsiveness. Cytotoxicity and confocal microscope imaging studies were done in cervical and breast cancer cell lines in comparison with wild-type MEF (normal) cell line. The present investigation reports new classes of biodegradable and biocompatible L-lysine aliphatic polyurethanes and opens new avenue for L-lysine based thermal and enzyme multi-stimuli-responsive nano-carriers for drug delivery in cancer therapy.

## 2.2. Experimental procedure

### 2.2.1. Materials

L-Lysine monohydrochloride, 2-ethylhexan-1-amine, phenylmethanamine, cyclohexylamine, PEG-mono methyl ether-350, p-toluene sulfonyl chloride, sodium azide, 1-ethyl-3-(3-dimethylaminopropyl)carbodiimide. HCl (EDC.HCl), 1,12 dodecanediol, titanium tetrabutoxide (Ti(OBu)<sub>4</sub>), pyrene, hydrochloride salt of doxorubicin, horse liver esterase enzyme, **4',6-diamidino-2-phenylindole dihydrochloride ( DAPI 2HCl)**, dimethylthiazol-2, 5-diphenyltetrazolium bromide (MTT), paraformaldehyde, and glycerol were purchased from Aldrich chemicals and used without further purification. HPLC DMSO was obtained from Rankem. Thionyl chloride, 1-hydroxybenzotriazole (HOBt), N, N-Diisopropylethylamine (DIPEA), NaOH, Na<sub>2</sub>CO<sub>3</sub> and all other reagents and solvents were purchased locally and used as it is. WT-MEF (Wild Type Mouse Embryonic Fibroblast) and MCF 7 (breast cancer cells) cell lines were employed for studies in the present paper. The WTMEFs were a generous gift from the lab of Dr. Richard Anderson and MCF 7 cells are from Dr. Amit Dutt's lab in ACTREC. The cells have been maintained in phenol red containing DMEM media (purchased from Gibco). The media was supplemented with 10% v/v FBS (fetal bovine serum), along with 1.0 % v/v penicillin-streptomycin (anti-biotic). The cells were maintained and grown in 5.0 % CO<sub>2</sub> saturated incubator at 37°C. For experiments, cells were washed with 1.0 mL autoclaved 1X PBS, and trypsinization of cells was carried out for 1 min in CO<sub>2</sub> incubator using 0.05 % trypsin obtained from Gibco. Phalloidin conjugated with Alexa 488 was purchased from Invitrogen (Molecular Probes). The live cell imaging was carried out in Lab TEK 4 well cover

glass chamber purchased from Nunc Lab Tek. LysoTracker Green DND-26 for lysosomal imaging was purchased from Cell Signaling Technologies (CST).

### 2.2.2. General procedures:

$^1\text{H}$  NMR spectra of all the monomers and polymers were recorded using 400 MHz Jeol spectrometer and  $^{13}\text{C}$  NMR was recorded using 100 MHz Jeol spectrometer in  $\text{CDCl}_3$  containing a trace amount of TMS as an internal standard. Mass of all the monomers was confirmed by high resolution mass spectrometry using Micro Mass ESI-TOF MS spectrometer. MALDI-TOF MS of the polymers was recorded using APPLIED Biosystems 4800 PLUS Analyzer. IR spectra of all the samples were recorded using a Thermo-Scientific Nicolet 6700FT-IR spectrometer with the solid state in KBr. Purity of polymers was determined by Gel permeation chromatography (GPC) using Viscotek VE 1122 pump, VE 3580 RI detector and Viscotek VE 3210 UV/V is detector in tetrahydrofuran (THF) using polystyrene as a standard. Thermo gravimetric analysis (TGA) of monomers and polymers was determined by using Perkin Elmer thermal analyzer STA 6000 model at a heating rate of  $10\text{ }^\circ\text{C}/\text{min}$  under inert atmosphere. Differential scanning calorimetry (DSC) measurements were performed on a TA Q20 differential scanning calorimeter (DSC) at heating and cooling rates of  $10\text{ }^\circ\text{C}/\text{min}$  under nitrogen atmosphere. Size of polymeric nanoparticle was measured by dynamic light scattering (DLS), using a Nano ZS-90 apparatus utilizing a 633 nm red laser from Malvern instruments. Field emission scanning electron microscopy (FE-SEM) images were obtained by using Zeiss Ultra Plus scanning electron microscope. The Atomic Force Microscopy (AFM) images were obtained using Veeco Nanoscope IV instrument in tapping mode. Confocal imaging was performed by using LSM710 microscope. Synthetic details for PEG-amine (compounds 5 to 7) are given in the supporting information. Encapsulation details, *in vitro* drug release studies, MTT assay Flow Cytometry and live cell confocal imaging details are given in the supporting information.

**2.2.3. Synthesis of  $\text{N}^2$ ,  $\text{N}^6$ -bis(methoxycarbonyl)-L-lysine (1):** L-Lysine monohydrochloride (10.00 g, 0.0526 mol) was dissolved in saturated solution of sodium carbonate (8.40 g, 0.078 mol). Methyl chloroformate (4.90 mL, 0.063 mol) in THF (60.0 mL) was added drop wise at  $0\text{ }^\circ\text{C}$  and the reaction was continued for 12 h at room temperature. The reaction mixture was neutralized with 1N HCl and extracted with dichloromethane and the organic layer was dried over anhydrous  $\text{Na}_2\text{SO}_4$ . The viscous liquid was further purified by passing through silica gel column using pet ether and ethyl acetate (1:1 v/v) as eluent. Yield = 12.40 g (90 %).  $^1\text{H}$ -NMR

(400 MHz, CDCl<sub>3</sub>)  $\delta$  ppm: 1.39-1.46 (m, 2H, -CH-CH<sub>2</sub>-CH<sub>2</sub>), 1.50-1.52 (m, 2H, NH-CH<sub>2</sub>-CH<sub>2</sub>-), 1.65-1.85 (m, 2H, CH-CH<sub>2</sub>-), 3.17-3.19 (b, m, 2H, -NH-CH<sub>2</sub>-CH<sub>2</sub>-), 3.67 (s, 3H, -NH-COOCH<sub>3</sub>), 3.69 (s, 3H, -NH-COOCH<sub>3</sub>), 4.13 (s, 1H, -NH-CH-), 5.92 (s, -CH<sub>2</sub>-NH-), 5.61 (b, s -CH-NH-). <sup>13</sup>C-NMR (100 MHz, CDCl<sub>3</sub>)  $\delta$  ppm: 22.09, 29.24, 30.89, 31.67, 40.95, 52.12, 52.37, 53.48, 157.01, 157.57, 175.79. FT-IR (cm<sup>-1</sup>) 3331, 2946, 2865, 1700, 1532, 1451, 1365, 1221, 1057, 780, 751, 646. HRMS (ESI+): m/z calcd. for C<sub>10</sub>H<sub>18</sub>N<sub>2</sub>O<sub>6</sub>Na [M+Na]<sup>+</sup>: 285.1057; found: 285.1062.

**2.2.4. Synthesis of dimethyl((5S)-6-((2-ethylhexyl)amino)-6-oxohexane-1,5-diyl)dicarbamate (2):** Compound (1) (5.00 g, 0.019 mol) was taken in a 250 mL two neck flask and dissolved in 60.0 mL of dry DMF. EDC.HCl (4.30 g, 0.023 mol), HOBt (2.50 g, 0.019 mol) and DIPEA (9.80 mL, 0.057 mol) were added and reaction was stirred for 15 min under nitrogen purging. 2-ethylhexan-1-amine (3.70 mL, 0.022 mol) was added dropwise and reaction was continued for 24 h at room temperature under nitrogen atmosphere. Excess solvent was removed by vacuum distillation; residue was dissolved in 1M sodium bicarbonate solution and extracted with dichloromethane. The organic layer was passed through anhydrous Na<sub>2</sub>SO<sub>4</sub> and compound was further purified through silica gel column using pet ether ethyl acetate (1:4 v/v) as eluent. Yield = 5.10 g (73 %). <sup>1</sup>H-NMR (400 MHz, CDCl<sub>3</sub>)  $\delta$  ppm: 0.77 - 0.98 (m, 6 H, -CH<sub>2</sub>-(CH<sub>3</sub>)<sub>2</sub>), 1.26 -1.33 (m, 8H, -(CH<sub>2</sub>)<sub>4</sub>-CH<sub>3</sub>) 1.35 - 1.45 (m, 3 H, -CH<sub>2</sub>-CH<sub>2</sub>-CH and -NH-CH<sub>2</sub>-CH), 1.48 - 1.57 (m, 2 H, -NH-CH<sub>2</sub>-CH<sub>2</sub>-), 1.60-1.69 ( m, 1 H, -CH<sub>2</sub>-CH), 1.80 - 1.89 (m, 1H, -CH<sub>2</sub>-CH), 3.17-3.26 (m, 4 H, -NH-CH<sub>2</sub>-CH<sub>2</sub>-) and -NH-CH<sub>2</sub>-CH), 3.66 (s, 3H, -CH<sub>2</sub>-NH-COOCH<sub>3</sub>), 3.67 (s, 3H, -CH-NH-COOCH<sub>3</sub>) 4.10 (s, 1H, CH-NH-) 4.88 (s, 1H, NH) 5.51 ( s, 1H, NH) 6.22 ( s, 1H, NH). <sup>13</sup>C-NMR (100 MHz, CDCl<sub>3</sub>)  $\delta$  ppm: 10.69, 10.76, 13.97, 22.30, 22.91, 24.05, 28.72, 29.36, 30.84, 31.87, 39.22, 40.18, 42.28, 51.95, 52.27, 54.81, 157.01, 157.29, 171.87. FTIR (cm<sup>-1</sup>) 3315, 2931, 2864, 1715, 1656, 1530, 1452, 1365, 1241, 1142, 1058, 899,780,729. HRMS (ESI): m/z calcd. for C<sub>18</sub>H<sub>35</sub>N<sub>3</sub>O<sub>5</sub> [M+H]<sup>+</sup>: 374.5015; found: 374.2656.

**2.2.5. Dimethyl (6-(benzylamino)-6-oxohexane-1,5-diyl)dicarbamate (3):** Compound 1 (5.00 g, 0.019 mol) benzylamine (2.50 mL, 0.023 mol) were reacted together using the EDC.HCl, HOBt and DIPEA as described for monomer (2). The crude product was purified through silica gel column using pet ether ethyl acetate (1:4 v/v) as eluent. Yield = 5.00 g (72 %). <sup>1</sup>H-NMR (400 MHz, CDCl<sub>3</sub>)  $\delta$  ppm: 1.36-1.42 (m, 2H, -CH<sub>2</sub>-CH<sub>2</sub>-CH), 1.46-1.58 (m, 2H, -NH-CH<sub>2</sub>-CH<sub>2</sub>-), 1.64-1.73 (m, 1H, -CH<sub>2</sub>-CH), 1.83-1.93 (m, 1H, -CH<sub>2</sub>-CH), 3.16 (t, 2H, -

NH-CH<sub>2</sub>-CH<sub>2</sub>), 3.64 (s, 3H, -CH<sub>2</sub>-NH-COOCH<sub>3</sub>), 3.65 (s, 3H, -CH-NH-COOCH<sub>3</sub>), 4.19 (s, 1H, -CH<sub>2</sub>CH), 4.38-4.49 (m, 2H, -CH<sub>2</sub>-C<sub>6</sub>H<sub>5</sub>), 4.94 (s, 1H, NH), 5.63 (s, 1H, NH), 6.82 (s, 1H, -NH-CH<sub>2</sub>-C<sub>6</sub>H<sub>5</sub>), 7.25-7.36 (m, 5H, -CH<sub>2</sub>-C<sub>6</sub>H<sub>5</sub>). <sup>13</sup>C-NMR (100 MHz, CDCl<sub>3</sub>) δ ppm: 22.24, 29.37, 31.88, 40.14, 43.44, 52.01, 52.33, 54.80, 127.48, 127.61, 128.64, 137.89, 157.03, 157.34, 171, 78. FTIR (cm<sup>-1</sup>) 3305, 2938, 2862, 2314, 1707, 1655, 1530, 1449, 1363, 1241, 1145, 1066, 1031, 902, 780, 736, 698, 610. HRMS (ESI): m/z calcd. for C<sub>17</sub>H<sub>26</sub>N<sub>3</sub>O<sub>5</sub> [M+H]<sup>+</sup>: 352.4105; found: 352.1872.

**2.2.6. Dimethyl (6-(cyclohexylamino)-6-oxohexane-1,5-diyldicarbamate (4):** Compound 1 (5.00 g, 0.019 mol) cyclohexyl amine (2.60 mL 0.023 mol) were coupled together using the EDC.HCl, HOBt and DIPEA as described for monomer (2). The crude product was purified through silica gel column using pet ether ethyl acetate (1:4 v/v) as eluent. Yield = 4.80 g (71 %). <sup>1</sup>H-NMR (400 MHz, CDCl<sub>3</sub>) δ ppm: 1.05 - 1.24 (m, 3 H), 1.28 - 1.44 (m, 4 H), 1.45 - 1.57 (m, 2 H), 1.62 (m, 2 H), 1.66 - 1.76 (m, 2 H), 1.76 - 1.95 (m, 3 H), 3.04 - 3.26 (m, 2 H), 3.56 - 3.80 (m, 7 H), 3.98 - 4.18 (m, 1 H), 4.90 (br. s, 1 H), 5.54 (d, 1 H), 6.12 (br. s, 1 H). <sup>13</sup>C-NMR (100 MHz, CDCl<sub>3</sub>) δ ppm: 22.55, 25.04, 25.72, 29.68, 32.46, 33.23, 40.55, 48.57, 52.30, 52.61, 55.10, 77.31, 77.64, 77.75, 157.29, 157.62, 171.06. FTIR (cm<sup>-1</sup>) 3307, 2930, 2856, 1737, 1698, 1644, 1541, 1446, 1365, 1262, 1230, 1148, 1042, 893, 784, 669, 539. HRMS (ESI): m/z calcd. for C<sub>16</sub>H<sub>30</sub>N<sub>3</sub>O<sub>5</sub> [M+H]<sup>+</sup>: 344.4315; found: 344.2189.

**2.2.7. Synthesis of amphiphilic L-lysine monomer (8):** Compound (1) (5.00 g, 0.019 mol) and polyethylene glycol monomethyl ether amine (7) (8.00 g, 0.022 mol) were reacted in dry DMF using EDC.HCl (4.30 g, 0.023 mol), HOBt (2.50 g, 0.019 mol) and DIPEA (9.80 mL, 0.057 mol) as described for monomer 2. The crude product was purified through silica gel column using chloroform as an eluent. Yield = 8.00 g (70 %). <sup>1</sup>H-NMR (400 MHz, CDCl<sub>3</sub>) δ ppm: 1.35 (q, 2 H), 1.40 - 1.54 (m, 2 H), 1.61 (d, 1 H), 1.79 (d, 1 H), 3.13 (d, 2 H), 3.34 (s, 3 H), 3.41 (q, 2 H), 3.48 - 3.55 (m, 4 H), 3.55 - 3.72 (m, 26 H), 5.10 (s, 1 H), 5.66 (d, 1 H), 6.90 (s, 1 H). <sup>13</sup>C-NMR (100 MHz, CDCl<sub>3</sub>) δ ppm: 22.18, 29.25, 32.42, 39.18, 40.36, 51.89, 52.15, 54.55, 58.93, 69.65, 70.03, 70.37, 70.39, 71.80, 156.77, 157.24, 171.94. FTIR (cm<sup>-1</sup>) 3334, 2928, 2856, 1741, 1543, 1451, 1364, 1220, 1098, 795.

**2.2.8. Synthesis of L-lysine polyurethane P-EH:** Melt polymerization technique is described for P-EH polymer. Monomer (2) (0.50 g, 1.3 mmol) and 1,12-dodecanediol (0.27 g, 1.3 mmol) and titanium tetrabutoxide (1.0 mol %) were taken in a test tube shaped polymerization setup



and melted by placing in oil bath at 150 °C. The polymerization setup was degassed by applying vacuum and condensation was carried out for 4 h under steady nitrogen flow to produce oligomeric viscous liquid. After 4 h this viscous liquid was subjected under high vacuum (0.01 bar) for 2 h at 150 °C to give moderate to high molecular weight polymer. If required, the polymer was purified by dissolving in tetrahydrofuran (THF) and re-precipitating in methanol. <sup>1</sup>H-NMR (400 MHz, CDCl<sub>3</sub>) δ ppm: 0.81 - 0.94 (m, 6 H), 1.26 - 1.44 (m, 27 H), 1.51 - 1.65 (m, 7 H), 1.82 (s, 1 H), 3.15 - 3.25 (m, 4 H), 4.03 (s, 4 H), 4.10 - 4.13 (t, 1 H), 4.94 (s, 1 H), 5.58 (s, 1 H), 6.42 (s, 1 H). <sup>13</sup>C-NMR (100 MHz, CDCl<sub>3</sub>) δ ppm: 10.69, 10.76, 13.97, 22.30, 22.91, 24.05, 28.72, 29.36, 30.84, 31.87, 39.22, 40.18, 42.28, 51.95, 52.27, 54.81, 157.01, 157.29, 171.87. FTIR (cm<sup>-1</sup>) 3316, 2926, 2859, 1715, 1528, 1453, 1364, 1230, 1137, 1065, 897, 781, 732, 536.

**2.2.9. Synthesis of L-lysine polyurethane P-Bz:** Monomer (**3**) (0.50 g, 1.4 mmol) 1,12-dodecanediol (0.28 g, 1.4 mmol) and titanium tetrabutoxide (1 mol%) were taken in a test tube shaped polymerization setup and subjected for polycondensation at 150 °C following similar procedure as described for **P-EH**. <sup>1</sup>H-NMR (400 MHz, CDCl<sub>3</sub>) δ ppm: 1.27-1.36 (m, 17 H), 1.47-1.50 (m, 2 H), 1.56 (m, 4 H), 1.66 (s, 1 H), 1.82 (s, 1 H), 3.12 (s, 2 H), 3.97-4.01 (m, 4 H), 4.22 (s, 1 H), 4.41 (s, 2 H), 5.04 (s, 1 H), 5.75 (s, 1 H), 7.11 (s, 1 H), 7.28 (s, 2 H), 7.24 (s, 3 H). <sup>13</sup>C-NMR (100 MHz, CDCl<sub>3</sub>) δ ppm: 13.34, 19.57, 23.79, 25.57, 28.21, 29.06, 29.34, 37.28, 54.52, 58.93, 66.73, 66.78, 110.16, 112.98, 115.82, 130.41, 159.56, 159.98, 179.93. FTIR (cm<sup>-1</sup>) 3305, 2926, 2856, 2312, 1728, 1531, 1449, 1364, 1226, 1139, 1063, 783, 697.

**2.2.10. Synthesis of L-lysine polyurethane P-Cy:** Monomer (**4**) and (0.50 g, 1.4 mmol) 1,12-dodecanediol (0.30 g, 1.4 mmol) and titanium tetrabutoxide (1.0 mol %) were taken in a test tube shaped polymerization setup and subjected for polycondensation following similar procedure as described for **P-EH**. <sup>1</sup>H-NMR (400 MHz, CDCl<sub>3</sub>) δ ppm: 1.15 (q, 3 H), 1.21 - 1.33 (m, 16 H), 1.33 - 1.44 (m, 5 H), 1.44 - 1.55 (m, 2 H), 1.55 - 1.65 (m, 6 H), 1.65 - 1.74 (m, 3 H), 1.74 - 1.83 (m, 2 H), 1.86 (s, 2 H), 2.99 - 3.27 (m, 2 H), 3.60 - 3.83 (m, 1 H), 4.03 (s, 4 H), 5.0 (s, 1 H), 5.63 (s, 1 H), 6.41 (s, 1 H). <sup>13</sup>C-NMR (100 MHz, CDCl<sub>3</sub>) δ ppm: 22.19, 24.79, 25.48, 25.85, 27.81, 28.96, 29.26, 29.47, 32.30, 32.94, 48.31, 65.01, 65.41, 68.58, 156.79, 157.09, 171.02. FTIR (cm<sup>-1</sup>) 3733, 3302, 2925, 2854, 2312, 1734, 1641, 1535, 1447, 1365, 1223, 1037, 919, 777, 727, 665, 524.

**2.2.11. Synthesis of P-PEG-400:** Monomer (**2**) (0.40 g, 1.1 mmol), PEG-400 (0.42 g, 1.1 mmol) and titanium tetrabutoxide (1.0 mol %) were taken in a polymerization setup and allowed for polycondensation following similar procedure as described for **P-EH**. <sup>1</sup>H-NMR (400 MHz, CDCl<sub>3</sub>) δ ppm: 0.84 (q, 6 H), 1.25 (m, 8 H), 1.47 (m, 3 H), 1.61 (m, 1H), 1.81 (m, 1 H), 3.14 (m, 4 H), 3.62 (m, 32 H), 4.06 (m, 1H), 4.17 (m, 4 H), 5.16 (s, 1 H), 6.31 (s, 1 H).

**2.2.12. Synthesis of P-PEG-600:** Monomer (**2**) (0.40 g, 1.1 mmol), PEG- 600 (0.64 g, 1.1 mmol) and titanium tetrabutoxide (1.0 mol %) were taken in polymerisation setup and subjected for polycondensation under continuous nitrogen flow following same procedure as for **P-EH**. <sup>1</sup>H-NMR (400 MHz, CDCl<sub>3</sub>) δ ppm: 0.86 (q, 6 H), 1.24 (m, 8 H), 1.35 (m, 3 H), 1.50 (m, 2 H), 1.61 (m, 1 H), 1.80 (m, 1 H), 3.12 (m, 4 H), 3.62 (s, 56 H), 4.06 (s, 1 H), 4.18 (s, 4 H), 5.02 (s, 1 H), 5.50 (s, 1 H), 6.22 (s, 1 H).

**2.2.13. Synthesis of Polyethylene glycol monomethyl ether-tosylate (5):** PEG-350 monomethyl ether (20.00 g, 0.057 mol) was dissolved in sodium hydroxide solution (2.20 g, 0.057 mol). p-Toluene sulfonyl chloride (13.00 g, 0.068 mol) in THF (50.00 ml) was added dropwise in reaction mixture at 0<sup>o</sup>C and reaction was continued for 12 h at room temperature. The product was concentrated under reduced vacuum on a rotary evaporator and residue was further purified by silica gel column using pet ether ethyl acetate (1:1 v/v) as eluent. Yield = 26.00 g (90%). <sup>1</sup>H-NMR (400 MHz, CDCl<sub>3</sub>) δ ppm: 2.44 (s, 3H, -C<sub>6</sub>H<sub>4</sub>-CH<sub>3</sub>), 3.37 (s, 3H, -O-CH<sub>3</sub>), 3.53-3.69 (m, 28H, -O-CH<sub>2</sub>-CH<sub>2</sub>-O-), 4.15 (t, 2H, -CH<sub>2</sub>-CH<sub>2</sub>-O-SO<sub>2</sub>-C<sub>6</sub>H<sub>4</sub>-), 7.32-7.34 (d, 2H, -C<sub>6</sub>H<sub>4</sub>-), 7.78-7.80 (d, 2H, -C<sub>6</sub>H<sub>4</sub>-). <sup>13</sup>C-NMR (100 MHz, CDCl<sub>3</sub>) δ ppm: 58, 68, 69, 70, 71, 127, 129, 132, 144.

**2.2.14. Synthesis of Polyethylene glycol monomethyl ether azide (6):** Polyethylene glycol monomethyl ether-tosylate (15.00 g, 0.029 mol) was taken in 250 mL two neck flask and dissolved in 60.00 mL of dry DMF. Sodium azide (3.80 g, 0.059 mol) was added in above mixture and reaction was refluxed under nitrogen for 12 h. Excess solvent was distilled by vacuum distillation and residue was filtered by whatman filter paper to get brown colour liquid. Yield = 10.20 g (99%). <sup>1</sup>H-NMR (400 MHz, CDCl<sub>3</sub>) δ ppm: 3.37 (s, 3H, -O-CH<sub>3</sub>), 4.38 (t, 2H, -O-CH<sub>2</sub>-CH<sub>2</sub>-N<sub>3</sub>), 3.52-3.67 (m, 28H, -O-CH<sub>2</sub>-CH<sub>2</sub>-O-). <sup>13</sup>C-NMR (100 MHz, CDCl<sub>3</sub>) δ ppm: 50.47, 58.85, 61.36, 69.85, 70.36, 71.73, 72.38.

**2.2.15. Synthesis of Polyethylene glycol monomethyl ether amine (7):** Lithium aluminium hydride (3.80 g, 0.102 mol) was dissolved in 50.00 mL of freshly dried THF and purged with

nitrogen for 15 min. A suspension of Polyethylene glycol monomethyl ether azide (10.00 gm, 0.028 mol) in freshly dried THF (15.00 mL) was added dropwise in above mixture at 0°C and reaction was continued for 6 h under nitrogen atmosphere. The reaction mixture was neutralized at ice cold condition with saturated KOH (2.00 gm in 10.00 mL) solution and filtered by whatman filter paper. The filtrate was concentrated by rota evaporator to get brown coloured product. Yield = 8.80 g (89.2) %. <sup>1</sup>H-NMR (400 MHz, CDCl<sub>3</sub>) δ ppm: 2.82 (t, 2H, -O-CH<sub>2</sub>-CH<sub>2</sub>-NH<sub>2</sub>), 3.36 (s, 3H, -O-CH<sub>2</sub>-CH<sub>2</sub>-O-CH<sub>3</sub>), 3.48 (t, 2H, -O-CH<sub>2</sub>-CH<sub>2</sub>-NH<sub>2</sub>), 3.52-3.67 (m, 28H, -O-CH<sub>2</sub>-CH<sub>2</sub>-O-). <sup>13</sup>C-NMR (100 MHz, CDCl<sub>3</sub>) δ ppm: 41.64, 58.87, 61.41, 70.13, 70.34, 70.40, 71.77, 72.49, 73.30.

**2.2.16. Synthesis of PEG substituted amphiphilic L-lysine polyurethane (APU):** Monomer (**8**) and (0.50 g, 0.8 mmol) 1,12-dodecanediol (0.17 g, 0.8 mmol) and titanium tetrabutoxide (1.0 mol %) were taken in a test tube shaped polymerization setup and subjected for polycondensation following similar procedure as described for **P-EH**. The polymer is purified by dissolving in THF and re-precipitate in methanol. <sup>1</sup>H-NMR (400 MHz, CDCl<sub>3</sub>) δ ppm: 1.27 (m, 15 H), 1.51 (m, 2 H), 1.60 (m, 4 H), 1.79 (s, 6 H), 3.15 (s, 2 H), 3.38 (s, 3 H), 3.45 (m, 2 H), 3.57 (m, 3 H), 3.66 (m, 22 H), 4.03 (m, 4 H), 4.13 (s, 1 H), 4.99 (s, 1 H), 5.57 (s, 1 H), 7.03 (s, 1 H). <sup>13</sup>C-NMR (100 MHz, CDCl<sub>3</sub>) δ ppm. 21.39, 22.30, 25.74, 29.15, 29.21, 29.37, 29.44, 32.66, 37.65, 39.17, 40.23, 54.45, 56.84, 58.82, 58.88, 64.78, 64.85, 67.15, 69.57, 69.96, 70.05, 70.37, 70.39, 70.79, 156.88, 156.93, 174.25. FTIR (cm<sup>-1</sup>) 3322, 2927, 2864, 1728, 1531, 1451, 1451, 1364, 1220, 1098, 795.

**2.2.17. Optical transmittance measurement:** The optical transmittance of all the samples was measured by using PerkinElmer Lambda 45 UV-visible spectrophotometer connected with temperature controlled peltier system. The concentration of polymer was maintained as 1.0 mg/mL. The heating cycle was recorded by continuous heating from 20 °C - 80 °C, similarly cooling cycle was recorded by continuous cooling from 80 °C - 20 °C.

**2.2.18. Encapsulation of anticancer drugs in the polymer nanoparticles:** Anticancer drug doxorubicin was encapsulated using dialysis method. DOX.HCl was neutralized with tri-ethyl amine prior to use. 5.0 mg of polymer and 0.5 mg of doxorubicin were dissolved in 2.0 mL of DMSO. 3.0 mL of deionized water was added dropwise to above solution and stirred for 4 h in dark. This solution was transferred into dialysis membrane (MWCO 1kD) and dialyzed against milli-Q water for 48 h. Fresh milli-Q water was replaced periodically to remove the un-

encapsulated drug. To measure the encapsulation efficiency 200 $\mu$ L of dialysed solution was diluted upto 2.0 mL with milli Q water and absorbance at 510 nm was measured by UV spectrophotometer. DLC and DLE were calculated by using following formulae.

$$\text{DLE (\%)} = \{ \text{weight of drug in NPs} / \text{weight of drug in feed} \} \times 100$$

$$\text{DLC (\%)} = \{ \text{weight of drug in NPs} / \text{weight of polymer taken} \} \times 100$$

**2.2.19. In vitro drug release studies:** DOX loaded APU nanoparticles were employed to study the drug release behaviour of the new class of polyurethanes using horse liver esterase enzyme. In order to accomplish this, the DOX loaded nanoparticles dispersed in PBS (3.0 mL) were taken in a Spectro-chem dialysis bag of cut off 1 kD, keeping the concentration as 1.0 mg/mL. To understand the behaviour of the polymeric nanoparticles under the hydrolytic enzyme rich environments of the lysosomes of the cells the similar experiments were carried out under the presence of the horse liver esterase enzyme under the mentioned set up. The effect of the enzyme on the polymeric architecture reflected on the escape of the loaded drug into the reservoir and therefore, at specific time interval 2.0 mL of PBS was withdrawn from the reservoir and its absorbance was measured. The PBS withdrawn for the measurement was replaced back into the reservoir in order to ensure the concordant concentration throughout the experiment. To mimic the physiological conditions, as a control, the dialysis tube was immersed in PBS buffer solution and incubated at 37 °C, and similar reading were procured at the same time intervals. The amount of release of the DOX from the polymeric nano-carrier cavity was recorded as the intensity of the absorbance of DOX at  $\lambda$  510 nm. This intensity was plotted as relative concentration with respect to the initial DOX concentration, against the time to generate the release profile of the APU DOX loaded nanoparticles in presence and absence of Esterase enzyme at 37°C. The thermo-responsive behaviour of the APU nanoparticles were studied using the similar approach of dialysis tube immersed in PBS solution. These solutions were maintained at 42 °C and 37 °C to simulate the cancer tissue environment and physiological environment at *in vitro* level. The release of the loaded cargoes were plotted against time using similar approach as that of enzyme release and the plots were generated against time. The relative amount of drug released during the experiment was calculated using the following equations:

The amount of drug released at time 't' was calculated by using following equation:

$$\text{Cumulative drug release} = \{ [\text{Amount of drug released at time 't'}] / [\text{Total amount of drug in nanoparticles taken in dialysis tube}] \} \times 100.$$

**2.2.20. Cell viability assay (MTT assay):** The toxicity of the APU polyurethane nanoparticles were studied as a function of cell viability in MCF 7 (cancerous cells) and WT-MEF (normal cells) using 3-(4,5-dimethylthiazol-2-yl)-2,5-diphenyltetrazolium bromide (MTT) assay. The typical experiment involved exposure of various concentrations of the polymeric nanoparticles to a fixed number of cells for a specific time period to study their toxicity effect. Sterile 96 well plate was seeded with a cell density 1000 cells per well in 100  $\mu$ L DMEM (with 5% FBS) and incubated at 37°C for 16 h for cell growth. Further these cells were revealed to various concentrations (ranging from 1.0 – 80.0  $\mu$ g/mL) of the nascent polymeric nanoparticles. Further, they were incubated at 37 °C for 72 h. The cells were prepared for the MTT assay, by aspirating the media and replacing it with freshly made MTT 100  $\mu$ L (0.5mg/mL in DMEM containing 5 % FBS) solution, and further incubated for 4 h at 37 °C to let the MTT react to the living cells. MTT solution was then aspirated and 100  $\mu$ L of DMSO was added to each well to dissolve the formazan crystal formed after reduction of MTT by mitochondrial dehydrogenase enzyme from the living cells. Further, the absorbance from purple colour formazan crystals was measured using a micro plate reader at 570 nm (Varioskan Flash) and the triplet readings were plotted by taking their mean against the concentration of the polymer nanoparticles. The cell killing as a function of cell viability was carried out by the same experimental procedure for various concentrations of the free DOX and polymer nanoparticles loaded with DOX with concentration of DOX maintained at 0.1 – 1.0  $\mu$ g/mL respectively. Same experimental procedure was followed as that of the nascent polymer, and plots were reported.

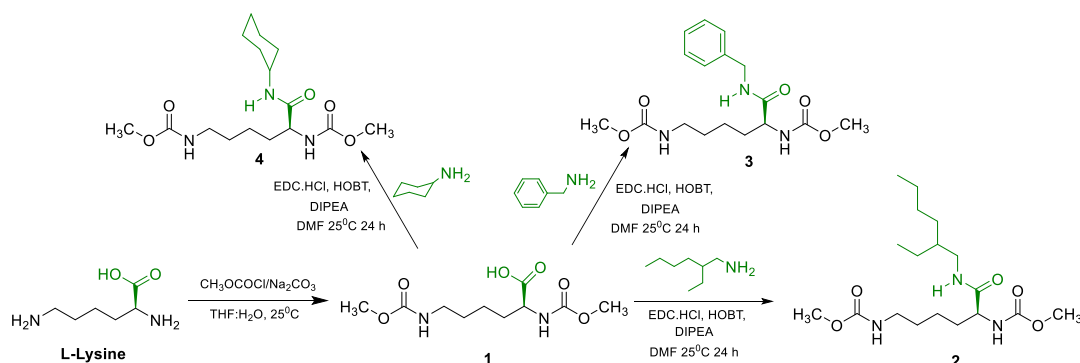
**2.2.21. Live cell imaging experiments:** The internalization of the free DOX and polymer loaded with DOX inside the cells via endocytosis was studied using lyso tracker dye for staining the lysosomal compartments of the cells. In a representative experiment, an 8-well live chamber was seeded with  $2.5 \times 10^4$  MCF 7 cancer cells in each well, and were incubated and grown for 16 h at 37 °C. Followed by aspiration of the media, DOX loaded APU, free DOX were administered to the cells at a concentration of 2.0  $\mu$ g/mL of DOX in fresh media and continued the cell incubation for 4 h. The media was aspirated and cells were washed with PBS (2.0 mL) once, 50.0 nM Lyso tracker® Green DND-26 in fresh media was exposed to the cells. The live cells were immediately imaged using confocal laser microscope (CLSM). The DOX and lyso-tracker were excited at 561 nm and 488 nm respectively and they were imaged in the red and green channel respectively.

**2.2.22. Flow Cytometry Measurements:** The quantification of uptake of DOX in free as well as the confined in core of APU nanoparticles in MCF 7 cells were studied using FACS analysis. Typically, a 6-well plate was employed and seeded with MCF 7 cells (at a density of  $1 \times 10^5$  per well), and incubated and grown for 16 h at  $37^\circ\text{C}$ . This was followed by aspiration of media and were exposed to free DOX and APU nanoparticles loaded with DOX, keeping the concentration of DOX ( $2.0 \mu\text{mL}$ ) correspondingly. After the exposure for 9 h the media was aspirated and cells were washed with PBS ( $1.0 \text{ mL} \times 2$ ) to ensure removal of traces of free DOX and nanoparticles that were not taken up by the cells, if any. The cells for observation were further treated with  $500.0 \mu\text{L}$  trypsin enzyme to detach the cells from the 6-well plate walls by incubating at  $37^\circ\text{C}$  for 1.0 min. Further these cell suspensions were centrifuged at 10,000 RPM for 5 minutes and pelletized, resuspended in 1 mL of 1X PBS, and were used for flow cytometric analysis. Prior to each recording, the pellets were vortexed to ensure homogeneous mixing of the cells. BD LSRFortessa SORP cell analyser was employed for carrying out the studies, and were well equipped with five lasers, capable of detecting 18 colours simultaneously. DOX was excited using 561nm laser and detected using a band pass filter of  $610 \pm 10 \text{ nm}$ . Each measurement was carried out at a population of 10000 events per recording.

## 2.3. Results and Discussion.

### 2.3.1. Melt Transurethane Process for L-Lysine Polyurethanes.

The synthesis of L-lysine multifunctional monomers is shown in scheme 2.1. The amine functional group in the L-lysine was converted into urethane (or carbamate) functional group by reacting with methyl chloroformate under basic condition. The carboxylic acid group in compound **1** was masked as amide by reacting with amines such as 2-ethylhexylamine, benzylamine, cyclohexylamine to yield monomers **2**, **3** and **4**, respectively. The structure of the monomers were characterized by  $^1\text{H}$  and  $^{13}\text{C}$ -NMR as shown in Figure 2.5. and Figure 2.6.



**Scheme 2.1.** Synthesis of lysine based di-urethane monomers.

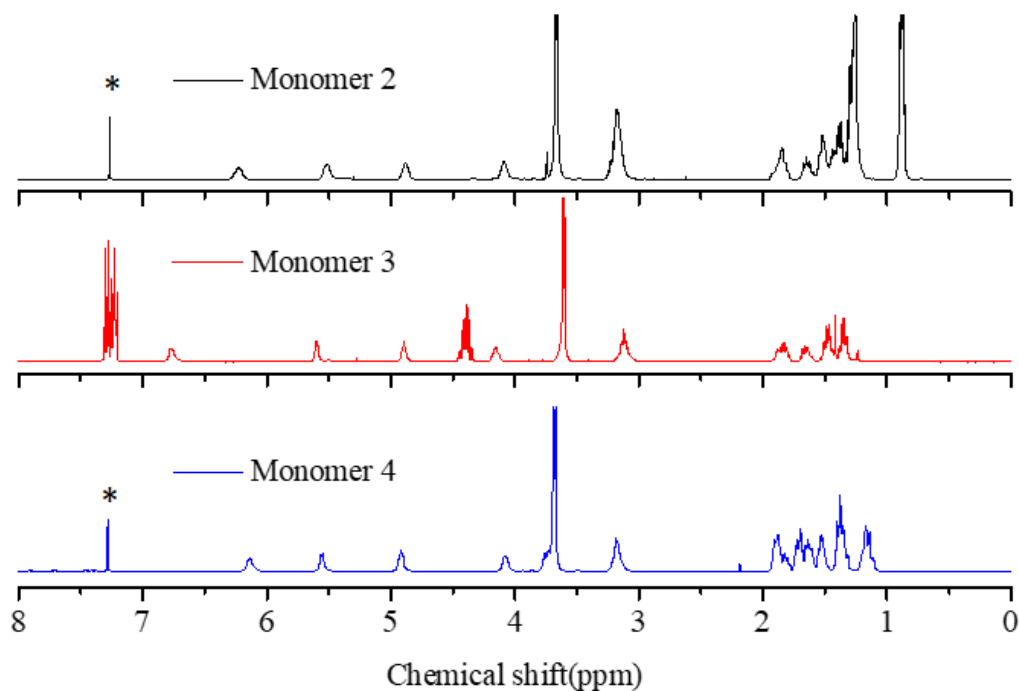


**Figure 2.5.**  $^1\text{H}$  NMR spectra of monomers in  $\text{CDCl}_3$ . The solvent peak is indicated by asterisks (\*).

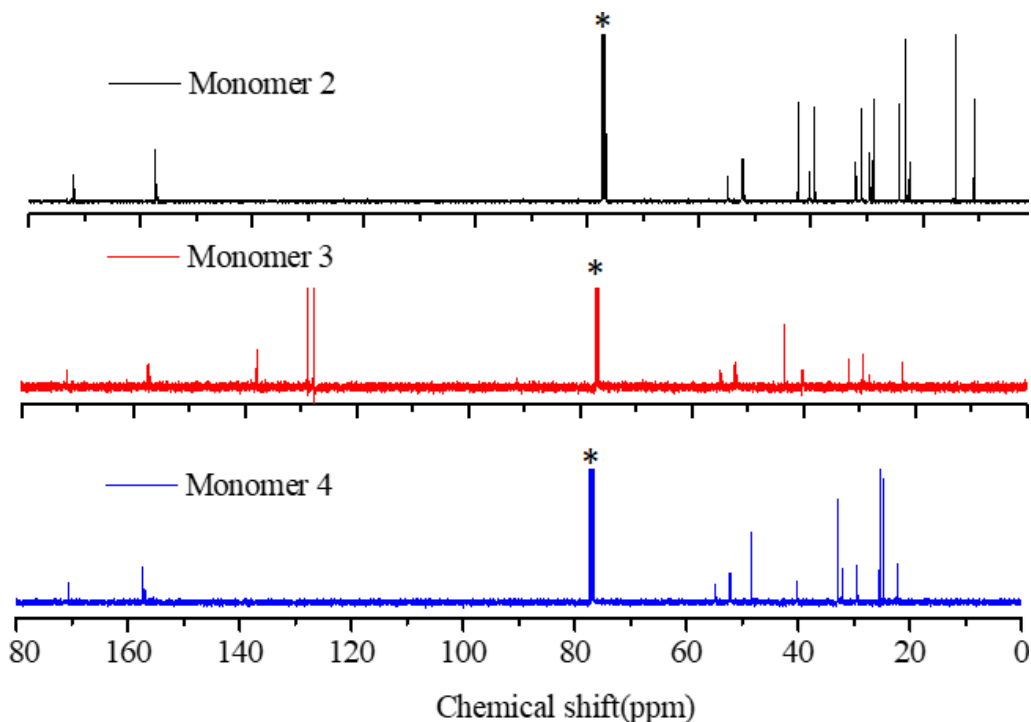
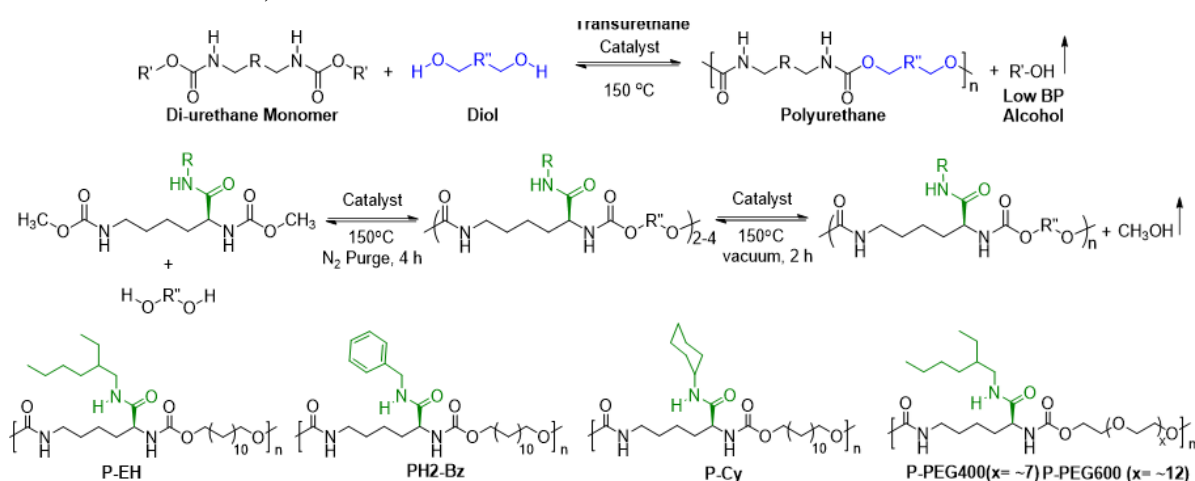


**Figure 2.6.**  $^{13}\text{C}$  NMR spectra of monomers in  $\text{CDCl}_3$ . The solvent peak is indicated by asterisks (\*).

Thermal stability of the monomers was investigated by thermogravimetric analysis and the TGA plots showed that these newly designed monomers were stable up to 250 °C under nitrogen atmosphere which revealed their suitability for melt polycondensation. The melt transurethane polymerization reaction is shown in scheme 2.2. The urethane chemical linkage

(-HN-CO-OR') is a typical combination of half-amide (-HN-CO) and half-ester (-CO-OR); thus, the selective nucleophilic attack at the carbonyl carbon by the R''-OH results in the formation of new urethane linkages (-HN-CO-OR''). This reaction is controlled by both, the type of catalyst as well as the temperature of the reaction<sup>60</sup>. Under the melt conditions, the reaction of di-urethane and diol produces moderate to high molecular weight linear polyurethanes. In this process, low boiling alcohol, typically methanol in the present case was continuously removed from the equilibrium to increase the % conversion. The polymerization was carried out in one-pot but in two steps. In the first step, the monomer and diols were melted at 150 °C along with catalyst (1.0 mole %, Ti (OBu)<sub>4</sub>) and degassed with nitrogen and evacuated under vacuum to make it moisture free. This step was repeated three times and the polycondensation was carried out by stirring at 150 °C for 4 h under nitrogen purge. During this process, the di-urethane monomer reacted with diols to produce oligomers and the methanol was removed from the reaction mixture by the carrier nitrogen gas. In the second step, the resultant melt was subjected for stirring at 150 °C under vacuum (0.01 bar) for 2 h to produce a viscous polymer. The polymers were purified by dissolving in THF and precipitating in methanol to remove the catalysts and other monomeric impurities. The different L-lysine polyurethanes produced under melt transurethane process from monomers (2) to (4) in condensation with 1,12-dodecandiol are shown in scheme 2.2.



**Scheme 2.2.** Synthesis of polyurethanes through melt transurethane polycondensation process and the structures of the L-lysine based polyurethanes.

The polymers are referred as **P-EH**, **P-Bz** and **P-Cy** with respect to the types of amide units in the side chains in monomers (2) to (4), respectively. Polyethylene glycols of molecular weight 400 and 600 g/mol were also polymerized with monomer 2 to produce polyurethanes **P-PEG-**



**400** and **P-PEG-600**, respectively. The structures of these polyurethanes are shown in scheme 2.2.

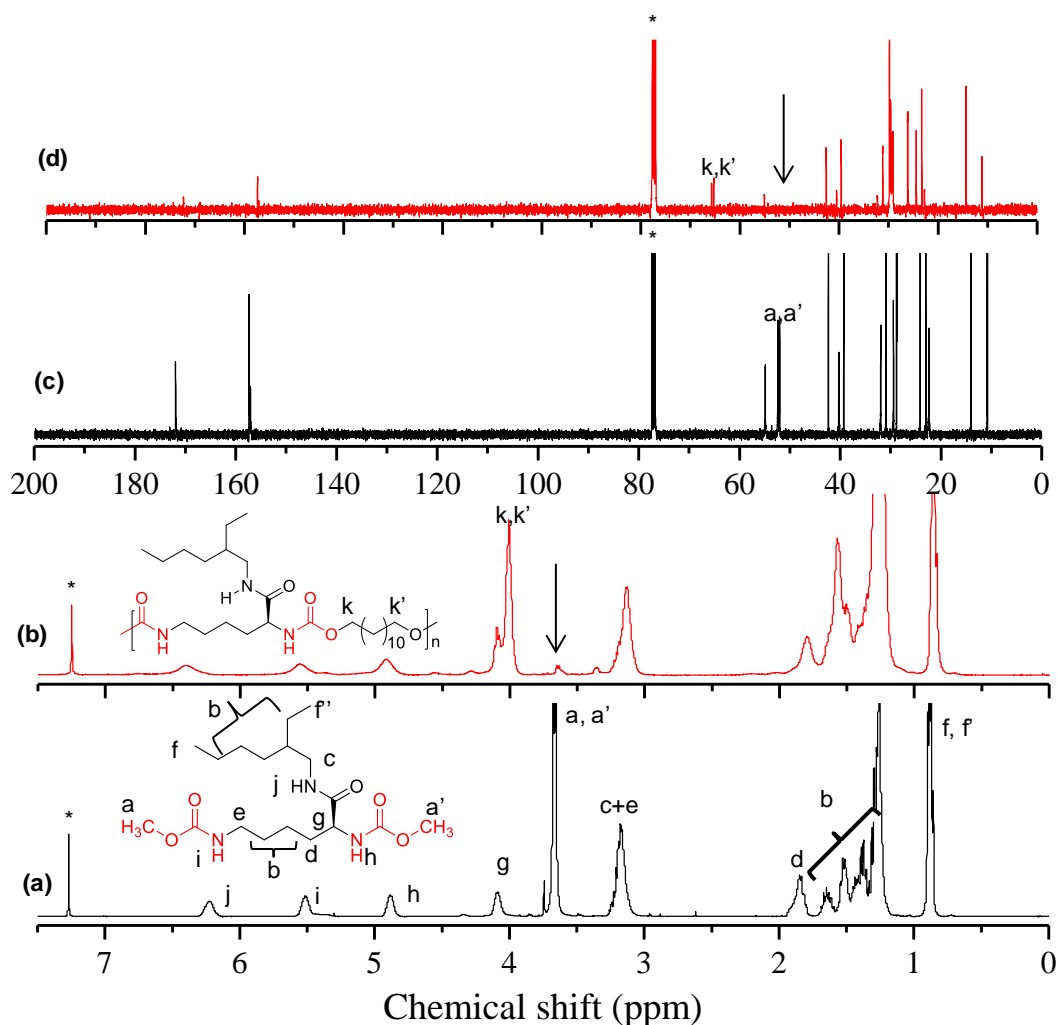


**Figure 2.7.** (a)  $^1\text{H}$ -NMR spectra of monomer **2** and (b) polymer **P-EH** in  $\text{CDCl}_3$ . (c)  $^{13}\text{C}$ -NMR spectra of monomer **2** and (d) polymer **P-EH** in  $\text{CDCl}_3$ . The solvent peaks are shown by asterisks and the different types of protons in the chemical structure are assigned alphabetically with respect to peaks in the NMR spectra. (e) GPC chromatograms of polymers in THF at  $25^\circ\text{C}$ . (f) Table containing molecular weights of polymer determined from GPC and NMR, and glass transition temperature ( $T_g$ ) determined by DSC.

The occurrence of the melt transurethane process in the L-lysine monomer was confirmed by NMR spectroscopy. The  $^1\text{H}$ -NMR spectrum of monomer (**2**) (Figure 2.7.a) showed peaks at 3.65 ppm (proton a and a') with respect to  $\text{R-HN-COOCH}_3$ . Upon polymerization, these peaks disappeared, and new urethane peaks appeared at 4.05 ppm (proton k and k') with respect to the  $\text{R-HN-COOCH}_2\text{CH}_2-$  in the polymer spectrum (Figure 2.7.b). The  $\text{R-CH}_2\text{-NH-CO}$  peak at 3.17 ppm was not disturbed both in the monomer and polymer spectra indicating that the amide unit is inert during the melt-transurethane process.  $^{13}\text{C}$ -NMR

spectrum of monomer showed two peaks at 51.95 and 52.27 ppm with respect to R-HN-COOCH<sub>3</sub> (shown by arrow in Figure 2.7.c) which completely disappeared in the polymer spectrum (Figure 2.7.d). Thus, the disappearance of R-HN-COOCH<sub>3</sub> groups in the monomer (or at the chain ends) and appearance of new peaks for R-HN-COOCH<sub>2</sub>CH<sub>2</sub>- in the polymer spectra confirmed the occurrence of melt transurethane process. Similar NMR spectra analysis was done for other polymers P-Cy and P-Bz, P-PEG-400 and P-PEG-600, and their details are given in the Figure 2.8.

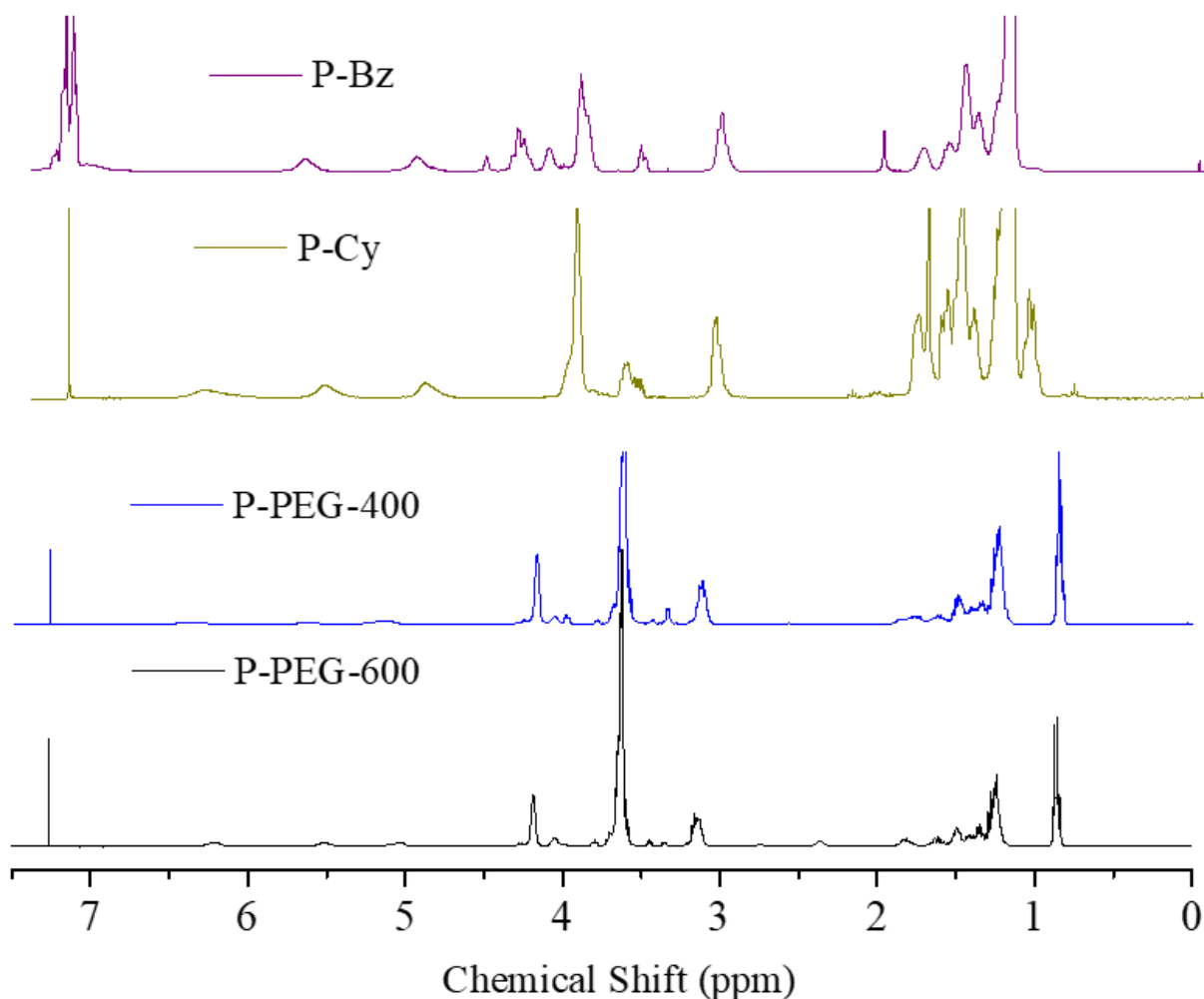


**Figure 2.8.** <sup>1</sup>H NMR Spectra of Polymers in CDCl<sub>3</sub>.

The degree of polymerization  $X_n$  was determined by comparing the integral intensities of the new polyurethane peak for R-HN-COOCH<sub>2</sub>CH<sub>2</sub> at 4.05 ppm with the end groups R-HN-COOCH<sub>3</sub> at 3.65 ppm. The comparison of the peak integrals revealed that the polymer **P-EH** was produced with 30-32 repeating units. The substitution of this value in the Carothers expression:  $X_n = 1/(1-p)$ , gave the extent of the reaction “p” calculated as  $\geq 98\%$ . The number average molecular weights of the polyurethanes  $M_n = X_n \times \text{repeating unit mass}$ , showed  $M_n = 15,000$  g/mol for the polymer **P-EH**. Laboratory level demonstration (1.0 to 2.0 g scale) of new

polycondensation approach with more than 98 % conversion is really good.<sup>30</sup> Thus, it may be concluded that the newly developed melt transurethane process for L-lysine monomers is very robust in producing moderate to high molecular weight L-lysine polyurethanes. The GPC chromatograms of polymers in figure 2.9.a showed mono-modal distribution with respect to the formation of homogeneous molecular weights. The  $M_n$  and  $M_w$  of the P-EH were determined as 8000 g/mol and 16,000 g/mol with polydispersity of 2.0. The  $M_n$  determined by GPC was much lower compared to the  $M_n$  values obtained from  $^1\text{H-NMR}$  analysis ( $M_n = 15000\text{g/mol}$ ) thus, the GPC molecular weights seemed to be relatively underestimated. The molecular weights of polymers are given in table in figure 2.9.b. Among all the monomers, the 2-ethylhexyl amide substituted L-lysine monomer appeared to be good for the melt transurethane process in producing moderate to high molecular weight polymers.

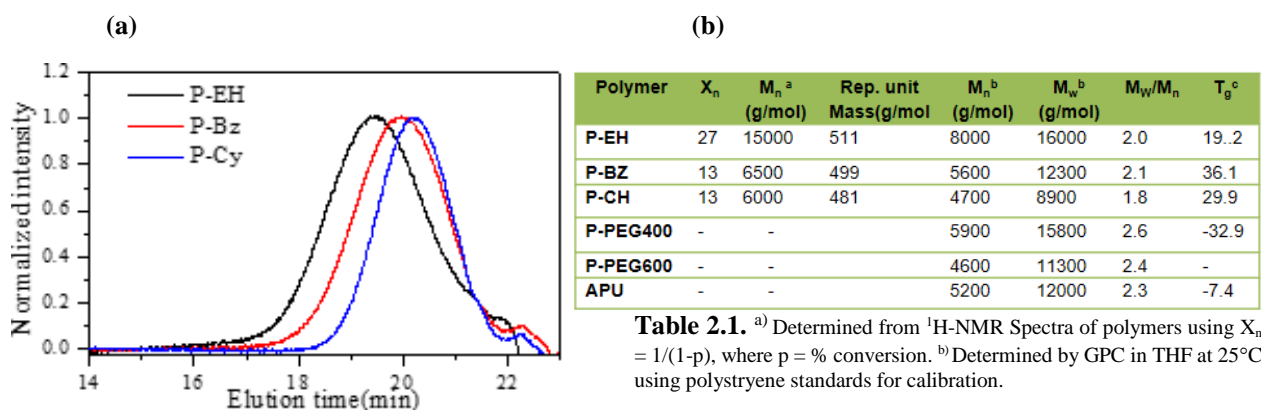


**Figure 2.9.** (a) GPC chromatograms of polymers in THF at  $25^\circ\text{C}$ . (b) Table containing molecular weights of polymers determined from GPC and NMR, and glass transition temperature ( $T_g$ ) determined by DSC.

To study the role of the catalyst on the melt transurethane process, five different catalysts such as  $\text{Ti}(\text{OBU})_4$ ,  $\text{Fe}(\text{acac})_3 \cdot 6\text{H}_2\text{O}$ ,  $\text{LaCl}_3$ ,  $\text{Zn}(\text{OAc})_2$  and  $\text{Cd}(\text{OAc})_3$  were chosen based on our earlier observation in dual ester-urethane condensation process.<sup>60</sup> The polymerization was tested for monomer **2** with 1,12-dodecanediol using 1.0 mole % of catalyst at  $150^\circ\text{C}$ . The molecular weights of the polymers were determined by GPC and the data is summarized in Table 2.2. Among all the catalysts, both  $\text{Ti}(\text{OBU})_4$  and  $\text{Fe}(\text{acac})_3$  produced moderate to high molecular weight polymers. The role of diols on the polymerization process was investigated for monomer (**2**) with 1,6-hexanediol, 1,8-octanediol, 1,10-decanediol and 1,12-dodecanediol. The GPC molecular weights (Table 3) suggested that the long aliphatic diol 1,12-dodecanediol produced higher molecular weight polymers in the melt transurethane process.

**Table 2.2.** Molecular weights of the polymers produced using produced using different catalyst.

Catalyst	M <sub>n</sub> (gm/mol)	M <sub>w</sub> (gm/mol)	PDI
Ti(OBu) <sub>4</sub>	8000	15400	1.9
Fe(acac) <sub>3</sub>	6500	11300	1.7
Zn(OAc) <sub>2</sub>	5900	11000	1.8
Cd(OAc) <sub>2</sub>	3000	4300	1.4
LaCl <sub>3</sub>	2000	2300	1.2

**Table 2.3.** Molecular weights of the synthesized using different diols

Diol	M <sub>n</sub> gm/mol	M <sub>w</sub> gm/mol	PDI
1,12 dodecane	8000	16000	2
1,10 decane	3600	5200	1.4
1,8 octane	3500	4800	1.3
1,6 Hexane	2200	2500	1.2

The kinetics of the polymerization was studied for the polymerization of monomer 2 with 1,12-dodecanediol using 1.0 mole % of Ti(OBu)<sub>4</sub> as a catalyst at 150 °C. Polymer aliquots were taken at various time intervals. The TGA profiles of the aliquots (Figure 2.10.a) suggested that the melt transurethane polymerization typically proceeded towards more thermally stable polymer products with an increase in the reaction time. As the reaction time increases the molecular weight of the polymer also increases. A high molecular weight polymer reaction mixture acquires high thermal stability due to the reduction of end group functionality per unit volume. The GPC plots of the aliquots in Figure 2.10.b confirmed the building up of high molecular weight chains with an increase in the reaction time. The plots of M<sub>n</sub> determined from GPC and NMR showed very good correlation up to the 5000 g/mol (Figure 2.10.c). From NMR it was clear that till 4 h the polymer melt was in oligomeric form. But after 4h, when we apply the vacuum, the equilibrium between reactant and product shifts in a forward direction, resulting in a sudden increase in molecular weight. So when we calculate the molecular weight from NMR (exact molecular weight) it shows a sudden increase in the molecular weight after 4 h. The GPC used to determine the molecular weights was calibrated with Polystyrene standards. There is a large structural variation in polystyrene, and these amino acid-based poly(urethane)s because of this the GPC was underestimating the molecular weights and a discrepancy in the molecular between NMR and GPC arises for higher reaction time.

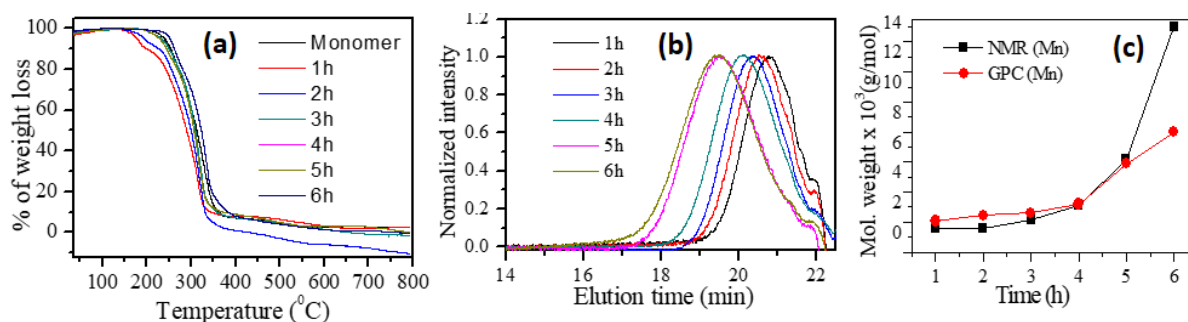


**Figure 2.10.** (a) TGA Profile of the polymer aliquots are taken at different time interval in the transurethane reaction of monomer (2) with 1,2-dodecadiol. (b) Gel permeation chromatograms

of aliquots taken at different time interval for P-EH polymerization kinetic study in tetrahydrofuran at 25 °C. (c) Comparison of molecular weight determined from GPC and NMR.

The polydispersity of the aliquots  $M_w/M_n$  was obtained in the range of 1.9 to 2.7. The polydispersity was increasing with extent of reaction because, In the case of condensation polymerization, the polydispersity is given by the expression  $X_w/X_n = 1+P$  where “P” is the percent conversion or extent of the reaction. So as the P increases (higher percentage conversion) the polydispersity also increases..

MALDI-TOF mass spectroscopy analysis of polymer end groups were further explored to study the thermal stability of urethane and hydroxyl functional groups in the polymer chains during the melt transurethane process. Typically, the A-A + B-B polymerization process is known to produce three types of end groups in the polymer chains: A-P<sub>n</sub>-A, B-P<sub>n</sub>-B, A-P<sub>n</sub>-B and macrocyclic P<sub>n</sub>. The peaks in the MALDI-TOF spectra were estimated for these different types for these different types of species as shown in Figure 2.11. In the aliquot sample 2 (after 2 h of N<sub>2</sub> purge), all three types of end groups were visible for A and B functionality There are two important facts that are clear from the MALDI-TOF analysis: (i) both the urethane and hydroxyl functional groups at the chains ends were clearly visible and it suggested that they were very stable in the melt process, and (ii) there is no evidence for the macro-cycle formation, which is feasible for proceeding the polycondensation process to yield high molecular weight linear polyurethanes.

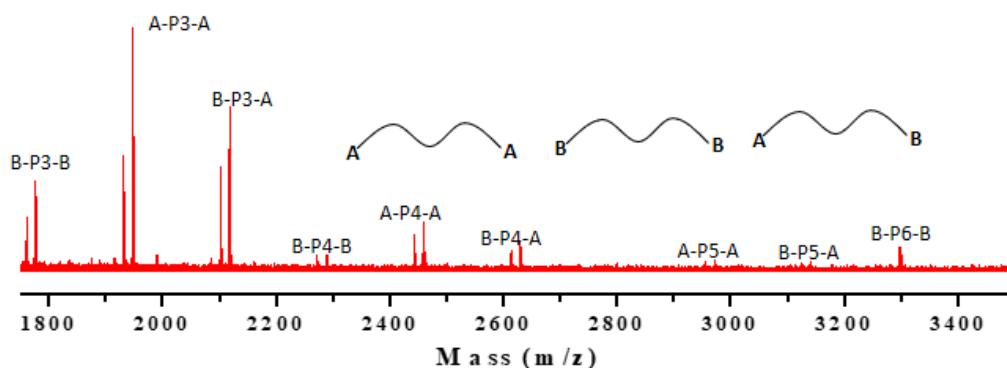


**Figure 2.11.** MALDI-TOF spectrum of P-EH polymer aliquots after 2 h.

Thus, based on the above studies, it may be concluded that the melt transurethane process is very good methodology for producing linear polyurethanes based on L-amino acid resources. To study the thermal properties of the polymers, they were subjected to TGA and DSC analysis under N<sub>2</sub> atmosphere. DSC plots in Figure 2.12.b showed glass transition temperature with respect to amorphous nature of the polyurethanes. The T<sub>g</sub> of the polymers (see table in Figure 2.9) were found to significantly vary with respect to their structure. The polymers with benzyl amide side chain was found to exhibit higher T<sub>g</sub> compared to 2-

ethylhexyl amide side chains and this was attributed to the possibility of strong hydrogen bonding interaction facilitated by the pendant groups. The introduction of flexible PEG chains in the backbone induced a higher degree of flexibility which reduced the  $T_g$  below  $-30\text{ }^\circ\text{C}$ . The TGA plots of the polymers showed thermal stability up to  $250 - 280\text{ }^\circ\text{C}$  (Figure 2.12.a). Hence, it may be concluded that the newly designed L-lysine based aliphatic polyurethanes are moderate to high molecular weights, thermally stable and their thermal properties such as  $T_g$  could be tuned by choosing appropriate amide pendants.

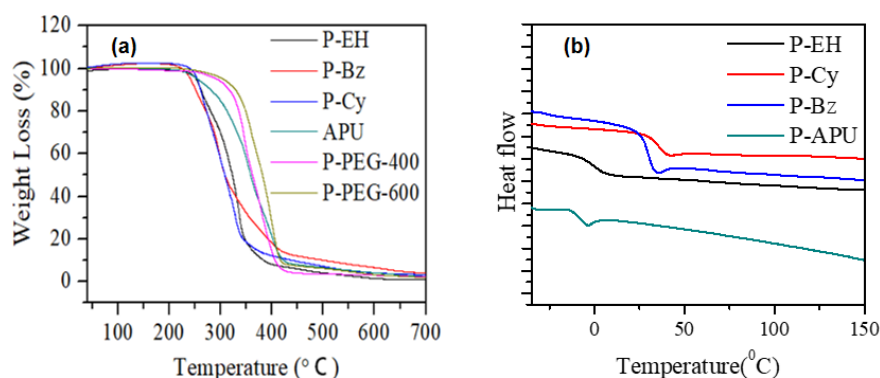
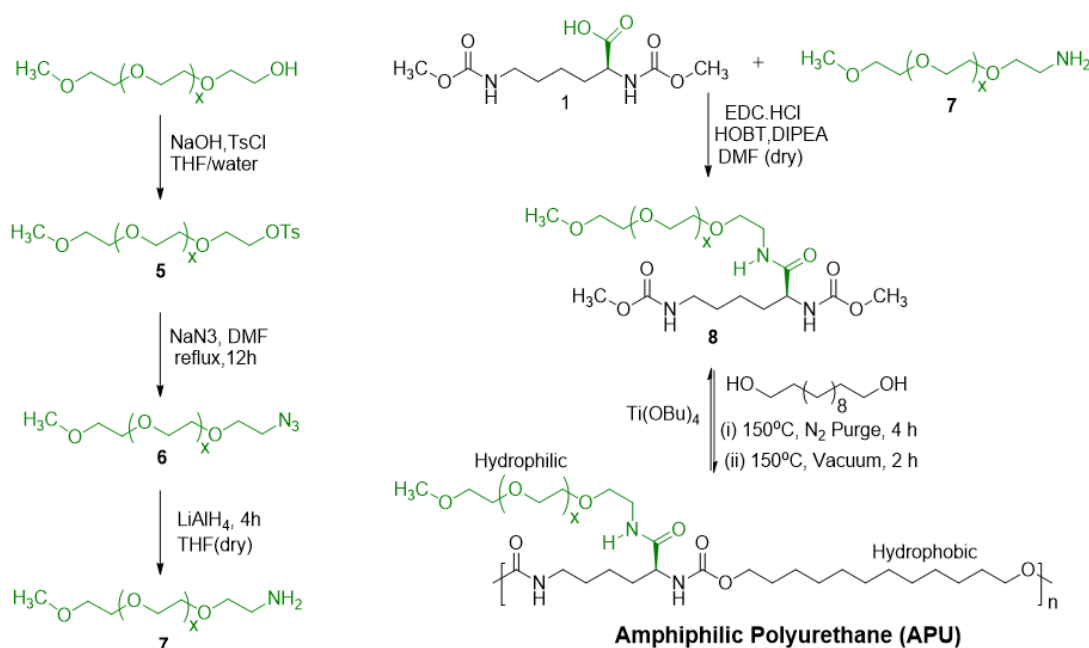


**Figure 2.12** (a) TGA Profile of Polymers. (b) DSC thermograms of polymers.

### 2.3.2 Amphiphilic Polyurethanes (APU)

Having established the melt transurethane process for L-amino acid-based polyurethanes; attempts were made to synthesize amphiphilic L-lysine polyurethanes to demonstrate their capabilities in drug delivery application.



**Scheme 2.2.** Synthesis of polyurethanes through melt transurethane polycondensation process and the structures of the L-lysine based polyurethanes

For this purpose, the carboxylic acid functional group in the L-lysine part in compound (1) was anchored with polyethylene glycol monomethyl ether of molecular weight 350 g/mol as shown in scheme 2.2. The hydroxyl chain end in MeO-PEG<sub>350</sub>-CH<sub>2</sub>OH was converted into MeO-PEG<sub>350</sub>-CH<sub>2</sub>OTs (compound 5). It was converted into MeO-PEG<sub>350</sub>-CH<sub>2</sub>N<sub>3</sub> azide (compound 6). The azide was reduced to yield amine MeO-PEG<sub>350</sub>-CH<sub>2</sub>NH<sub>2</sub> amine (compound 7). The reaction of amine (7) with compound (1) yielded amphiphilic L-lysine monomer (8). The structure of monomer (8) was confirmed by <sup>1</sup>H and <sup>13</sup>C-NMR (Figure 2.13.a). MALDI-TOF spectrum of the monomer showed peaks with respect to repeating unit mass CH<sub>3</sub>O-(CH<sub>2</sub>CH<sub>2</sub>O)<sub>n</sub>-CH<sub>2</sub>CH<sub>2</sub>NH-CO-Lysine monomer (8) and exactly matched with expected structure.

The polymerization of monomer (8) with 1,12-dodecanediol yielded amphiphilic polyurethane (APU). The structure of the polymer was confirmed by <sup>1</sup>H and <sup>13</sup>C NMR spectroscopy (Figure 2.13.b) and the molecular weights were determined by GPC. APU was found to be thermally stable up to 250 °C and the DSC profile showed amorphous trend with T<sub>g</sub> at -7.4 °C (see table 1 in figure 2.9.b).

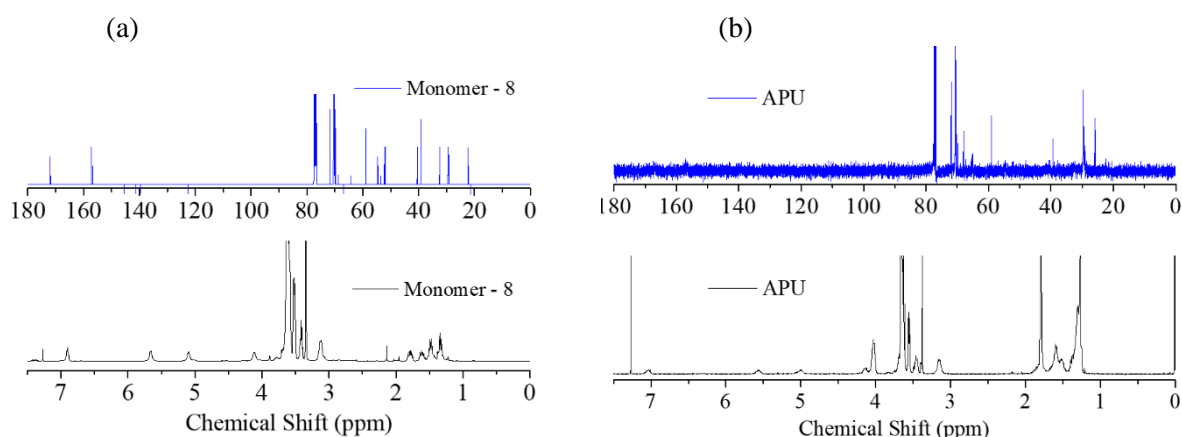


**Figure 2.13.** (a) <sup>1</sup>H and <sup>13</sup>C -NMR Spectra of monomer (8) in CDCl<sub>3</sub>. (b) <sup>1</sup>H and <sup>13</sup>C -NMR Spectra of APU in CDCl<sub>3</sub>.

The APU has a unique structural feature to self-assemble in water, the hydrophobic polyurethane backbone tends to bend inwards away from water and the PEG chains are projected outside toward the aqueous medium. The segregation of hydrophilic and hydrophobic segments in the APU yielded hair-pin type of polymer amphiphiles which underwent self-assembly to produce polymer nanoparticles in aqueous medium (2.14.a). The nanoparticles possessed well-defined hydrophobic core and PEG in the periphery to produce core-shell type nanoparticles. The APU nanoparticles were produced by dialysing the polymer in DMSO +

water combination for 48 h using a semi-permeable membrane with MWCO = 1.0 kD. Dynamic light scattering of the dialyzed APU solutions showed the formation of  $180 \pm 10$  nm nanoparticles in water 2.14.b. Atomic force microscopic analysis of aqueous dialysed solution on mica-support revealed the existence of  $180 \pm 10$  nm spherical nanoparticles. Field emission scanning electron microscopic images further confirmed the formation of  $180 \pm 10$  nm spherical nanoparticles. All the above three independent techniques confirmed the self-assembly of APU spherical nanoparticles in aqueous medium. The critical micelle concentration of the APU nanoparticles was determined using pyrene as probe. Typically,  $0.6 \mu\text{M}$  concentration of Pyrene was dissolved in acetone and was added to vials and the solvent was evaporated<sup>61</sup>. The concentration of the polymer solution was varied from  $34.0 \mu\text{g/mL}$  to  $0.82 \mu\text{g/mL}$  and the solutions were sonicated and equilibrated for 12 h. The pyrene encapsulated solutions were purged with nitrogen for 30 minutes and subjected to fluorescence measurements (2.14.c).

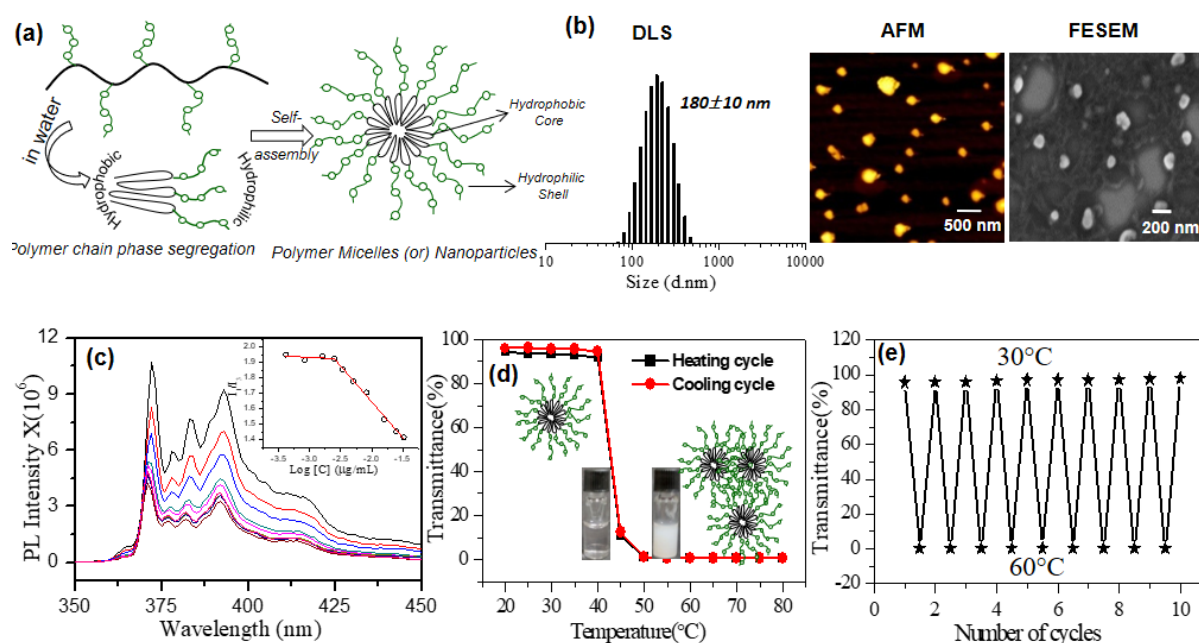


**Figure 2.14.** (a) Self-assembly of amphiphilic polyurethane (APU) into core-shell nanoparticles. (b) Dynamic light scattering (DLS) histogram, atomic force microscopy (AFM) image and FE-SEM image of APU nanoparticles. (c) Critical micellar concentration of APU nanoparticles determined by Pyrene probe in water. The plot of  $I_1/I_3$  is shown as inset. (d) Plot showing % transmittance for the thermo-responsiveness of APU nanoparticles in water in heating and cooling cycles. (e) Plot showing the change in the % transmittance of APU nanoparticles in ten consecutive heating and cooling at 30 and  $60^{\circ}\text{C}$ . The concentration of the polymer was maintained as  $1.0 \text{ mg/mL}$  for % transmittance measurement



The  $I_1/I_3$  values are plotted and shown as inset in Figure 2.14.c and from the break point, the CMC of the APU nanoparticle was estimated  $\sim 5.0 \mu\text{g/mL}$ . The CMC of the APU was comparable to that of other L-amino acid based aqueous nanoparticles.<sup>14,28</sup> The APU nanoparticles showed very unique thermo-responsive behaviour upon heating by transforming from clear to turbid solution. In the subsequent cooling cycle, the turbid solution turned back to clear solution. The plots of % transmittance at different temperatures of cooling and heating cycles are shown in figure 2.14.d. The lower critical solution temperature (LCST) of the APU nanoparticles was determined as 40-42°C. .

Further, the dynamic light scattering histograms of the APU nanoparticles showed significant size change from 200 nm to 600 nm upon heating; confirming the aggregation of nanoparticles. Based on this, the model for the APU polymer nanoparticles aggregation is shown in figure 2.15. The plots did not show any hysteresis indicating that the self-assembly is perfectly reversible in nature. The % transmittance measured at consecutive heating and cooling at 30 and 80 °C in ten cycles (see Figure 2.14.e) showed perfect reproducibility and reversibility of the nano-aggregates.

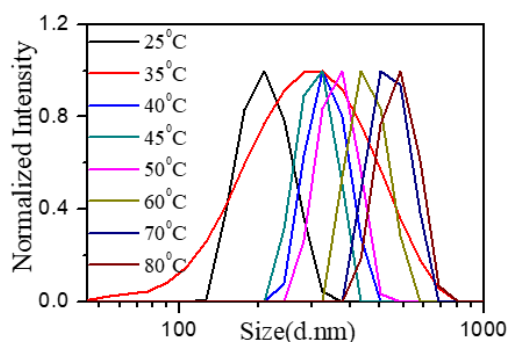


**Figure 2.15.** DLS histograms of APU nanoparticle at various temperatures

To study the encapsulation capabilities of APU nanoparticles, hydrophobic anticancer drug doxorubicin was selected to be loaded in the APU nanoparticles. In a typical experiment, 5.0 mg of polymer and 0.5 mg of pre-neutralized doxorubicin was stirred in 2.0 mL of DMSO + 3.0 mL of Milli Q water. The mixture was allowed to stir in dark at room temperature for 4 h. The mixture was transferred to 1.0 kD dialysis bag and dialysed against Milli Q water for 48 h. The drug encapsulation efficiency (DLE) and drug loading content (DLC) was estimated by absorption spectroscopy as 35.0 % and 3.5 %, respectively. The DLE and DLCs are comparable to that reported for typical polymer nanoparticles.<sup>28,62</sup> Different groups have reported different encapsulation methods, such as nano-precipitation, sonication and dialysis method. The typical dialysis method includes dissolving amphiphilic polymer in a good solvent in presence of the

cargo (soluble in the good solvent) and dialysing it against large volume of water (acting as a bad solvent). This forces the amphiphilic polymer chains collapse into nano-assemblies yielding hydrophobic domains ideal for encapsulation of cargoes of interest. The dialysis method ensures removal of any un-encapsulated cargo, and it seems to be one of the best ways to produce stable nanoparticles<sup>61,62</sup>. The reproducibility of the drug loading content reported by the dialysis method in the present study was checked for more than 18 months with multiple independent drug loading experiments and the data was perfectly reproducible. Attempts were also made to employ sonication method for encapsulation of the drug. However, substantial amount of the drug was found to precipitate from nanoparticle aqueous solution after 72 h and the DLC was estimated to be < 2.5 %. Further attempts on structural-optimization on L-lysine based polyurethane may help to enhance the DLC and DLE. The DLS histogram of DOX-loaded APU nanoparticle is shown in Figure 2.16.a

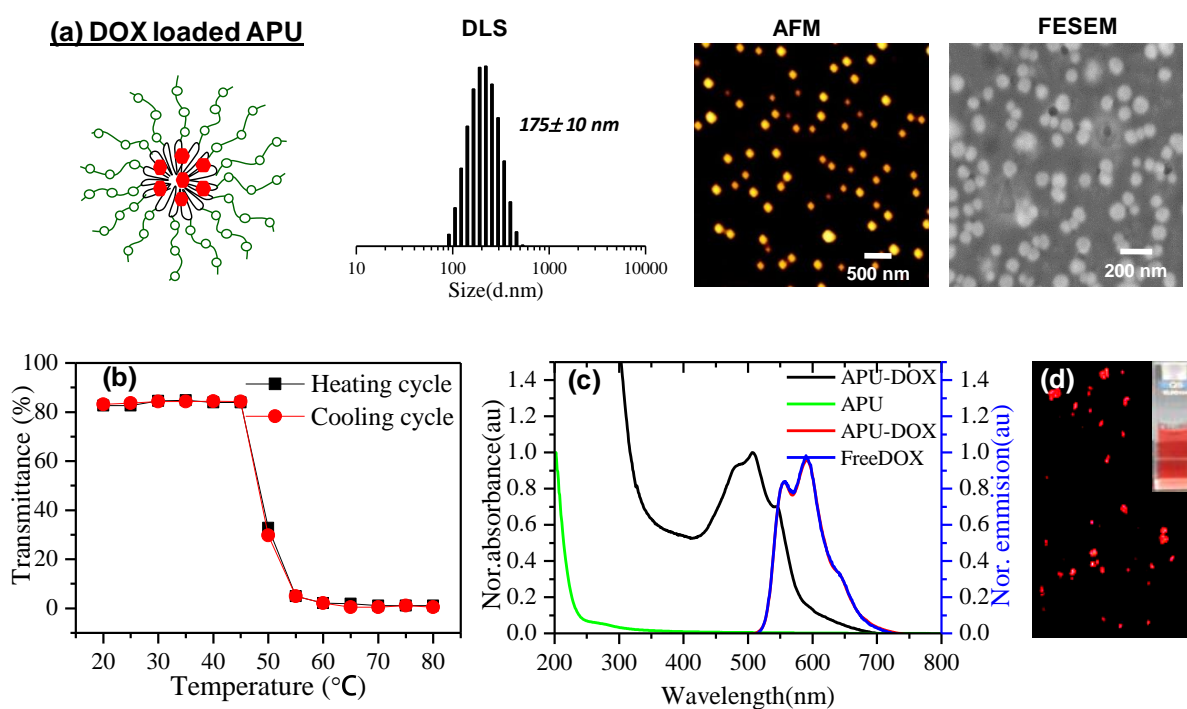


**Figure 2.16.** (a) Schematic representation of DOX-loaded APU nanoparticle, DLS histogram, and AFM and FESEM images of DOX-loaded APU nanoparticle. (b) Transmittance of DOX-loaded APU nanoparticle in the heating and cooling cycle. (c) Absorbance and emission spectra of free DOX and DOX-loaded APU nanoparticle. (d) Fluorescence microscope image of DOX-loaded APU nanoparticle.

The DLS histogram showed mono-modal distribution having size around  $175 \pm 10$  nm which was further confirmed by AFM and FESEM (see Figure 2.16.a). DLS showed the size of the polyurethane nanoparticles before and after DOX encapsulation as  $180 \pm 10$  nm (see Figure 2.14.a) and  $175 \pm 10$  nm (see Figure 2.16.a), respectively. The polymer nanoparticles

are produced by the chain folding of hydrophobic polymer backbone away from the aqueous medium and it constitutes the hydrophobic pocket at the core of the nanoparticles as shown in Figure 2.14.a. Since the chains are expected to be present in the highly entangled state within the hydrophobic pockets, it still persists enough cavity or vacant space to occupy the drug molecules which are relatively smaller in size compared to that of the core of nanoparticles.

This attributes to the retention of the size of the nanoparticles even after encapsulation of drug molecules within the experimental error bar of  $\pm 10$  nm. Thus, the size of the nanoparticles did not change much during the DOX encapsulation. These all results collectively confirmed the formation of spherical nanoparticle and these APU nanoparticles retained their size and morphology even after loading of anticancer drug doxorubicin. To study the thermoresponsive behavior, DOX-loaded APU nanoparticles were subjected for transmittance studies (Figure 2.16.b). It is clear that the nanoparticles retained their thermo-responsive behavior after the drug loading. Since doxorubicin is fluorescent in nature so these DOX-loaded nanoparticles were subjected for photophysical studies. The absorbance spectra of DOX-loaded APU nanoparticle showed absorption maxima at 510 nm and emission maxima at 610 nm corresponding to DOX (see figure 2.16.c). The absorption and emission spectra of free DOX and DOX-loaded APU nanoparticle was found to be same suggesting that DOX preserved its characteristic properties. Figure 2.16.d shows the fluorescence microscopy image of APU DOX nanoparticle drop casted on glass slide and the inset shows the DOX stabilized APU nanoparticle.

### **2.3.3. Thermo- and Enzyme-responsive Drug Releases**

It is proven now that the cancer tissues have slightly higher temperature compared to normal tissues due to the faster proliferation and *increased* metabolic activity.<sup>63</sup> Thermo-responsive polymer nano-carriers are particularly important and are used to exploit this higher temperature of cancer tissues; since the polymer nano-carriers have advantage of accumulating passively through enhance permeability and retention (EPR) effect.<sup>64</sup> The thermo-responsiveness further enhances the accumulation and delivery of drugs due to the collapsing of the chains above LCST from the solution. Hence, the thermo-responsive polymers having LCST closer to 42-43 °C are very useful for drug delivery to cancer cells.<sup>65</sup>

To check the thermo-responsive release of doxorubicin from APU; DOX-loaded APU nanoparticles were incubated at two different temperatures in PBS buffer at pH=7.4 at 37 °C (normal body temperature) and at 42 °C. The cumulative drug release profile is shown in Figure

2.17.a. APU nanoparticles showed < 25% drug release at 37 °C. At 42 °C more than 90 % DOX was released in less than 10 h.

These results suggest that APU nanoparticles are stable under normal physiological

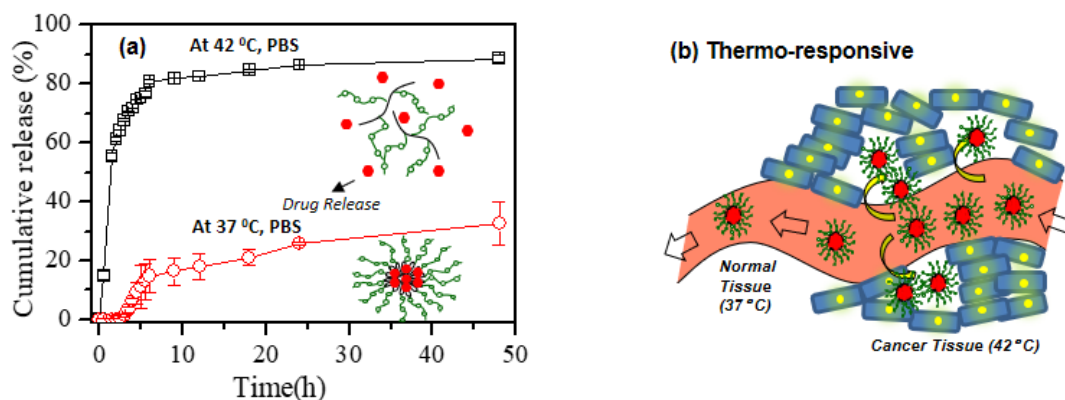


**Figure 2.17.** (a) Cumulative drug release profile at 37°C and 42 °C in PBS. (b) Schematic representation of nanoparticle accumulation in cancer tissue from blood vessel.

conditions (at 37 °C, PBS) and underwent changes above LCST at 42 °C to release DOX. This study envisages that the thermo-responsive nano-particles could accumulate largely at the cancer tissue environment due to the collapsing and phase separation of the nano-carriers above LCST. This concept is schematically shown in Figure 2.17.b. This allows the retaining of the nano-carriers reasonably for longer duration so that they could be taken across the cell membrane via endocytosis process. Once they cross the cancer tissue environment, they would undergo transformation at physiological temperature and become completely dispersed in the transport medium without any phase separation (below LCST).

This type of reversible phase separation process would allow the enhancement of nano-carriers concentration at the cancer tissue environment which is only feasible by thermo-responsive carriers in passive targeting protocols. The premature release of the nanoparticles in PBS (< 30 %) is not resultant of the polydispersity or variation in the molecular weight of the polymers rather, this is attributed to the effect of salts present in the PBS on the self-assembled nano-objects by the Hofmeister effect as earlier shown in thermoresponsive polymer nanoassemblies.<sup>66</sup>

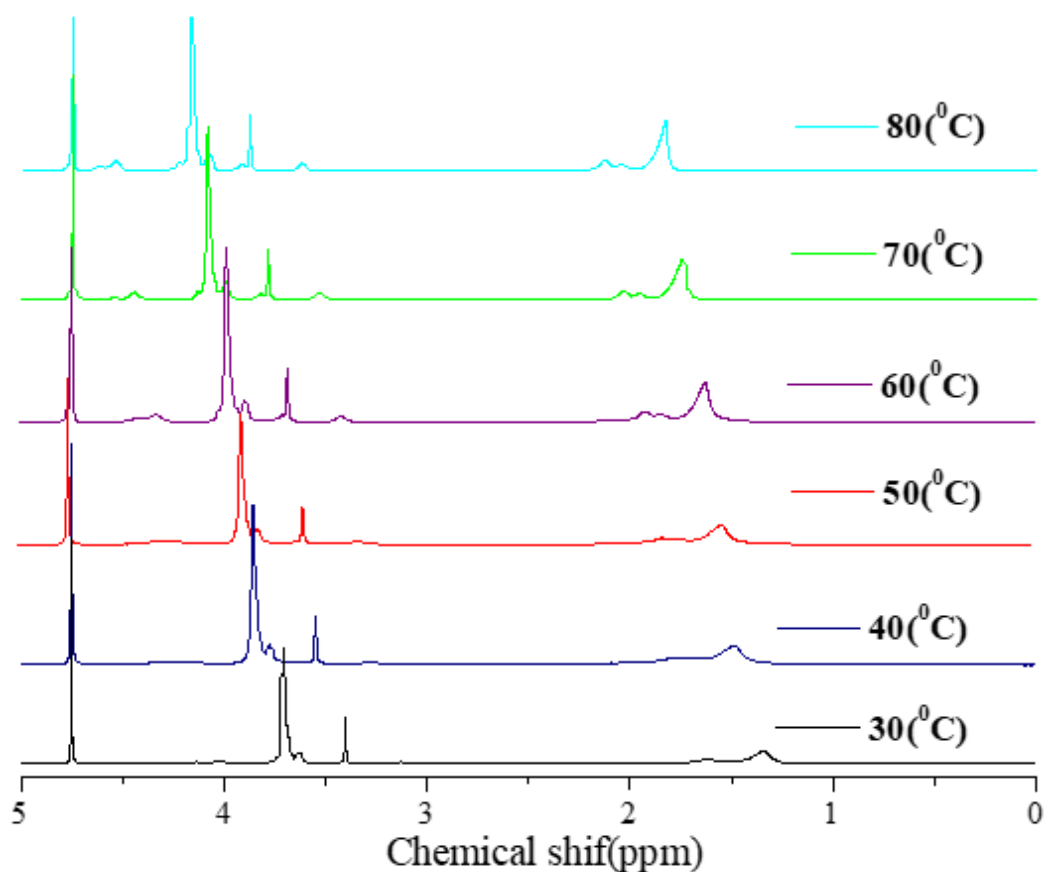


**Figure 2.18.**  $^1\text{H-NMR}$  spectra of APU in  $\text{D}_2\text{O}$  solvent in the heating cycle at various temperatures. The sample was recorded from 30 °C to 80 °C.

Though there is no appropriate *in vitro* or *in vivo* models that are currently available to test the hypothesis directly; however, it is worth to report the thermo-responsive polymer nano-carriers with a controlled release which may have significant influence on the long-term impact in cancer treatment. The mechanism for the thermo-responsiveness of APU was further studied by variable temperature  $^1\text{H-NMR}$  studies from 30 to 80 °C in  $\text{D}_2\text{O}$  in the heating cycle and subsequent cooling from 80 to 30 °C (see Figure 2.18). Below LCST the hydrogen bonding between water molecule and oxygen of polyethylene glycol (intermolecular hydrogen bonding) is dominant due to which the PEG chains are in highly hydrated state. The complete dispersion of nanoparticle in  $\text{D}_2\text{O}$  medium leads to globular confirmation of nanoparticle. The PEG pendants in the nano-assemblies are exposed to the solvent environment whereas the polymer backbone is buried in the interior of the nano-particles which has limited exposure to the solvent.<sup>65</sup> As a result, below 40 °C, the signals from the PEG part are clearly visible above 3.6 ppm compared to the polymer aliphatic proton signals at 1.5 to 2.0 ppm. At higher temperature (above LCST), the intermolecular hydrogen bonding between PEG chains and water molecule gets disturbed due to which the polymeric chains undergo phase separation in  $\text{D}_2\text{O}$ . Above

LCST, the PEG chains no longer shields the polymer backbone; thus, the closer contact of the polymer backbone in D<sub>2</sub>O medium enhances the NMR signal intensity at 1.5 to 2.0 ppm. The elevation in <sup>1</sup>H-NMR signal intensity at 50 to 80 °C for hydrophobic segment indicates that the nanoparticles undergo morphology transformation from globular to open chain confirmation. This transformation accounts for the release of loaded drug above LCST. A slight change in chemical shift was observed for each proton which is because chemical environment of molecules has a large effect on chemical shift so, as the chemical environment will change the chemical shift will also change. The chemical environment of self-assembled (APU nanoparticle) is changing with temperature, so it is showing an effect on chemical shift also.

Aliphatic urethane (or carbamate) linkages are reported to enzymatically biodegrade under physiological conditions and mechanism of the cleavage of the urethane linkages is similar to that of the aliphatic esters.<sup>59</sup> Lysosomal esterase enzyme is one of the highly active serine-protease enzyme at the intracellular level and accounts for the large number of the polymer degradation in drug delivery.<sup>61-62</sup> The bio-degradation of the APU nanoparticles across the cell membrane via esterase enzyme has been shown schematically in Figure 2.19.b.

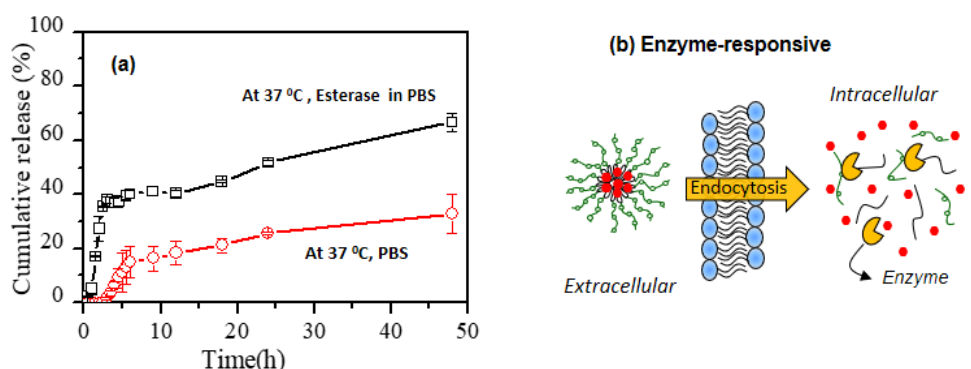


**Figure. 2.19.** (a) cumulative drug release profile of DOX loaded nanoparticle in presence and in absence of esterase enzyme at 37 °C in PBS buffer. (b) Schematic representation of drug release of DOX loaded APU nanoparticle at the intracellular level by esterase enzyme.

This was selected to study the enzymatic biodegradation of the DOX loaded APU nano-carriers. The sample was incubated in PBS buffer at 37 °C and the drug release profiles were studied by dialysis method using absorption spectroscopy and the drug release profile has been shown in figure 2.19.a. The DOX loaded sample was taken in semi-permeable membrane dialysis tube having with MWCO 1.0 kD and drug release in the reservoir was monitored. In PBS buffer at 37 °C (in the absence of enzyme) only less than 20 % drug leaching was observed even after 24 h. This observation revealed that the APU nanoparticle was stable and preserves the drug in high concentration under extracellular conditions. When the APU nanoparticle was incubated with 10 U esterase enzymes in PBS at 37 °C, about 70 % drug was released in

controlled manner. This study clearly proves that the custom designed aliphatic polyurethanes are readily enzymatically-biodegraded exclusively at the intracellular level to release the loaded drug DOX.

#### 2.3.4. Cytotoxicity of APU Nanoparticle.

The biocompatibility and cytotoxicity of the L-lysine based APU nanoparticles were tested by carrying out various biological studies. The bio-compatibility in terms of toxicity of APU polyurethane nanoparticles were studied as cell viability in MCF 7 by the (MTT) assay as explained in the experimental section. The APU concentration was varied from 1.0  $\mu\text{g/mL}$  to 80.0  $\mu\text{g/mL}$  for testing the cytotoxicity of the polymer to cells, and the relative cell killing is shown in figure 2.20, which suggests that the newly designed APU nanoparticle was non-toxic to cells up to 80.0  $\mu\text{g/mL}$  and exhibits high biocompatibility as good as 100 %. Cytotoxicity of DOX-loaded APU nanoparticles were compared and tested by varying the DOX concentration ranging from 0.1  $\mu\text{g/mL}$  to 1.0  $\mu\text{g/mL}$  in both MCF 7 and WT-MEF cell lines. In MCF 7 cell line (see Figure 2.20), both the free DOX and DOX-loaded APU exhibited  $\text{IC}_{50}$  values  $\sim 0.4$   $\mu\text{g/mL}$  which is in accordance with the literature values for free DOX and newly designed polymer nano-carriers. Interestingly, in WT-MEF cells (see Figure 2.20), the DOX-loaded APU exhibited much lower cell killing compared to free DOX. The cytotoxicity studies confirmed that the newly designed APU nanoparticle is suitable for delivering DOX in breast cancer cell line.

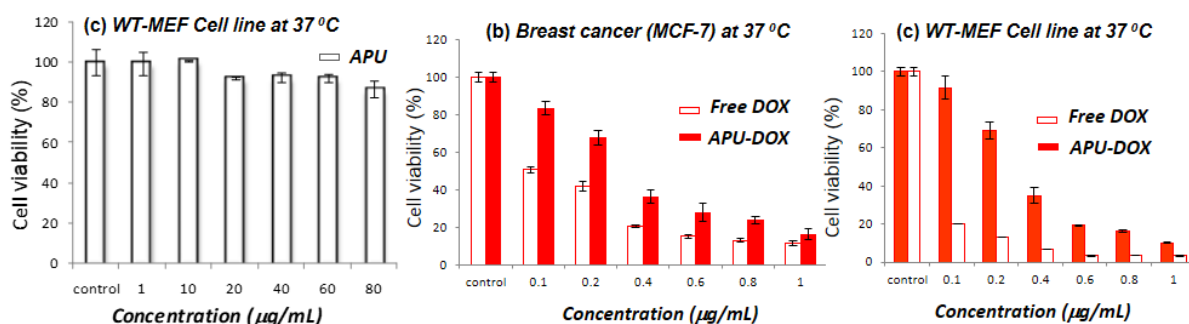


**Figure.2.20.** Cytotoxicity of APU in WT-MEF cell line., free DOX and DOX-loaded APU nanoparticle in MCF 7 and WT-MEF cell line.

**2.3.5. Cellular Uptake and confocal imaging.** Further to demonstrate the cellular uptake of free DOX and DOX-loaded nanoparticles, confocal scanning laser microscopy (CSLM) assisted imaging was carried out for the MCF 7 cell line. The cells were incubated with free DOX and DOX-loaded nanoparticle at 37 °C for 9 h and the nucleus was stained with DAPI ( $\lambda_{exc} = 405 \text{ nm}$ ) and monitored at blue channel, and the cytoskeleton was stained with phalloidin ( $\lambda_{exc} = 488 \text{ nm}$ ) and visualised through green channel.

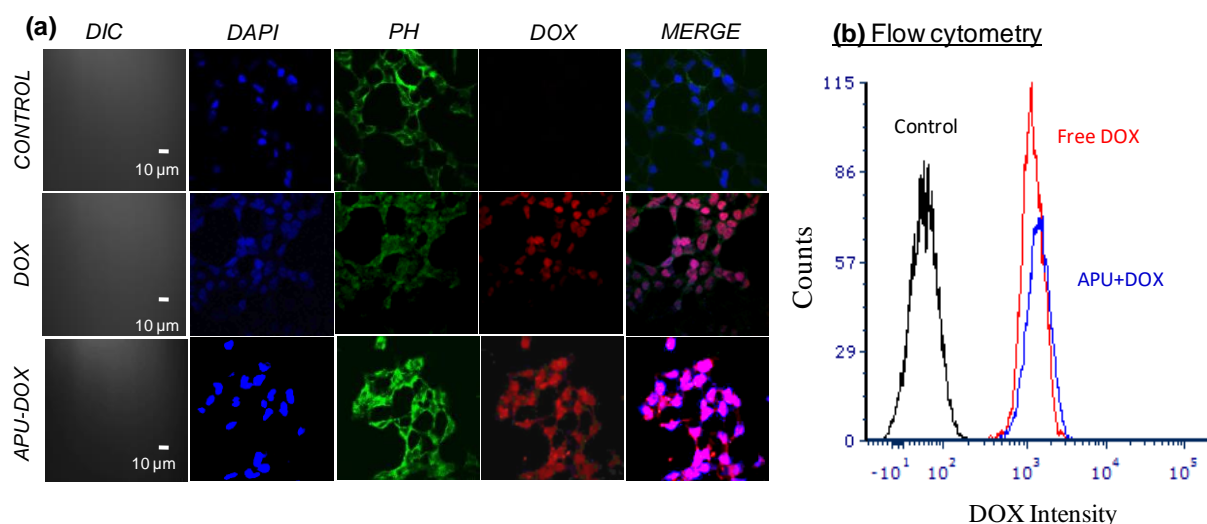


**Figure 2.21.** (a) CLSM images of free DOX and DOX-loaded APU nanoparticle incubated for 4 h in fixed MCF 7 cells. The merged images are shown for the blue (DAPI) and red (DOX) channels together. (b) Flow cytometry plot for control, free DOX, DOX-loaded APU nanoparticles in MCF 7 cell lines (9h) incubation, DOX concentration = 2.0  $\mu\text{g/mL}$  and 10,000 cells were counted).

The panel in Figure 2.21.a corresponding to free DOX clearly showed that the free DOX preferentially accumulated in nucleus which was further confirmed by magenta colour of nucleus in merged image (due to selective blue staining of DAPI in nucleus). While in the panel for merged image showed dispersion of magenta colour in nucleus and red colour in cytosol suggesting that the nanoparticle is getting cleaved in cytosol and DOX was getting subsequently delivered to nucleus. The difference in cellular uptake of free DOX to DOX-loaded nanoparticle was further quantified by flow cytometry analysis see Figure 2.21.b. The histogram corresponding to DOX loaded nano-particle showed maxima which is 2-fold higher than that free DOX. From these results, it is evident that APU nanoparticles were able to deliver higher amounts of DOX anti-cancer drugs to the cells compared to free counterpart suggesting their use as ideal candidates for delivery of anticancer drug DOX.



### 2.3.6. Live-cell Imaging.

Live cell imaging of MCF 7 cell lines was carried out to understand the mechanism of uptake of APU nanoparticles loaded with the luminescent DOX as well as the free DOX. As anticipated, to prove that internalisation of the nanoparticles via endocytosis, the aid of Lyso tracker® Green DND-26 was taken, which are highly efficient dyes used for staining the acidic compartments of cells (mostly the endosomes and the lysosomes). As mentioned in the experimental section a typical experiment involved growing of cells in an 8-well live cell chamber at 37 °C and exposing them to required amount of free DOX and DOX-loaded nanoparticles for 4 h. The cells' endosomal and lysosomal compartments were further stained with the lyso tracker green prior to imaging. For DOX molecules, the cells were excited at laser 561 nm and imaged in red channel, and for the lysotracker imaging the cells were excited at 488 nm and imaged under green channel. Figure 2.22 shows representative live cell confocal (CSLM) microscopy images.

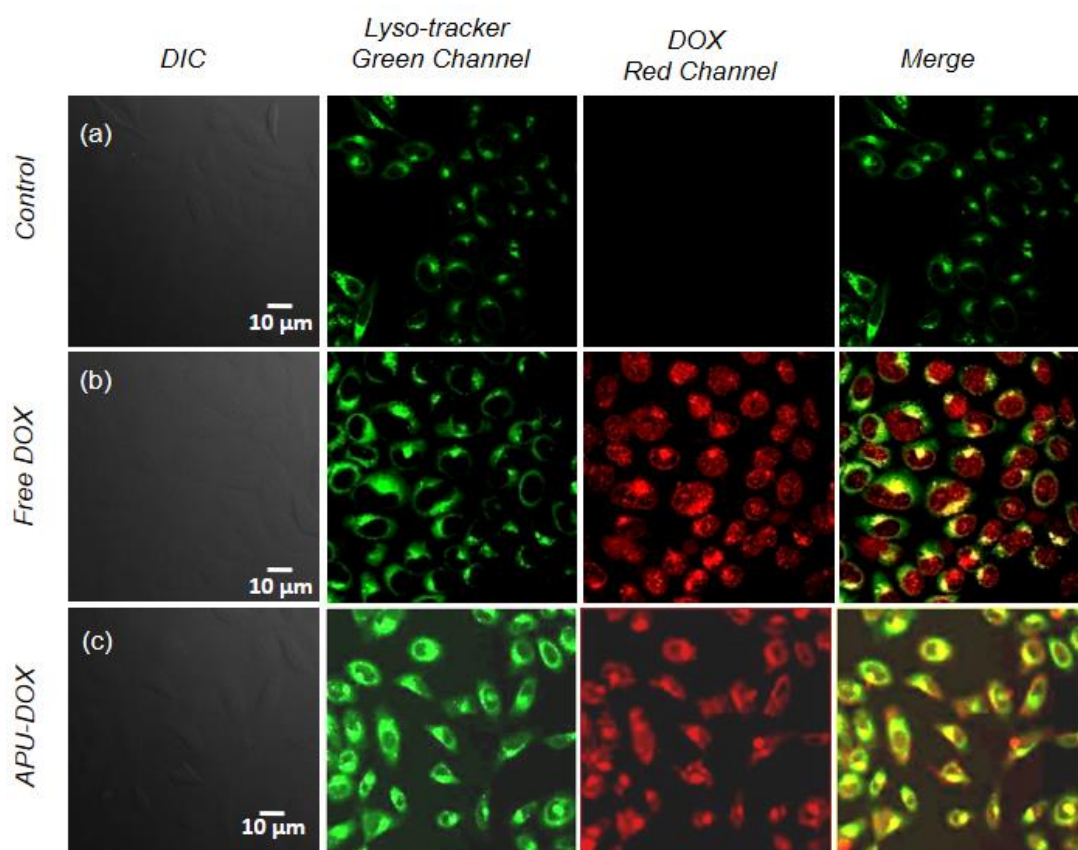


**Figure 2.22.** MCF 7 live cell confocal microscope imaging. (a) With lysotracker, (b) free DOX along with lysotracker and (c) DOX loaded APU along with lysotracker [4 h incubation, DOX concentration = 2.0  $\mu\text{g/mL}$ ]

The panel in first row shows the images corresponding to the presence of lysosomes at the intracellular level which are illuminated in bright green colour. In panel b, the images corresponding to free DOX (as mentioned in figure 2.22.b), the red emission was predominantly observed from the nuclear region and the merged image showed very less overlap of green and red emission suggesting the non-involvement of endocytosis in the case of free DOX. This suggested the small size DOX molecules accumulated in the cells via a diffusion process. On the other hand, the APU loaded DOX nanoparticles demonstrated a different pathway for entry of the nanoparticles as the red emission of DOX was also observed from the perinuclear region and in the cytosol of the cells. Interestingly, the APU nanoparticle shown in merged panel (Figure 2.22.c) confirmed the colocalization of DOX in lysosomal compartments in the merged images as the red and green color gave a bright yellow merger. The presence of DOX in the lysosome and the nuclear regions suggested that the nanoparticles were taken up by endocytosis and cleaved in the lysosomal compartment to trigger the DOX release which was subsequently delivered to the nucleus. This live-cell imaging study supports the enzymatic biodegradation mechanism of the L-lysine based aliphatic polyurethane nanocarriers.

Endocytosis of polymer nanoparticles across the cell membrane is an energy driven process; thus, variable temperature cellular uptake studies were carried out at 4 °C, 37 °C and 42 °C using the APU-DOX nanoparticles. At 4 °C, slower rate or absence of ATP to ADP conversion (exothermic process) at the intracellular level indirectly slowdown or suppress the transportation of nano-carriers across the cell membrane. On the other hand at physiological temperature (at 37 °C), the endocytosis is facilitated by the expenditure of energy associated with the ATP-to-ADP conversion<sup>69,70</sup>. Further, the APU is also thermo-responsive nano-carrier; and hence, the cellular uptake of APU-DOX at 37 °C and 42 °C would provide direct evidence for the effect of thermo-responsive disassembly of the nano-carriers below and above the APU LCST temperature, respectively. For this purpose, the APU-DOX samples were dispersed in media at 25 °C and then administered to the cells. The cells were further incubated at 4 °C on ice, 37 °C and 42 °C (in CO<sub>2</sub> incubator) for 4h; subsequently they were fixed for confocal microscope imaging. The microscopic images of the APU-DOX uptake at 4 °C, 37 °C and 42 °C are shown in Figure 2.23.a and the corrected total cell fluorescence intensity with respect to DOX at the intracellular level was estimated by Image J software and plotted in Figure 2.23.b. It is quite clear from the images that the endocytosis of APU-DOX was not significant at 4 °C whereas almost 8-fold enhancement in the uptake of the APU-DOX

nanoparticles under physiological temperature (at 37 °C) was observed. This clearly supports that the APU-DOX nanoparticles were taken up via the endocytosis process. Confocal microscope images at 42 °C incubation exhibited significant enhancement in the DOX uptake compared to 37 °C.

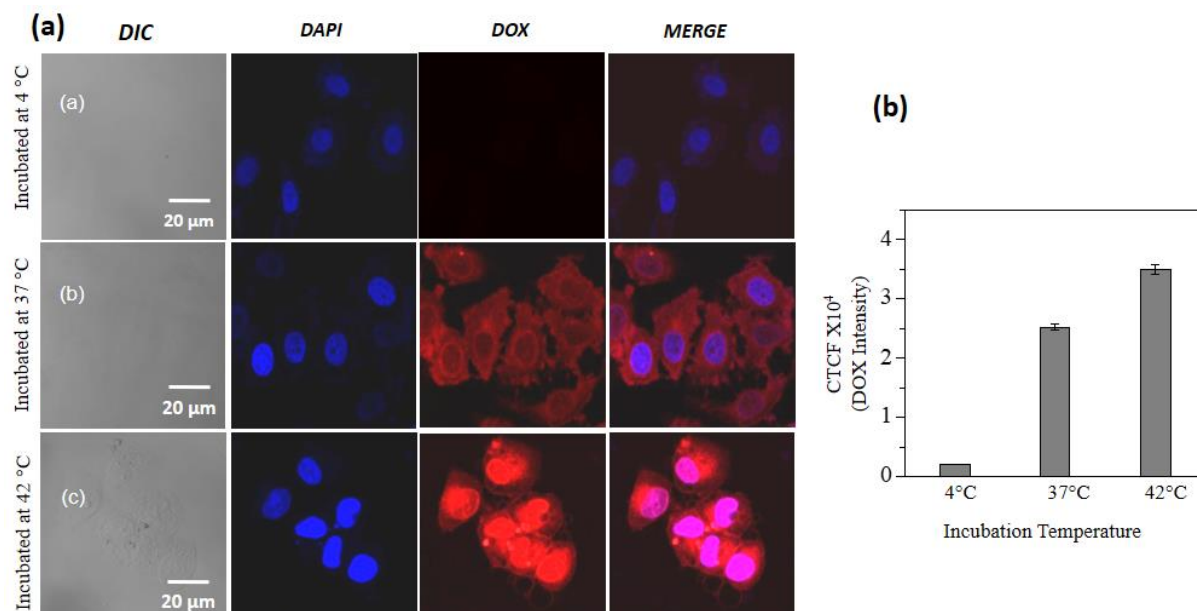


**Figure.2.23.** (a) Confocal microscope images of MCF 7 cell line exposed to APU DOX nanoparticles, incubated at variable temperature. (b) plot demonstrating corrected total cell fluorescence of DOX against the incubation temperature. The APU-DOX was administered to MCF 7 cells at 25 °C and then the cells were incubated at desired temperature (4 °C, 37 °C and 42 °C) [incubation time = 4 h, DOX concentration = 2.0 μg/mL].

This experiment is directly evident for the thermo-responsive disassembly of APU nanoparticles above LCST for more DOX release. From the cumulative drug release data for thermo-responsive delivery at 42 °C and esterase enzyme release data at 37 °C. It is obvious that the thermal stimuli exhibited much faster release of DOX (< 5 h) compared to slow release by the lysosomal esterase enzyme (~ 12 h). This implies that, disassembly of the APU nanoparticles at cancer tissue temperature is much faster than the bio-degradation by the lysosomal esterase enzyme at the intracellular level (at 37 °C). The comparison of APU DOX uptake in merged images (Figure 2.23.c) at 42 °C was higher than that of 37 °C which supported the above observation of the drug release kinetics by these thermo and enzyme dual stimuli responsiveness. Further, the cells corresponding to 42 °C incubation showed the DOX co-localisation with DAPI stained for the release of DOX at the cytosol and subsequent DOX intercalation of DNA in the nucleus.

Two more control experiments were carried out to confirm the thermo-responsive behaviours of APU nanoparticles. For this purpose, (i) the APU-DOX nanoparticle was

incubated at 37 °C for 2 h (below LCST) and at 42 °C for 2h (above LCST) prior to administrating to the cells. In these experiments, initial incubation of APU-DOX nanoparticles at 37 °C would reflect the stability of the nanoparticles similar to extracellular matrix under physiological conditions.

The incubation of APU nanoparticles at 42 °C would represent the exposure of APU-DOX at cancer tissue temperature environment.<sup>57</sup> In the latter case, the APU nanoparticles tend to undergo disassembly (as seen in Figure 2.17.a) and the resultant solution is expected to have both the free DOX (produced by the disassembly of APU) as well as APU-DOX nanoparticles.

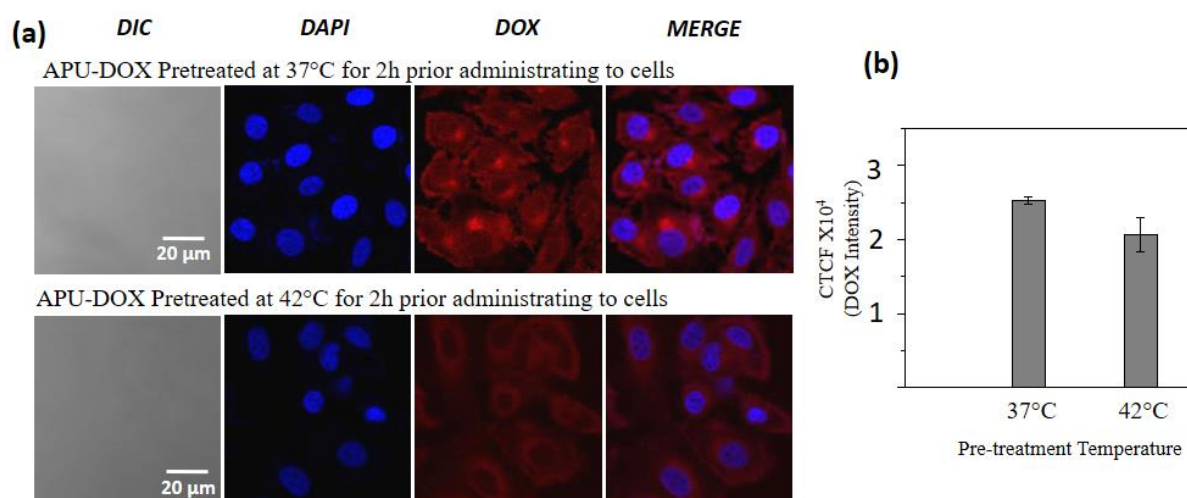


**Figure 2.24.** (a) Confocal microscope images of MCF 7 cell line exposed to APU DOX nanoparticles, incubated at variable temperature. (b) plot demonstrating corrected total cell fluorescence of DOX against the incubation temperature. The APU-DOX was administered to MCF 7 cells at 25 °C and then the cells were incubated at desired temperature (4 °C, 37 °C and 42 °C) [incubation time = 4 h, DOX concentration = 2.0 μg/mL].

Both these pre-treated samples were exposed to cells and were subsequently incubated at 37 °C for 4h and then fixed for imaging. Confocal microscope images for these samples are shown in Figure 2.24.a and, the data is summarized in Figure 2.24.b The 42 °C pre-treated samples were found to exhibit significantly low level of DOX uptake which was attributed to the partial disassembly of APU-DOX. On the other hand, the 37 °C pre-treated samples showed higher uptake of DOX indicating that the APU nanoparticles were stable under extracellular conditions. Further, the comparisons of the DOX uptake data for 25 °C administration followed by 42 °C incubation (see Figure 2.23.b) and 42 °C pre-treated sample (see Figure 2.24.b) revealed that the thermo-responsive nano-carriers would allow higher uptake of drugs when they do not undergo pre-mature disassembly prior to the endocytosis process. Thus, thermo-responsiveness would be beneficial in drug delivery application provided that the nano-carriers

exclusively undergo disassembly at the intracellular level to deliver the loaded cargoes. In the present study, the enzyme-responsiveness at the intracellular level, in addition to the thermo-responsive nature of nanoparticle complements the higher delivery of the loaded cargo. The above studies confirmed that L-lysine based aliphatic polyurethanes and their amphiphilic nano-carriers are excellent candidates for biomedical applications. In the present investigation, these new classes of the polyurethanes were designed and developed based on solvent free melt transurethane process and their potential application has been demonstrated in delivery of the DOX to breast cancer cell lines.

#### **2.4. Conclusion**

In summary, the present investigation reports one of the first examples for melt polycondensation approach for the development of L-amino acid based aliphatic polyurethanes and employs the polymerization methodology to make amphiphilic polyurethane nano-carriers for drug delivery applications. L-Lysine was converted into di-urethane monomers and they underwent melt polymerization with commercial diols to produce moderate to high molecular weight polyurethanes. The occurrence of the melt transurethane polycondensation was confirmed by NMR spectroscopy and kinetics of the polymerization reactions, the role of catalysts and diols segments were also investigated in detail. Both amide pendant substitutions in the polymer side chain and the polymer backbone were varied to study the structure-property relationship of these new classes of L-lysine polyurethanes. PEG-pendant L-lysine monomer produced amphiphilic polyurethane (APU) which was found to self-assemble as core shell nanoparticle in aqueous solution as  $175 \pm 10$  nm nanoparticles. The APU nanoparticles exhibited thermoresponsive behavior having LCST at 42 °C which is closer to cancer tissue temperature. The reversible thermoresponsive behavior was completely characterized by variable temperature transmittance analysis and NMR. Further, the aliphatic polyurethane backbone renders enzymatic-biodegradation of the polymer nanoparticles at the intracellular conditions under physiological conditions. Anticancer drug DOX was loaded in the APU nanoparticles and its application was tested for drug delivery breast cancer (MCF 7) cell line. *In vitro* drug release studies showed that the nanoparticles were stable at physiological temperature and undergoing phase transition at 42 °C to release the loaded cargo (stimuli-1). Lysosomal esterase enzyme (stimuli-2) was found to biodegrade the backbone and enables the controlled release of the drugs. The nascent APU nanoparticles were found to be the non-toxic and highly biocompatible whereas the DOX-loaded APU showed excellent cell growth inhibition in cancer cells. The cellular uptake of nanoparticle was confirmed by confocal laser

scanning microscopy in MCF 7 cell line. Further, the mechanism of cellular uptake was studied by live cell imaging in MCF 7 cell line which shows that nanoparticles cleaved in lysosomal compartment to release the loaded cargo which subsequently delivered to the nucleus. The melt transurethane process demonstrated here is not restricted to the L-lysine bio-resources alone and, in principle; it can be applied to a wide variety of other aliphatic diamine to make diverse polymer architectures. Similarly, the delivery of clinically important anticancer drug DOX was established in the APU platform; however, the APU nano-carrier could also be useful for a wide range of other drugs in combination therapy in cancers. Further, the amide-functionality in the polyurethane repeating units may also be expanded to anchor drugs, fluorophores and targeting ligands to make the APU nano-carriers as a multi-task platform in cancer therapy. In a nutshell, the present investigation provides the first insight into the designating of aliphatic polyurethane especially in L-lysine resources and opens a new platform of polymer synthesis opportunities based on melt polycondensation approach. Currently, the research work is progressed in these directions to exploit the unexplored aliphatic polyurethane system in biomedical applications.

## References

1. Shen, Y.; Fu, X.; Fu, W.; Li, Z. *Chem. Soc. Rev.* **2015**, *44*, 612-622.
2. Bauri, K.; Nandi, M.; De, P. *Polym. Chem.* **2018**, *9*, 1257-1287.
3. Sun, H.; Hong, Y.; Xi, Y.; Zou, Y.; Gao, J.; Du, J. *Biomacromolecules* **2018**, *19*, 1701-1720.
4. Deming, J. T. *Prog. Poly. Sci.* **2007**, *32*, 858-875.
5. Carlsen, A.; Lecommandoux, S. *Current Opinion in Colloid & Interface Science* **2009**, *14*, 329-339.
6. Osada, K.; Kataoka, K. *Adv. Polym. Sci.* **2006**, *202*, 113-153.
7. Deming, T. J. *Adv. Drug Deliv. Rev.* **2002**, *54*, 1145-1155.
8. Sun, H.; Meng, F.; Dias, A. A.; Hendricks, M.; Feijen, J.; Zhong, Z. *Biomacromolecules* **2011**, *12*, 1937-1955.
9. Deng, M.; Wu, J.; Reinhart-King, C. A.; Chu, C. C. *Biomacromolecules* **2009** *10*, 3037-3047.
10. Fonseca, A. C.; Gil, M. H.; Simões, P. N. *Prog. Polym. Sci.* **2014**, *39*, 1291-1311.
11. Sun, H.; Cheng, R.; Deng, C.; Meng, F.; Dias, A. A.; Hendriks, M.; Feijen, J.; Zhong, Z. *Biomacromolecules* **2015**, *16*, 597-605.

12. Wu, J.; Wu, D.; Mutschler, M. A.; Chu, C. C. *Adv. Funct. Mater.* **2012**, *22*, 3815-2823.
13. Wu, J.; Zhao, L.; Xu, X.; Bertrand, N.; Choi, W.; Yameen, B.; Shi, J.; Shah, V.; Mulvale, M.; MacLean, J. L.; Farokhzad, O. C. *Angew. Chem., Int. Ed.* **2015**, *54*, 9218–9223.
14. Lu, W.; Wang, X.; Cheng, R.; Deng, C.; Meng, F.; Zhong, Z. *Polym. Chem.* **2015**, *6*, 6001-6010.
15. Huyang, F.; Cheng, Ru.; Meng, F.; Deng, C.; Zhong, Z. *Biomacromolecules* **2015**, *16*, 2228-2236.
16. Liu, J.; Wang, P.; Chu, C. C.; Xi, T. *Colloids Surf. B* **2017**, *159*, 78-88.
17. Liu, J.; Wang, P.; Chu, C. C. Xi, T. *J. Mater. Chem. B.* **2017**, *5*, 1787-1802.
18. Yu, C.; Kohn, J. *Biomaterials* **1999**, *20*, 253-264.
19. Sheihet, L.; Piotrowska, K.; Dubin, R. A.; Kohn, J.; Devore, D. *Biomacromolecules* **2007**, *8*, 998-1003.
20. Sharon, L. B.; J, Kohn. *Adv. Drug. Deliv. Rev.* **2003**, *55*, 447–466.
21. Aamer, K. A.; Genson, K. A.; Kohn, J.; Becker, M. L. *Biomacromolecules* **2009**, *10*, 2418-2426.
22. Anantharaj S.; Jayakannan, M. *Biomacromolecules* **2012**, *13*, 2446-2455.
23. Aluri, R.; and Jayakannan, M. *Polym. Chem.* **2015**, *6*, 4641-4649.
24. Anantharaj S.; Jayakannan, M. *Biomacromolecules* **2015**, *16*, 1009-1020.
25. Saxena, S.; Jayakannan, M. *J. Polym. Sci., Part A: Polym. Chem.* **2016**, *54*, 3279-3293.
26. Anantharaj, S.; Jayakannan, M. *J. Polym. Sci., Part A: Polym. Chem.* **2016**, *54*, 2864-2875.
27. Aluri, R.; Jayakannan, M. *Biomacromolecules* **2017**, *18*, 189-200.
28. Aluri, R.; Saxena, S.; Joshi, C. D.; Jayakannan, M. *Biomacromolecules* **2018**, *19*, 2166-2181.
29. Saxena, S.; Jayakannan, M. *Biomacromolecules* **2017**, *18*, 2594-2609.
30. Rajdev, P.; Basak, D.; Gosh, S. *Macromolecules* **2015**, *48*, 3360-3367.
31. Shpaisman, N.; Sheihet, L.; Bushman, J.; Winters, J.; Kohn, J. *Biomacromolecules* **2012**, *13*, 2279-2286.
32. James, K.; Levene, H.; Parsons, R. J.; Kohn, J. *Biomaterials* **1999**, *20*, 2203-2212.
33. Ghaffar, A.; Draaisma, G. J. J.; Mihov, G.; Dias, A. A.; Schoenmakers, P. J.; Van der Wal, S. *Biomacromolecules* **2011**, *12*, 3243–3251.

34. Brannigan, P. R.; Walder, A.; Dove, P. A. *ACS Sustainable Chem. Eng.* **2017**, *5*, 6902-6909.
35. Hojabri, L.; Kong, X.; Nrine, S. S. *Biomacromolecules* **2010**, *11*, 911-918.
36. McKiernan, L. R.; Heintz, M. A.; Hsu, L. S.; Atkins, T. D. E.; Penelle, J.; Gido, P. *S. Macromolecules* **2002**, *35*, 6970-6974.
37. Osman, F. A.; Edwards, A. G.; Schiller, L. T.; Andriani, Y.; Jack, S. K.; Morrow, C. I.; Halley, J. P.; Martin, J. D. *Macromolecules* **2012**, *45*, 198-210.
38. Sun, X.; Gao, H.; Wu, G.; Wang, Y.; Fan, Y.; Ma, J. *Int. J. Pharm.* **2011**, *412*, 52–58.
39. Sardon, H.; Tan, J. P. K.; Chan, J. M. W.; Mantione, D.; Mecerreyes, D.; Hedrick, J. L.; Yang, Y. Y. *Macromol. Rapid Commun.* **2015**, *36*, 1761–1767.
40. Wang, A.; Goa, H.; Sun, H.; Sun, Y. L.; Yang, Y. W.; Wu, G.; Wang, W. *Int. J. Pharm.* **2013**, *441*, 30–39.
41. Maisonneuve, L.; Lamarzeiie, O.; Rix, E.; Grau, E.; Cramail, H. *Chem, Rev.* **2015**, *115*, 12407-12439.
42. Kreye, O.; Mutlu, H.; Meier, M. A. R. *Green Chem.* **2013**, *15*, 1431–1455.
43. Foti, S.; Giuffrida, M.; Maravigna, P.; Montaudo, G. *J Polym Sci Polym Chem Ed.* **1983**, *21*, 1599-1615.
44. Maisonneuve, L.; Wriotius, A.; Alfoss, C.; Grau, E.; Cramail, H. *Polym. Chem.* **2001**, *5*, 6142-6147
45. Bossion, A.; Aguirresarobe, H. R.; Irusta, L.; Taton, D.; Cramail, H.; Grau, E.; Mecerreyes, D.; Su, C.; Liu, G.; Muller, A. J.; Sardon, H. *Macromolecules* **2018**, *51*, 5556–5566.
46. Bossion, A.; Jones, G. O.; Taton, D.; Mecerreyes, D.; Hedrick, J. L.; Ong, Z. Y.; Sardon, H. *Langmuir* **2017**, *33*, 1959–1968.
47. Kahira, N.; Endo, T.; *J. Polym. Sci., Part A: Polym. Chem.* **1993**, *31*, 2765-2773.
48. Kumar, A.; Ramakrishnan, S. *J. Polym. Sci., Part A: Polym. Chem.* **1996**, *34*, 839-848.
49. Okaniwa, M.; Takeuchi, K.; Asia, M.; Ueda, M. *Macromolecules* **2002**, *35*, 6224-6231.
50. Lebarbe, T.; More, A. S.; Sane, P. S.; Grau, E.; Alfoss, C.; Cramail, H. *Macromol. Rapid Commun.* **2014**, *35*, 479–483.
51. Deepa, P.; Jayakannan, M. *J. Polym. Sci., Part A: Polym. Chem.* **2008**, *46*, 2445-2458.



52. Deepa, P.; Jayakannan M. *J. Polym. Sci., Part A: Polym. Chem.* **2008**, *46*, 5897-5915.
53. Palaskar, D. V.; Boyer, A.; Cloutet, E.; Alfos, C.; Cramail, H. *Biomacromolecules* **2010**, *11*, 1202–1211.
54. More, A. S.; Gadenne, B.; Alfos, C.; Cramail, H. *Polym. Chem.* **2012**, *3*, 1594-1605.
55. Yang, Y.; Zhou, Y.; Ge, J.; Wang, Y.; Chen, X. *Polymer* **2011**, *52*, 3745-3751.
56. Kudo, H.; Nagai, A.; Ishikawa, J.; Endo, T. *Macromolecules* **2001**, *34*, 5355-5357.
57. Hao, H.; Shao, J.; Deng, Y.; He, S.; Luo, F.; Wu, Y.; Li, J.; Tan, H.; Li, J.; Fu, Q. *Biomater. Sci.* **2016**, *4*, 1682-1690.
58. Hassan, K. M.; Mauritz, A. K.; Storey, F. R.; Wiggins, S. J. *J. Polym. Sci., Polym Chem.* **2006**, *44*, 2990-3000.
59. Rautio, J.; Kumpulainen, H.; Heimbach, T.; Oliyai, R.; Oh, D.; Järvinen, T.; Savolainen, J. *Nat. Rev. Drug Discovery.* **2008**, *7*, 255–270.
60. Anantharaj, S.; Jayakannan, M. *J. Polym. Sci., Part A: Polym. Chem.* **2016**, *54*, 1065-1077.
61. Malhotra, M.; Surnar, B.; Jayakannan, M. *Macromolecules* **2016**, *49*, 8098- 8112.
62. Surnar, B.; Jayakannan, M. *ACS Biomater. Sci. Eng.* **2016**, *2*, 1926-1941.
63. Abulateefeh, R. S.; Spain, G. S.; Thurecht, J. K.; Aylott, W. J.; Chen, C. W.; Garnett, C. M.; Alexander, X. *Biomater. Sci.* **2013**, *1*, 434-442.
64. Salmaso, S.; Caliceti, P.; Amendola, V.; Meneghetti, J.; Magnusson, P. J.; Pasparakis, G.; Alexander, C. *J. Mater. Chem.* **2009**, *19*, 1608-1615.
65. Kashyap, S.; Singh, N.; Surnar, B.; Jayakannan, M. *Biomacromolecules* **2016**, *1*, 384-398.
66. Kashyap, M.; Jayakannan, M. *J. Mater. Chem. B.* **2014**, *2*, 4142–4152.
67. Deshpande, U. N.; Jayakannan, M. *Biomacromolecules* **2018**, *19*, 3572-3585.
68. Deshpande, U. N.; Jayakannan, M. *Biomacromolecules* **2017**, *18*, 113-1126.
69. Zeng, X.; Zhang, Y.; Nystrom, A. *Biomacromolecules* **2012**, *13*, 3814–3822.
70. Wang, H. Y.; Hua, X. W.; Jia, H. R.; Liu, P.; Gu, N.; Chen, Z.; Wu, F. G. *J. Mater. Chem. B.* **2016**, *4*, 834–843.

# Chapter 3

---

**L-Amino acid Based Aromatic  $\pi$ - $\pi$  Interaction Driven  
Polymeric Drug Delivery System in Cancer Research**

## **Abstract**

*The present study report a new class of enzymatically biodegradable L-amino acid based poly(ester-urethane)s and their drug delivery applications in cancer cells. For that L-Tyrosine and L-DOPA resources were suitably modified into dual ester urethane monomer in which the –OH groups were protected as silyl ether. The newly designed monomers were subjected for solvent free melt polymerization with hydrophilic polyethylene glycol to get the poly(ester-urethane)s. The postpolymerisation deprotection of silyl ether yielded a new classes of enzyme-responsive phenol and catechol functionalized poly(ester-urethane)s in which the backbone of polymer contains polyethylene glycol and the side chain contains a pendent aromatic unit. The amphiphilic nature of polymer and hydrophobic interactions between aromatic units facilitates the formation of core shell type nanoparticle in aqueous medium having size around  $100 \pm 10$  nm. The electron rich aromatic nature of L-DOPA was explored for the encapsulation of drug molecules inside the hydrophobic core. The aromatic electron rich nature of polymeric backbone promotes the encapsulation of electron deficient drug molecules by aromatic pi-pi stacking interactions. The aromatic interactions between L-DOPA and drug molecule was confirmed by decrease in the fluorescent intensity of drug and L-DOPA by fluorescence spectroscopy. The backbone of polymer contains the ester linkages which underwent enzymatic biodegradation in presence of lysosomal enzymes, resulting the disassembly of nanoparticle and release of loaded cargo. Cytotoxicity studies in the breast cancer (MCF-7) and normal WT-MEFs cell lines revealed that the nascent nanoparticles were nontoxic, whereas the DOX and TPT drug-loaded polymer nanoparticles exhibited excellent cell killing in cancer cells. Confocal microscopic imaging confirmed the cellular internalization of drug-loaded nanoparticles. In conclusion, A new class of poly(ester-urethane)s were synthesized from L-tyrosine and L-DOPA amino acids via melt polycondensation approach and aromatic nature of L-DOPA amino acid was exploited to enhance the drug loading capability by  $\pi$ – $\pi$  stacking interactions. The present investigation opens up new opportunities to design L-amino acid based biodegradable nano-carriers for cancer treatment and the proof-of-concept was demonstrated in (MCF-7) breast cancer cell line.*

**Keywords:** *L-amino acid, Poly(ester-urethane)s, Enzyme-responsive, Drug Delivery, Cancer Therapy.*

### 3.1. Introduction

Polymeric drug delivery systems with well-defined architectures are crucial for both drug encapsulation efficiency and the stabilization of rigid-aromatic anticancer drugs that are water-insoluble<sup>1,2</sup>. Several non-covalent interactions, including van der Waals forces<sup>3-5</sup>, aromatic  $\pi$ - $\pi$  interactions, and hydrogen bonding<sup>6-8</sup>, were also implemented into the hydrophobic pocket of the amphiphilic macromolecular nanocarrier to ensure adequate drug stability against premature leaching. Anticancer drugs are predominately polyaromatic molecules (except metal based Pt-drugs); thus, aromatic  $\pi$ - $\pi$  interaction between the polymer chains and drug molecules become a natural choice to strengthen the molecular interactions at the nanoconfinement for enhancing the drug loading content in formulations.<sup>9-12</sup> Aromatic  $\pi$ - $\pi$  interactions between polymers and drug molecules are mainly achieved by introducing pi-conjugated chromophores into the polymer matrix.<sup>13-17</sup>

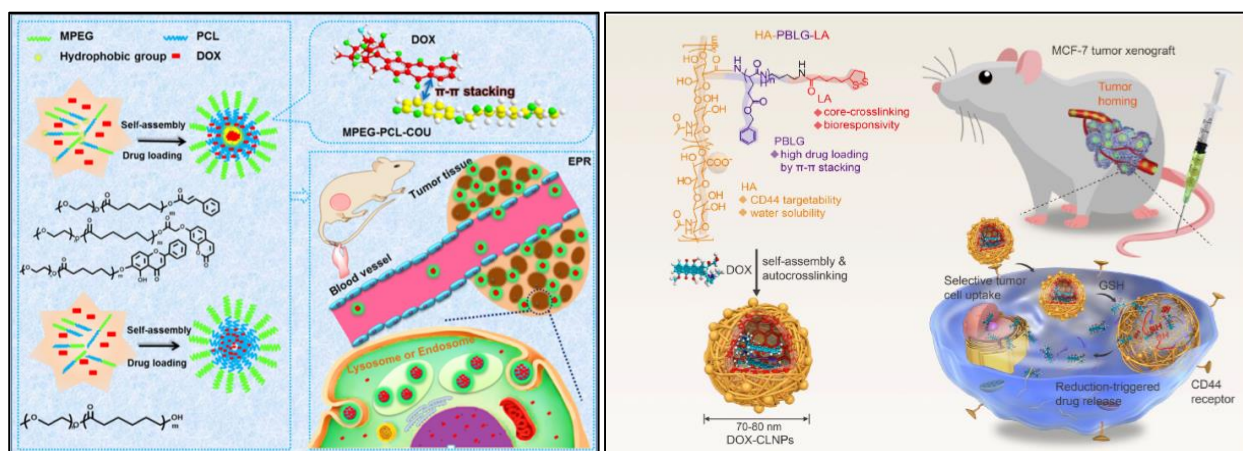


**Figure 3.1.** Different polymeric systems with  $\pi$ -conjugated moieties explored for enhanced drug loading. Adopted from Y. Liang et al. *Biomaterials* **2015**, 71, 1-10. and B. Sun et al. *Acta Biomater.* **2016**, 45, 223–233.

Often the fluorescent characteristics of  $\pi$ -conjugated chromophores and polyaromatic drug molecules such as doxorubicin<sup>18-21</sup> (DOX), camptothecin<sup>22-23</sup>, and curcumin<sup>24</sup> were explored to construct fluorescence resonance energy transfer (FRET) probes to accomplish both therapeutics and diagnostics together in single system. It is important to mention that majority of the  $\pi$ -conjugated chromophores reported for the above purpose were non-biodegradable; hence, the undesirable cytotoxicity of these species at internal organs and also their inability to clear through renal filtration under physiological conditions are still unresolved issues for their long-term impact

in biomaterial research. One of the elegant strategies to overcome the above limitation is by choosing the biologically derived aromatic molecules for designing monomers to build amphiphilic polymer structures and explore their  $\pi$ - $\pi$  interaction capability to stabilize the drug molecules in therapeutics. L-Amino acids residues such as L-tyrosine, L-phenylalanine and L-tryptophan are chosen by the bio-machinery to stabilize the incoming substrate molecules via  $\pi$ -stack interactions in the globular protein structures for particular enzymatic-action. Synthetic polypeptides such as PEG-b-poly(L-tyrosine) amphiphilic di-block copolymers were tailor made and their  $\pi$ -rich hydrophobic domains in the nanoparticles were exploited for outstanding 63 % of DOX encapsulation.<sup>25</sup> Lipoic acid units were also used as disulphide crosslinking agent to enhance the stability of the nanoparticles and protease-responsiveness of the polypeptide backbone was employed for drug delivery at the cellular level.<sup>26</sup>

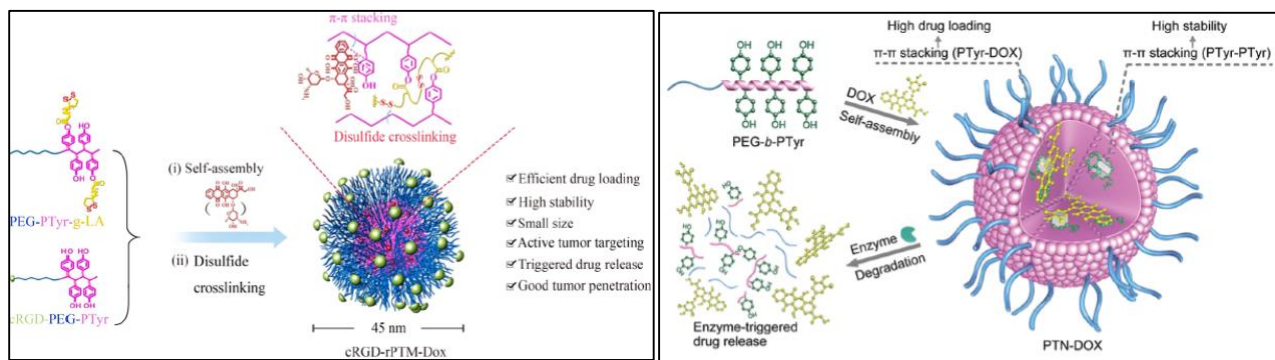


**Figure 3.2.** L-tyrosine based block copolymers for ultra-high loading and enzyme-responsive release of DOX. (Adopted from zhong et al. *Biomacromolecules* **2018**, *19*, 3586–3593 and *Biomater. Sci.* **2018**, *6*, 1526–1534)

PEGylated block copolymers of 4-phenyl-1 butanol modified polyaspartates were also reported for loading high paclitaxel (PTX) content in their nanoparticles<sup>27</sup>. L-DOPA (3,4-dihydroxyphenyl alanine) is important L-amino acid intermediates produced by tyrosinase enzymes in biological system as a neurotransmitter.<sup>28-30</sup> Synthetic polymers based on L-DOPA were also explored as bioadhesive<sup>31,32</sup> because of active catechol unit and cross-linked hydrogels through chemical oxidation of the electron rich aryl units.<sup>33-35</sup> Up to our knowledge, there is no effort has been taken to exploit the electron-rich aryl units for  $\pi$ -interaction driven drug delivery systems. Our group has been exploring melt polycondensation approach for L-amino acid resources for developing new classes of non-peptide biodegradable polymer analogues such as polyesters,<sup>36</sup> polyurethanes,<sup>37</sup> and poly(ester-urethane)s.<sup>38</sup> Amphiphilicity of these polymer structures were tailor-made for Ph<sup>39</sup>, enzyme<sup>39</sup>, thermo-responsive<sup>40-41</sup> nano-carriers, and FRET probes in cancer research.<sup>42-43</sup> Our expertise is expanded here to develop one of the first examples of L-DOPA based poly(ester-

urethane)s by melt polycondensation approach and explore the resultant polymers for aromatic  $\pi$ -stacking interaction driven drug delivery in cancer research. This new concept is shown in Figure 3.3. During the self-assembly of drug molecules and amphiphilic polymers, Hydrophobic drugs are known to precipitate in an aqueous solution by forming drug aggregates, instead of drug-embedded micelles which significantly lowers the drug loading efficiency in nanoparticles. So to increase the drug loading content the introduction of molecular interaction between polymers and drugs is strongly required. The drug molecules which are used for encapsulation have a polyaromatic electron-deficient core. So to introduce the strong polymer-drug interactions, an electron-rich aromatic pi system was explored so that the drug molecule will preferentially interact with polymer chains over self-aggregation.

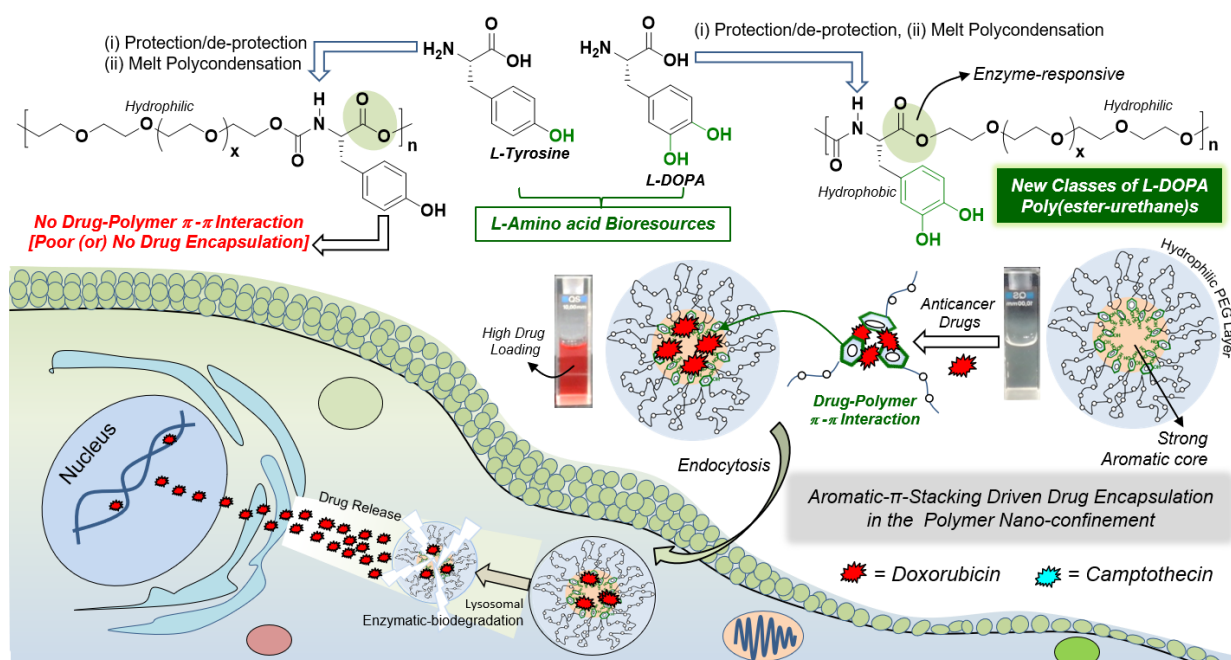


**Figure 3.3.** Aromatic  $\pi$ -Stack interaction driven drug delivery system based on enzymatic-biodegradable L-Amino acid poly(ester-urethane) nano-assemblies.

PTyr-PEG-400 in aqueous solvent formed  $120 \pm 10$  nm nanoparticles; however, it was rather surprising to note that L-tyrosine based polymers did not load DOX or TPT. Both L-DOPA and L-tyrosine polymers have appropriate hydrophilic and hydrophobic balance to self-assemble in water. They differ by the phenol or catechol units at the core of the nanoparticles; thus, they could vary in terms of aromatic  $\pi$ -interactions with the incoming polyaromatic drug molecules. Further, it is also important to note that we have employed the dialysis method for the encapsulation; thus the encapsulated DOX and TPT will be removed in the reservoir and only the stabilized drug molecules could stay in the nanoparticles. Therefore, the drug stabilization

exhibited by the L-DOPA polymer is attributed to the presence of strong aromatic  $\pi$ -interaction between DOX (or TPT) and electron-rich catechol units. On the other hand, the phenol units in the L-tyrosine polymers exhibited weak  $\pi$ -interaction towards the incoming drug molecules and thus failed to act as efficient host for incoming guest molecules.

The development of phenol-functional polymers from L-tyrosine and L-DOPA amino acid resources is fairly challenging task and it requires suitable protection/de-protection synthetic strategy to avoid the phenolic group interference in the polymerization reaction. For this purpose, the -OH functionality in L-tyrosine and L-DOPA were masked by silyl substitution and the amine and carboxylic acid were converted into polymerizable functional groups. These monomers underwent solvent free dual ester-urethane melt polycondensation reaction with PEG-diols (or diols) under to yield high molecular weight silyl-protected poly(ester-urethane)s. Post polymerization de-protection strategy was adopted to unmask the silyl-unit to yield phenol and catechol containing amphiphilic poly(ester-urethane)s, for the first time, in the literature (see Figure 1). Both the L-tyrosine and L-DOPA polymers self-assembled into <100 nm nanoparticles in water; the more electron rich aromatic  $\pi$ -core of the L-DOPA was exploited for encapsulation of polyaromatic anticancer drugs like doxorubicin (DOX) and topotecan (TPT). Detail photophysical studies further established the strong aromatic  $\pi$ -interaction driven drug encapsulation process. The aliphatic ester backbone of the polymers underwent enzymatic-biodegradation lysosomal compartment at the intercellular level to release more than 90 % of DOX. Cytotoxicity studies and cellular internalization studies were carried out in human breast cancer cell lines (MCF7). The drug loaded polymeric nanoparticles showed excellent cell killing in the cancer cells. The cellular internalization was confirmed by confocal microscope. The present investigation provides a new synthetic methodology for the synthesis of phenol and catechol containing poly(ester urethane)s and their drug delivery applications in cancer cell

## 3.2. Experimental Methods

**3.2.1. Material:** L-tyrosine, L-DOPA, sodium bicarbonate, tert-Butyldimethylsilyl chloride, imidazole, 4-Dimethylaminopyridine (DMAP), tetra-n-butylammonium fluoride (TBAF), 1,12 dodecanediol, 1,10 decanediol, 1,8 octanediol, 1,6 hexanediol, PEG-200 diol, PEG-400 diol, PEG-600 diol, titanium(IV) butoxide, europium nitrate, dibutyltin dilaurate, iron acetoacetate, zinc

acetate, cesium acetate, titanium(IV) isopropoxide, hydrochloride salt of doxorubicin, hydrochloride salt of topotecan, horse liver esterase enzyme, 3-(4,5- dimethylthiazol-2-yl)-5diphenyltetrazolium bromide (MTT), 4',6- diamidino-2-phenylindole dihydrochloride (DAPI. 2HCl), paraformaldehyde, glycerol and HPLC DMSO were purchased from Sigma-Merck chemicals and used directly without further purification. Breast cancer cell lines (MCF 7) cells were maintained in phenol red containing DMEM media with 10% (v/v) fetal bovine serum (FBS) and 1% (v/v) of penicillin-streptomycin (purchased from Gibco). Thionyl chloride, methyl chloroformate and other solvents were purchased locally and purified prior to use.

**3.2.2. Experimental methods:**  $^1\text{H}$  spectra of all compounds were recorded using 400 MHz JEOL NMR spectrophotometer and  $^{13}\text{C}$  spectra were recorded using 100 MHz JEOL NMR spectrophotometer in  $\text{CDCl}_3$  containing trace amount of TMS as an internal Standard. Purity of all the polymers were checked by Gel permeation chromatography (GPC) analysis. The concentration of all the polymers was maintained as 1 mg/mL and samples were performed using Viscotek VE 1122 pump, Viscotek VE 3580 RI detector and Viscotek VE 3210 UV/vis detector in tetrahydrofuran (THF) using polystyrene as standards. High resolution mass spectra of all the monomers were recorded using Micro Mass ESI-TOF MS spectrometer. MALDI-TOF MS of the polymers was determined using Applied Biosystems 4800 PLUS Analyzer. FT-IR spectra of all compounds were recorded using Bruker alphaT Fourier transform infrared spectrophotometer. Size of nanoparticles was determined by dynamic light scattering (DLS) using a Nano ZS-90 apparatus utilizing a 633 nm red laser from Malvern instruments. Thermal stability of the polymers was determined using Perkin Elmer thermal analyzer STA 6000 model at a heating rate of  $10^\circ\text{C}/\text{min}$  under nitrogen atmosphere. Thermal analysis of the polymers was performed using TA Q20 Differential Scanning Calorimeter. The instrument was calibrated with indium standards. Polymers were heated and cooled at  $10^\circ\text{C}/\text{min}$  under nitrogen atmosphere and their thermograms were recorded. For FE-SEM analysis, the samples were prepared by drop casting on silicon wafers. and coated with gold. FE-SEM images were recorded using Zeiss UltraPlus scanning electron microscope. Atomic force microscopy (AFM) imaging samples were prepared by dropcasting on mica sheets and images were generated by using Veeco Nanoscope IV instrument in tapping mode.



**3.2.3. Synthesis of (S)-3-(4-hydroxyphenyl)-1-methoxy-1-oxopropan-2-aminium chloride.** L-tyrosine hydrochloride salt (10.0 g, 0.045 mol) was dispersed in 70.0 mL of dry methanol. Under nitrogen environment and (4.0 ml, 0.055 mol) of thionyl chloride was added dropwise at ice cold condition. Reaction mixture was refluxed under nitrogen environment for 12 h. The excess of thionyl chloride and methanol was removed by vacuum distillation to get a white coloured solid which was directly used for next step. Yield = 10.6 g (100%)

**3.2.4. Synthesis of methyl (methoxycarbonyl)-L-tyrosinate:** (S)-3-(4-hydroxyphenyl)-1-methoxy-1-oxopropan-2-aminium chloride (10.0 g, 0.0431 mol) was taken in 250 mL round bottom flask and dissolved in 30 mL of 25% sodium bicarbonate solution at ice cold condition further 60 ml of DCM was added into it. (4.0 mL, 0.051 mol) of methyl chloroformate was added dropwise into reaction mixture at ice cold condition and reaction was continued at room temperature for 12 h. After 12 h reaction mixture was neutralized with 10 molar HCl and product was extracted with excess of DCM which was further purified by passing through silica gel column using ethyl acetate and pet ether (1:4 v/v) as an eluent to get a white crystalline compound yield = 11.3 g (87%). <sup>1</sup>H NMR (400 MHz, CDCl<sub>3</sub>) δ ppm: 2.99 - 3.04 (m, 2 H, CH-CH<sub>2</sub>-), 3.67 (s, 3 H, -NH-COOCH<sub>3</sub>), 3.73 (s, 3 H, -COOCH<sub>3</sub>), 4.61 (q, 1 H, -CH<sub>2</sub>-CH-), 5.23 (d, 1 H, CH-NH-), 6.71 (d, 2 H, ArH), 6.96 (d, 2 H, ArH). <sup>13</sup>C NMR (100 MHz, CDCl<sub>3</sub>) δ ppm: 37.42, 52.41, 52.50, 54.93, 115.53, 127.17, 130.30, 155.18, 156.56, 172.39. FT-IR (cm<sup>-1</sup>): 3333, 3019, 2955.20, 1699, 1614, 1596, 1516, 1445, 1362, 1223, 1105, 1061, 830, 802, 779.

**3.2.5. Synthesis of compound (2) methyl(S)-3-(4-((tert-butyldimethylsilyl)oxy)phenyl)-2-((methoxycarbonyl)amino)propanoate:** Compound (1) (10 g, 0.039 mol) and potassium carbonate (16.3 g, 0.118 mol) were dissolved in 90.0 mL of dry acetonitrile and reaction mixture was refluxed for 30 min under nitrogen purging. tert-butyldimethylsilyl chloride (8.9 g, 0.059 mol) was added into it and reaction was refluxed for 48h under nitrogen environment. After completion of reaction excess solvent was distilled and residue was poured into water, from which product was extracted with excess of DCM. The product was passed through dry sodium sulphate and purified by silica gel column chromatography using ethyl acetate and pet ether (1:5 v/v) to get colorless viscous liquid. Yield = 11.9 g (82%). <sup>1</sup>H NMR (400 MHz, CDCl<sub>3</sub>) δ ppm: 0.17 (s, 6 H, Si(CH<sub>3</sub>)<sub>2</sub>), 0.97 (s, 9 H, Si-C(CH<sub>3</sub>)<sub>3</sub>), 3.02 (d, 2 H, CH-CH<sub>2</sub>), 3.66 (s, 3 H, NH-COOCH<sub>3</sub>), 3.70 (s, 3 H, -COOCH<sub>3</sub>), 4.58 (q, 1 H, NH-CH), 5.17 (d, 1 H, CH-NH), 6.76 (d, 2 H, ArH), 6.97 (d, 2 H,

**ArH**).  $^{13}\text{C}$  NMR (100 MHz,  $\text{CDCl}_3$ )  $\delta$  ppm: -4.48, 18.13, 25.61, 37.47, 52.20, 52.29, 54.81, 120.14, 128.27, 130.16, 155.74, 156.24, 172.15, 191.58. FT-IR ( $\text{cm}^{-1}$ ): 3333, 2955, 2931, 2887, 2858, 1725, 1609, 1509, 1462, 1444, 1361, 1254, 1216, 1103, 1063, 914, 840, 803, 780, 690.

**3.2.6. Synthesis of PTyr-Si-12:** A typical procedure for polymer PTyr-Si-400 is described by melt condensation using monomer 2 and 1,12 dodecanediol. L-tyrosine monomer (0.65 g, 1.7 mmol) and (0.35 g, 1.7 mmol) of 1,12 dodecanediol were taken in a polymerization tube and melted at  $150\text{ }^\circ\text{C}$ . The polymerization tube was evacuated and degassed repeatedly by using vacuum and nitrogen purging to make it free from moisture and oxidizing gases. 1 mol % of catalyst was added and the polycondensation was continued at  $150\text{ }^\circ\text{C}$  for 4h with continuous stirring and nitrogen purging to get a viscous oligomeric liquid. After 4h polycondensation was continued under vacuum (0.01 bar) for 2h to get the polymer.  $^1\text{H}$  NMR (400 MHz,  $\text{CDCl}_3$ )  $\delta$  ppm: 0.18 (s, 6 H,  $\text{Si}(\text{CH}_3)_2$ ), 0.98 (s, 9 H,  $\text{Si}-\text{C}(\text{CH}_3)_3$ ), 1.27 (s, 16 H,  $-\text{CH}_2-\text{CH}_2-$ ), 1.57 - 1.65 (m, 4 H,  $\text{CH}_2$ ), 3.01(d, 2 H,  $\text{C}_6\text{H}_5-\text{CH}_2$ ), 4.02 - 4.11 (m, 4 H,  $\text{COOCH}_2$ ,  $\text{NHCOOCH}_2$ ), 4.56 (q, 1 H,  $\text{NH}-\text{CH}$ ), 5.10 (d, 1 H,  $\text{CH}-\text{NH}$ ), 6.73 (d, 2 H, **ArH**), 6.98 (d, 2 H, **ArH**).  $^{13}\text{C}$  NMR (100 MHz,  $\text{CDCl}_3$ )  $\delta$  ppm: -4.45, 18.14, 25.64, 25.81, 28.46, 28.94, 29.22, 29.29, 29.38, 29.49, 29.55, 29.57, 32.77, 37.61, 54.77, 63.04, 65.31, 65.53, 120.05, 128.44, 130.24, 154.67, 155.96, 171.84. FT-IR ( $\text{cm}^{-1}$ ): 3356, 2928, 2855, 1718, 1609, 1509, 1461, 1442, 1361, 1342, 1252, 1186, 1118, 1103, 1057, 1033, 985, 913, 838, 805, 779, 688.

**3.2.7. Synthesis of PTyr-Si-10:**  $^1\text{H}$  NMR (400 MHz,  $\text{CDCl}_3$ )  $\delta$  ppm: 0.18 (s, 6 H), 0.89 (s, 9 H), 1.29 (s, 12 H), 1.57 - 1.71 (m, 4 H), 3.02 (s, 2 H), 3.97 - 4.25 (m, 4 H), 4.58 (q, 1 H), 5.12 (d, 1 H), 6.72 (d, 2 H), 6.96 (d, 2 H).  $^{13}\text{C}$  NMR (100 MHz,  $\text{CDCl}_3$ )  $\delta$  ppm: -4.44, 18.15, 25.64, 25.72, 28.44, 29.21, 29.33, 29.44, 29.56, 29.53, 32.77, 54.77, 65.23, 65.46, 120.08, 128.45, 130.25, 154.70, 155.97, 171.87. FT-IR ( $\text{cm}^{-1}$ ): 3356, 2926, 2855, 1716, 1608, 1509, 1463, 1444, 1360, 1341, 1249, 1187, 1119, 1102, 1056, 1035, 985, 913, 837, 803, 776.

**3.2.8. Synthesis of PTyr-Si-8:**  $^1\text{H}$  NMR (400 MHz,  $\text{CDCl}_3$ )  $\delta$  ppm: 0.18 (s, 6 H), 0.98 (s, 9 H), 1.31 (s, 8 H), 1.59 (t, 4 H), 2.89 - 3.19 (m, 2 H), 4.02 - 4.10 (m, 4 H), 4.57 (q, 1 H), 5.13 (d, 1 H), 6.75 (d, 2 H), 6.98 (d, 2 H).  $^{13}\text{C}$  NMR (100 MHz,  $\text{CDCl}_3$ )  $\delta$  ppm: -4.44, 18.15, 25.64, 25.73, 28.45, 29.23, 54.77, 65.20, 65.44, 120.07, 128.43, 130.25, 154.71, 155.97, 171.85.

**3.2.9. Synthesis of PTyr-Si-6:**  $^1\text{H}$  NMR (400 MHz,  $\text{CDCl}_3$ )  $\delta$  ppm: 0.18 (s, 6 H), 0.97 (s, 9 H), 1.33 (s, 4 H), 1.60 (t, 4 H), 3.02 (s, 2 H), 4.02 - 4.14 (m, 4 H), 4.57 (q, 1 H), 5.14 (s, 1 H), 6.75(d, 2 H), 6.96 (d, 2 H).  $^{13}\text{C}$  NMR (100 MHz,  $\text{CDCl}_3$ )  $\delta$  ppm: -4.44, 18.15, 25.64, 25.73, 28.44, 28.90, 29.24, 54.76, 65.23, 65.45, 120.06, 128.43, 130.25, 154.73, 155.95, 171.83.

**3.2.10. Synthesis of PTyr-12:** PTyr-Si-12 (0.50 g, 1.0 mmol) was taken in a 10 ml flask and dissolved in 5 ml THF. (0.35 g, 1.1 mol) of TBAF was added into it and reaction was continued for 12 h at 25  $^\circ\text{C}$ . after completion of reaction polymer was first precipitated in hexane and then washed multiple times with distilled water and dried in vacuum oven. Yield = 0.38 gm (95%).  $^1\text{H}$  NMR (400 MHz,  $\text{CDCl}_3$ )  $\delta$  ppm: 1.27 (s, 16 H,  $-\text{CH}_2-\text{CH}_2-$ ), 1.57 (s, 4 H,  $\text{CH}_2$ ), 2.96-3.02 (m, 2 H,  $\text{C}_6\text{H}_5-\text{CH}_2$ ), 4.07 (t, 4 H,  $\text{COOCH}_2$ ,  $\text{NHCOOCH}_2$ ), 4.57 (s, 1 H,  $\text{NH}-\text{CH}$ ), 5.46 (d, 1 H,  $\text{CH}-\text{NH}$ ), 6.71-6.73 (m, 2 H,  $\text{ArH}$ ), 6.92-6.98 (m, 2 H,  $\text{ArH}$ ).  $^{13}\text{C}$  NMR (100 MHz,  $\text{CDCl}_3$ )  $\delta$  ppm: 25.47, 25.67, 28.09, 27.98, 29.33, 29.37, 29.38, 29.53, 29.57, 29.67, 32.93, 37.76, 54.79, 63.14, 65.31, 65.59, 119.12, 127.43, 129.24, 154.77, 156.29, 171.84. FT-IR ( $\text{cm}^{-1}$ ): 3325, 2925, 2854, 1697, 1615, 1595, 1515, 1456, 1397, 1344, 1260, 1216, 1189, 1104, 1057, 1033, 984, 921, 831, 806.

**3.2.11. Synthesis of PTyr-Si-PEG-600:** Monomer (2) (0.65 g, 1.7 mmol) and PEG 600 (1.06 gm, 1.7 mmol) was polymerized using same method as described for PTyr-Si-12.  $^1\text{H}$  NMR (400 MHz,  $\text{CDCl}_3$ )  $\delta$  ppm: 0.18 (s, 6 H,  $-\text{Si}(\text{CH}_3)_2$ ), 0.97 (s, 9 H,  $-\text{C}(\text{CH}_3)_3$ ), 3.03-3.06 (m, 2 H,  $\text{C}_6\text{H}_5-\text{CH}_2$ ), 3.52 - 3.83 (m, 58 H,  $-\text{O}-\text{CH}_2-\text{CH}_2-\text{O}-$ ), 4.19 - 4.29 (m, 4 H,  $\text{COOCH}_2$ ,  $\text{NHCOOCH}_2$ ), 4.60 (t, 1 H,  $-\text{CH}_2-\text{CH}$ ), 5.29 (d, 1 H,  $-\text{CH}-\text{NH}$ ), 6.73 (d, 2 H,  $\text{ArH}$ ), 6.99 (d, 2 H,  $\text{ArH}$ ).  $^{13}\text{C}$  NMR (100 MHz,  $\text{CDCl}_3$ )  $\delta$  ppm: -4.12, 18.41, 25.83, 25.92, 28.53, 28.98, 29.26, 29.34, 29.53, 29.57, 29.60, 37.53, 54.63, 65.33, 65.56, 120.98, 122.22, 128.74, 145.93, 146.67, 155.92, 171.72. FT-IR ( $\text{cm}^{-1}$ ): 3354, 2928, 2856, 1716, 1508, 1463, 1427, 1347, 1288, 1256, 1217, 1126, 1062, 983, 907, 836, 781, 695.

**3.2.12. Synthesis of PTyr-Si-PEG-400:** Monomer (2) (0.65 g, 1.7 mmol) and PEG 400 (0.70 gm, 1.7 mmol) was polymerized using same method as described for PTyr-Si-12.  $^1\text{H}$  NMR (400 MHz,

CDCl<sub>3</sub>)  $\delta$  ppm: 0.17 (s, 6 H, -Si(CH<sub>3</sub>)<sub>2</sub>), 0.96 (s, 12 H, -C(CH<sub>3</sub>)<sub>3</sub>), 3.02-3.04 (m, 2 H, C<sub>6</sub>H<sub>5</sub>-CH<sub>2</sub>), 3.62 – 3.66 (m, 30 H, -O-CH<sub>2</sub>-CH<sub>2</sub>-O-), 4.19-4.28 (m, 4 H, COOCH<sub>2</sub>, NHCOOCH<sub>2</sub>), 4.58 (q, 1 H, -CH<sub>2</sub>-CH), 5.30 (d, 1 H, -CH-NH), 6.73 (d, 2 H, ArH), 6.99 (d, 2 H, ArH). <sup>13</sup>C NMR (100 MHz, CDCl<sub>3</sub>)  $\delta$  ppm: -4.12, 18.39, 25.84, 25.91, 28.51, 28.96, 29.26, 29.34, 29.53, 29.57, 29.60, 37.53, 54.61, 65.31, 65.54, 120.99, 122.23, 128.76, 145.94, 146.69, 155.96, 171.76. FT-IR (cm<sup>-1</sup>): 3356, 2928, 2857, 1719, 1508, 1463, 1429, 1347, 1288, 1253, 1217, 1126, 1062, 985, 906, 838, 783, 696.

**3.2.13. Synthesis of PTyr-Si-PEG-200:** Monomer (2) (0.65 g, 1.7 mmol) and PEG 200 (0.035 gm, 1.7 mmol) was polymerized using same method as described for PTyr-Si-12. <sup>1</sup>H NMR (400 MHz, CDCl<sub>3</sub>)  $\delta$  ppm: 0.17 (s, 6 H, -Si(CH<sub>3</sub>)<sub>2</sub>), 0.97 (s, 12 H, -C(CH<sub>3</sub>)<sub>3</sub>), 3.0-3.06 (m, 2 H, C<sub>6</sub>H<sub>5</sub>-CH<sub>2</sub>), 3.59 – 3.24 (m, 15 H, -O-CH<sub>2</sub>-CH<sub>2</sub>-O-), 4.19-4.28 (m, 4 H, COOCH<sub>2</sub>, NHCOOCH<sub>2</sub>), 4.57 (q, 1 H, -CH<sub>2</sub>-CH), 5.29 (d, 1 H, -CH-NH), 6.73 (d, 2 H, ArH), 6.99 (d, 2 H, ArH). <sup>13</sup>C NMR (100 MHz, CDCl<sub>3</sub>)  $\delta$  ppm: -4.12, 18.39, 25.83, 25.91, 28.52, 28.96, 29.26, 29.34, 29.60, 37.53, 54.63, 65.33, 65.52, 120.95, 122.21, 128.73, 145.91, 146.67, 155.93, 171.74. FT-IR (cm<sup>-1</sup>): 3354, 2927, 2855, 1717, 1507, 1467, 1429, 1346, 1286, 1253, 1216, 1126, 1060, 984, 906, 842, 781, 698.

**3.2.14. Synthesis of PTyr- PEG-600:** PTyr-Si-PEG-600 (0.70 gm, .77 mmol) was taken in a 10 mL flask and dissolved in 5 mL of THF. TBAF (0.51 gm, 1.6 mmol) was added into it and reaction was continued for 12 h at 25 °C. After 12 h polymer was precipitated in hexane and precipitate was dissolved in 2 ml of DMSO which was dialyzed against milliQ water for 24 h. <sup>1</sup>H NMR (400 MHz, CDCl<sub>3</sub>)  $\delta$  ppm: 2.97-3.06 (m, 2 H, C<sub>6</sub>H<sub>5</sub>-CH<sub>2</sub>), 3.46 – 3.73 (m, 56 H, -O-CH<sub>2</sub>-CH<sub>2</sub>-O-), 4.15-4.30 (m, 4 H, COOCH<sub>2</sub>, NHCOOCH<sub>2</sub>), 4.58 (q, 1 H, -CH<sub>2</sub>-CH), 5.34 (s, 1 H, CH-NH), 6.75 (d, 2 H, ArH), 6.96 (d, 2 H, ArH). <sup>13</sup>C NMR (100 MHz, CDCl<sub>3</sub>)  $\delta$  ppm: 25.81, 25.91, 28.54, 28.92, 29.24, 29.51, 29.63, 37.53, 54.63, 65.33, 65.57, 120.76, 122.11, 128.64, 145.83, 146.65, 155.96, 171.72. FT-IR (cm<sup>-1</sup>): 3353, 2925, 2854, 1717, 1504, 1461, 1431, 1343, 1284, 1255, 1215, 1123, 1059, 987, 907, 841, 786, 698.

**3.2.15. Synthesis of PTyr-PEG-400:** <sup>1</sup>H NMR (400 MHz, CDCl<sub>3</sub>)  $\delta$  ppm: 2.89-3.04 (m, 2 H, C<sub>6</sub>H<sub>5</sub>-CH<sub>2</sub>), 3.54 – 3.73 (m, 30 H, -O-CH<sub>2</sub>-CH<sub>2</sub>-O-), 4.17-4.27 (m, 4 H, COOCH<sub>2</sub>, NHCOOCH<sub>2</sub>),

4.58 (d, 1 H, CH<sub>2</sub>-CH), 5.39 (d, 1 H, CH-NH), 6.76 (d, 2 H, ArH), 6.98 (d, 2 H, ArH). <sup>13</sup>C NMR (100 MHz, CDCl<sub>3</sub>) δ ppm: 25.81, 25.91, 28.54, 28.92, 29.24, 29.51, 29.63, 37.53, 54.63, 65.33, 65.57, 120.76, 122.11, 128.64, 145.83, 146.65, 155.96, 171.72.

**2.2.16. Synthesis of PTyr-PEG-200:** <sup>1</sup>H NMR (400 MHz, CDCl<sub>3</sub>) δ ppm: 2.98-3.07 (m, 2 H, C<sub>6</sub>H<sub>5</sub>-CH<sub>2</sub>), 3.55 – 3.76 (m, 15 H, -O-CH<sub>2</sub>-CH<sub>2</sub>-O-), 4.15-4.24 (m, 4 H, COOCH<sub>2</sub>, NHCOOCH<sub>2</sub>), 4.54-4.55 (s, 1 H, CH<sub>2</sub>-CH), 5.60 (s, 1 H, CH-NH), 6.76 (d, 2 H, ArH), 6.96 (d, 2 H, ArH). <sup>13</sup>C NMR (100 MHz, CDCl<sub>3</sub>) δ ppm: 25.73, 25.87, 28.49, 28.84, 29.21, 29.52, 29.63, 37.52, 54.61, 65.29, 65.52, 120.72, 122.06, 128.63, 145.78, 146.61, 155.91, 171.69.

**2.2.17. Synthesis of methyl (S)-3-(3,4-dihydroxyphenyl)-2-((methoxycarbonyl)amino)propanoate (compound 3):**

(5.0 g, 0.025 mol) of (S)-2-amino-3-(3,4-dihydroxyphenyl)propanoic acid was dispersed in 50.0 ml of dry methanol. Reaction mixture was placed in ice bath and thionyl chloride (2.2 mL, 0.30 mol) was added dropwise into it. Reaction was continued for 12 h at room temperature. After completion of reaction, excess of solvent was removed by distillation to get a white coloured powder which was further dissolved in 15 mL of 30 % sodium bicarbonate solution. The reaction mixture was further diluted with 40 ml of DCM and cooled to 0 °C. Methyl chloroformate (2.3 ml, 0.03 mol) was added into it and reaction was allowed to warm slowly. Reaction was continued for 12 h at 25 °C. After 12 h reaction mixture was neutralized by 1N HCl and product was extracted in DCM and organic layer was dried over anhydrous Na<sub>2</sub>SO<sub>4</sub> to obtain a colourless liquid which was further purified by passing through silica gel column using ethyl acetate and pet ether (1:4 v/v) as eluent. Yield = 6.2 g (92%). <sup>1</sup>H NMR (400 MHz, CDCl<sub>3</sub>) 2.82 - 3.09 (m, 2 H, CH-CH<sub>2</sub>), 3.66 (s, 3 H, -NHCOOMe), 3.73 (s, 3 H, CHCOOMe), 4.59 (m, 1 H, -CH<sub>2</sub>-CH), 5.32 (d, 1 H, CH-NH), 6.26 (s, 2 H, Ar-OH), 6.47 - 6.58 (dd, 1 H, ArH), 6.65 (d, 1 H, ArH), 6.75 (d, 1 H, ArH). <sup>13</sup>C NMR (100 MHz, CDCl<sub>3</sub>) δ ppm: 37.62, 52.50, 54.93, 115.38, 116.05, 121.47, 128.00, 143.15, 143.93, 156.76, 172.52. FT-IR (cm<sup>-1</sup>): 3335, 2955, 1697, 1607, 1519, 1444, 1363, 1283, 1220, 1197, 1114, 1063, 1024, 869, 803, 777.

**3.2.18. Synthesis of methyl(S)-3-(3,4-bis((tert butyldimethylsilyl)oxy)phenyl)2((methoxycarbonyl)amino)propanoate:**

(3 gm, 0.011 mol) of compound 3, (2.2 g, 0.33 mol) of imidazole and (0.25g, 2.2 mmol) of 4-Dimethylaminopyridine were dissolved in 40 mL of dry DMF and reaction was stirred for 10 min at 25<sup>0</sup>C. tert-Butyldimethylsilyl chloride (5.0 g, 0.033 mol) was added into it and reaction was continued for 24 h at 25<sup>0</sup>C. After 24 h excess of solvent was distilled and residue was poured in 100 ml of water from which product was extracted with dichloromethane. The organic layer was dried over Na<sub>2</sub>SO<sub>4</sub> and further purified by passing through silica gel column chromatography using ethyl acetate and pet ether (1:4 v/v) as eluent. Yield =5.4 g (98%). <sup>1</sup>H NMR (400 MHz, CDCl<sub>3</sub>) δ ppm: 0.19 (s, 12 H, Si(CH<sub>3</sub>)<sub>4</sub>), 0.98 (s, 18 H, Si-C(CH<sub>3</sub>)<sub>6</sub>), 2.98 (d, 2 H, CH-CH<sub>2</sub>), 3.67 (s, 3 H, NH-COOCH<sub>3</sub>), 3.71 (s, 3 H, -COOCH<sub>3</sub>), 4.56 (q, 1 H, NH-CH), 5.11 (d, 1 H, CH-NH), 6.53-6.56 (dd, 1 H, ArH), 6.60 (d, 1 H, ArH), 6.74 (d, 1 H, ArH). <sup>13</sup>C NMR (100 MHz, CDCl<sub>3</sub>) δ ppm: -4.12, 18.39, 25.88, 37.41, 52.25, 54.70, 60.38, 121.05, 122.14, 128.58, 146.03, 146.79, 156.22, 172.08. FT-IR (cm<sup>-1</sup>): 3333, 2954, 2930, 2887, 2858, 1725, 1509, 1471, 1462, 1443, 1422, 1361, 1289, 1253, 1219, 1163, 1125, 1062, 1034, 982, 905, 838, 803, 780, 695.

**3.2.19. Synthesis of PDOPA-Si-12:** Monomer (4) (0.65 g, 1.3 mmol) and dodecane diol (0.26 gm, 1.3 mmol) were taken in a polymerization tube and melted at 150<sup>0</sup>C. Polymerization tube degassed and evacuated multiple time by applying vacuum. 1 mol% of titanium tetrabutoxide was added into it and polymerization was continued at 150<sup>0</sup>C for 4 h. After 4 h polymer was subjected under high vacuum (0.01 bar) for 2 h at 150<sup>0</sup>C to get viscous polymer. polymerized following the same procedure as described for P1. <sup>1</sup>H NMR (400 MHz, CDCl<sub>3</sub>) δ ppm: 0.18 (s, 12 H, -Si(CH<sub>3</sub>)<sub>4</sub>), 0.99 (s, 18 H, -C(CH<sub>3</sub>)<sub>6</sub>) 1.27 - 1.29 (m, 16 H, CH<sub>2</sub>), 1.57- 1.62 (m, 4 H, CH<sub>2</sub>) 2.98 (d, 2 H, CH-CH<sub>2</sub>), 4.02 - 4.12 (m, 4 H, -NHCOO-CH<sub>2</sub>-, -CHCOO-CH<sub>2</sub>-), 4.56 (q, 1 H, CH<sub>2</sub>-CH), 5.09 (d, 1 H, CH-NH), 6.53-6.56 (dd, 1 H, ArH), 6.61 (d, 1 H, ArH), 6.73 (d, 1 H, ArH). <sup>13</sup>C NMR (100 MHz, CDCl<sub>3</sub>) δ ppm: -4.12, 25.91, 25.91, ,28.51, 28.96, 29.26, 29.34, 29.53, 29.57, 29.60. 37.53, 54.61, 65.31, 65.54, 120.99, 122.23, 128.76, 145.94, 146.69, 155.96, 171.76. FT-IR (cm<sup>-1</sup>): 3356, 2928, 2857, 1719, 1508, 1463, 1429, 1347, 1288, 1253, 1217, 1126, 1062, 985, 906, 838, 783, 696.

**3.2.20. Synthesis of PDOPA-12:** PDOPA-Si-12 (0.70 gm, 1.1 mmol) was taken in a 10 mL flask and dissolved in 5 mL of THF. TBAF (0.72 gm, 2.3 mmol) was added into it and reaction was continued at 25<sup>0</sup>C for 12 h in dark. After 12 h polymer was precipitated in hexane and dialysed

against milli Q water for 24 h.  $^1\text{H}$  NMR (400 MHz,  $\text{CDCl}_3$ )  $\delta$  ppm: 1.24 - 1.31 (m, 16 H,  $\text{CH}_2$ ), 1.55- 1.62 (m, 4 H,  $\text{CH}_2$ ) 2.96 (s, 2 H,  $\text{CH-CH}_2$ ), 3.92 - 4.19 (m, 4 H,  $-\text{NHCOO-CH}_2-$ ,  $-\text{CHCOO-CH}_2-$ ), 4.56 (d, 1 H,  $\text{CH}_2\text{-CH}$ ), 5.09 (d, 1 H,  $\text{CH-NH}$ ), 6.55 (dd, 1 H, **ArH**), 6.61 (d, 1 H, **ArH**), 6.67 (d, 1 H, **ArH**).  $^{13}\text{C}$  NMR (100 MHz,  $\text{CDCl}_3$ )  $\delta$  ppm: 25.84, 25.89, 28.51, 28.93, 29.26, 29.34, 29.53, 29.57, 29.60, 37.53, 54.61, 65.29, 65.51, 120.95, 122.19, 128.72, 145.91, 146.65, 155.92, 171.74. FT-IR ( $\text{cm}^{-1}$ ): 3354, 2923, 2852, 1717, 1508, 1459, 1429, 1343, 1283, 1253, 1212, 1122, 1062, 983, 906, 839, 781, 698.

**3.2.21. Synthesis of PDOPA-Si-PEG-400:** Monomer (4) (0.65 g, 1.3 mmol) and PEG-400 (0.52 gm, 1.3 mmol) was taken in a polymerization tube and polymerized using the same method as reported for PDOPA-Si-12.  $^1\text{H}$  NMR (400 MHz,  $\text{CDCl}_3$ )  $\delta$  ppm: 0.16 (s, 12 H,  $-\text{Si}(\text{CH}_3)_4$ ), 0.95 (s, 18 H,  $-\text{C}(\text{CH}_3)_6$ ), 2.91-3.01 (m, 2 H,  $\text{CH-CH}_2$ ), 3.62-3.67 (m, 30 H,  $-\text{O-CH}_2\text{-CH}_2\text{-O-}$ ), 4.13-4.27 (m, 4 H,  $-\text{NHCOO-CH}_2-$ ,  $\text{CHCOO-CH}_2-$ ), 4.52-4.55 (q, 1 H,  $-\text{CH}_2\text{-CH}$ ), 5.22 (d, 1 H,  $\text{CH-NH}$ ), 6.53-6.57 (m, 2 H, **ArH**), 6.70 (d, 1 H, **ArH**).  $^{13}\text{C}$  NMR (100 MHz,  $\text{CDCl}_3$ )  $\delta$  ppm: -4.12, 25.88, 37.29, 54.65, 61.65, 64.14, 64.30, 68.78, 69.41, 70.40, 70.50, 72.57, 120.96, 122.16, 122.23, 128.58, 145.94, 146.66, 155.55, 171.47. FT-IR ( $\text{cm}^{-1}$ ): 3353, 2926, 2857, 1717, 1505, 1463, 1425, 1345, 1286, 1256, 1217, 1126, 1064, 985, 906, 838, 783, 692.

**3.2.22. Synthesis of PDOPA-PEG-400:**  $^1\text{H}$  NMR (400 MHz,  $\text{CDCl}_3$ )  $\delta$  ppm: 2.90-3.07 (m, 2 H,  $\text{CH-CH}_2$ ), 3.63-3.72 (m, 30 H,  $-\text{O-CH}_2\text{-CH}_2\text{-O-}$ ), 4.14-4.36 (m, 4 H,  $-\text{NHCOO-CH}_2-$ ,  $\text{CHCOO-CH}_2-$ ), 4.59 (s, 1 H,  $-\text{CH}_2\text{-CH}$ ), 5.39-5.22 (m, 1 H,  $\text{CH-NH}$ ), 6.53-6.57 (m, 1 H, **ArH**), 6.71-6.79 (m, 2 H, **ArH**).  $^{13}\text{C}$  NMR (100 MHz,  $\text{CDCl}_3$ )  $\delta$  ppm: 37.30, 54.62, 61.63, 64.11, 64.27, 68.75, 69.39, 70.37, 70.49, 72.55, 120.91, 122.10, 122.18, 128.52, 145.91, 146.61, 155.52, 171.42. FT-IR ( $\text{cm}^{-1}$ ): 3353, 2922, 2853, 1717, 1503, 1463, 1422, 1348, 1283, 1258, 1215, 1122, 1064, 983, 903, 835, 782, 696.

**3.2.23. Drug encapsulation and *in vitro* release:** The drug loading experiment was carried out with the anticancer drugs DOX and TPT by using the dialysis method. The procedure followed was adopted from the previously reported protocol. The dialyzed solution was filtered, lyophilized and stored in dark condition at 4 °C. The drug loading content (DLC) and drug loading efficiencies (DLE) were determined by absorption spectroscopy using the molar extinction coefficients of

11500 L mol<sup>-1</sup> cm<sup>-1</sup> and 20000 L mol<sup>-1</sup> cm<sup>-1</sup> for DOX and TPT, respectively. DLC and DLE were calculated by using the following formulae.

$$\text{DLE (\%)} = \{\text{weight of drug in NPs} / \text{weight of drug in feed}\} \times 100$$

$$\text{DLC (\%)} = \{\text{weight of drug in NPs} / \text{weight of polymer taken}\} \times 100$$

The release profiles of drug loaded polymer nanoparticles were studied by dialysis method using absorbance spectroscopy. The typical experiment protocol was followed as reported earlier. The cumulative drug release was calculated using the following equation.

$$\text{Cumulative drug release} = \{[\text{Amount of drug released at time 't'}] / [\text{Total amount of drug in nanoparticles taken in dialysis tube}]\} \times 100.$$



**3.2.24. Cell viability assay and Cellular Uptake by Confocal microscopy:** These studies were carried out following our reported procedure.<sup>39,40</sup> The cytotoxicity of nascent polymer and drug loaded polymer nanoparticles was studied in WTMEF cell line and MCF 7 cell lines using the MTT assay. The protocol for cell viability assay and cellular uptake was same as that reported earlier by us.<sup>41</sup> The absorbance from the purple formazan crystals formed as a result of MTT reduction by mitochondrial dehydrogenase enzyme was the measure of viable cells. Values from triplicate run for each control and treated set were noted and their mean value was used for calculations. The cellular uptake was studied using a LSM 710 confocal microscope wherein the fluorophores were excited using the  $\lambda=405$  nm (blue channel) and  $\lambda=561$  nm (red channel) lasers. Images thus obtained were analyzed using ImageJ analysis software.

### 3.3. Results and Discussion

#### 3.3.1. Synthesis and characterization of L-tyrosine and L-DOPA based polymers:

Synthetic methodologies for phenol-containing polyesters or polyester urethane are very rare in the literature, and therefore, new strategies are required to make polymers from L- tyrosine and L- DOPA amino acid resources. For this purpose, the acid and amine functional groups were converted into ester and urethane functionality, respectively, and the –OH groups were concealed as silyl ether by reacting with tert-Butyldimethylsilyl chloride. The structures of the new L-tyrosine and L-DOPA monomers are shown in Scheme 3.1 and their chemical structures were characterized by NMR spectroscopy (see Figure 3.4.)

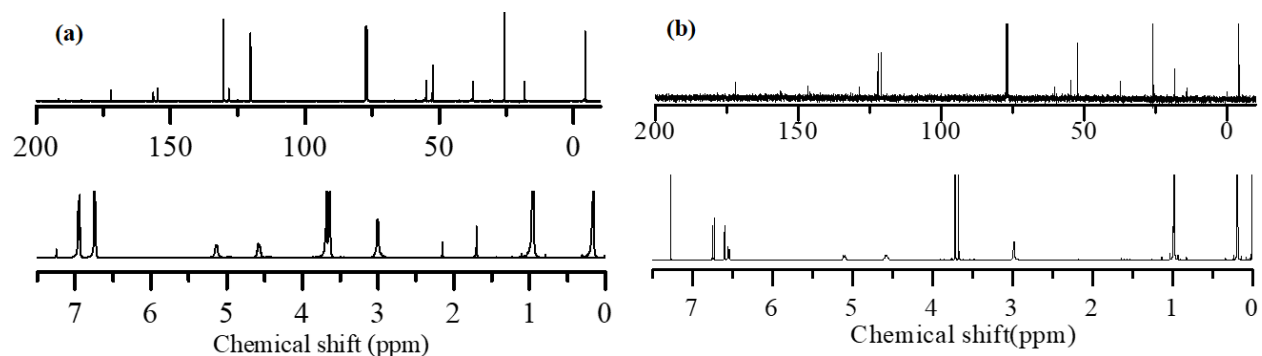
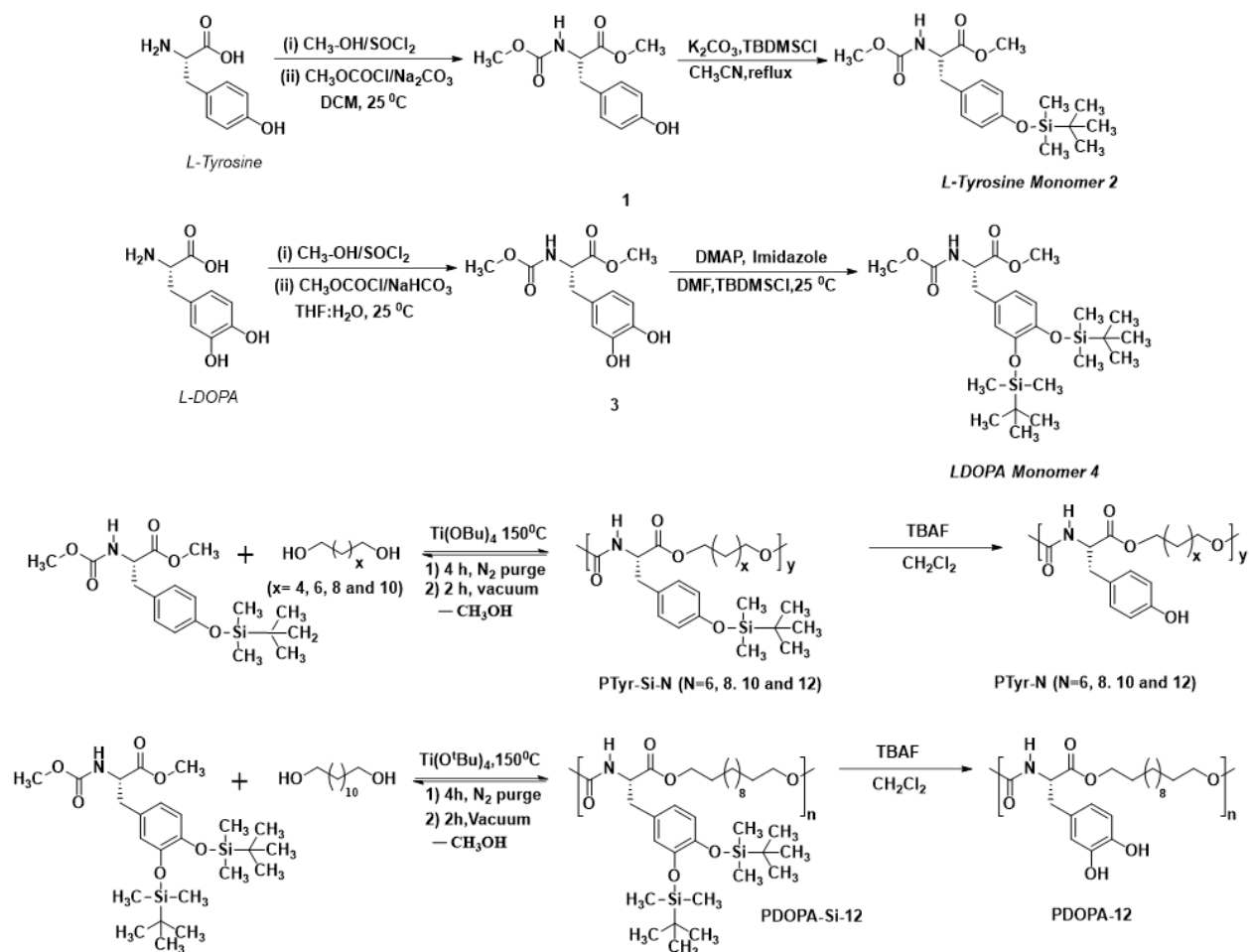


**Figure 3.4.** (a)  $^1\text{H}$  NMR and  $^{13}\text{C}$  NMR spectra of L-tyrosine-monomer (2) and (b) L-DOPA monomer (4) in  $\text{CDCl}_3$ .

Thermogravimetric analysis demonstrated excellent thermal stability of both the monomers up to 200  $^\circ\text{C}$  and their suitability for melt polymerization. L-tyrosine monomer-2 was subjected to polymerization along with different commercial diols under melt conditions at 150  $^\circ\text{C}$  using 1 mol % of  $(\text{Ti}(\text{O}i\text{Bu})_4)$  catalyst. The melt polymerization was carried out in two steps in a

single pot: (i) in first step amino acid monomer and diol were allowed to react for 4 h in presence of catalyst at 150 °C. Continuous nitrogen gas was purged as a carrier to remove the methanol during polycondensation reaction to produce viscous oligomers, and (ii) In the second stage, polycondensation was carried out under high vacuum (0.01 mm of Hg) for 2 h to yield highly viscous polymers. These polymers are referred to as PTyr-Si-12, PTyr-Si-10, PTyr-Si-8 and PTyr-Si-6 for the usage of aliphatic diols, 1, 12-dodecanediol, 1, 10-decanediol, 1, 8-octane diol, 1, 6-hexane diol, respectively, and their structures are shown in Scheme 3.1.



**Scheme 3.1.** Synthesis of L-Tyrosine and L-DOPA based monomers and poly(ester-urethane)s.

The polymerization process was confirmed by NMR and a representative NMR spectrum for PTyr-Si-12 is shown in Figure 3.5.a. The singlet at 3.66 ppm and at 3.70 ppm corresponding to methyl protons of urethane and ester groups in monomer-2 (Figure 3.5.a) were completely disappeared in the polymer spectrum. A multiplet at 4.08 (proton b+b') was appeared in polymer spectrum corresponding to the formation of new ester and urethane chemical linkages (Figure 3.5.b).  $^{13}\text{C}$ -NMR spectrum of monomer 2 showed two peaks at 54.2 and 54.4 ppm for the methyl

carbon of urethane and ester respectively, which were completely vanished and new peak appeared at 60.4 ppm in the polymer  $^{13}\text{C}$ -NMR spectrum. The disappearance of end groups and appearance of newly formed ester and urethane peaks in  $^1\text{H}$  and  $^{13}\text{C}$  NMR confirmed the polymerization of monomer 2 and 1,12- dodecanediol to give PTyr-Si-12.

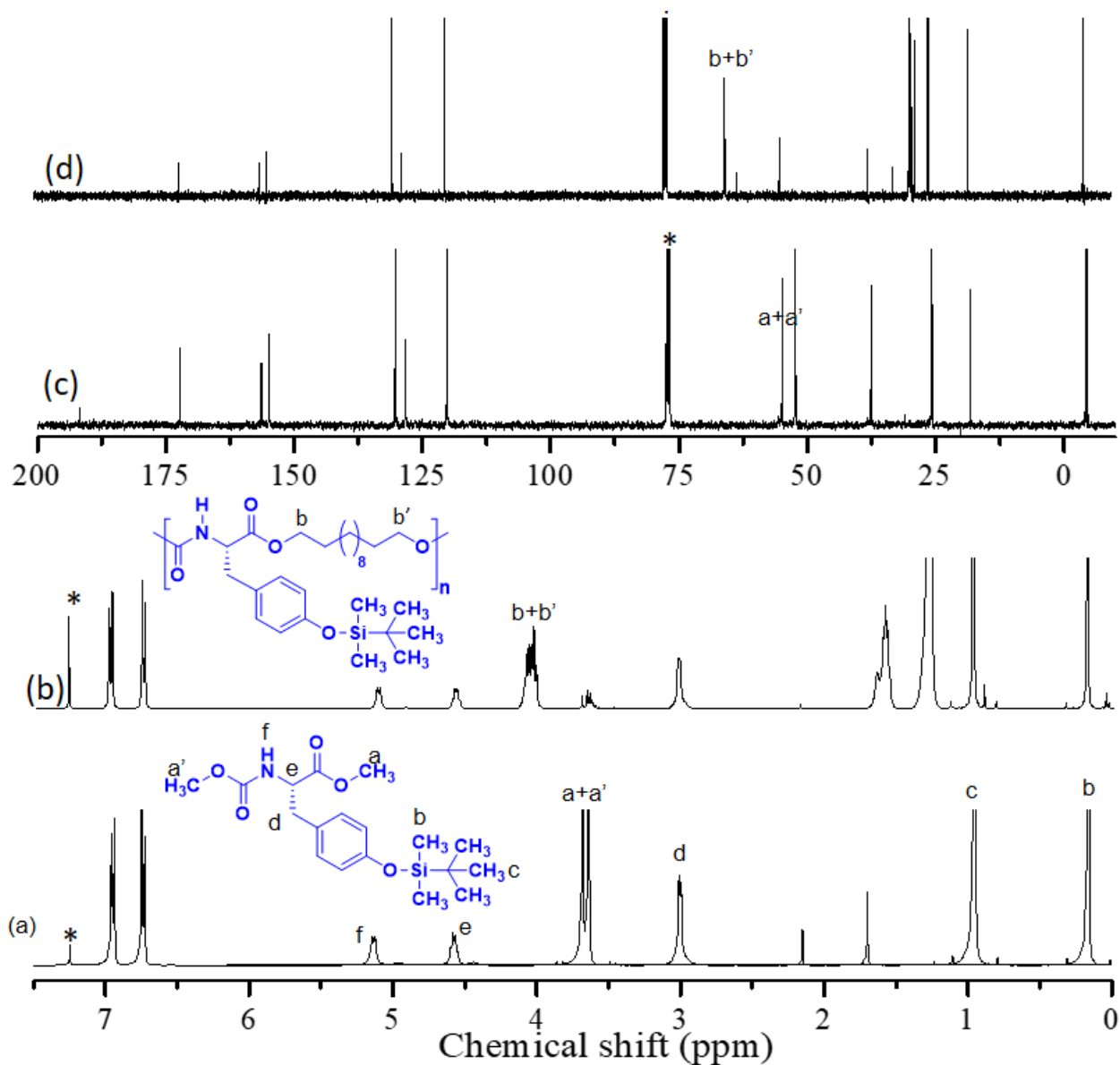


**Figure 3.5.** (a)  $^1\text{H}$  NMR and  $^{13}\text{C}$  NMR spectra of monomer L-tyrosine-monomer 2 and (b) polymer PTyr-Si-12 in  $\text{CDCl}_3$ . The solvent peaks are indicated by asterisks and the different types of protons in the chemical structure are assigned alphabetically with respect to peaks in the NMR spectra.

Similarly, the melt polymerization of L-tyrosine monomer-2 with other diols were confirmed by NMR and the details are given in Figures 3.6. The molecular weight of the polymers

was determined by gel permeation chromatography and it was found that all the silyl-protected polymers showed mono-model distribution (Figure 3.7.a). The number average molecular weight was varying from  $5.0 \times 10^3$  gm/mol to  $12.0 \times 10^3$  gm/mol while weight average molecular weight was varying from  $12.3 \times 10^3$  gm/mol to  $25.3 \times 10^3$  gm/mol depending upon the diol. (see table 3.1) The molecular weights of the polymers were found to be higher when 1,12-dodecanediol was employed in the synthesis as noticed in our previous investigation(ref).

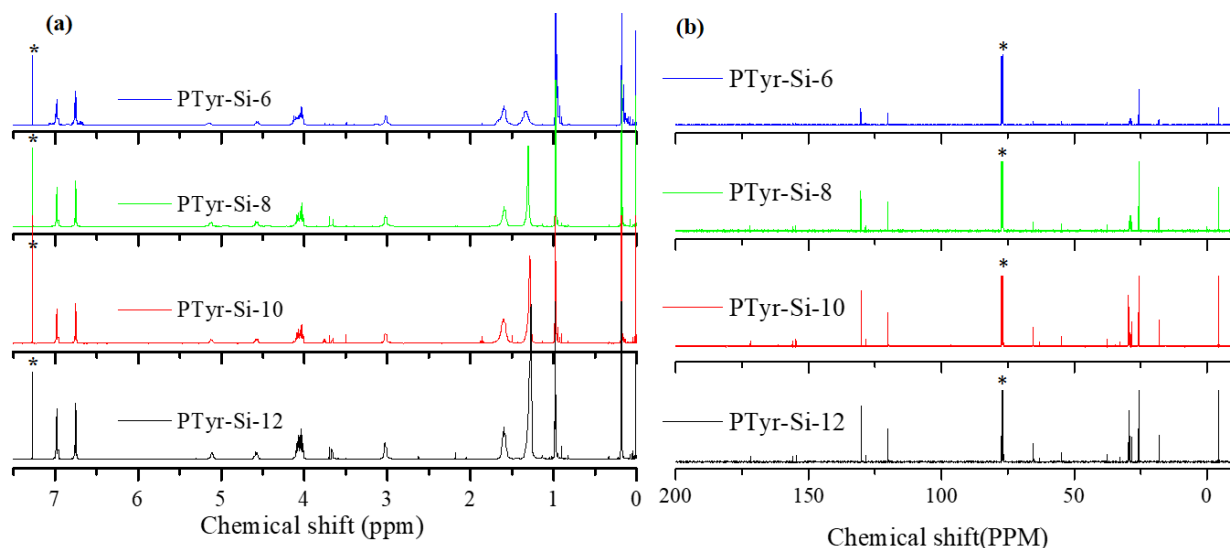


**Figure 3.6.** (a)  $^1\text{H}$  NMR and (b)  $^{13}\text{C}$  NMR spectra of polymers in  $\text{CDCl}_3$ . The solvent peaks are indicated by asterisks.

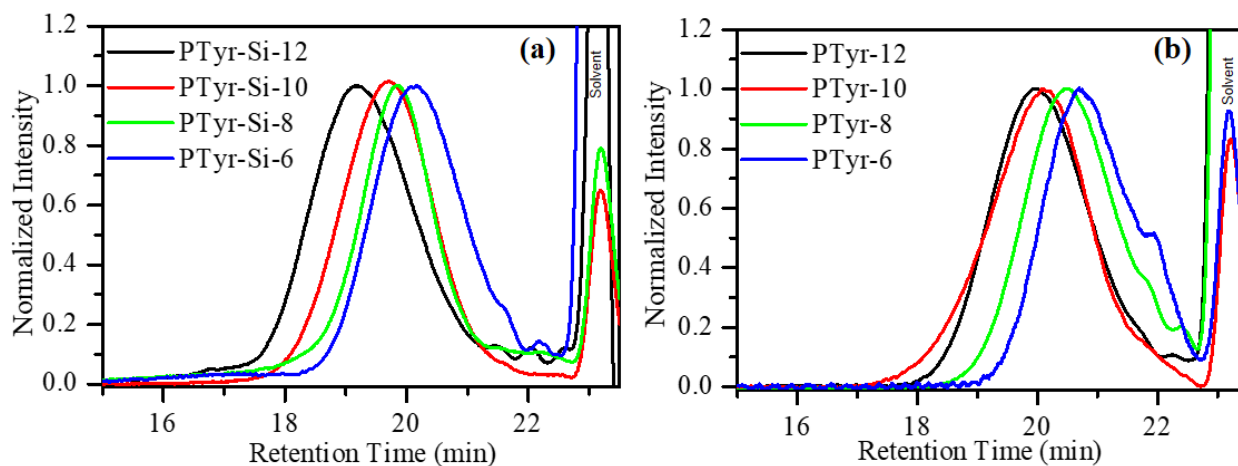


**Figure 3.7:** GPC chromatograms of polymers in THF at  $25^\circ\text{C}$ .

Post-polymerization deprotection of silyl group in these poly(ester-urethane)s using TBAF yielded the phenol-group containing L-tyrosine based poly(ester-urethane)s (PTyr-X) as shown

in Scheme-3.1. The deprotection was confirmed by  $^1\text{H}$  NMR analysis that which showed the complete disappearance of peaks at 0.17 ppm and 0.98 ppm corresponding to methyl and t-butyl protons of silyl group. Further, the comparison of the peak intensities of the other protons in the polymer structure revealed that the de-protection did not affect the backbone the polymer chains and retaining the degree of polymerizations. GPC plots of the phenol-functionalized polymers PTyr-X showed mono-modal distribution in Figure 3.7.b. however, their molecular weights were found to be slightly lower (table 3.1) than that of their silyl-counterpart. In the case of PTyr-Si-N, the polymer structure is completely hydrophobic and resembles the polystyrene standard used for the GPC calibration. But after silyl deprotection, there is structural variation between the polymer structure and polystyrene standards used for GPC calibration. Therefore, in the case of PTyr-N the GPC is underestimating the molecular weights.

**Table 3.1.** <sup>a</sup>Molecular weights are determined by GPC in THF at 25 °C. <sup>b</sup>DSC thermograms are recorded under nitrogen atmospheres at 10°/min heating/cooling cycles. <sup>c</sup>Decomposition temperature was estimated from TGA plots at 5% decomposition under a nitrogen atmosphere at 10°/min heating rate.

Polymer	Diol	$M_n^a$ (g/mol)	$M_w$ (g/mol)	Mw/Mn	$T_g^b$ (°C)	$T_D^c$ (°C)	Deprotected Polymer	$M_n$ (g/mol)	$M_w$ (g/mol)	Mw/Mn	$T_g$ (°C)	$T_D$ (°C)
PTyr-Si-12	C12-diol	12000	25300	2.1	8.3	327	PTyr-12	4000	11000	2.7	22.1	315
PTyr-Si-10	C10-diol	7000	14000	2	13.8	300	PTyr-10	4500	8200	1.8	26.2	287
PTyr-Si-8	C8-diol	7000	11700	1.6	15.4	290	PTyr-8	3500	8000	2.1	31.6	270
PTyr-Si-6	C6-diol	5000	12300	2.9	23.8	280	PTyr-6	2000	4000	2	34.3	254
PDOPA-Si-12	C12-diol	9800	21000	2.1	18.0	305	PDOPA-12	7000	14000	2.0	24.0	290

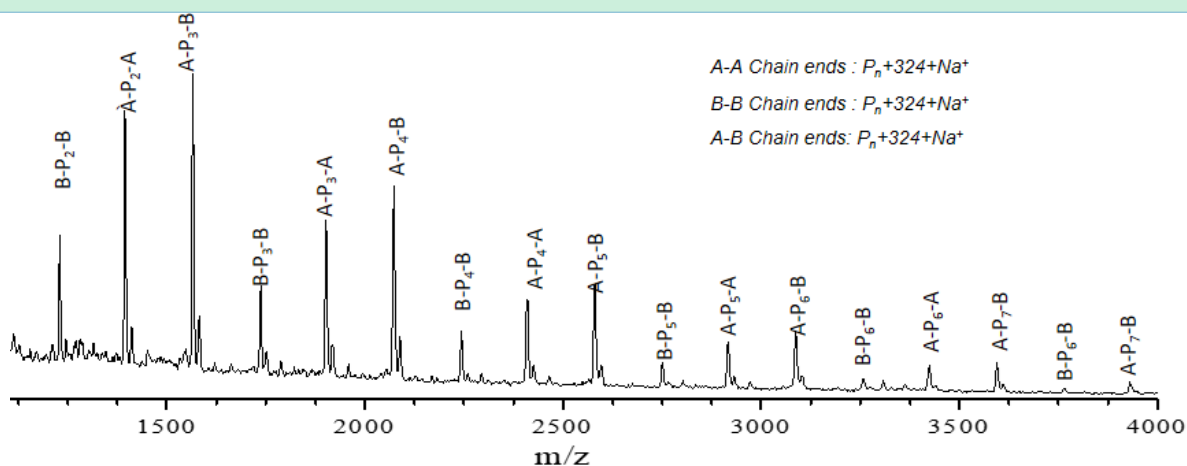


**Figure 3.8.** MALDI-TOF spectrum of PTyr-Si-12 polymer aliquots after 3 h.

MALDI-TOF end group analysis was carried out to analyze the stability of the silyl groups in the melt polycondensation process. In a typical A-A+ B-B type polycondensation, four different end groups are expected: (i) polymer chains having A-P<sub>n</sub>-A type, (ii) polymer chains having B-P<sub>n</sub>-B types, (iii) polymer chains having A-P<sub>n</sub>-B type, and (iv) macrocycles P<sub>n</sub>, if any (n= repeating unit). Polymer aliquots in the N<sub>2</sub> purge stage showed peaks corresponding to A-P<sub>n</sub>-A, B-P<sub>n</sub>-B and A-P<sub>n</sub>-B and no peaks with respect to macrocycle was found (Figure 3.8). L-Tyrosine monomer-2 was subjected for melt polymerization with 1,12 dodecanediol using 1 mol % of catalyst at 150 °C. All the polymers were subjected for NMR and GPC analysis and molecular weights obtained from GPC are summarized in Figure 3.9. Among all the catalyst Eu(NO<sub>3</sub>)<sub>3</sub>, Ti(OBu)<sub>4</sub>, DBTDL and Fe(acac)<sub>3</sub> were giving high molecular weight polymers.

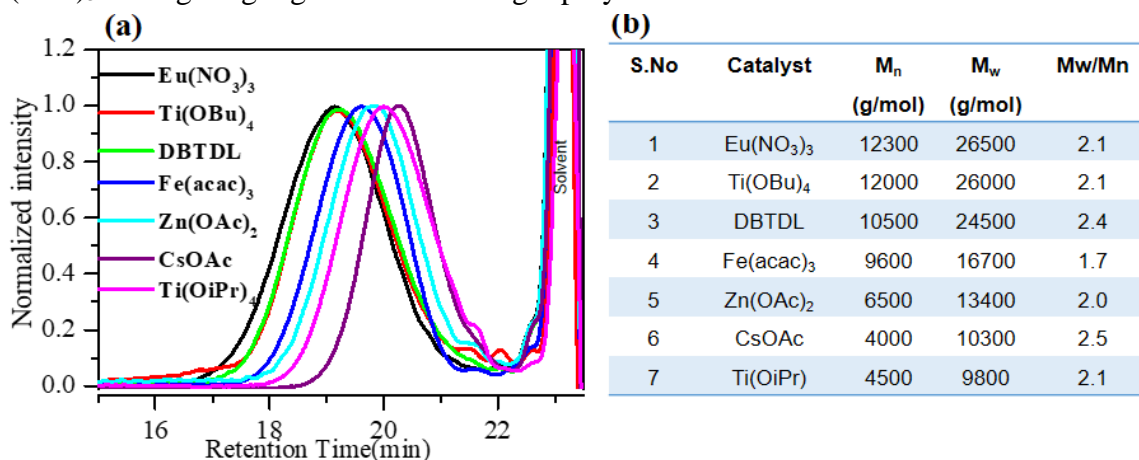


**Figure 3.9.** (a) GPC chromatograms of polymers with various catalysts. (b) Table containing molecular weights of polymers with different catalysts.

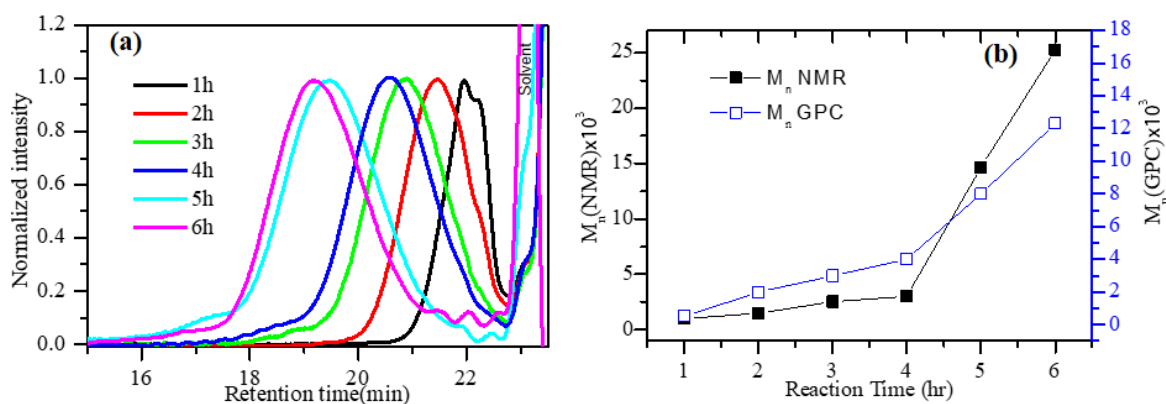


**Figure 3.10.** Gel permeation chromatograms of aliquots taken at different time interval for L-tyrosine monomer 2 polymerization kinetic study in tetrahydrofuran at 25 °C. (b) Comparison of molecular weight determined from GPC and NMR.

Further monomer-2 polymerization with 1,12 dodecanediol was subjected kinetic analysis using 1 mol % of Ti(OBu)<sub>4</sub>. Polymer aliquots were taken at different time interval and subjected

for GPC and NMR analysis. NMR analysis showed that the intensity of end groups at 3.66 ppm and 3.70 ppm was decreasing with time and intensity of newly formed ester urethane peak at 4.08 ppm was increasing with time.

Number average molecular weights from GPC and NMR showed good correlation, and completion of the reaction with more than 97 % conversion (Figure 3.10). Having established the polymerization process for L-tyrosine system, L-DOPA monomer-4 was polymerized with 1,12-dodecanediol using similar polycondensation approach (see Scheme-1) to produce silylated L-DOPA based poly(ester-urethane) (PDOPA-Si-12).

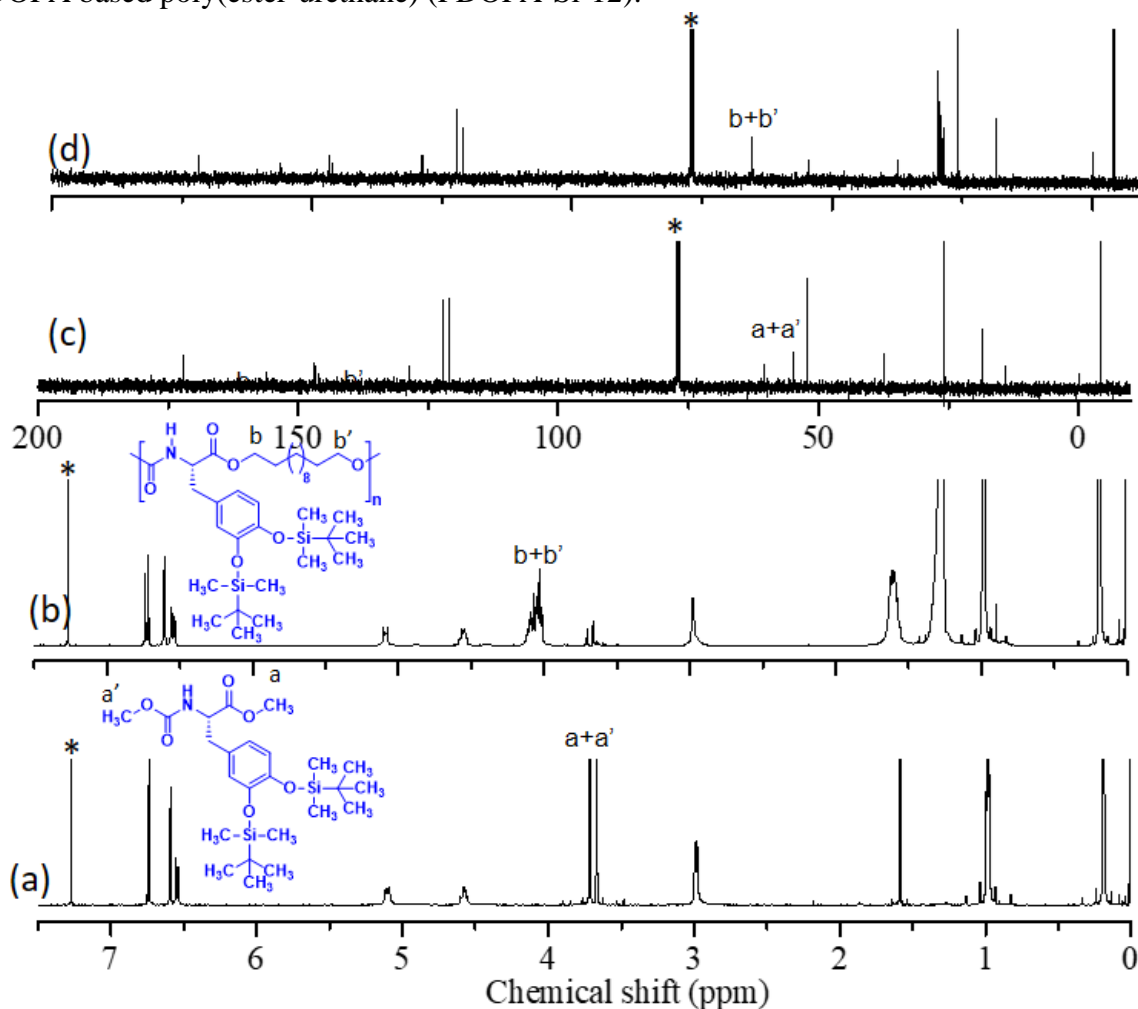
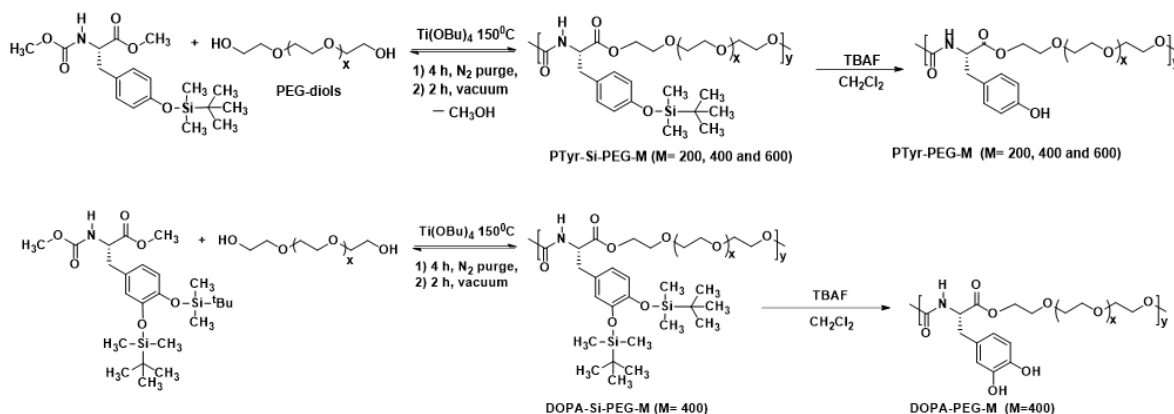


**Figure 3.11.** (a)  $^1\text{H}$  NMR and  $^{13}\text{C}$  NMR spectra of monomer L-tyrosine-monomer 2 and (b) polymer PTy-Si-12 in  $\text{CDCl}_3$ . The solvent peaks are indicated by asterisks and the different types of protons in the chemical structure are assigned alphabetically with respect to peaks in the NMR spectra.

produce silylated L-DOPA based poly(ester-urethane) (PDOPA-Si-12). NMR and GPC analysis showed the expected polymer structure with good molecular weight distribution and these details

are shown in Table 3.1. The silyl-groups were successfully de-protected to yield PDOPA-12 confirmed by its NMR analysis. The GPC molecular weights of the L-DOPA polymers are comparable to that of the L-tyrosine polymer (see table 3.1.)

To produce amphiphilic L-tyrosine and L-DOPA polymers, polyethylene glycols having molecular 200, 400 and 600 g/mol were chosen for the polymerization reaction (scheme 3.2.) and their NMR are shown in Figures 3.12. NMR spectra showed the complete disappearance of the end groups with respect to the formation of high molecular weight polymers; however, the GPC underestimated the molecular weights (see table 3.2). This observation is in agreement with earlier observations, in these classes of PEGylated polymers due to the large structural variation between the polymers and polystyrene standards used for GPC calibration.<sup>44</sup> Further, the silyl deprotection of these polymers yielded amphiphilic L- tyrosine and L-DOPA based PEGylated polymers.



**Scheme-3.2.** Synthesis of L-Tyrosine and L-DOPA based amphiphilic PEGylated poly(ester urethane)s.

**Table 3.2** <sup>a</sup>Molecular weights are determined by GPC in THF at 25 °C. <sup>b</sup>DSC thermograms are recorded under nitrogen atmospheres at 10°/min heating/cooling cycles. <sup>c</sup>Decomposition temperature was estimated from TGA plots at 5% decomposition under a nitrogen atmosphere at 10°/min heating rate.

Polymer	Diol	$M_n^a$ (g/mol)	$M_w^a$ (g/mol)	Mw/Mn	$T_g^b$ (°C)	$T_D^d$ (°C)	Deprotected Polymer	$M_n$ (g/mol)	$M_w$ (g/mol)	Mw/Mn	$T_g$ (°C)	$T_D$ (°C)
PTyr-Si-PEG-200	PEG-200	5200	11300	2.1	-8.9	270	PTyr-PEG-200	3800	5700	1.5	-1.3	268
PTyr-Si-PEG-400	PEG-400	5500	10000	1.8	-33.0	290	PTyr-PEG-400	3400	5300	1.4	-26.0	311
PTyr-Si-PEG-600	PEG-600	4500	9500	2.1	-41.0	340	PTyr-PEG-600	3500	6300	1.8	-33.0	317
PDOPA-Si-PEG-400	PEG-400	5500	10000	1.8	-33.0	310	PDOPA-PEG-400	3400	5300	1.4	-26.0	295



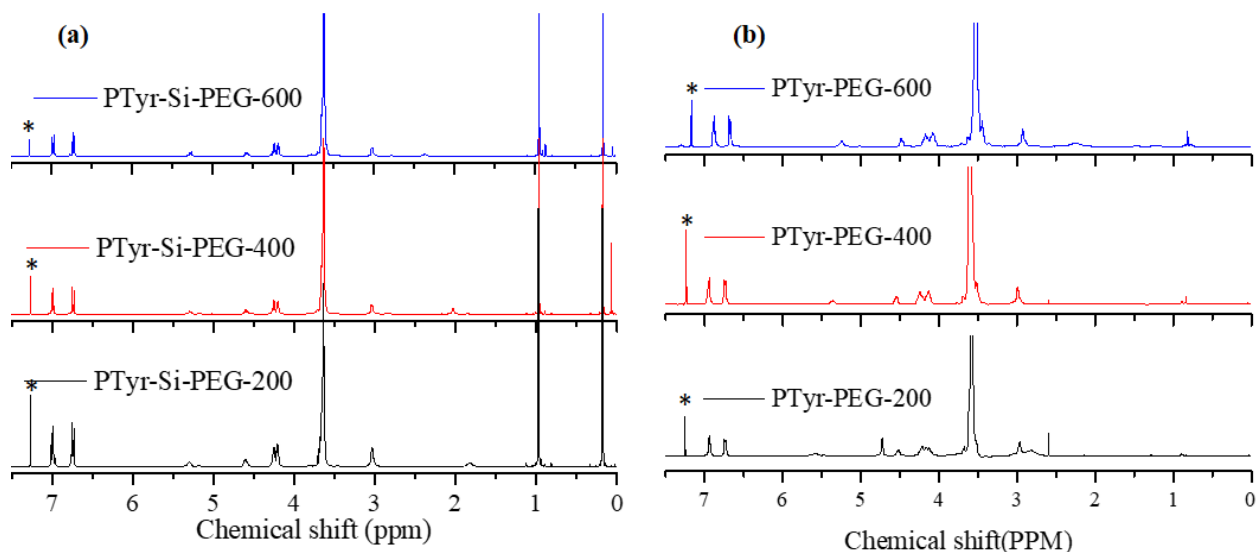


**Figure 3.12.** (a)  $^1\text{H}$  NMR spectra of PTyr-Si-PEG-M and (b) PTyr-PEG-M in  $\text{CDCl}_3$ . The solvent peaks are indicated by asterisks.

The thermal properties of polymers was determined by TGA and DSC analysis under nitrogen atmosphere. The TGA plots of polymers showed that all the polymers were stable more than 270-300  $^{\circ}\text{C}$  (see Figure 3.13).

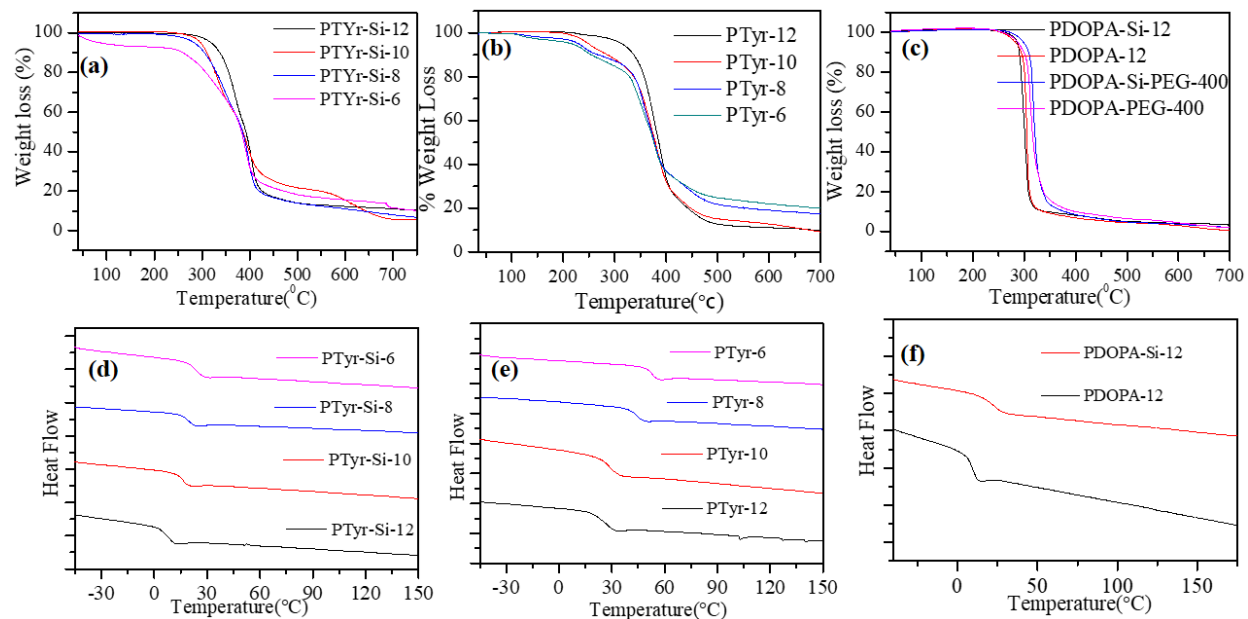


**Figure 3.13.** (a) TGA Profile of L-tyrosine Polymers before and (b) after silyl deprotection. (c) TGA profiles of LDOPA polymers before and after silyl deprotection. (d) DSC thermograms of L-tyrosine Polymers before and (e) after silyl deprotection. (f) DSC thermograms of LDOPA polymers before and after silyl deprotection

DSC thermograms of polymers showed that the polymers were predominately amorphous and exhibited only glass transition temperature ( $T_g$ ).  $T_g$  was increased from 8.3 to 23.8 with decrease in the aliphatic diol segment in PTyr-Si-X series which is attributed to higher flexibility of the polymers with increase in the diol chain length. Interestingly, the  $T_g$  of the phenolic-polymers were found to be almost 20 °C higher than the Si-polymers and this elevation in glass transition temperature is attributed to the hydrogen bonding between free –OH groups.

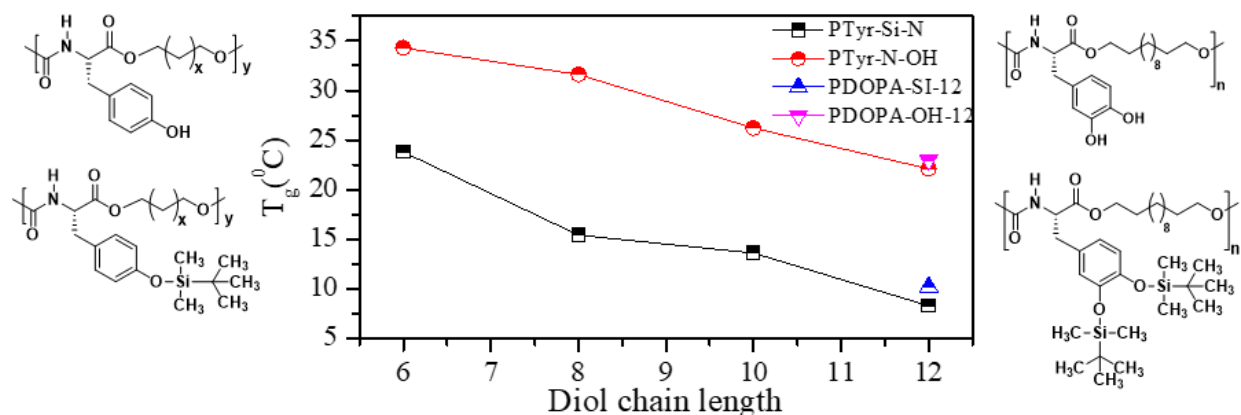


**Figure 3.14.** Comparison of  $T_g$  values of polymers before and after silyl deprotection.

$T_g$  of the PEG-polymers were very low and the values were observed in the sub-ambient region below  $-20$  °C due to the high degree of flexibility contributed by the PEG-chains. Based on the above analysis, it may be summarized that the newly developed melt polycondensation strategy in the L-tyrosine and L-DOPA amino acid resources is very elegant to produce new classes of silylated poly(ester-urethane)s and phenolic-poly(ester-urethane)s with good molecular weights and thermal properties and it may be highly useful as thermoplastic engineering materials. Further, the solvent free melt process is also eco-friendly and enabled diverse structural modification like phenolic, catechol functionality and amphiphilic PEGylated polymers.

### 3.3.2. Self-assembly in Thin-film and Aqueous Medium:

Aromatic amino acid polymers can demonstrate higher order self-assembled structures in a solid state or thin film due to their chirality and noncovalent interactions. Self-assembly of polymers was studied for drop-caste films by field-emission scanning electron microscope (FE-SEM) and atomic force microscopy (AFM). Both PDOPA-Si-12 and PDOPA-12 were dissolved in THF and their drop-caste film was subjected for FESEM and AFM imaging. FESEM images in Figure 3.15.a showed helical nanofibrous morphology having thickness of 40 nm and length of few micrometers. AFM images also confirmed the nanofibrous morphology and similar size range. PDOPA-12 polymer in Figure 3.15.b did not alter the nano-fibrous morphology.

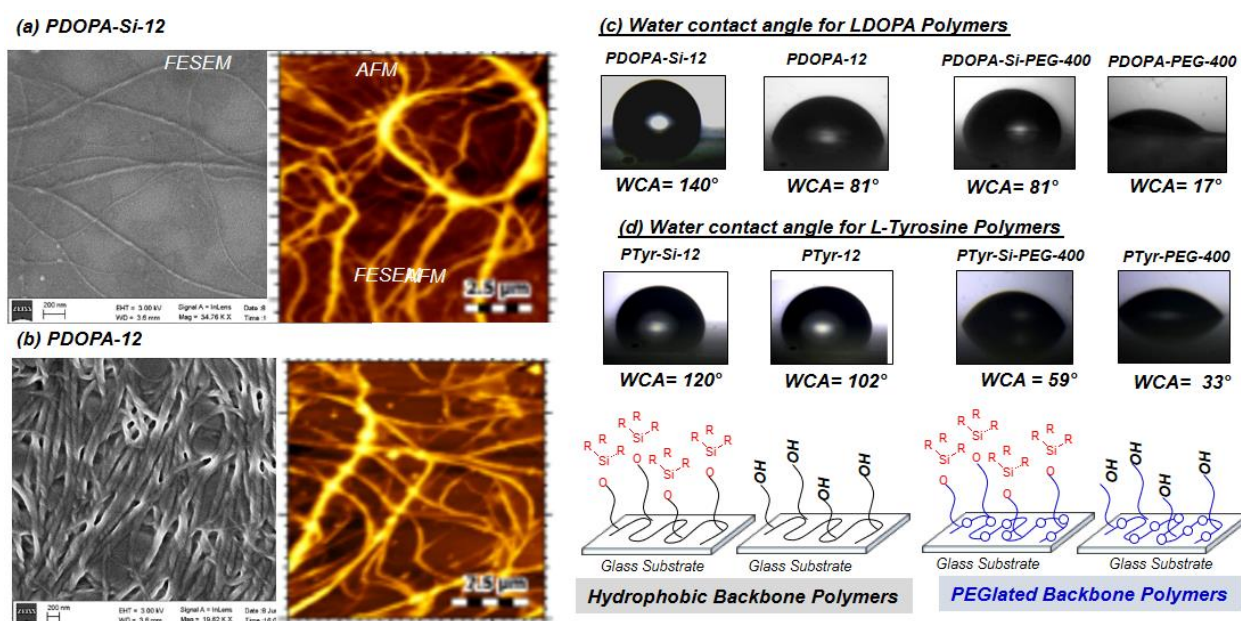


**Figure 3.15.** (a) FESEM and AFM images of polymer film drop cast from THF before and (b) after silyl deprotection. (c) Water contact angle images of polymers.

These results suggest that the bulky silyl-substitution or the -OH groups did not alter the self-assembly of the poly(ester-urethane) backbone and the chains adopted expanded conformation to produce very well-defined helical nano-fiber morphology. Water contact angle measurements is an excellent method to understand the hydrophilic or hydrophobic nature of the polymeric material. Highly hydrophobic surface or polymer materials exhibit WCA  $\theta > 90^\circ$  whereas  $\theta < 90^\circ$  is typically obtained for hydrophilic layers or materials. Since, the silyl and phenolic L-tyrosine and L-DOPA polymers are new entity in the literature, determination of their WCA would enable their long-term application for both material and biomedical application. WCA of the L-DOPA

and L-Tyrosine polymers was measured for thin films on glass substrate by low bond axisymmetric drop shape analysis (LB-ADSA method) and photographs polymers shown in. (Figure 3.15.c.) and (Figure 3.15.d.) respectively. Silyl groups are completely hydrophobic in nature; thus P-DOPA-Si-12 and PTyr-Si-12 showed completely hydrophobic in nature having water contact angle value  $140^{\circ}$  and  $120^{\circ}$ , respectively. The higher WCA for L-DOPA silyl polymer compare to L-tyrosine silyl polymer was attributed to the presence of one extra silyl group in each repeating unit. One would anticipate change in the hydrophobicity of these polymers upon deprotection of silyl unit. As expected, the phenolic polymers PDOPA-12 value (WCA=  $81^{\circ}$ ) PTyr-12 (WCA=  $105^{\circ}$ ) showed significant reduction in WCA. The value was found to large shift in L-DOPA polymer system by nearly  $60^{\circ}$  (from  $140^{\circ}$  to  $80^{\circ}$ ). So based on WCA values it may be concluded that all the polymers were hydrophobic in nature. The water contact angle of PEGylated polymers was also measured before and after silyl deprotection. The water contact angle for PDOPA-Si-PEG-400 and PTyr- Si-PEG-400 polymer was measured as  $81^{\circ}$  and  $59^{\circ}$  respectively. After silyl deprotection there was a significant decrease in water contact angle value for both the polymers. The water contact angle for PDOPA-PEG-400 and PTyr-PEG-400 was measured as  $19^{\circ}$  and  $33^{\circ}$  respectively (Figure 3.15.c.) and (Figure 3.15.d.). Since the PDOPA-PEG-400 polymer exhibited the maximum water solubility among all the polymers, it was selected for further aqueous self-assembly and drug loading studies. The new class of L-DOPA based poly(ester-urethane)s consists of hydrophilic PEG (-CH<sub>2</sub>CH<sub>2</sub>O-)x in the backbone and an aromatic substituent as a pendant. This design is similar to the comb-type amphiphilic polymer structures as shown in Figure 3.16.a.

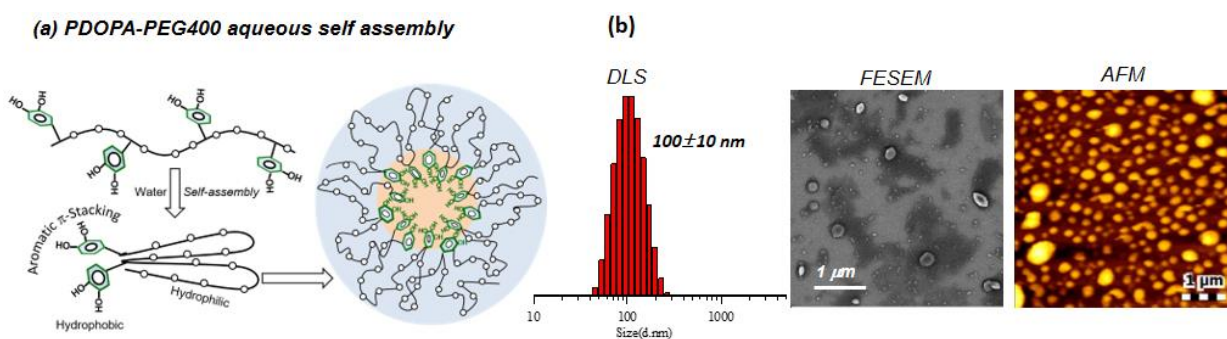


**Figure 3.16.** (a) Self-assembly PDOPA-PEG-400 into core-shell nanoparticles. (b) Dynamic light scattering (DLS) histogram, FE-SEM image and (AFM) atomic force microscopy image of PDOPA-PEG-400 nanoparticles. Samples concentration = 0.1 mg/ml of PTyr-PEG-400.

Due to secondary interactions between the pendent aromatic units the aromatic tails interact with each other and form a hydrophobic bundle, while the hydrophilic backbone folds into tiny hairpin structures due to likewise interactions. A higher-order self-assembly of these polymer aggregates produced micellar nanoparticles in aqueous solution. The polymer was showing formation of  $100 \pm 10$  nm nanoparticle in aqueous medium. Further, AFM and FESEM analysis confirmed the formation of spherical nanoparticles of  $100 \pm 10$  nm size in aqueous medium (Figure 3.16.b.)

### 3.3.3. Aromatic $\pi$ -Stack Driven Drug Encapsulation:

To check the drug loading capabilities of polymer two electron deficient polyaromatic anticancer drugs DOX.HCl and TPT.HCl was explored. in a typical procedure 0.5 mg of preneutralized drug and 5 mg of polymer was dissolved in 2 mL of DMSO. 3 mL of water was added dropwise into it and mixture was stirred in dark for 4 h. After 4 h mixture was transferred in a semipermeable membrane MWCO = 1.0 kDa and dialyzed against deionized water for 48 h. After Dialysis the samples were filtered through syringe filter and DLC was calculated by absorbance spectroscopy and it was found 7% and 4% respectively for DOX and TPT and DLE was determined 70% and 40% respectively. The DLS measurement of DOX and TPT loaded PDOPA-PEG-400 showed the formation of  $116 \pm 8$  nm and  $138 \pm 8$  nm size nanoparticles respectively which indicates there was not much change in the size of nanoparticle after drug loading (see Figure 3.17.). In order to confirm the size and shape of drug loaded nanoparticles, AFM and FESEM analysis were performed, which confirmed the formation of size  $>100$  nm spherical nanoparticles.

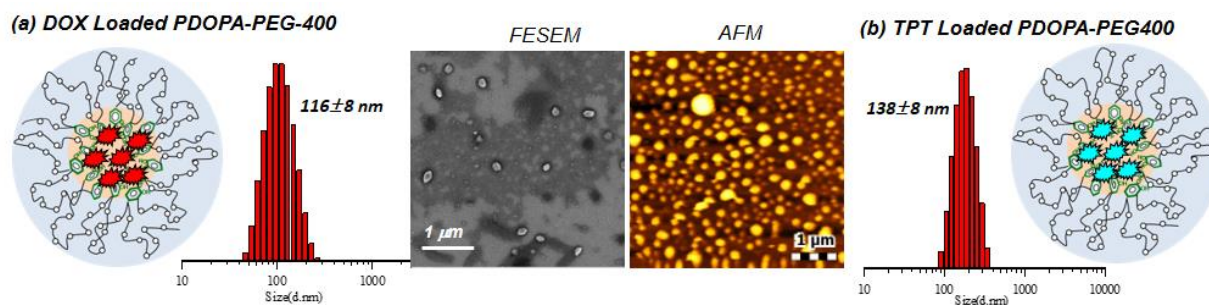


**Figure 3.17.** (a) DLS histogram, AFM and FESEM images of aqueous self-assembly of DOX loaded PDOPA-PEG-400. (b) DLS histogram of TPT loaded loaded PDOPA-PEG-400.

Aromatic electron-rich moieties are known for stabilizing of electron deficient drug molecules within hydrophobic core through aromatic pi-pi stacking interactions. So to check the aromatic interactions between L-DOPA and drug molecules a detailed photophysical study was carried out. The aqueous solution of free DOX, PDOPA-PEG-400, and DOX loaded nanoparticles was subjected for absorbance and emission spectroscopy (see Figure 3.18).

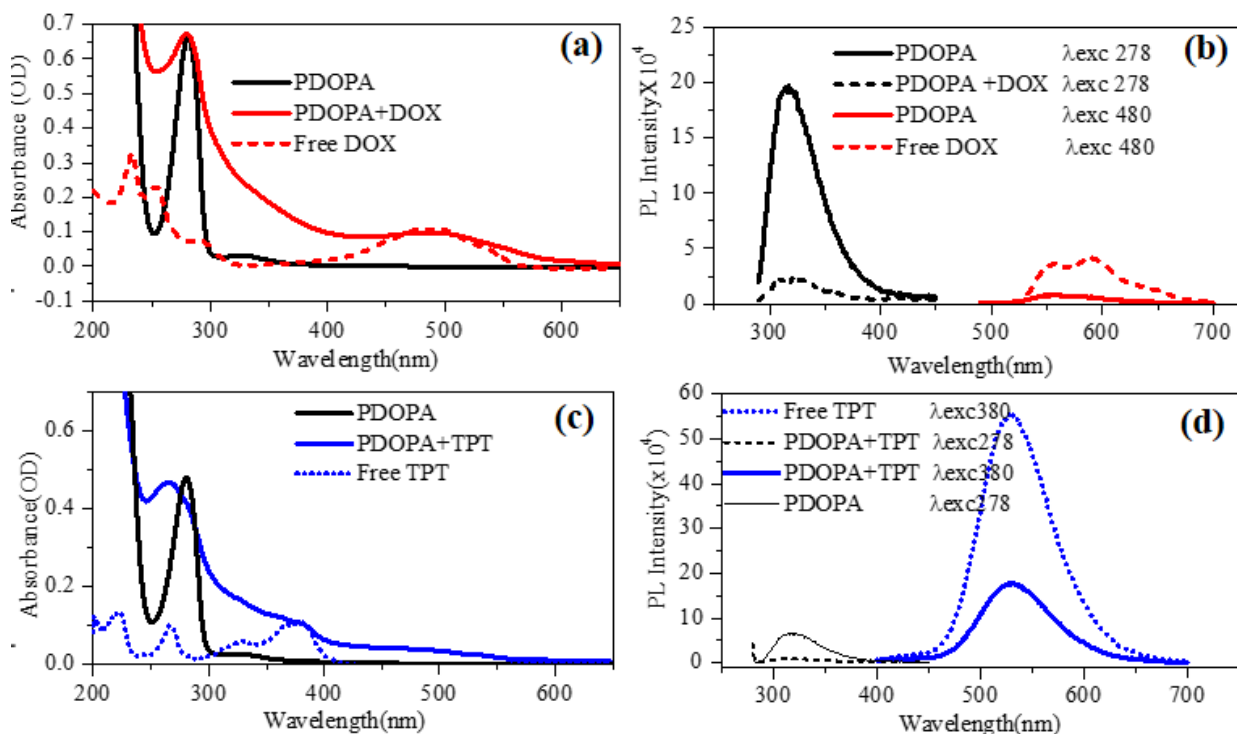


**Figure 3.18.** (a) Schematic representation of drug release of DOX loaded nanoparticle at the intracellular level by esterase enzyme. (b) Cumulative drug release profiles of (a) DOX (b) TPT in presence of esterase enzyme at 37°C in PBS buffer.

The concentration of DOX was maintained as 0.1 OD in free DOX and DOX loaded PDOPA-PEG-400 and concentration of L-DOPA was maintained as 0.67 OD in PDOPA-PEG-400 and DOX loaded PDOPA-PEG-400 (see Figure 3.18.a). The absorbance maxima corresponding to L-DOPA and DOX was observed at 287 nm and 480 nm in DOX loaded PDOPA-PEG400. When free DOX and DOX loaded PDOPA-PEG-400 was excited at 480 nm, free DOX showed an emission maximum at 560 nm while DOX loaded PDOPA-PEG-400 showed very weak emission band at 560 nm similarly when PDOPA-PEG-400 and DOX loaded PDOPA-PEG-400 was excited at 287 nm, PDOPA-PEG-400 showed a strong emission band at 310 nm which was getting quenched in DOX loaded PDOPA-PEG-400 (see Figure 3.18.b). The quenching of

fluorescent intensity at 310 nm and 560 nm in DOX loaded nanoparticle suggest the strong molecular interactions between L-DOPA and DOX.

Similar photophysical experiments were carried out for free TPT, PDOPA-PEG-400 and TPT loaded PDOPA-PEG-400 in which concentration of TPT and L-DOPA was maintained as 0.1 OD and 0.52 OD respectively (see Figure 3.18.c.) Free TPT and TPT loaded PDOPA-PEG-400 was excited at 380 nm free TPT showed a strong emission peak at 510 nm which got quenched in case of TPT loaded PDOPA-PEG-400. Similarly, PDOPA-PEG-400 and TPT loaded PDOPA-PEG-400 was excited at 287 nm corresponding to L-DOPA excitation; PDOPA-PEG-400 was showing an emission band at 310 nm which was quenched in TPT loaded PDOPA-PEG-400 (see Figure 3.18.d.). Thus the quenching of characteristic emission peak of drug and LDOPA in drug loaded nanoparticles indicates the efficient  $\pi$ - $\pi$  stacking between drug and electron rich LDOPA moieties.

### 3.3.4. In vitro drug release studies:

The backbone of newly designed L-DOPA based polymer contains an ester linkage in polymer backbone which is susceptible to esterase enzyme and after endocytosis these nanoparticles can be readily cleaved by lysosomal enzymes. So the enzyme responsive drug release behaviour was measured in presence and absence of esterase enzyme at 37 °C. The DOX loaded nanoparticles were dispersed in PBS buffer and placed in a dialysis tube (MWCO = 1 kDa) at 37 °C, the amount of DOX released in the reservoir was measured at different intervals using UV/visible spectroscopy. The cumulative drug release of DOX loaded nanoparticle was plotted and results are shown in Figure 3.19.a.

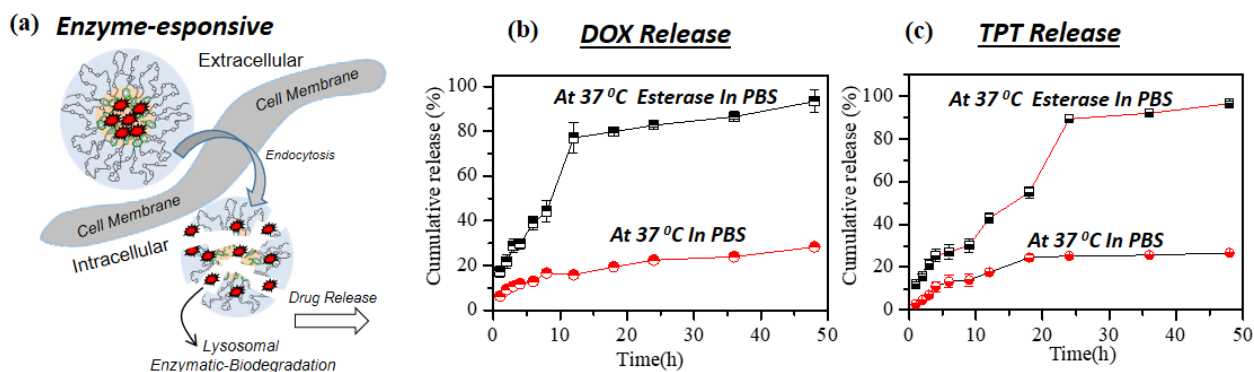


**Figure 3.19.** (a) Schematic representation of drug release of DOX loaded nanoparticle at the intracellular level by esterase enzyme. (b) Cumulative drug release profiles of (a) DOX (b) TPT in presence of esterase enzyme at 37°C in PBS buffer.

From drug release profile it is clear that nanoparticles were showing better stability in PBS buffer at 37°C with 25 % DOX release and showing almost 90 % drug release in presence of esterase enzyme within 24 h (Figure 3.19.b). Similarly, TPT loaded nanoparticles were showing good stability in PBS buffer at 37°C (leaching = 25%) and selectively getting cleaved in presence of esterase enzyme to release the loaded TPT (Figure 3.19.c).

Polymer chains with the optimal hydrophilic and hydrophobic balance are able to self-assemble in aqueous solution to form compact nanoparticles. During degradation, nanoparticles lose their hydrophilic- hydrophobic balance, which results in the aggregation of hydrophobic bundles in an aqueous medium, resulting in a gradual increase in nanoparticle size time. The degradation of drug loaded nanoparticles was further studied by DLS measurement. The drug loaded nanoparticles was treated with required amount of esterase enzyme and incubated at 37 °C for 48 hours. The change in size with time was monitored with DLS and results are shown in Figure 3.20. In presence of esterase enzyme, the drug loaded nanoparticles were changing from monomodal size distribution to bimodal size distribution and showing a gradual increase in size with time.

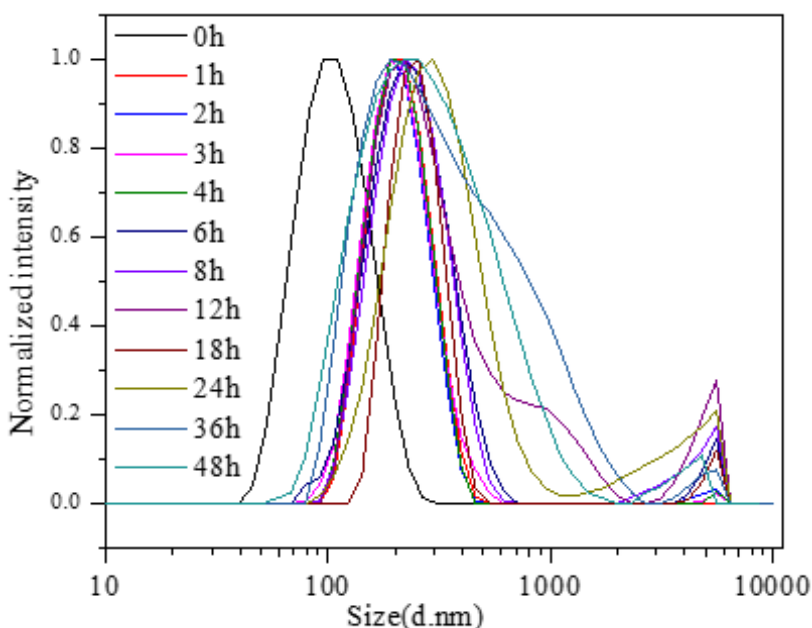


**Figure 3.20.** DLS histograms of drug loaded nanoparticles incubated at 37°C in presence of esterase enzyme.



From drug release profile and DLS size measurements it is clear that the polymer nanoparticles were stable under physiological condition but getting selectively cleaved in presence of esterase enzyme to release the loaded cargo.

### 3.3.5. Cytotoxicity and cellular uptake:

The biocompatibility of these newly designed poly(ester-urethane) scaffolds was investigated in noncancerous embryonic fibroblast cell line (WTMEF) and breast cancer cell line (MCF7) using MTT. A 96-well plate was seeded with  $10^3$  cells per well in a triplicate and incubated for 18 h at  $37^{\circ}\text{C}$  in  $\text{CO}_2$  incubator. The cells were treated with different polymer concentrations ranging from  $1\ \mu\text{g/mL}$  to  $80\ \mu\text{g/mL}$ , and subsequently incubated at  $37^{\circ}\text{C}$  for 72 hours. The media was aspirated and  $100\ \mu\text{L}$  of fresh MTT solution ( $0.5\text{mg/mL}$  in complete media) was added in each well. After 4h incubation the media was removed and  $100\ \mu\text{L}$  of DMSO was added in each well to dissolve the MTT-formazan crystals.

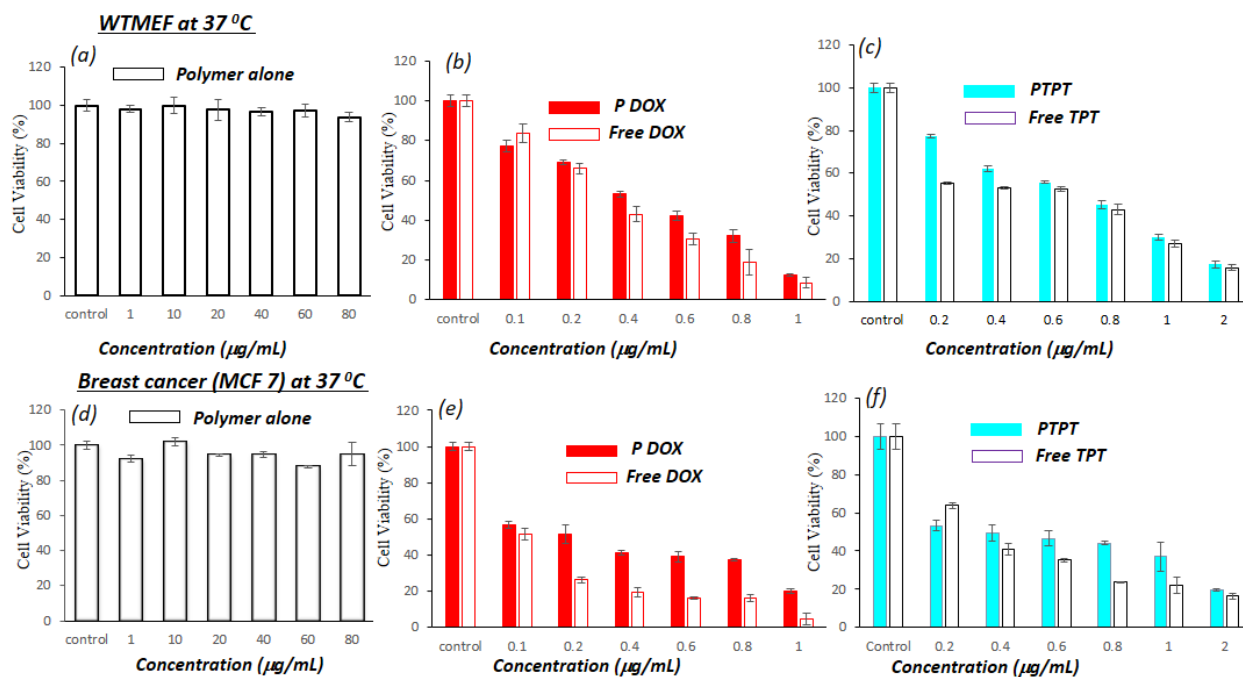


**Figure 3.21.** (a) Cytotoxicity of PDOPA-PEG-400 nascent nanoparticles (b) free DOX and DOX loaded PDOPA-PEG-400 (c) free TPT and TPT loaded PDOPA-PEG-400 nanoparticles in WTMEF cell line. (d) Cytotoxicity of nascent PDOPA-PEG-400 nanoparticles (e) free DOX and DOX loaded PDOPA-PEG-400 (f) and free TPT and TPT loaded PDOPA-PEG-400 nanoparticles in the MCF7 cell line (incubation time = 72 h)

The absorbance of formazan crystals was measured at 570 nm and the results of MTT experiment are shown in Figure 3.21. The cell viability plots in Figure 3.21.a shows that the newly

designed L-DOPA based polyester urethane nanoparticle were highly biocompatible and there was no cytotoxicity observed even up to 80  $\mu\text{g/mL}$ . A cytotoxicity test was performed for DOX loaded and TPT loaded nanoparticles in (WTMEF) and MCF-7 cell lines with DOX concentrations ranging from 0.1  $\mu\text{g/mL}$  to 1  $\mu\text{g/mL}$  and TPT concentrations ranging from 0.2  $\mu\text{g/mL}$  to 2  $\mu\text{g/mL}$  respectively and the viability plots are shown in Figure 3.21.b. and 3.21.c. In WTMEF cell line both PDOX and PTPT exhibited less toxicity compare to free drug and in MCF-7 cells the nanoformulations were efficiently inhibiting the cell growth. The DOX loaded nanoparticles were showing almost 20% cell viability at the concentration of 1  $\mu\text{g/mL}$  (see Figure 3.21.e.) The TPT loaded nanoparticles showed almost the same cytotoxicity as free TPT and free TPT became stagnant at higher concentrations, whereas the TPT loaded nanoparticles showed a linear cell growth inhibition with a cell viability of 20 % at the concentration of 2  $\mu\text{g/mL}$  (see figure 3.21.f.)

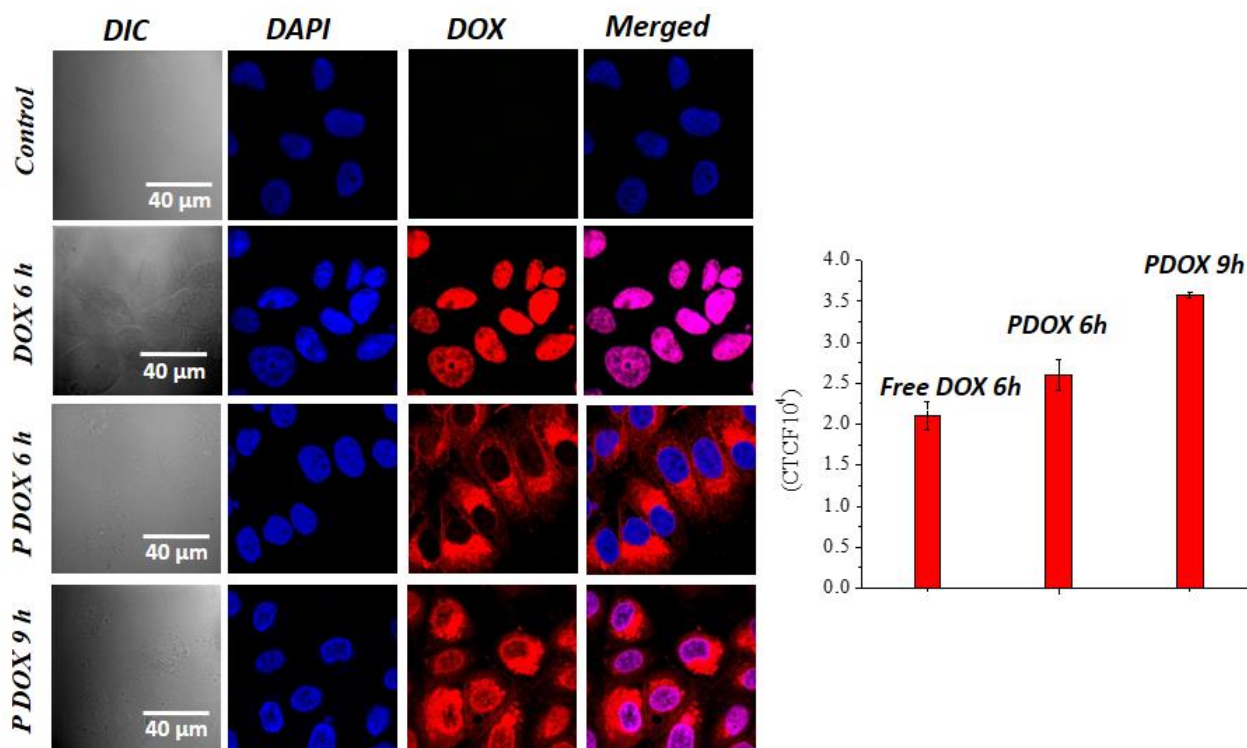


**Figure. 3.22** (a) CLSM images for free DOX and DOX loaded nanoparticles in MCF 7 cell line at two different time points. (b) bar diagram showing the CTCF for free DOX and DOX-loaded nanoparticles in MCF 7 cells at two different time points. ( $[\text{DOX}] = 2.0 \mu\text{g/mL}$  and 10,000 cells used).

The time dependent cellular uptake was monitored using Confocal microscopy. The six-well plate was seeded with 10,000 MCF-7 cells per well and incubated for 24 hours. Media was aspirated from the cells, they were exposed to DOX loaded nanoparticles (2.0  $\mu\text{g}/\text{mL}$  DOX) at two different time points at 6 and 9 hours. Free DOX (2.0  $\mu\text{g}/\text{mL}$ ) was also exposed to the cells for 6 hours as a control. In addition, a control for cells without DOX was also maintained to eliminate the possibility of signal interference from other chromophores. The inherent fluorescence property of DOX was exploited for imaging. For free DOX and PDOX treated samples the cells were excited at 561 nm and images were visualized in the red channel and the nucleus of the cells were stained with DAPI ( $\lambda = 405$  nm) and visualized at blue channel. The images processed in Image J software are shown in Figure. After 6 h incubation the red emission of free DOX was found in nuclear region which was confirmed by the magenta color of nucleus in merged image whereas, in case of DOX loaded nanoparticles the merged image shows that the red emission of DOX was mainly localized in the cytoplasm and very less in the nuclear region. After 9 h of treatment, the intense red emission of DOX was coming from both the cytoplasm and the nucleus suggesting that DOX was released from the nanoparticles and began to accumulate in the nuclei. These results suggest that the free DOX quickly gets transported into the cells via passive diffusion mechanism whereas, DOX loaded nanoparticles were effectively taken up via endocytosis and then released DOX into the nuclei. The intensity of DOX emission increased significantly upon increasing the incubation time of the nanoparticles from 6 h to 9 h so to quantify the DOX emission CTCF calculations was carried shown in Figure 2.22. The CTCF calculations indicate that the amount of nanoparticles taken up by the cell increased significantly with time, and it was almost 1.5 times higher after 9 h incubation compared with 6 h incubation.

### **3.3.6. Live cell imaging:**

Further, Live cell imaging experiment was used to examine the internalization of drugs inside the cells. A four-well live cell chamber was populated with MCF 7 cells at a density of 35,000 cells per well. The cells were exposed to free DOX and DOX loaded nanoparticles by maintaining the concentration of DOX at 2  $\mu\text{g}/\text{mL}$ . The cells were incubated at 37  $^{\circ}\text{C}$  in a 5%  $\text{CO}_2$  incubator for 9 hours and LysoTracker green DND 26 was used for staining the acidic compartments in live cells. The cells were imaged using a confocal instrument equipped with a stage incubator at 37  $^{\circ}\text{C}$  with humidified atmosphere and 5%  $\text{CO}_2$  throughout the experiment. The LysoTracker green was excited using the 488 nm laser, DOX was excited using 561 nm laser and imaged in the green and

red channel respectively. The obtained images were processed Image J analysis software and are shown in Figure 3.23. The live cell imaging of the free DOX in Figure 3.23 illustrates the abundance of free DOX in the nucleus and not in the cytosol or lysosomes. In case of nanoparticle assisted delivery there is a strong red emission can be seen in both cytosol and nucleus.

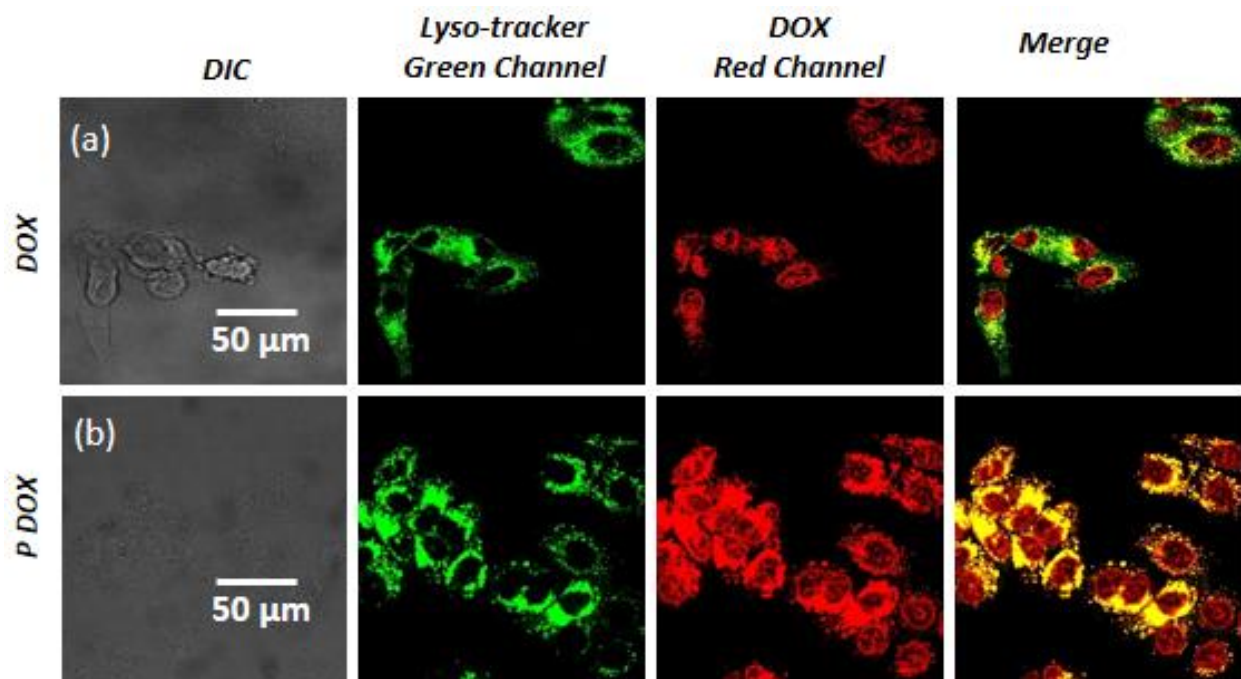


**Figure 3.23.** *live cell confocal microscope imaging: (a) with free DOX along with lysotracker, and (b) DOX loaded nanoparticle along with lysotracker [9 h incubation, DOX concentration = 2.0  $\mu\text{g}/\text{mL}$ .]*

It is clear from the polymer nanocarrier-assisted delivery images in Figure 2.23 that DOX was colocalized in the lysosomes as evidenced by the yellow fluorescence that became apparent due to the combination of green and red fluorescence. From live cell experiment it is evident that the colocalization of DOX in the lysosomal compartment, possibly caused by initial endosomal uptake of DOX loaded nanoparticles which further underwent degradation by lysosomal enzymes to release the DOX. The red emission of DOX in nucleus suggest that the released DOX was subsequently accumulated in the nucleus.

### 3.4. Conclusion

In summary, a new classes of biodegradable poly(ester urethane) nanocarriers were developed from L-DOPA and L-tyrosine bio-resources using solvent free melt polycondensation. For this

purpose, the trifunctional aromatic amino acid L-tyrosine and L-DOPA were suitably modified into melt polymerizable dual ester urethane monomer in which the phenolic and catechol functional groups were protected as silyl ether. These silyl protected amino acid monomers were subjected for melt polymerization with various PEG and to get L-Tyrosine and L-DOPA based silylated poly(ester urethanes). The postpolymerisation deprotection of silyl ether yielded a new classes of enzyme-responsive PEGylated amphiphilic poly(ester-urethane)s. The amphiphilic poly(ester urethane)s self-assembled in aqueous solvent to give  $100 \pm 10$  nm nanoparticles. The electron rich aromatic nature of PEGylated LDOPA polymer was explored for pi- stacking interaction driven drug encapsulation. Two different electron deficient anticancer drugs DOX, and TPT were loaded and the interactions between L-DOPA and drug molecules was confirmed by detailed photophysical studies. These drugs loaded nanocarriers were found to be stable at extracellular conditions, but experienced biodegradation in the presence of esterase enzyme, releasing the drug under physiological conditions. The biocompatibility of nanocarriers was tested in WT-MEFs and MCF 7 cell line and nanocarriers were showing no cytotoxicity up to 80  $\mu\text{g/mL}$  concentration whereas, the DOX and TPT drug-loaded polymer nanoparticles exhibited excellent cell killing in cancer cells. The cellular uptake of drug loaded nanoparticles in MCF 7 cells was confirmed by confocal microscopy. The present investigation offers new possibilities for designing biodegradable nanocarriers for cancer treatment based on L-amino acids.

## References

- (1) Beltrán-Gracia, E.; López-Camacho, A.; Higuera-Ciapara, I.; Velázquez-Fernández, J. B.; Vallejo-Cardona, A. A. *Cancer Nanotechnol.* **2019**, *10*, 11.
- (2) Shi, C.; Guo, D.; Xiao, K.; Wang, X.; Wang, L.; Luo, J. *Nat. Commun.* **2015**, *6*, 7449.
- (3) Zoratto, N.; Montanari, E.; Viola, M.; Wang, J.; Coviello, T.; Di Meo, C.; Matricardi, P. *Carbohydr. Polym.* **2021**, *266*, 118119.
- (4) Lombardo, D.; Calandra, P.; Barreca, D.; Magazù, S.; Kiselev, M. A. *Nanomaterials* **2016**, *6*, 125.
- (5) Li, Y.; Yang, L. *J. Microencapsul.* **2015**, *32*, 255.
- (6) Cheng, C.-C.; Sun, Y.-T.; Lee, A.-W.; Huang, S.-Y.; Fan, W.-L.; Chiao, Y.-H.; Chiu, C.-W.; Lai, J.-Y. *Polym. Chem.* **2020**, *11*, 2791.
- (7) Kothari, K.; Ragoonanan, V.; Suryanarayanan, R. *Mol. Pharmaceutics* **2015**, *12*, 162.
- (8) Kim, B.-S.; Lee, H.-i.; Min, Y.; Poon, Z.; Hammond, P. T. *Chem. Commun.* **2009**, 4194.
- (9) Yang, D.; Gao, S.; Fang, Y.; Lin, X.; Jin, X.; Wang, X.; Ke, L.; Shi, K. *Nanomedicine* **2018**, *13*, 3159.
- (10) Shi, Y.; van Steenberg, M. J.; Teunissen, E. A.; Novo, L. s.; Gradmann, S.; Baldus, M.; van Nostrum, C. F.; Hennink, W. E. *Biomacromolecules* **2013**, *14*, 1826.
- (11) Zhuang, W. R.; Wang, Y.; Cui, P. F.; Xing, L.; Lee, J.; Kim, D.; Jiang, H. L.; Oh, Y. K. *J. Control. Release* **2019**, *294*, 311.
- (12) Kim, S.; Shi, Y.; Kim, J. Y.; Park, K.; Cheng, J.-X. *Expert Opin. Drug Deliv.* **2010**, *7*, 49.
- (13) Liang, Y.; Deng, X.; Zhang, L.; Peng, X.; Gao, W.; Cao, J.; Gu, Z.; He, B. *Biomaterials* **2015**, *71*, 1.
- (14) Zhang, P.; Huang, Y.; Liu, H.; Marquez, R. T.; Lu, J.; Zhao, W.; Zhang, X.; Gao, X.; Li, J.; Venkataramanan, R.; Xu, L.; Li, S. *Biomaterials* **2014**, *35*, 7146.
- (15) Zhang, P.; Huang, Y.; Kwon, Y. T.; Li, S. *Mol. Pharm.* **2015**, *12*, 1680.
- (16) Zhu, S.; Gao, H.; Babu, S.; Garad, S. *Mol. Pharm.* **2018**, *15*, 97.
- (17) Wei, X.; Wang, Y.; Xiong, X.; Guo, X.; Zhang, L.; Zhang, X.; Zhou, S. *Adv. Funct. Mater.* **2016**, *26*, 8266.
- (18) Dong, Y.; Du, P.; Liu, P. *Int J Pharm.* **2020**, *588*, 119723.
- (19) Wang, T.-T.; Wei, Q.-C.; Zhang, Z.-T.; Lin, M.-T.; Chen, J.-J.; Zhou, Y.; Guo, N.-N.; Zhong, X.-C.; Xu, W.-H.; Liu, Z.-X.; Han, M.; Gao, J.-Q. *Biomater. Sci.* **2020**, *8*, 118.

- (20) Chen, K. J.; Chiu, Y. L.; Chen, Y. M.; Ho, Y. C.; Sung, H. W. *Biomaterials* **2011**, *32*, 2586.
- (21) Virmani, M.; Deshpande, N. U.; Pathan, S.; Jayakannan, M. *ACS Polym. Au* **2021**.
- (22) He, X.; Cai, K.; Zhang, Y.; Lu, Y.; Guo, Q.; Zhang, Y.; Liu, L.; Ruan, C.; Chen, Q.; Chen, X.; Li, C.; Sun, T.; Cheng, J.; Jiang, C. *ACS Appl. Mater. Interfaces* **2018**, *10*, 39455.
- (23) Qiu, L.; Li, J.-W.; Hong, C.-Y.; Pan, C.-Y. *ACS Appl. Mater. Interfaces* **2017**, *9*, 40887.
- (24) Saxena, S.; Pradeep, A.; Jayakannan, M. *ACS Appl. Bio Mater.* **2019**, *2*, 5245.
- (25) Gu, X.; Qiu, M.; Sun, H.; Zhang, J.; Cheng, L.; Deng, C.; Zhong, Z. *Biomater. Sci.* **2018**, *6*, 1526.
- (26) Xue, S.; Gu, X.; Zhang, J.; Sun, H.; Deng, C.; Zhong, Z. *Biomacromolecules* **2018**, *19*, 3586.
- (27) Hamaguchi, T.; Matsumura, Y.; Suzuki, M.; Shimizu, K.; Goda, R.; Nakamura, I.; Nakatomi, I.; Yokoyama, M.; Kataoka, K.; Kakizoe, T. *Br. J. Cancer* **2005**, *92*, 1240.
- (28) Misu, Y.; Ueda, H.; Goshima, Y. In *Adv. Pharmacol.*; August, J. T., Anders, M. W., Murad, F., Coyle, J., Eds.; Academic Press: 1995; Vol. 32, p 427.
- (29) Misu, Y.; Kitahama, K.; Goshima, Y. *Pharmacology & therapeutics* **2003**, *97*, 117.
- (30) Bove, C.; Travagli, R. A. *J. Neurophysiol.* **2019**, *121*, 1856.
- (31) Zhang, L.; Xue, H.; Gao, C.; Carr, L.; Wang, J.; Chu, B.; Jiang, S. *Biomaterials* **2010**, *31*, 6582.
- (32) Lu, D.; Li, Y.; Wang, X.; Li, T. e.; Zhang, Y.; Guo, H.; Sun, S.; Wang, X.; Zhang, Y.; Lei, Z. *J. Mater. Chem. B* **2018**, *6*, 7511.
- (33) Guo, Q.; Chen, J.; Wang, J.; Zeng, H.; Yu, J. *Nanoscale* **2020**, *12*, 1307.
- (34) Brubaker, C. E.; Messersmith, P. B. *Biomacromolecules* **2011**, *12*, 4326.
- (35) Holowka, E. P.; Deming, T. J. *Macromol Biosci.* **2010**, *10*, 496.
- (36) Saxena, S.; Jayakannan, M. *Biomacromolecules* **2020**, *21*, 171.
- (37) Joshi, D. C.; Saxena, S.; Jayakannan, M. *ACS Appl. Polym. Mater.* **2019**, *1*, 1866-1880.
- (38) Anantharaj, S.; Jayakannan, M. *Biomacromolecules* **2015**, *16*, 1009.
- (39) Saxena, S.; Jayakannan, M. *J. Polym. Sci. A: Polym. Chem.* **2016**, *54*, 3279.

- (40) Aluri, R.; Saxena, S.; Joshi, D. C.; Jayakannan, M. *Biomacromolecules* **2018**,
- (41) Aluri, R.; Jayakannan, M. *Biomacromolecules* **2017**, *18*, 189.
- (42) Saxena, S.; Pradeep, A.; Jayakannan, M. *ACS Appl. Bio Mater.* **2019**, *2*, 5245.
- (43) Saxena, S.; Jayakannan, M. *Biomacromolecules* **2017**, *18*, 2594.



# **Chapter 4**

---

## **Development of Melt Polycondensation Strategy for L-Amino acids and Sugar Based Hybrid Polymers**

## Abstract

*In this work we are reporting a completely biomass-based amino acid sugar hybrid polyester(urethane)s synthesis by eco-friendly solvent free melt condensation approach. D-mannitol was converted into two different bicyclic diacetalized monomers leaving the two primary hydroxyl group free for polymerization reaction. The structure of both the diols was confirmed by their single crystal structure analysis. The second reacting partner was selected from amino acid resources and converted into dual ester-urethane monomer by suitable modifications. Both, amino acid monomer and diacetalized sugar diol was subjected for melt polymerisation at 150 °C to synthesise completely renewable resource based polyester(urethane)s. The dual ester-urethane condensation was successfully demonstrated for variety of amino acids including glycine, L-alanine, L-valine, L-leucine, L-isoleucine and L-phenylalanine. The occurrence of melt polymerisation and structure of polymers was confirmed by NMR technique. The end group analysis by MALDI-TOF-MS confirmed the stability of both the monomers under melt condition. The newly synthesized polyester(urethane)s were showing relatively high glass transition temperature ( $T_g \geq 80$  °C) compare to their aliphatic diol based polyester(urethane)s counterparts. Further the acetal unit in the polymer was deprotected to get amphiphilic amino acid sugar hybrid polyester(urethane)s which was forming  $200 \pm 10$  nm size nanoparticle in aqueous solvent. The biocompatibility of these sugar based diols were checked in normal (WT-MEFs) cell line and it was found that polymers were highly biocompatible. The present investigation is emphasized to design one of the first example of completely renewable resource based polymers by using two naturally abundant raw materials i.e. sugar and amino acids and these polymers could be a replacement for various petroleum based polymers in future.*

**Keywords:** Biomass-based, L-amino acid, Poly(ester-urethane)s, Melt Polymerisation.

## 4.1. Introduction

Fully biodegradable polymers undergo competitive digestion under biological conditions and eventually breakdown into biological monomers to minimize the adverse effects on the environment.<sup>1,2</sup> Aliphatic polyesters based on poly(L-lactide)s and poly(L-glycolide)s are very good examples for enzymatically-biodegradable polymers into their elementary subunits<sup>3</sup> like H<sub>2</sub>O and CO<sub>2</sub>, etc. Efforts have been taken to improve the PLLA and PLGA molecular weight, mechanical stability, processability, environmental stability and making them successful replacement for the existing petroleum-based polymers.<sup>4-7</sup> In the last 2-3 decades, different bio resources including L-amino acids,<sup>8,9</sup> carbohydrates,<sup>10-12</sup> fatty acids,<sup>13,14</sup> phenols<sup>15,16</sup> etc. have been screened for the development of biodegradable polymers.

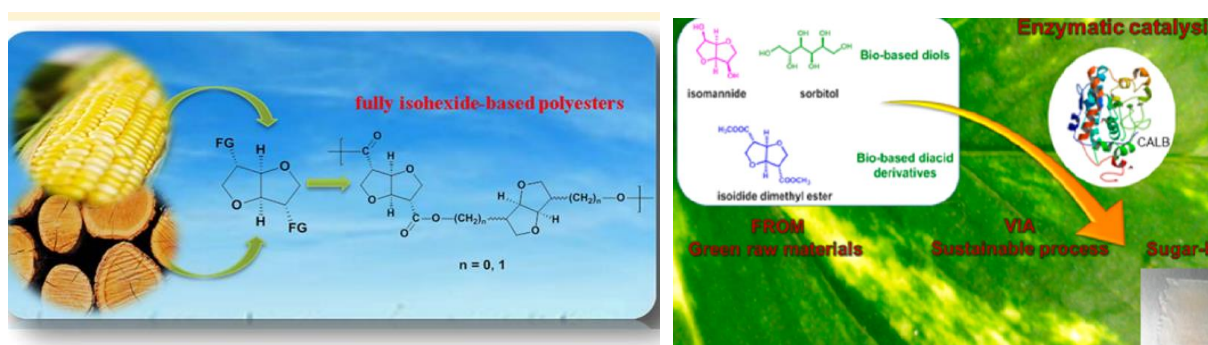


**Figure 4.1.** Bio based polymers from renewable resources. (Adopted from et al. Wu *Macromolecules* **2013**, 46, 384–394 and Gustni et al. *Biomacromolecules* **2016**, 17, 3404–3416)

The bio-resources have been modified into polymerizable monomers and copolymerized with petroleum-based monomers in order to synthesise partially biobased polymers.<sup>17,18</sup> In this approach, the polymer structure is not completely biodegradable, and nearly 50% of the degraded waste is not able to be recycled back into its natural state even after many decades. Aliphatic polyesters are natural choice for the biodegradable polymers;<sup>19-21</sup> however, the commercial aliphatic polyesters like polycaprolactone, poly(alkylene sebacate) and poly(alkylene adipate) are slow degradable<sup>22</sup> and required 8-10 years for complete biodegradation into monomeric units. Similarly, the existing protease enzyme bio-machinery in microbes are not capable of degrading high molecular weight polypeptides that are produced from L-amino acid bio-resources. Carbohydrate monomers are the most desirable bio-resources because of their low cost, high abundance, structural diversity, as well as their biocompatibility and biodegradability.<sup>23,24</sup> Stereoisomers of 1,4:3,6-Dianhydrohexitol known

as isosorbide, isoidide and isomannide synthesized by dehydration of corresponding hexitol are well explored building blocks for the synthesis of biopolymer by condensation polymerisation<sup>25-27</sup> but the secondary nature and unfavorable spatial arrangement of hydroxyl groups in these monomers seriously hamper the molecular weight of polymers. Acyclic carbohydrates like mannitol, glucitol and galactitol have both 1° and 2°- hydroxyl groups; thus, they required additional protection strategy to mask the middle 2°- hydroxyl groups to make the primary hydroxyl groups available for polycondensation reaction.

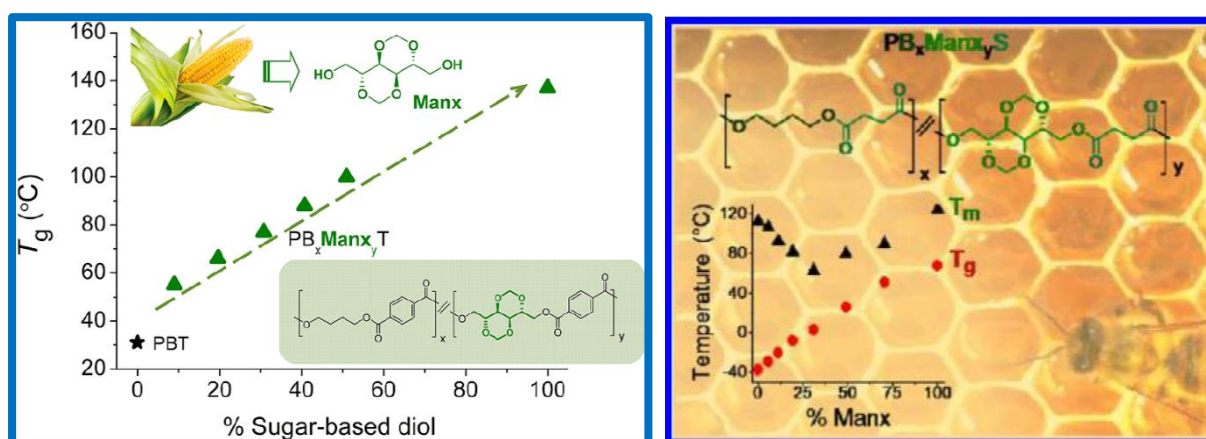


**Figure 4.2.** Bio based polyesters from bicyclic D-mannitol. Lavilla et al. *Macromolecules* **2012**, *45*, 8257–8266 and *Biomacromolecules* **2013**, *14*, 781–793.

In this case, the secondary hydroxyl groups were routinely protected by methyl, benzyl, silyl ethers or cyclic acetal and the resultant protected-sugar diols (having free  $-\text{CH}_2\text{OH}$  groups) were successfully employed for polycondensation with diacids or its di-esters to produce high molecular weight polyesters.<sup>12,28,29</sup> Poly(ethylene terephthalate),<sup>30,31</sup> poly(butylene terephthalate),<sup>32,33</sup> poly(alkylene adipate),<sup>34</sup> and poly(alkylene sebacate),<sup>34</sup> etc, were also synthesised by modifying these sugar based monomers to obtain value-added polymers. Sugar-based amines, isocyanates were also developed for polyamides, polycarbonates and polyurethanes, etc. and very recently poly(anhydride-esters) was reported for the delivery of anti-inflammatory drug ibuprofen.<sup>35</sup> Muñoz-Guerra co-workers and Galbis co-workers have pioneered in developing sugar-based polymers and this topic has been reviewed to impart the importance of sugar-based polymers for the futuristic bioplastic development.<sup>12</sup>

L-amino acids are another class of naturally abundant biologically active molecules and they routinely employed for the synthesis of polypeptides by the ring opening polymerization of their NCA monomers. Significant efforts have been taken to make new classes of non-peptide polymer such as poly(ester-amide)s, poly(ester-urea), poly(disulfide-urethane)s,

poly(ester-urea-urethane), polyurethanes and polycarbonates, etc. through polycondensation route. From our group, we reported the new classes of poly(ester-urethane)s<sup>36</sup> by melt polycondensation approach in which amino acid monomers were suitably modified into dual ester urethane monomers which upon reaction with a diol gives polyester(urethane)s. Further, thermo-selective polycondensation approach was also developed to multi-functional L-amino acid resources such as L- aspartic and L-serine to make new classes of linear polyesters and hyperbranched poly(ester-urethane)s.<sup>37,38</sup> This approach has been extended to make thermo-responsive L-tyrosine and L-lysine based poly(ester-urethane)s<sup>39</sup> and polyurethanes<sup>40</sup> for delivering the anticancer drugs. The amphiphilic polyesters and poly(ester-urethane)s were self-assembled into nano-carriers for the enzyme-responsive drug delivery in cancer therapy as well as fluorophore tagged FRET bio-probes to study their real-time action at the intracellular compartments in live-cancer cells.<sup>41</sup> In all these non-peptide polymer analogues reported by us and others, one of the polymerizable monomer, i.e. diol component was predominately chosen from the petroleum-based resources. The selection of non-bioresource based aliphatic diols in the polycondensation reaction has limited the possibility of accomplishing 100 % bioresource based L-amino acid polymers. This limitation has been cleverly overcome in the present investigation by clearly choosing melt polymerization monomer partners from L-amino acids (A-A monomer, from our lab chemistry) and D-mannitol sugar-based diols (B-B-monomer, from the literature) and successfully employed the solvent free melt polycondensation chemistry to make the first report on fully bio-resource L-amino acid + sugar poly(ester-urethane)s. This new methodology is shown in Figure 1.

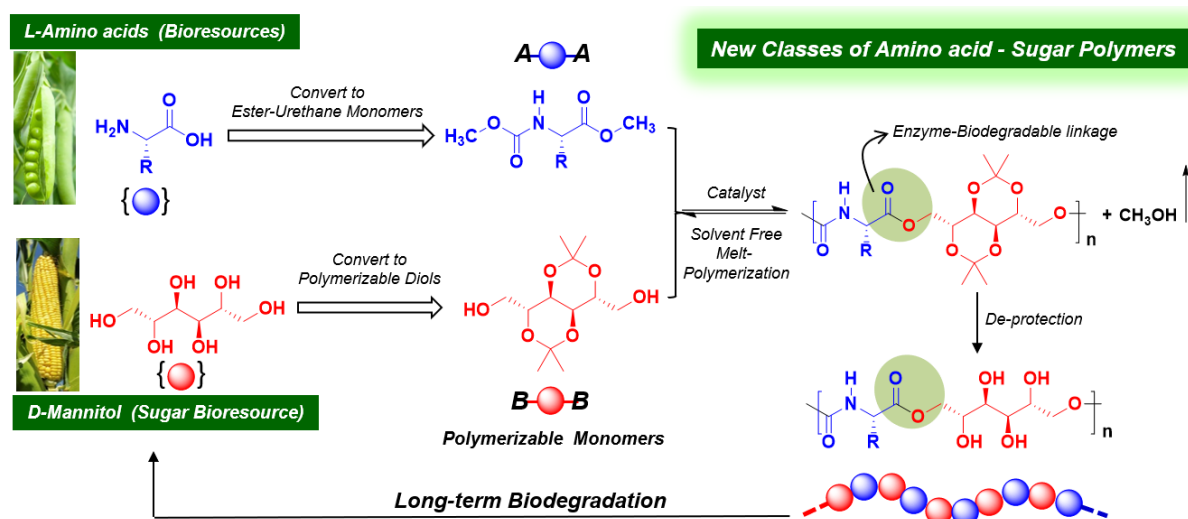


**Figure 4.3.** Development of new classes of L-amino acid+ sugar hybrid polymers by solvent-free eco-friendly melt condensation route.

D-mannitol was successfully converted into two different bicyclic diacetalized 5-member and 6-member diol monomers and the chemical structures of the sugar diols were completely characterized by X-ray single crystal structure and 2D NMR analysis. L-Amino acids were readily converted into polymerizable ester-urethane monomers following our earlier report. Melt polymerization of the sugar diols and L-amino acid ester urethane monomers produced high molecular weight acetal-masked aliphatic poly(ester-urethane)s. Special attention is paid to check the effect of sugar diol on glass transition temperature of polyester(urethane) and we found that incorporation of sugar diol in place of aliphatic diol significantly increases the glass transition temperature of polymers. Further the acetal unit in the polymer was deprotected to get amphiphilic amino acid sugar hybrid polyester(urethane)s which was forming  $200 \pm 10$  nm size nanoparticle in aqueous solvent. Biocompatibility tests of amphiphilic nanocarriers were performed in WT-MEF cells, and polymer nanocarriers were found to be biocompatible up to  $250 \mu\text{g/mL}$ . The present investigation is emphasized to design one of the first example of completely renewable resource-based polymers by using two naturally abundant raw materials i.e. sugar and amino acids and these polymers could be a replacement for various petroleum based polymers in future. Post polymerization deprotection of the acetal unit yield fully bio-resourced based L-amino acid-sugar based poly(ester-urethane)s which is a new entry in the literature.

## 4.2. Experimental procedure

**4.2.1. Materials:** D-mannitol, benzoyl chloride, 2,2-dimethoxypropane, 1,12-dodecanediol, and the catalyst dibutyl tin oxide (DBTO, 98%) were purchased from Sigma-Aldrich and used without further purification. methyl chloroformate, trifluoroacetic acid, L-phenyl alanine, L-valine, L-leucine, L-isoleucine, L-alanine, L-glycine were purchased from Avra Synthesis. Thionyl chloride, DMSO and other solvents were purchased locally and purified prior to use.

**4.2.2. General Methods.**  $^1\text{H}$  and  $^{13}\text{C}$  NMR spectra of monomers and polymers were recorded on a Bruker 400 spectrometer at  $25.0^\circ\text{C}$  operating at 400 and 100 MHz, respectively. Samples were dissolved in deuterated dimethyl sulfoxide containing a trace amount of tetramethylsilane (TMS) as an internal standard. About 15 and 30 mg of sample dissolved in 0.7 mL of solvent were used for  $^1\text{H}$  and  $^{13}\text{C}$  NMR. Purity of polymers was determined by gel permeation chromatography (GPC) using Viscotek VE 1122 pump, VE 3580 RI detector, and Viscotek VE

3210 UV/Vis detector in tetrahydrofuran (THF) using polystyrene as a standard. Thermogravimetric analysis (TGA) of monomers and polymers was done by using PerkinElmer thermal analyzer STA 6000 model at a heating rate of 10 °C/min under an inert atmosphere. Differential scanning calorimetry (DSC) measurements were performed on a TA Q20 differential scanning calorimeter (DSC) at heating and cooling rates of 10 °C/min under nitrogen atmosphere. The size of the polymeric nanoparticle was measured by dynamic light scattering (DLS), using a Nano ZS-90 apparatus utilizing a 633 nm red laser from Malvern instruments. Field emission scanning electron microscopy (FE-SEM) images were obtained by using Zeiss Ultra Plus scanning electron microscope.

**4.2.3. Synthesis of (2R,3R,4R,5R)-2,3,4,5-tetrahydroxyhexane-1,6-diyl dibenzoate (compound 1):** D-mannitol (20 gm, 0.11 mol) was dissolved in 500 ml of dry pyridine. The reaction mixture was kept in ice bath and cooled up to 0°C. Benzyl chloride (23.1 ml, 0.198 mol) was added dropwise into reaction mixture and reaction was continued at room temperature for 6 h then poured in ice water. The white precipitated solid was filtered and washed twice with water and chloroform. The solid was dried and washed with hot ethanol to get white coloured powder Yield = 17.1 gm (40%). <sup>1</sup>H NMR (400 MHz, DMSO-*d*<sub>6</sub>) δ ppm: 3.78 (d, 2 H, OH-CH<sub>2</sub>-CHOH-CHOH) 3.86 (m, 2 H, OH-CH<sub>2</sub>-CHOH-CHOH) 4.27 (6.24 Hz, 2 H, OH-CH<sub>2</sub>-CHOH) 4.49-4.51 (d, 2 H, OH-CH<sub>2</sub>-CHOH), 4.52-4.56 (dd, 2H, OH-CH<sub>2</sub>-CHOH), 5.05 (d, 2 H, OH-CH<sub>2</sub>-CHOH), 7.45 - 7.59 (m, 4 H, *o*-ArH) 7.59 - 7.74 (m, 2 H, *p*-ArH) 7.96 - 8.15 (m, 4 H, *m*-ArH). <sup>13</sup>C NMR (100 MHz, CDCl<sub>3</sub>) δ ppm: 68.1, 68.9, 69.6, 129.3, 129.9, 130.5, 134.0, 167.0.

**4.2.4. Synthesis of 3-((((4R,4aR,8R,8aR)-8-((benzoyloxy)methyl)-2,2,6,6-tetramethyltetrahydro-[1,3]dioxino[5,4-d][1,3]dioxin-4-yl)methoxy)carbonyl)benzene-1-ylidene and (((4R,4'S,5S)-2,2,2',2'-tetramethyl-[4,4'-bi(1,3-dioxolane)]-5,5'-diyl)bis(methylene) dibenzoate:** 16 gm, 0.04 mol of compound 1 and toluene-*p*-sulfonic acid hydrate (1.4 gm, 0.008 gm) was dispersed in 120 ml of dry acetone. 2,2 dimethoxypropane (15 ml, 0.12 mol) was added dropwise into reaction mixture at ice cold condition. The suspension was stirred for 6 h at room temperature then solvent was distilled and compound was repeatedly extracted in hexane and passed through sodium sulphate which was further purified by silica gel column chromatography using hexane and ethyl acetate mixture (1:5 v/v) to get a colourless oil. Yield = 13.4 gm, (70%). <sup>1</sup>H NMR (400 MHz, DMSO-*d*<sub>6</sub>) δ ppm: 1.26 (s,

4 H), 1.28 (s, 2 H), 1.33 (s, 4 H), 1.42 (s, 2 H), 3.94 - 4.08 (m, 3 H), 4.31 - 4.48 (m, 5 H), 7.43 - 7.61 (m, 4 H), 7.61 - 7.76 (m, 2 H), 7.97 (m, 4 H).

**4.2.5. Synthesis of ((4R,4aR,8R,8aR)-2,2,6,6-tetramethyltetrahydro-[1,3]dioxino[5,4-d][1,3]dioxine-4,8-diyl)dimethanol (Manx6):** A suspension of mixture compound 2 (13.0 gm, 0.027 mol) in dry chloroform was stirred with sodium methoxide (4.48 gm, 0.082 mol) was stirred for 12 h under nitrogen environment then reaction mixture was filtered through whatman filter paper and filtrate was concentrated through rota evaporator to get a viscous yellow liquid which was further recrystallized using acetone and hexane mixture (1:5 v/v) to get compound 3. Yield = (3.9 gm, 55 %). <sup>1</sup>H NMR (400 MHz, DMSO-*d*<sub>6</sub>) δ ppm: 1.23 (s, 6 H, CH(CH<sub>3</sub>)<sub>2</sub>), 1.29 (s, 6 H, CH(CH<sub>3</sub>)<sub>2</sub>), 3.36 - 3.44 (m, 2 H, CH-CH<sub>2</sub>-OH), 3.44 - 3.49 (m, 2 H, CH-CH<sub>2</sub>-OH), 3.50 - 3.56 (m, 2 H, CH-CH<sub>2</sub>-OH), 3.70- 3.75 (m, 2 H, -CH-CH-CH<sub>2</sub>-OH), 4.71 (t, 2 H, -CH<sub>2</sub>-OH). <sup>13</sup>C NMR (100 MHz, CDCl<sub>3</sub>) δ ppm: 23.80, 24.42, 61.52, 67.47, 71.02, 99.94. FT-IR (cm<sup>-1</sup>): 3294, 2989, 2938, 2920, 2890, 1373, 1331, 1247, 1214, 1170, 1114, 1079, 1026, 969, 907, 867, 844.

**4.2.6. Synthesis of ((4R,4'S,5S)-2,2,2',2'-tetramethyl-[4,4'-bi(1,3-dioxolane)]-5,5'-diyl)dimethanol (Manx5):** The remaining mixture was concentrated and purified by silica gel column chromatography using hexane and ethyl acetate to get compound 4. Yield = 1.8 gm, 26%). <sup>1</sup>H NMR (400 MHz, DMSO-*d*<sub>6</sub>) δ ppm: 1.23 (s, 6 H, CH(CH<sub>3</sub>)<sub>2</sub>), 1.29 (s, 6 H, CH(CH<sub>3</sub>)<sub>2</sub>), 3.36 - 3.44 (m, 2 H, CH-CH<sub>2</sub>-OH), 3.44 - 3.49 (m, 2 H, CH-CH<sub>2</sub>-OH), 3.50 - 3.56 (m, 2 H, CH-CH<sub>2</sub>-OH), 3.70- 3.75 (m, 2 H, -CH-CH-CH<sub>2</sub>-OH), 4.71 (t, 2 H, -CH<sub>2</sub>-OH). <sup>13</sup>C NMR (100 MHz, CDCl<sub>3</sub>) δ ppm: 25.47, 27.54, 60.48, 74.54, 77.39, 107.31. FT-IR (cm<sup>-1</sup>): 3295, 2986, 2938, 2922, 2890, 1375, 1333, 1249, 1214, 1174, 1116, 1077, 1024, 972, 909, 869, 842.

**4.2.7 Synthesis (valine ester urethane) monomer:** L-valine hydrochloride salt (5 gm, 0.03 mol) was dispersed in 50 ml of dry methanol and thionyl chloride (2.1 ml, 0.036) was added into it at ice cold condition. Reaction was refluxed at 80 °C under nitrogen environment for 12 h then extra solvent was distilled to get the methyl ester of L-valine which was further dissolved in 25 % sodium bicarbonate solution and reaction mixture was diluted with 25 ml of dichloromethane. Methyl chloroformate (2.82 mL, 0.036 mol) was added at ice cold condition and reaction was continued for 12 h at room temperature. After completion of reaction mixture was neutralized with 1N HCl and product was extracted in dichloromethane which was further



purified by silica gel column chromatography using ethyl acetate and hexane mixture (1:4 v/v). Yield = (88%).  $^1\text{H}$  NMR (400 MHz, DMSO- $d_6$ )  $\delta$  ppm: 0.87 (dd, 6 H,  $-\text{CH}(\text{CH}_3)_2$ ), 1.91 - 2.10 (m, 1 H  $-\text{CH}(\text{CH}_3)_2$ ), 3.55 (s, 3 H,  $-\text{NHCOOCH}_3$ ), 3.63 (s, 3 H,  $-\text{CHCOOCH}_3$ ), 3.90 (dd, 1 H,  $-\text{CHCOOCH}_3$ ), 7.52 (d, 1 H,  $-\text{NHCOOCH}_3$ ).  $^{13}\text{C}$  NMR (100 MHz, CDCl $_3$ )  $\delta$  ppm: 18.2, 18.9, 29.7, 51.4, 51.5, 59.7, 156.9, 172.4. FT-IR ( $\text{cm}^{-1}$ ): 3355, 2986, 2962, 2939, 1723, 1528, 1460, 1372, 1332, 1310, 1217, 1170, 1119, 1091, 1033, 979, 911, 869, 845

**4.2.8. Phenyl alanine ester urethane:**  $^1\text{H}$  NMR (400 MHz, DMSO- $d_6$ )  $\delta$  ppm: 2.86 (dd, 1 H,  $-\text{CH}_2\text{-Ar}$ ), 3.03 (dd, 1 H,  $-\text{CH}_2\text{-Ar}$ ), 3.48 (s, 3 H,  $-\text{NHCOOCH}_3$ ), 3.62 (s, 3 H,  $-\text{CHCOOCH}_3$ ), 4.25 (dd, 1 H,  $-\text{CH-CH}_2$ ), 7.15 - 7.37 (m, 5 H,  $-\text{ArH}$ ), 7.69 (d, 1 H,  $-\text{NHCOOCH}_3$ ).  $^{13}\text{C}$  NMR (100 MHz, CDCl $_3$ )  $\delta$  ppm: 36.4, 51.4, 51.9, 55.5, 126.5, 128.2, 129.0, 137.4, 156.5, 172.4. FT-IR ( $\text{cm}^{-1}$ ): 3346, 2987, 2939, 1714, 1511, 1455, 1372, 1332, 1216, 1169, 1127, 1084, 1066, 1038, 980, 929, 910, 871, 846, 751, 701.

**4.2.9. Leucine ester urethane:**  $^1\text{H}$  NMR (400 MHz, DMSO- $d_6$ )  $\delta$  ppm: 0.82 (d, 3 H,  $-\text{CH}(\text{CH}_3)_2$ ) 0.87 (d, 3 H,  $-\text{CH}(\text{CH}_3)_2$ ) 1.40 - 1.47 (m, 1 H,  $-\text{CH}(\text{CH}_3)_2$ ), 1.51-1.68 (m, 2H,  $-\text{CH}_2\text{-CH}(\text{CH}_3)_2$ ), 3.54 (s, 3 H,  $-\text{NHCOOCH}_3$ ) 3.62 (m, 3 H,  $-\text{CHCOOCH}_3$ ) 4.04 (dd, 1 H,  $-\text{CH}_2\text{-CH-NH-}$ ) 7.56 (d, 1 H,  $-\text{CH-NH-}$ ).  $^{13}\text{C}$  NMR (100 MHz, CDCl $_3$ )  $\delta$  ppm: 21.0, 22.7, 24.2, 51.4, 51.8, 52.1, 156.7, 173.4. FT-IR ( $\text{cm}^{-1}$ ): 3337, 2986, 2955, 1724, 1530, 1458, 1372, 1332, 1217, 1169, 1120, 1090, 1037, 978, 911, 870, 846.

**4.2.10. Isoleucine ester urethane:**  $^1\text{H}$  NMR (400 MHz, DMSO- $d_6$ )  $\delta$  ppm: 0.89 - 0.83 (m, 6 H,  $-\text{CH}_3\text{-CH}_2\text{-CH-CH}_3$ ), 1.16 - 1.41 (m, 2 H,  $-\text{CH-CH}_2\text{-CH}_3$ ) 1.73-1.79 (m, 1 H,  $-\text{CH-CH}_2\text{-CH}_3$ ) 3.54 (s, 3 H,  $-\text{NHCOOCH}_3$ ) 3.95 (s, 3 H,  $-\text{CHCOOCH}_3$ ), 3.95 (dd, 1H  $-\text{NH-}$ ,  $-\text{CH-CH}_2$ ) 7.53 (d, 1 H,  $-\text{CH-NH-}$ ).  $^{13}\text{C}$  NMR (100 MHz, CDCl $_3$ )  $\delta$  ppm: 11.0, 15.4, 24.7, 36.1, 51.4, 51.5, 58.5, 156.8, 172.4. FT-IR ( $\text{cm}^{-1}$ ): 3356, 2985, 2963, 2938, 2879, 1724, 1530, 1459, 1380, 1332, 1217, 1170, 1124, 1090, 1035, 978, 911, 869.

**4.2.11. Alanine ester urethane:**  $^1\text{H}$  NMR (400 MHz, DMSO- $d_6$ )  $\delta$  ppm: 1.25 (d, 3 H,  $-\text{CH-CH}_3$ ), 3.53 (s, 3 H,  $-\text{NHCOOCH}_3$ ), 3.62 (s, 3 H,  $-\text{CHCOOCH}_3$ ), 4.07 (q, 1 H- $-\text{CH-CH}_3$ ) 7.60 (d, 1 H,  $-\text{CH-NH-}$ ).  $^{13}\text{C}$  NMR (100 MHz, CDCl $_3$ )  $\delta$  ppm: 16.9, 49.2, 51.4, 51.8, 156.3, 173.4. FT-IR ( $\text{cm}^{-1}$ ): 3363, 2986, 2963, 1724, 1529, 1460, 1372, 1333, 1310, 1217, 1170, 1118, 1091, 1033, 979, 911, 869, 846, 773.

**4.2.12. Glycine ester urethane:**  $^1\text{H}$  NMR (400 MHz, DMSO- $d_6$ )  $\delta$  ppm: 3.57 (s, 3 H,  $-\text{NHCOOCH}_3$ ), 3.65 (s, 3 H,  $-\text{CHCOOCH}_3$ ), 3.6 (d, 2 H,  $-\text{NH-CH}_2\text{-}$ ), 7.51 (t, 1 H,  $-\text{CH-NH-}$ ).  $^{13}\text{C}$  NMR (100 MHz, CDCl $_3$ )  $\delta$  ppm: 42.1, 51.6, 51.7, 157.2, 170.8. FT-IR ( $\text{cm}^{-1}$ ): 3362,

2986, 2940, 1724, 1530, 1459, 1380, 1332, 1216, 1168, 1118, 1089, 1039, 978, 908, 866, 844, 776.

**4.2.13. Valine polymer (Manx6-Val):** L-valine ester urethane monomer (0.5 gm, 0.002 mmol) and Manx6 (0.69 gm, 0.002 mol) was taken in a polymerisation tube and melted at 150 °C under nitrogen atmosphere to prevent thermal oxidation. The polymerisation setup was degassed twice and 1 mol % of DBTO was added in to it. polymerisation was carried out at 150 °C under continuous nitrogen purging for 4 h to get a viscous oligomeric liquid. After 4 h polymerisation tube was subjected under vacuum (0.01 m bar) for 2 h to get the polymer. <sup>1</sup>H NMR (400 MHz, DMSO-*d*<sub>6</sub>) δ ppm: 0.88-0.91 (m, 6 H, -CH-(CH<sub>3</sub>)<sub>2</sub>), 1.24 (s, 6 H, -C(CH<sub>3</sub>)<sub>2</sub>), 1.29 (s, 6 H, -C(CH<sub>3</sub>)<sub>2</sub>) 3.78-3.93 (m, 5 H, OCH<sub>2</sub>-CH-CH-CH-, NH-CH-), 4.05-4.25 (m, 4 H, O-CH<sub>2</sub>-CH-), 7.70 (d, 1 H, -NH-CH-). <sup>13</sup>C NMR (100 MHz, CDCl<sub>3</sub>) δ ppm: 18.2, 18.9, 23.5, 24.2 29.5, 59.7, 63.7, 63.9, 67.3, 67.6, 67.9, 100.5, 156.3, 171.6.

**4.2.14. Phenyl alanine polymer:** The synthetic procedure was similar to the Manx6-Val. <sup>1</sup>H NMR (400 MHz, DMSO-*d*<sub>6</sub>) δ ppm: 1.17-1.30 (m, 12 H), 2.85-3.0 (m, 2H), 3.70-3.88 (m, 4 H), 3.93-3.43 (m, 3 H), 4.19-4.29 (m, 2 H), 7.16-7.27 (m, 5 H), 7.82 (d 1 H). <sup>13</sup>C NMR (100 MHz, CDCl<sub>3</sub>) δ ppm: 23.3 24.06, 35.94, 55.3 63.7, 63.8 67.1, 67.4, 67.7, 70.6, 100.3, 126.3, 128.0, 128.7, 137.2, 155.7, 171.4.

**4.2.15. Leucine polymer:** The synthetic procedure was similar to the Manx6-Val. <sup>1</sup>H NMR (400 MHz, DMSO-*d*<sub>6</sub>) δ ppm: 0.86 (m, 6 H) 1.24- (s, 6 H) 1.29 (s, 6 H) 1.40- 1.70 (m, 3 H) 3.77 - 3.87 (m, 4 H) 4.0 - 4.1 (m, 4 H) 4.18-4.22 (m, 1 H) 7.74 (d, 1 H). <sup>13</sup>CNMR (100 MHz, DMSO-*d*<sub>6</sub>) δ ppm: 22.41, 22.89, 23.67, 24.42, 24.53, 52.48, 64.11, 67.58, 67.61, 67.71, 68.18, 100.73, 156.25, 172.72.

**4.2.16. Isoleucine polymer:** The synthetic procedure was similar to the Manx6-Val. <sup>1</sup>H NMR (400 MHz, DMSO-*d*<sub>6</sub>) δ ppm: <sup>1</sup>H NMR (400 MHz, DMSO-*d*<sub>6</sub>) δ ppm: 0.81-0.86 (m, 6 H) 1.24- 1.41 (m, 14 H), 1.76-1.79 (m, 1H), 3.76-3.79 (m, 5 H), 4.05-4.22 (m, 4 H), 7.82 (d 1 H). <sup>13</sup>C NMR (100 MHz, CDCl<sub>3</sub>) δ ppm: 22.47, 22.86, 23.63, 24.47, 24.56, 52.46, 64.10, 67.58, 67.61, 67.73, 68.16, 100.74, 156.29, 173.1.

**4.2.17. Alanine polymer:** The synthetic procedure was similar to the Manx6-Val. <sup>1</sup>H NMR (400 MHz, DMSO-*d*<sub>6</sub>) δ ppm: <sup>1</sup>H NMR (400 MHz, DMSO-*d*<sub>6</sub>) δ ppm: 1.25-1.31 (m, 15 H),

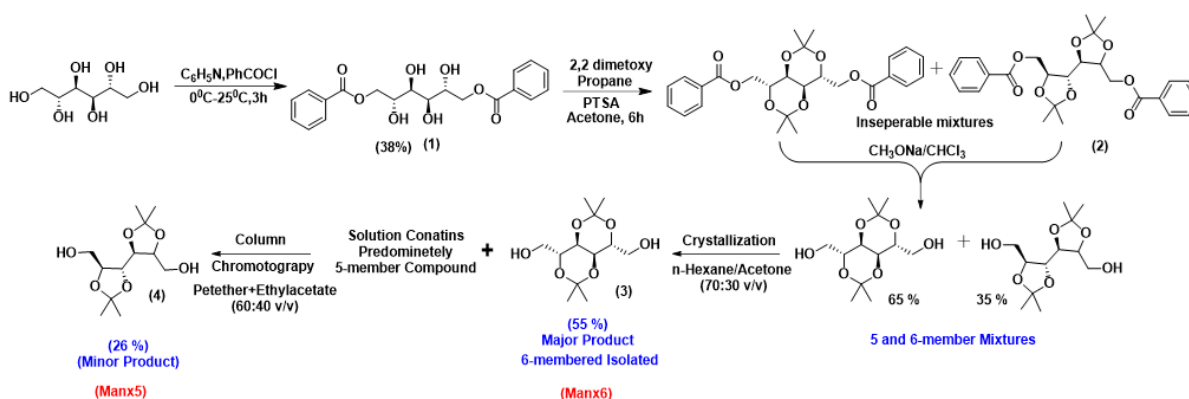
3.77-3.86 (m, 4H), 4.02-4.09 (m, 4 H), (m, 3 H), 4.19-4.22 (m, 1 H), 7.75 (d, 1 H).  $^{13}\text{C}$  NMR (100 MHz,  $\text{CDCl}_3$ )  $\delta$  ppm: 23.34, 24.06, 25.94, 55.3 63.76, 63.83, 67.1, 67.43, 67.69, 70.54, 100.41, 155.74, 172.41.

**4.2.18. Glycine polymer:** The synthetic procedure was similar to the Manx6-Val.  $^1\text{H}$  NMR (400 MHz,  $\text{DMSO}-d_6$ )  $\delta$  ppm:  $^1\text{H}$  NMR (400 MHz,  $\text{DMSO}-d_6$ )  $\delta$  ppm: 1.25 (s, 12 H), 1.31 (s, 12 H), 3.75-3.88 (m, 6 H), 4.03-4.14 (m, 4 H), 7.82 (d, 1 H).  $^{13}\text{C}$  NMR (100 MHz,  $\text{CDCl}_3$ )  $\delta$  ppm: 23.3 24.06, 35.94, 55.3 63.73, 63.8 67.1, 67.4, 67.7, 70.6, 100.3, 155.7, 171.4.

### 4.3. Result and discussion

#### 4.3.1. Synthesis of Acetal-masked D-Mannitol Sugar-diols:

Two sugar-diols were synthesised from D-mannitol by masking the middle secondary hydroxyl groups either as 6-member acetal or 5-member acetal as shown in Scheme 4.1. The primary hydroxyl groups of D-mannitol were first selectively protected by benzoyl chloride to get the compound **1** as reported earlier. Compound **1** was reacted with 2,2 dimethoxypropane to get mixtures of 6-member and 5-member isomeric products of **2** which are not separable by standard procedures. The percentage composition of these isomeric mixture was estimated by comparing the integration at 1.26 ppm and 1.28 ppm corresponding to the methyl protons of acetal group. From proton NMR it was observed that the 6 membered isomer was forming predominantly. Finally, benzoyl groups in Compound **2** were deprotected using sodium methoxide yield mixtures of 6-membered acetal protected sugar diol (compound **3**) abbreviated as **Manx6** and 5-membered acetal protected sugar diol (compound **4**) abbreviated as **Manx5**.



**Scheme 4.1.** Synthesis of D-mannitol based diols six membered (Manx6) and (b) five membered (Manx5)

$^1\text{H}$ -NMR analysis revealed that both compound **3** and **4** present in 65 % and 35 % in the product mixture. Fortunately, the recrystallization of the mixture in hot n-hexane/acetone 70/30 v/v solvent combination resulted in the selective crystallization of Manx6 in 55 % yield. Subsequent column purification of the mother liquor facilitated the isolation of Manx5 in 26

% yield. The structure of both the diols was confirmed by NMR (see figure 4.4) spectroscopy and chemical shift of each proton was confirmed by 2D NMR (HSQC and COSY) (see Figure 4.5) Analysing the COSY spectra of six membered diol allows the assignment of CH<sub>2</sub> proton at 3.4-3.5 ppm which was showing correlation with -OH proton. Further the direct correlation of peak at 3.5 ppm with -CH<sub>2</sub> protons suggest that the peak at 3.5 ppm corresponds to the -CH<sub>2</sub>-CH- proton. which was further confirmed by HSQC spectra. Similar analysis was done for five membered diol and chemical shift of each proton was assigned alphabetically

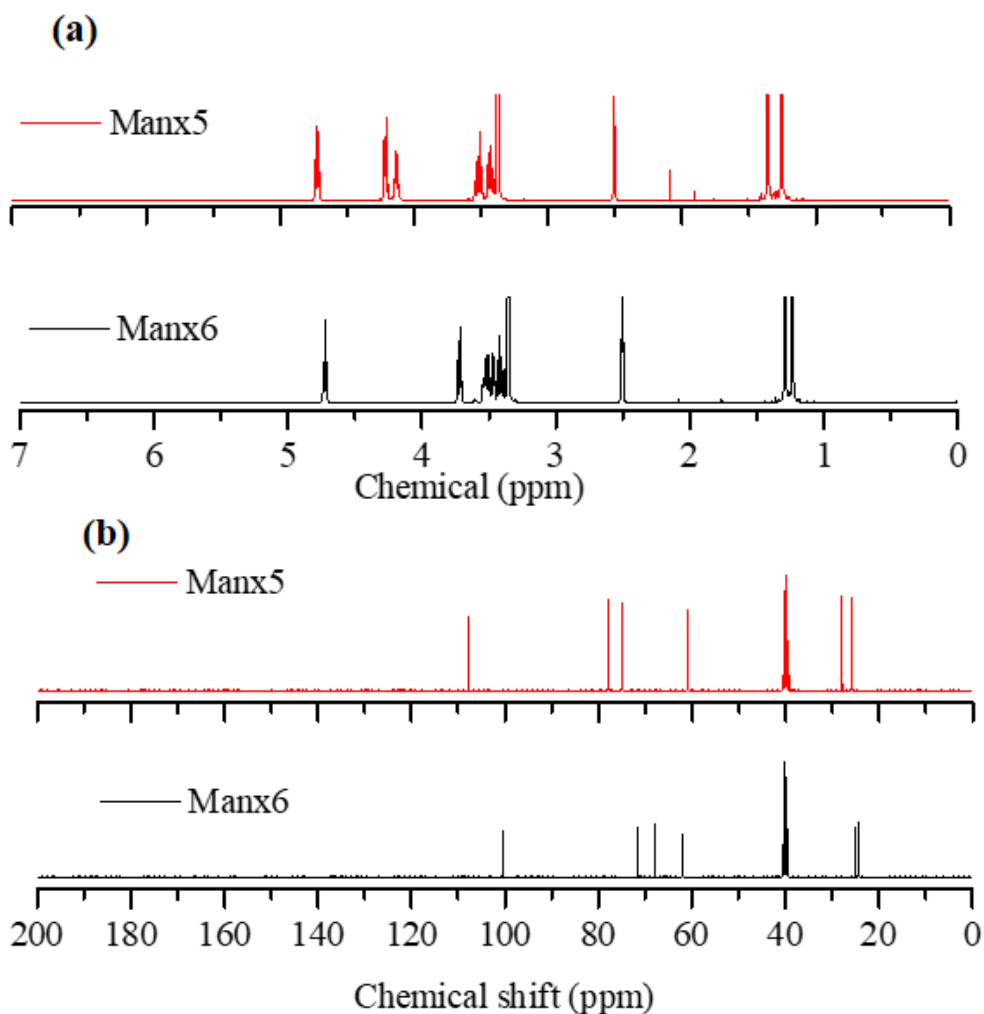


**Figure 4.4.** (a) <sup>1</sup>H NMR and (b) <sup>13</sup>C NMR spectra of compound 3 (Manx6) and compound 4 (Manx5) in DMSO-*d*<sub>6</sub>.

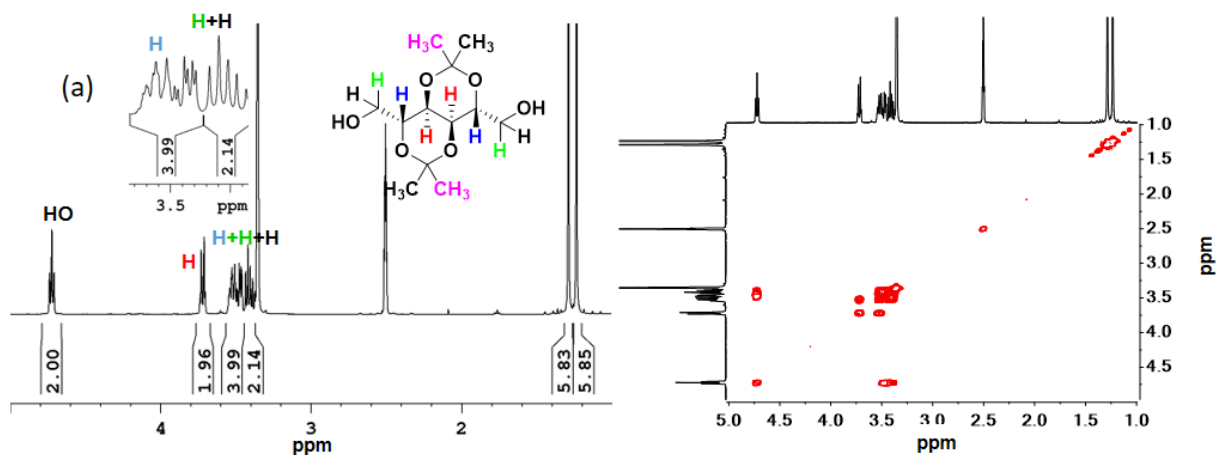


**Figure 4.5.** 2D NMR COSY Spectrum of Compound 3 (Manx6).

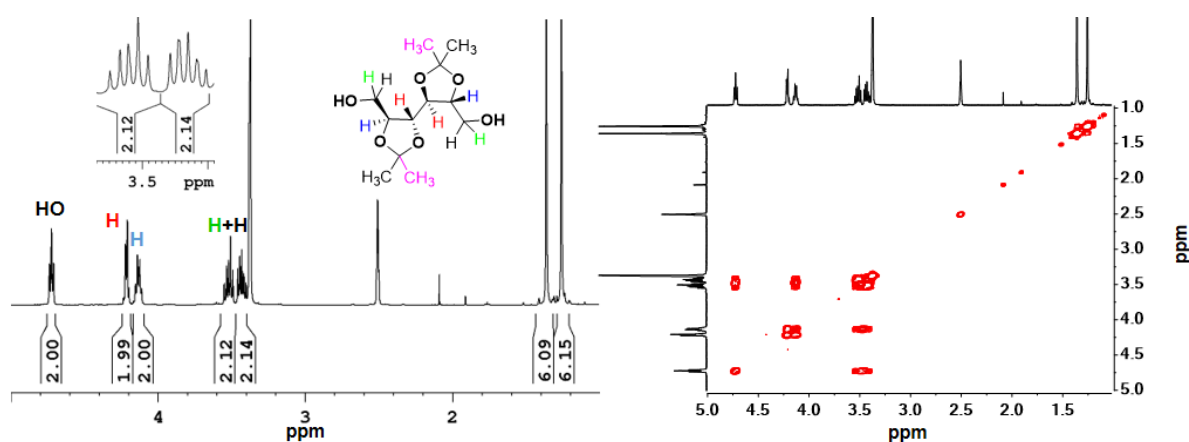


**Figure 4.6.** 2D NMR COSY Spectrum of Compound 4 (Manx5)

The structure of the sugar diols has been further confirmed by single-crystal X-ray diffraction analysis. Single crystal of both the diols was obtained in acetone: hexane mixture (1:3 v/v). The crystal structure studies showed that the both the diols have a 2-fold axis of symmetry which gives equal reactivity to both the  $\text{-OH}$  groups. In case of six membered diol both the fused rings are in chair confirmation keeping the bulkier  $\text{-CH}_2\text{OH}$  group in equatorial position. The molecule crystallises in a monoclinic space group of  $P2_1$  and the unit cell parameter for crystal was determined as  $a = 11.247 \text{ \AA}$ ,  $b = 11.459 \text{ \AA}$ ,  $c = 12.039 \text{ \AA}$ ,  $\alpha = 90.00 \text{ \AA}$ ,  $\beta = 116.06 \text{ \AA}$ ,  $\gamma = 90.00 \text{ \AA}$ . The crystallographic R factor for the final structure was  $R = 0.09$ . The crystal structure analysis for five membered diol showed that the diol crystallizes in a monoclinic space group,  $P2_1$  with the unit cell parameter of  $a = 12.802 \text{ \AA}$ ,  $b = 10.988 \text{ \AA}$ ,  $c = 20.21 \text{ \AA}$ ,  $\alpha = 90.00 \text{ \AA}$ ,  $\beta = 108.47 \text{ \AA}$ ,  $\gamma = 90.00 \text{ \AA}$ .

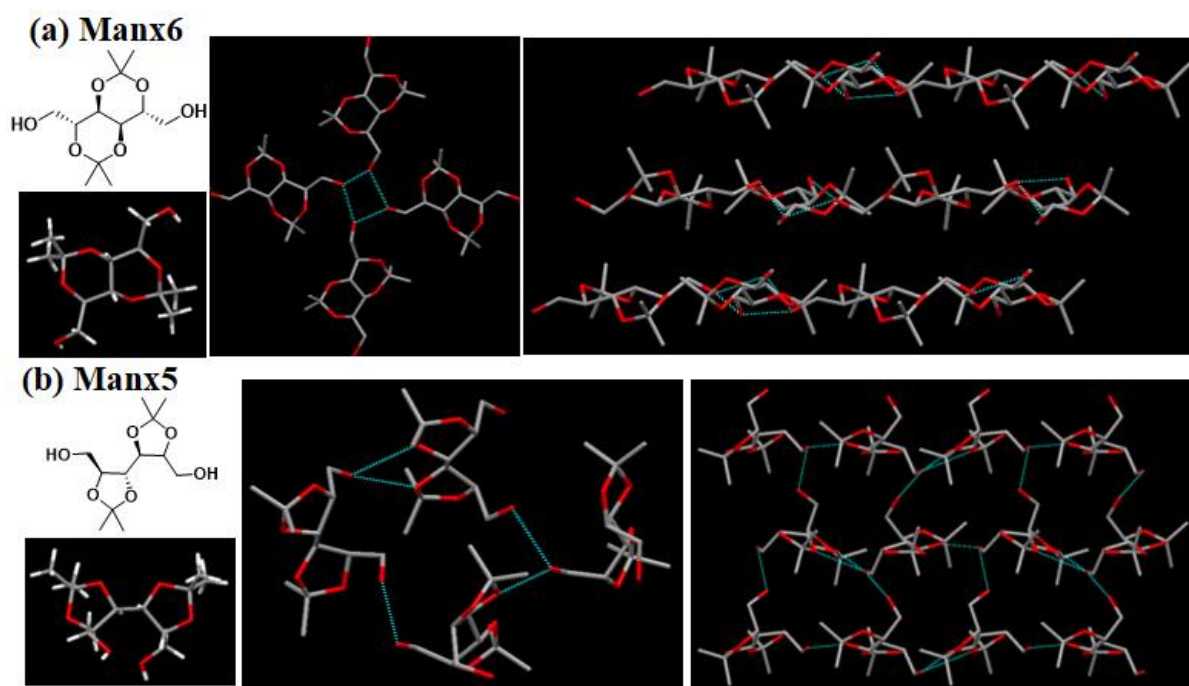


**Figure 4.7.** (a) Crystal structure of Manx6 and (b) Manx5

The thermal properties of monomers was measured by TGA and DSC analysis. The TGA analysis showed that the diols were stable up to 170 °C. The DSC measurements were carried out to understand the packing abilities of both the diols. The enthalpy of the melting ( $\Delta H_m$ ) and enthalpy of crystallisation ( $\Delta H_c$ ) was calculated under inert atmosphere with a heating and cooling rate of ten degrees per minute and values are shown in Table 4.1.

**Table 4.1.** Thermal properties measured from DSC analysis.

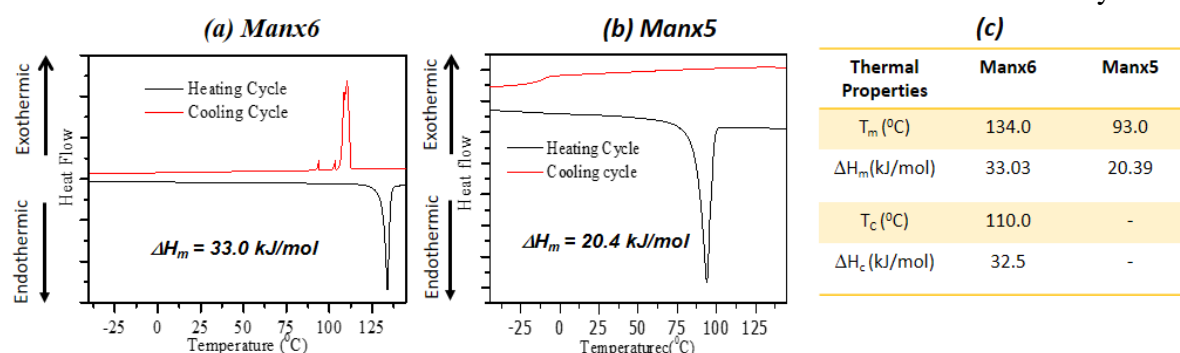


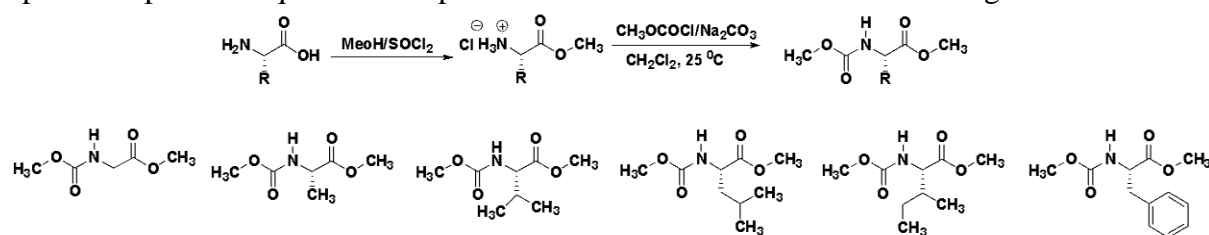
**Figure 4.8.** (a) DSC thermograms of compound 3 (Manx6) and (b) compound 4 (Manx5) in heating and cooling cycle (c) enthalpy of melting and crystalline transition of monomers.

The DSC thermogram of six membered diol showed a melting point 136 °C and enthalpy of melting was obtained as ( $\Delta H_m = 33.1$  kJ/mol) similarly, cooling DSC thermogram

from molten sample showed a crystallization peak at 110 °C and enthalpy of crystallisation was found to be ( $\Delta H_c = 32.5$  kJ/mol). The five membered diol was showing a melting point at 96 °C and enthalpy of melting was obtained as ( $\Delta H_m = 20.3$  kJ/mol). and there was no crystallization peak in cooling cycle which shows five membered diol is sluggish to crystallise. The higher value of ( $\Delta H_m$ ) for six membered diols compare to five membered diols can be attributed to the rigid fused structure of six membered diol which results in better packing and higher ( $\Delta H_m$ ).

#### 4.3.2. Synthesis of L-Amino acid Monomers:

Naturally abundant L-Amino acids were chosen to synthesise the ester urethane monomers. Amino acid was converted into methyl ester hydrochloride salt which was further reacted methyl chloroformate to get the desired ester urethane monomer (see scheme 4.2). Ester urethane monomer of L-phenyl L-alanine, L-leucine, L-isoleucine, L-valine, L-alanine and glycine, was synthesised and structure of these monomers was confirmed by NMR and other spectroscopic techniques. NMR spectrum of all the monomer is shown in Figure 4.9.



**Scheme 4.2.** Synthesis of L-Amino amino acid based ester urethane monomers.

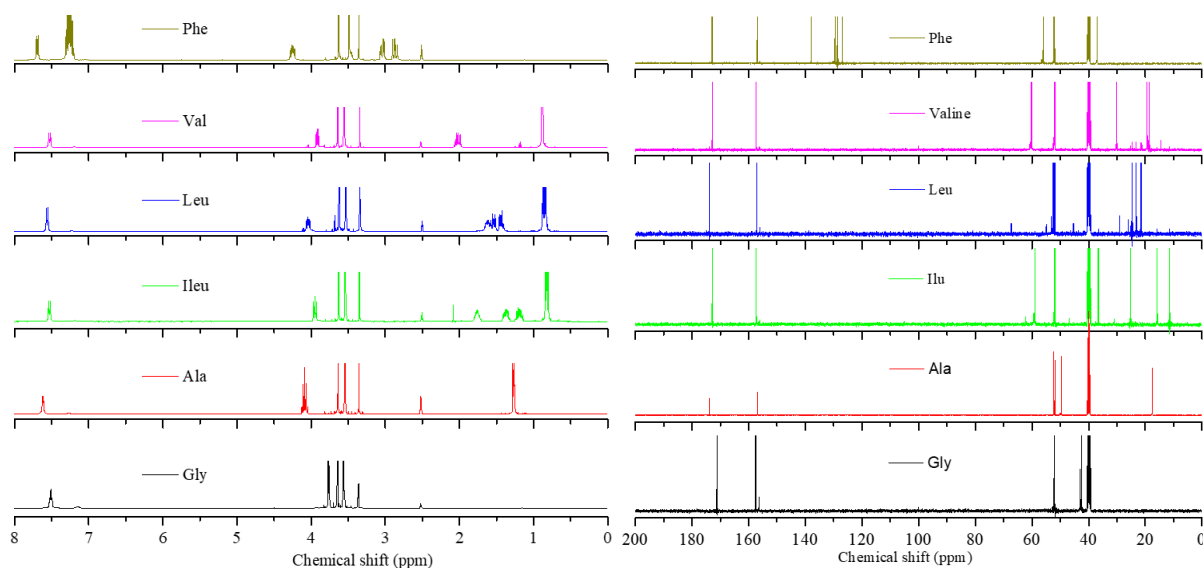
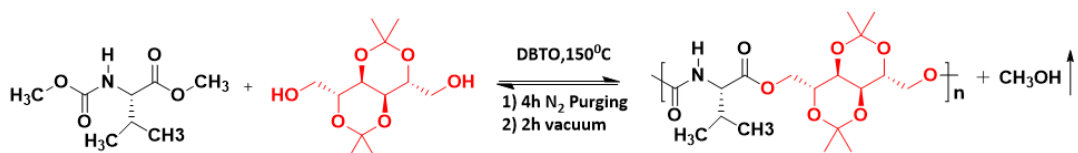


**Figure 4.9.**  $^1\text{H}$  NMR and  $^{13}\text{C}$  NMR spectra of Amino acid ester urethane monomers in  $\text{DMSO-}d_6$ .



**Scheme 4.3.** Synthesis of amino acid and sugar based poly(ester urethane)s.

Polymerisation was carried out by solvent free melt polycondensation technique for which equimolar amount of diol and amino acid was taken in a polymerisation tube equipped with four arm magnetic bead. The polymerisation tube was placed in oil bath at 150 °C and monomers were allowed to melt with continuous string. The polymerisation setup was made oxygen free by applying vacuum and 1 mol % of catalyst (Dibutyltin oxide) was added into it. The polycondensation was carried out at 150<sup>o</sup>C under continuous nitrogen purging for 4h to get a viscous oligomeric liquid. This oligomeric liquid was further subjected to vacuum (0.01 mm of Hg) for 2h to get the polyester(urethane)s see scheme 4.3. The NMR spectrum of Manx6-Val is shown in Figure 4.10.

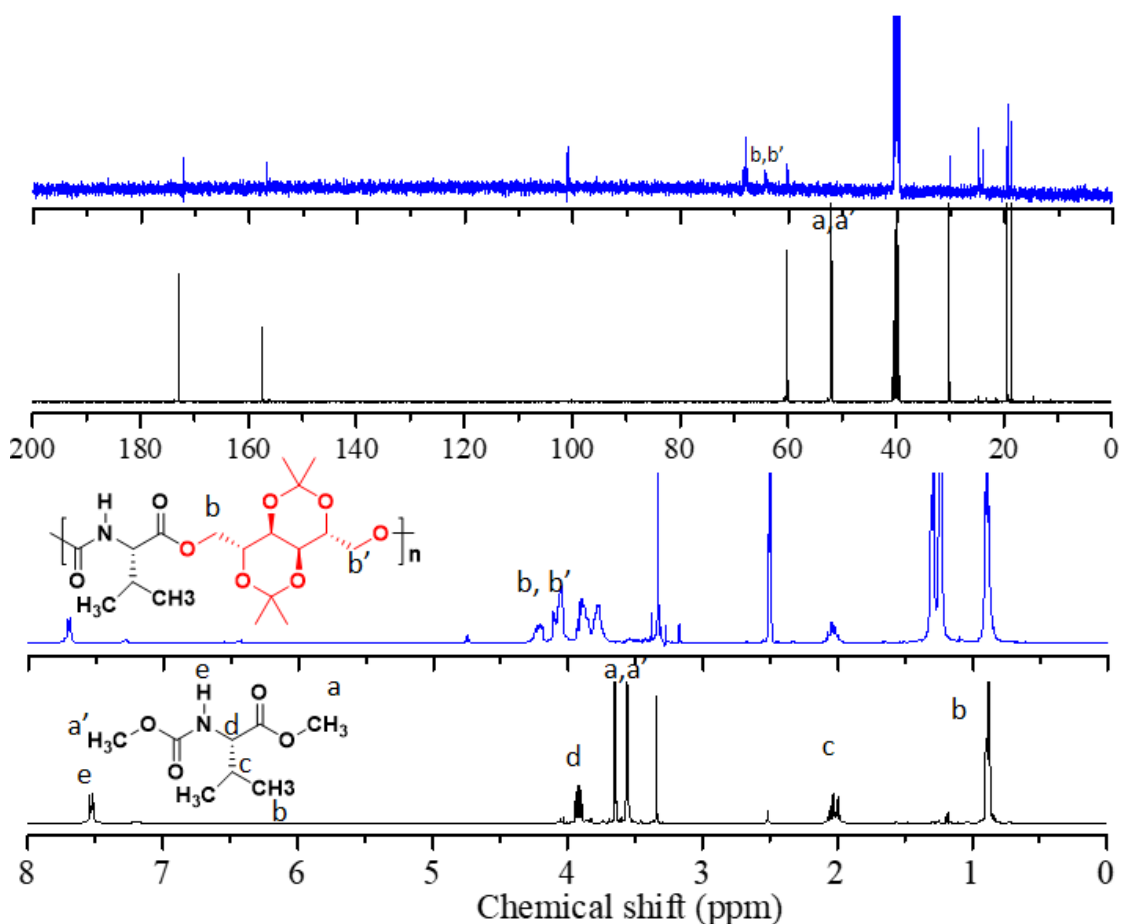


**Figure 4.10.** (a) <sup>1</sup>H NMR spectra of Val monomer and (b) polymer in DMSO-*d*<sub>6</sub>. (c) <sup>13</sup>C NMR spectra of Val monomer and (d) Polymer in DMSO-*d*<sub>6</sub>.



Other amino acid monomers were also subjected for melt polymerisation to give different polyester(urethane)s and their NMR characterisation is given in Figure 4.11. The formation of polymer was confirmed from NMR spectroscopy. The proton NMR of amino acid monomer shows two singlet at 3.63 ppm and 3.67 ppm corresponding to methyl protons of urethane and ester group which were completely disappeared in polymer  $^1\text{H}$  NMR spectrum. To find the chemical shift value of newly formed ester and urethane methylene  $-\text{CH}_2$  2D NMR was recorded and it was found that the newly formed ester and urethane  $-\text{CH}_2$  was showing a multiplet at 4.12-4.25 ppm.

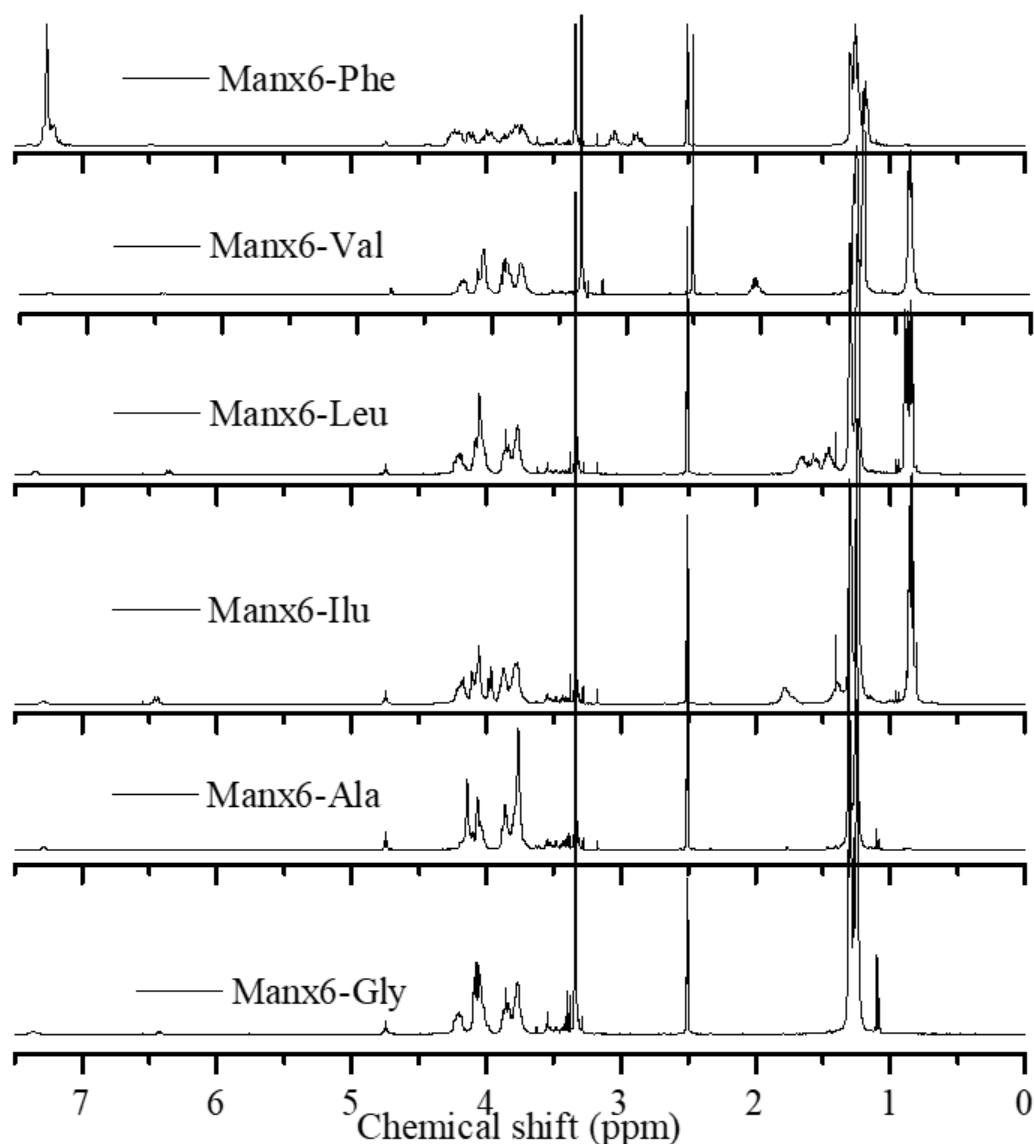


**Figure 4.11.**  $^1\text{H}$  NMR spectrum of polymers in  $\text{DMSO}-d_6$ .

Similarly, the  $^{13}\text{C}$  NMR of sugar diol shows peaks at 51.5 ppm corresponding to methylene carbon ( $-\text{CH}_2\text{-OH}$ ) which was completely vanished in the  $^{13}\text{C}$  NMR of polymer and two new peaks at 62.3 and 62.5 ppm was appeared corresponding to newly formed ester and urethane carbon. From  $^1\text{H}$  and  $^{13}\text{C}$  NMR of monomers and polymers it was evident that the

acetal group was stable under polymerisation condition and both the monomers were getting completely consumed to give the polyester(urethane).

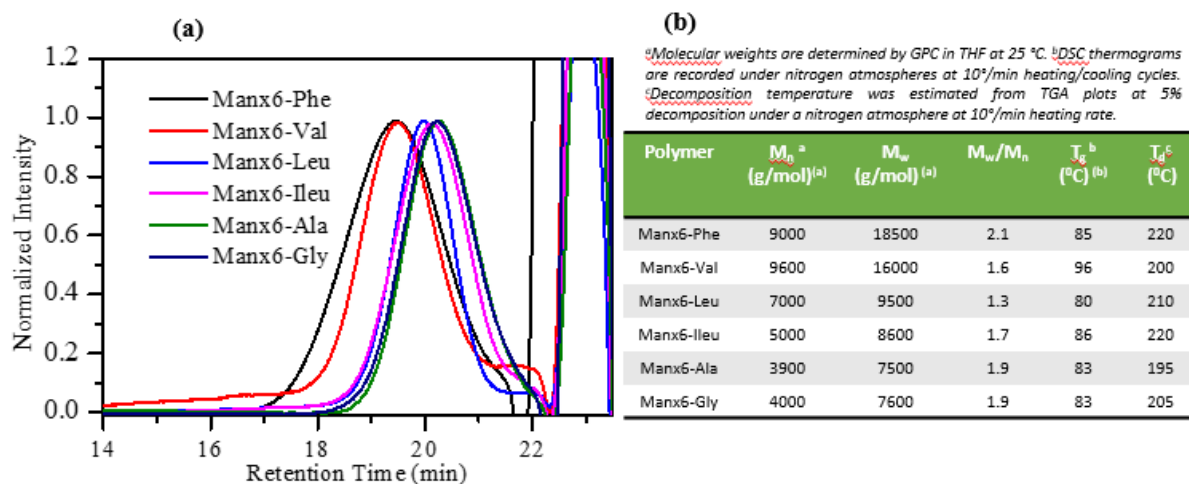


**Figure 4.12.** (a) GPC chromatograms of polymers in THF at 25°C. (b) Table containing molecular weight of polymers determined from GPC and glass transition temperature ( $T_g$ ) determined by DSC analysis and decomposition temperature determined from TGA analysis.

The molecular weight of these newly designed polymers was measured by GPC using THF as solvent. The GPC chromatograms of all these polymers showed monomodal distribution having number average molecular weight in the range of  $4 \times 10^3$  to  $9.5 \times 10^3$  see Figure 4.12.a. To check the stability of acetal group during melt condensation MALDI-TOF analysis was carried out see Figure 4.13. In a typical A-A+ B-B type polycondensation four different types of end groups are possible (i) polymer chains having A-P<sub>n</sub>-A type end groups (ii) polymer chains having B-P<sub>n</sub>-B types end groups (iii) polymer chains having A-P<sub>n</sub>-B type end groups and (iv) macrocycle due to back biting of end groups which gives the mass of repeating unit. MALDI-TOF spectra of aliquot after 4 h time interval was recorded and it was found all three types of end groups (A-P<sub>n</sub>-A, B-P<sub>n</sub>-B and A-P<sub>n</sub>-B) were present without any macrocyclic product which suggest the stability of end groups during polycondensation and absence of macrocyclic product suggest that polymer end groups are active for further polycondensation reaction and all other functional groups are stable during melt condensation.

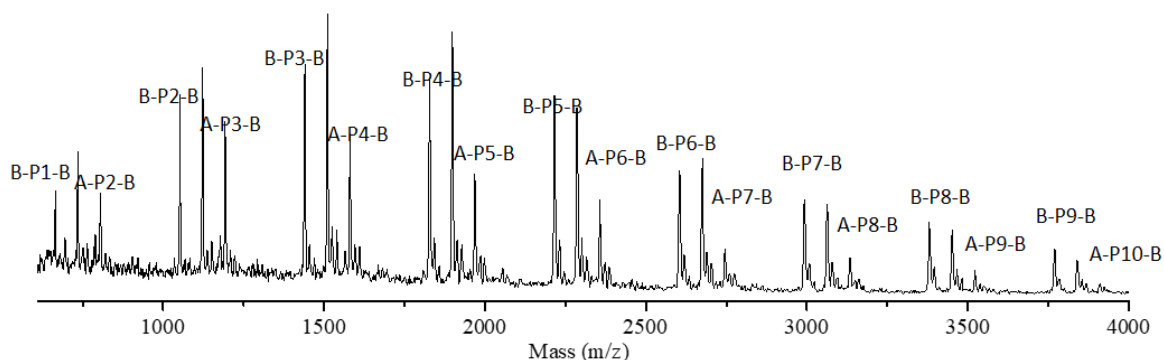


**Figure 4.13.** MALDI-TOF spectrum of Manx6-Val aliquot after 4 h.

Thermal properties of these polymers was measured by TGA and DSC analysis. The TGA analysis was carried out under inert condition with 10 °C/min heating rate and it was observed that all the polymers were thermally stable up to 200 °C see Figure 4.14.

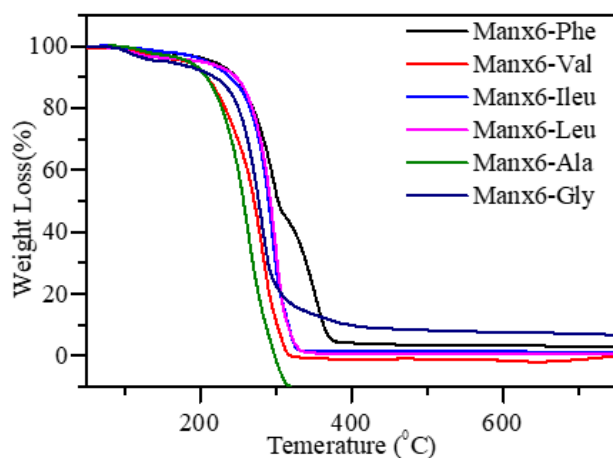


**Figure 4.14.** TGA Profile of Polymers.

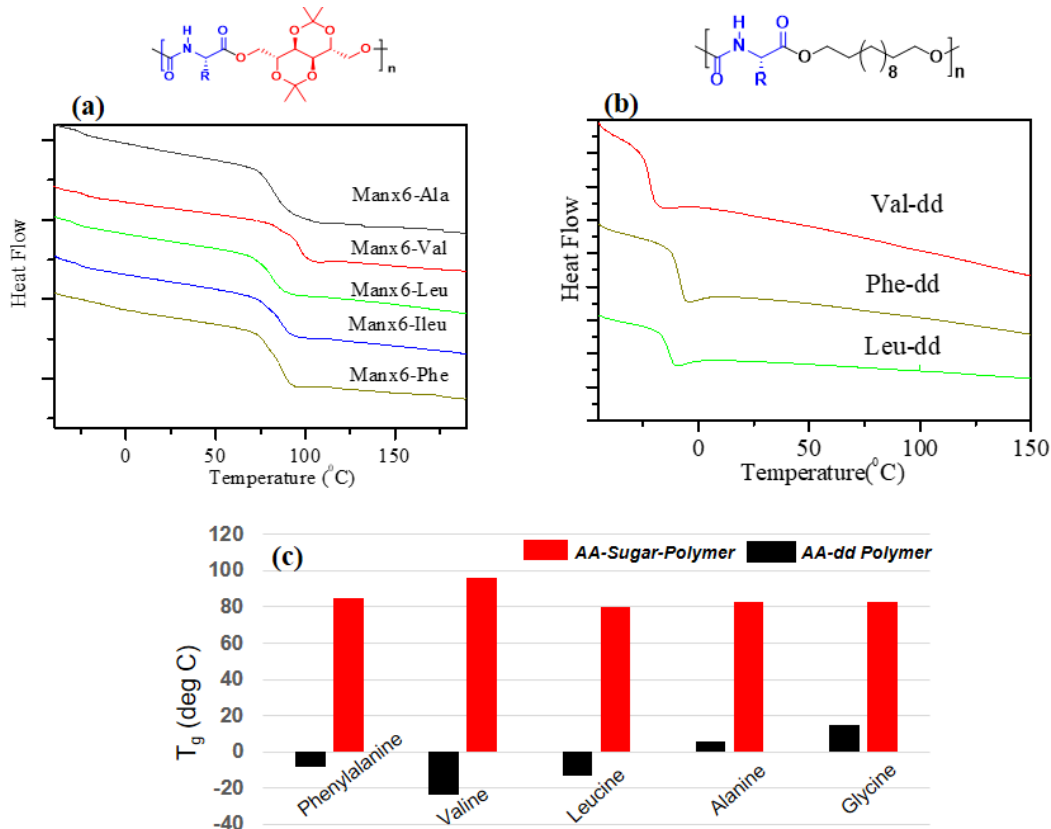
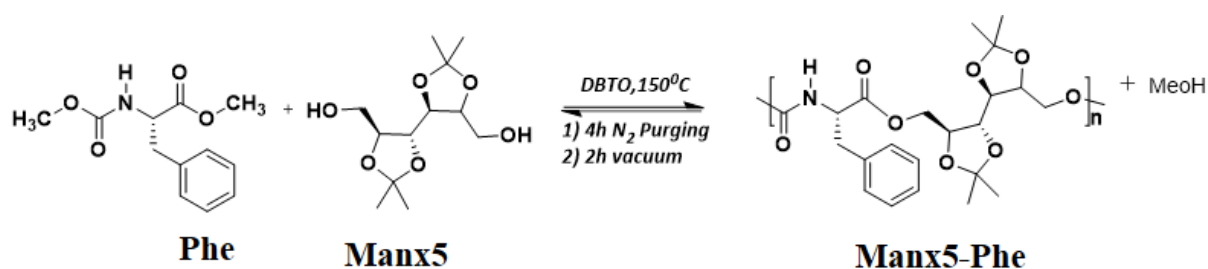


**Figure 4.15.** (a) DSC thermograms of different Polymers synthesised from Manx6 and (b) dodecanediol (c) bar diagram, showing glass transition temperature of polymers synthesised from Manx6 and dodecanediol.

Differential scanning calorimetry (DSC) analysis of all polymers showed that all the polymers were amorphous in nature and glass transition temperature of these polymers was varying from 80 °C to 96 °C and results are shown in Figure 4.15.a. To check the effect of sugar

diol on glass transition temperature we have replaced sugar diol with aliphatic 1,12 dodecanediol and a series of polymers was synthesised with different amino acids. The glass transition temperature of both the series of polymers was compared and we found that the polymers synthesised from aliphatic diol were showing much lower glass transition temperature (-23 °C to 15 °C) compare to the polymers synthesised from sugar diol (see Figure 4.15.c.) which shows that the rigid structure of sugar diol is responsible for high glass transition temperature. The Tg value for glycine polymer was found slightly higher compare to other polymers because, the thermal properties of polymers are affected by molecular weight. The Valine polymer has the highest molecular weight so it is expected that it will show slightly higher glass transition temperature compare to other polymers



**Scheme 4.4.** Synthesis of amino acid and sugar based poly(ester urethane)s.

The six membered diol (Manx6) contains two fused bicyclic ring which is more rigid structure compare to five membered diol (Manx5) so to check the effect of these two diols on glass transition temperature, polymer was synthesised with phenylalanine monomer using Manx5 diol Manx5 (see scheme 4.4.). Melt polymerisation reaction was monitored by NMR analysis. The phenyl alanine monomer was having two singlets at 3.48 and 3.62 ppm (see Figure 4.16.a.) which were completely disappeared in polymer NMR and a new peak was appeared at 4.30 ppm corresponding to newly formed ester and urethane -CH<sub>2</sub>. The disappearance of end groups and appearance of a multiplet at 4.30 in polymer <sup>1</sup>H NMR spectrum confirmed the formation of polymer. The molecular weight of the polymer was determined by GPC analysis and GPC chromatogram is shown in Figure 4.16.b. GPC analysis revealed that the polymer had a monomodal distribution with a molecular weight of 7 X 10<sup>3</sup> g/mol. To check the effect of diol structure on glass transition temperature polymer was subjected for DSC analysis. The DSC analysis confirmed the amorphous nature of polymer having a glass transition temperature 83 °C (see Figure 4.17.a) which tells that the polymer synthesised from both the diols are having almost same glass transition temperature Figure 4.17.b. The polymers were produced amorphous due to the sluggish nature of the polymer backbone towards crystallinity. The polymer synthesized from sugar diols was mostly reported

as amorphous in nature. It was seen that only polymers synthesized from diethyl sebacate are semicrystalline while other polymers were amorphous in nature which suggests that the crystallinity of polymers was controlled by the choice of the monomer. It was earlier reported from our lab that L-amino acid-based poly(ester urethane)s are predominately amorphous in nature except even they have very high molecular weight up to 38,000 g/mol. Only alanine, glycine and  $\beta$ -alanine based systems showed semi-crystallinity with clear melting transition at 80-90 deg C. The sugar-based polymers reported here were produced with a degree of polymerization of 25-30 units which is sufficient enough to show the semicrystallinity if present.

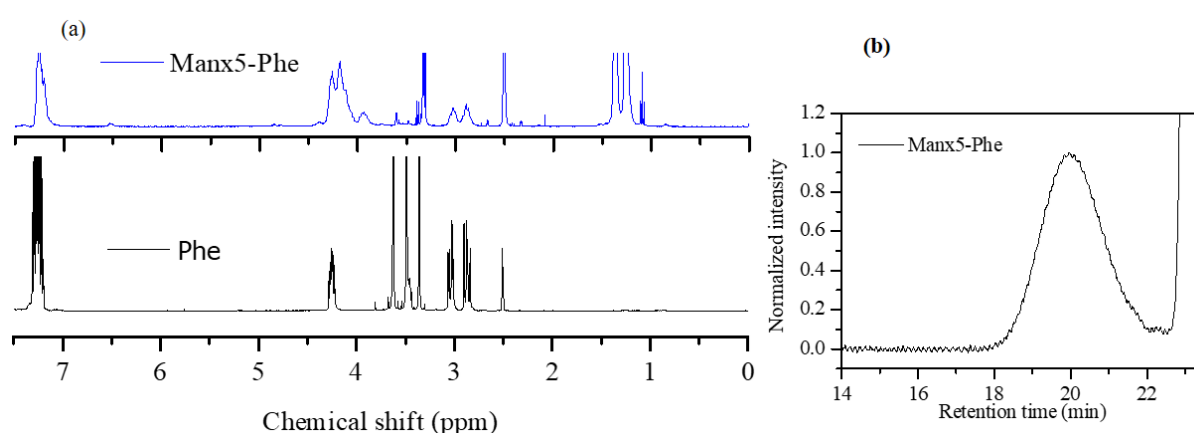


**Figure 4.16.** (a)  $^1\text{H}$  NMR spectrum of Manx5-Phe in  $\text{DMSO-}d_6$ . (b) GPC chromatogram of Manx5-Phe

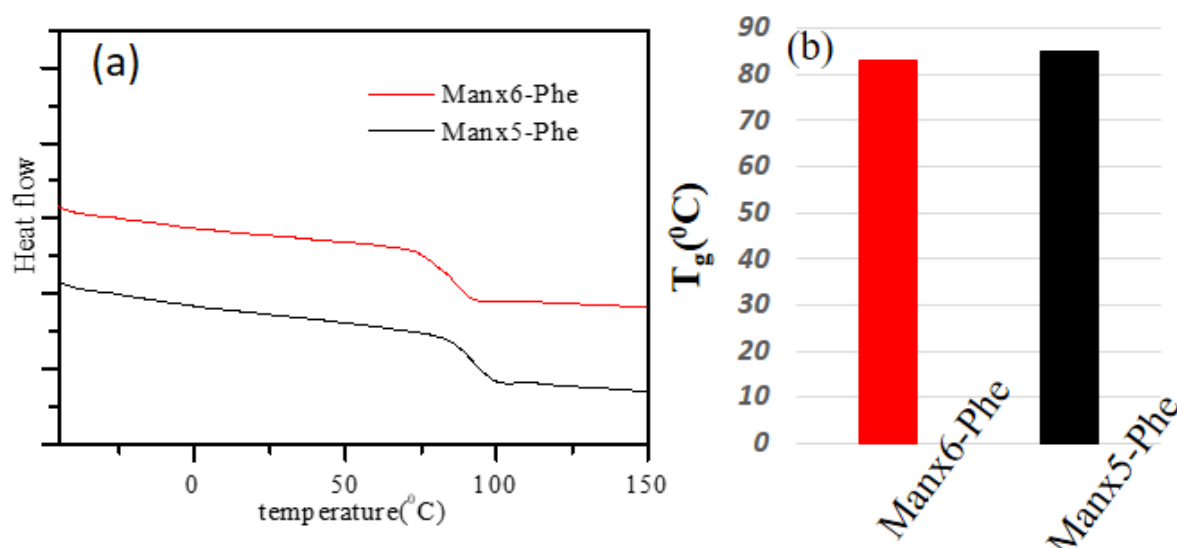
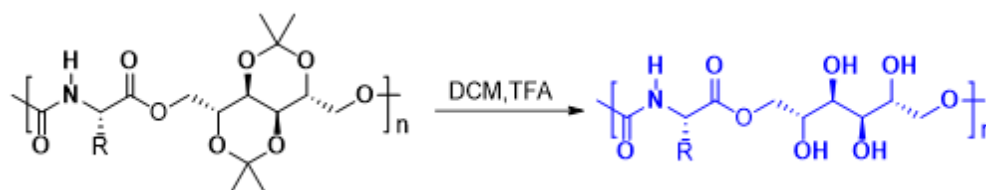


**Figure 4.17.** (a) DCS thermograms and (b) bar diagram showing glass transition temperature of Manx6-Phe and Manx5-phe.

The polymer synthesized from sugar diol and amino acid were hydrophobic in nature so to bring the amphiphilicity, the acetal group in the polymer was deprotected using TFA to synthesize amphiphilic amino acid sugar hybrid polymer as shown in scheme 4.5.



**Scheme 4.5.** Synthesis of amino acid-sugar hybrid polymers.

Deprotection of acetal group polymer was confirmed by proton NMR. The proton NMR of polymer contains two singlets at 1.33 and 1.43 ppm corresponding to two methyl groups of acetal unit which were completely disappeared after acetal deprotection confirming the deprotection of acetal group without affecting the polymer backbone. GPC chromatograms of polymers indicated a shift in retention time after deprotection, further suggesting the deprotection of acetal group.

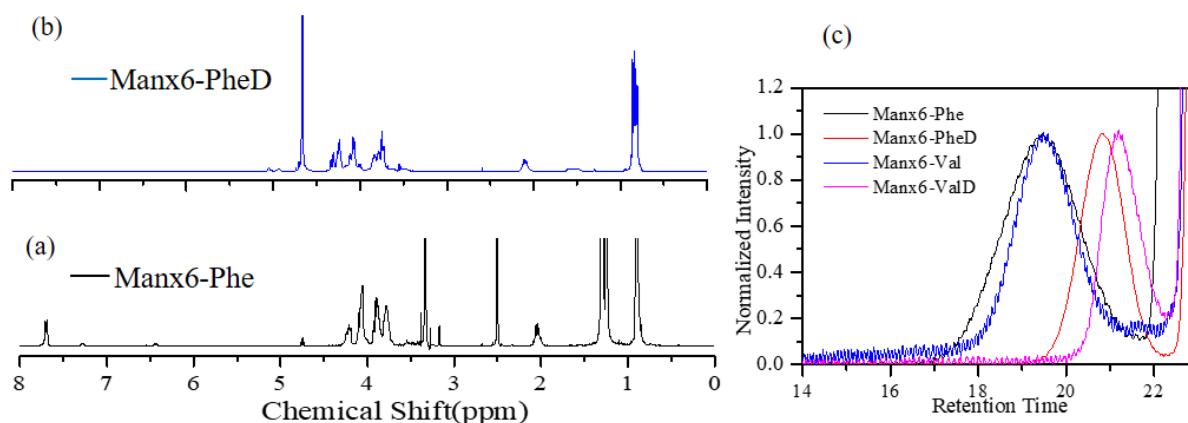


**Figure 4.18.** (a) <sup>1</sup>H NMR spectrum of Manx6-Phe and (b) Manx6-PheD in DMSO-d<sub>6</sub>. (before and after acetal deprotection) (c) GPC chromatogram of polymers before and after acetal deprotection.

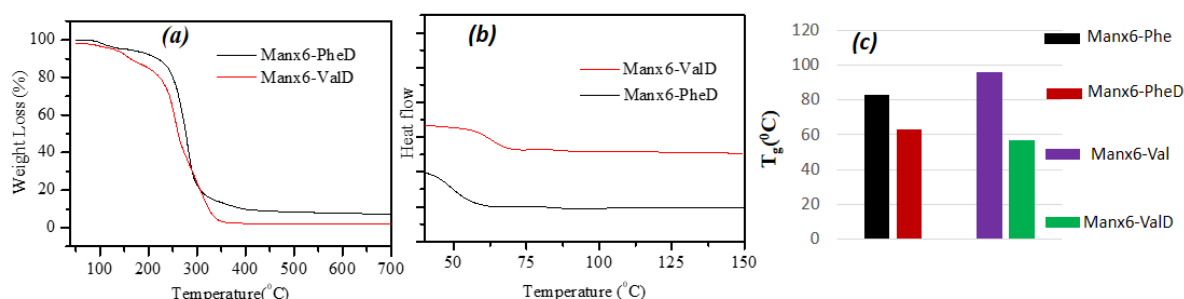


**Figure 4.19.** (a) TGA and (b) DSC thermograms of polymers (c) bar diagrams showing the glass transition temperature of polymers before and after acetal deprotection.

To check the thermal properties, polymers was subjected for TGA and DSC analysis. TGA thermograms of polymers are shown in Figure 4.19 a. which revealed thermal stability

of polymers up to 200 °C. DSC thermograms of polymer revealed amorphous nature of polymer and glass transition temperature at 65 °C (see Figure 4.19. b) which is slightly lower than acetal protected polymer Figure 4.19.c. These results suggest that after acetal deprotection the polymer chains have more conformational mobility which results in decrease in the glass transition temperature. The newly synthesised polyester(urethane)s were obtained from optically active amino acid monomers like L-phenyl alanine, L-valine, L-isoleucine, L-leucine and L-alanine so to check their secondary structure in solution state polymers were dissolved in THF and circular dichroism (CD) analysis was carried out the CD spectra are shown in Figure 4.20.

All the polymers were showing a positive CD band around 220-230 nm indicating the helical coil confirmation of these polymers while the acetal deprotected polymers were showing a negative CD band around 225-230 nm for  $n-\pi^*$  transition and a positive CD band around 215-220 nm for  $\pi-\pi^*$  transitions suggesting the  $\beta$  sheet conformation in THF.

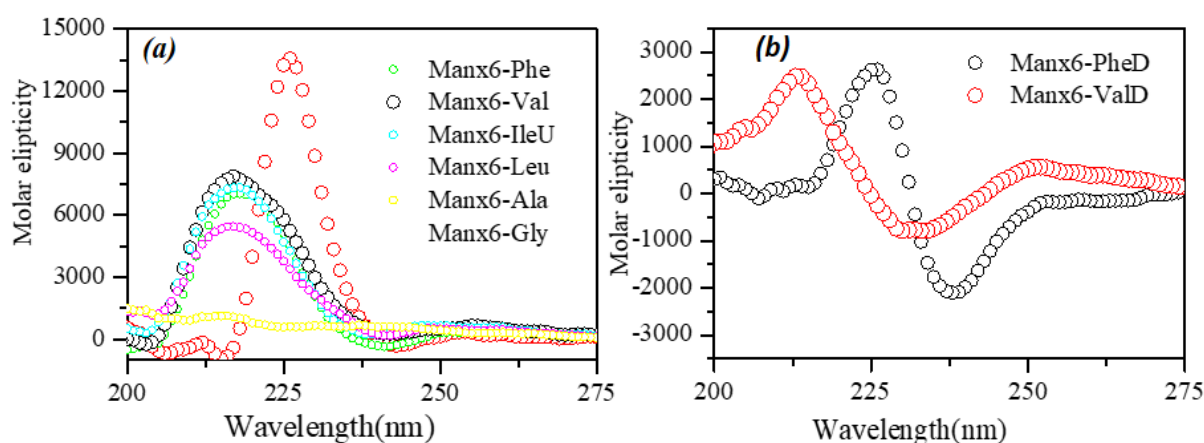


**Figure 4.20.** (a) CD spectra of polymers in THF before and (b) after acetal deprotection.

Free hydroxyl groups in the polymer chain can promote hydrogen bonding more effectively, resulting in the formation of  $\beta$ -sheet conformation for deprotected polymers while in case of non-deprotected polymers the hydrogen bonding was not effective which resulted in helical self-assembly. Water contact angle (WCA) measurements directly gives the information about hydrophilic and hydrophobic nature of polymer. To check the nature of these newly synthesised polymers water contact angle was measured before and after acetal deprotection by low bond axisymmetric drop shape analysis (LB-ADSA method) and photographs are shown in Figure 4.21.a and 4.21.b. The WCA value greater than  $90^{\circ}$  for these polymer suggest the hydrophobic nature of polymers but after acetal deprotection the free hydroxyl groups in

the polymer backbone are bringing enough hydrophilicity which is responsible for lower water contact angle.

The acetal protected polymers was not water soluble so their self-assembly behaviour was studied in organic solvent. For that 0.20 mg/mL of polymer solution in tetrahydrofuran (THF) was dropcasted on silicon wafers and subjected for FESEM analysis and photographs are shown in Figure 4.21.c The FESEM analysis of showed that polymers were showing nanofibril morphology in organic solvent. The thickness of these nanofibrils was found around  $60 \pm 10$  nm and length were varying up to few micrometre. The acetal deprotected polymers was hydrophilic in nature so there self-assembled behaviour was studied in aqueous solvent for that 5 mg polymer was dissolved in 2 ml of DMSO and 3 ml of double distilled water was added dropwise in to it and solution was transferred into 1 kDa dialysis membrane and dialyzed against double distilled water for 48 h.

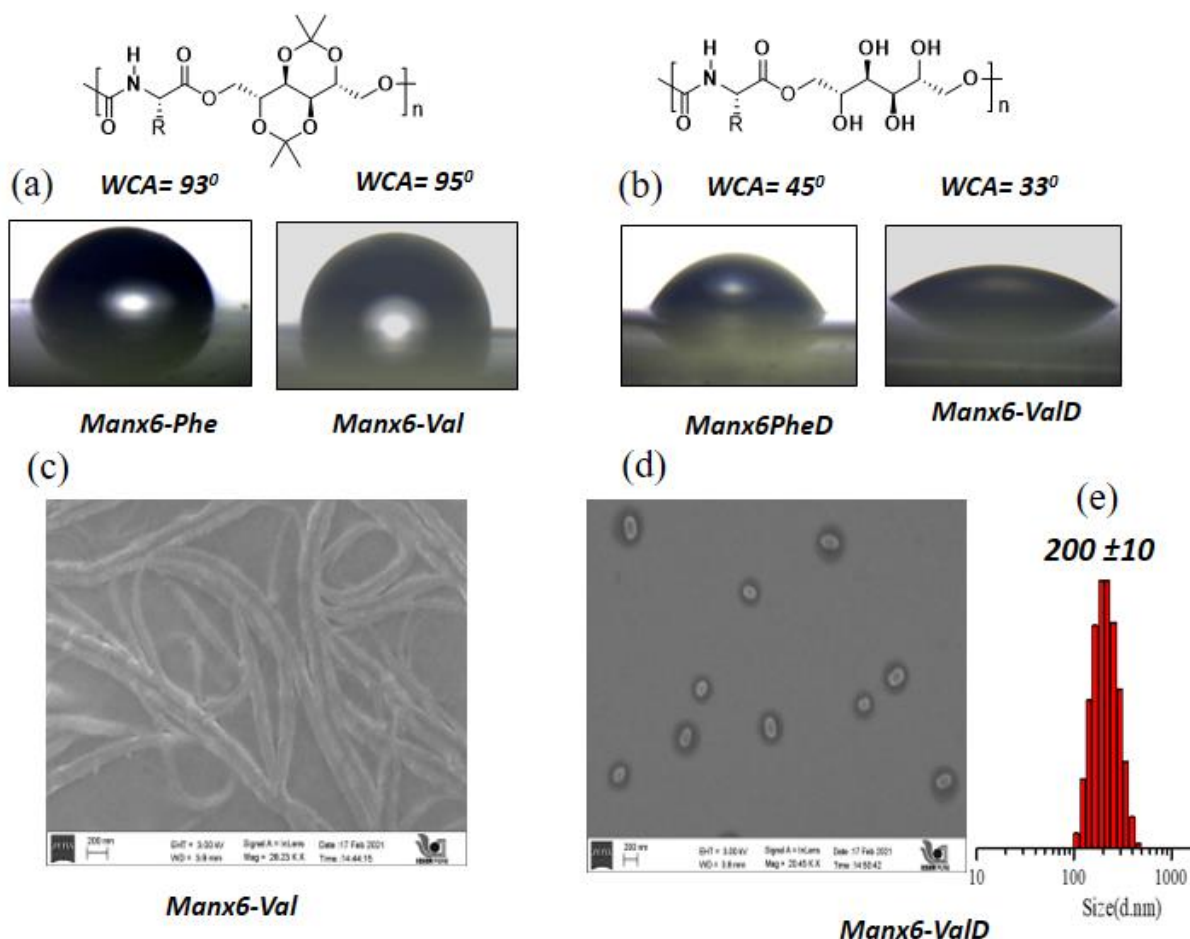


**Figure 4.21.** (a) Water contact angle image of Manx6-Phe and Manx6-Val (b) Water contact angle image of Manx6-PheD and Manx6-ValD (c) FESEM image of Manx6-Val, images were recorded for drop cast film of polymer solution (in THF, 0.1mg/mL) at 25°C. (d) FESEM image of Manx6-ValD, images were recorded for drop cast film of polymer solution (in H<sub>2</sub>O,



0.1mg/mL) at 25°C. (e) DLS histogram of aqueous self-assembly of polymer Sample concentration = 0.2 mg/ML.

The polymer solution was subjected for DLS measurements which shows that polymer is getting self-assembled in water to give  $200 \pm 10$  nm size nanoparticles see Figure 4.21.e. The formation of nanoparticle in aqueous medium was further confirmed by FESEM analysis which further supports the formation of  $190 \pm 10$  nm size nanoparticle see Figure 4.21.d The Cytotoxicity of these polymer nanoparticle was measured in WT-MEF cell line using MTT assay. Different concentration of polymer was exposed to cells and it was found that nanoparticles were showing excellent biocompatibility the cell viability results are given in Figure 4.22.

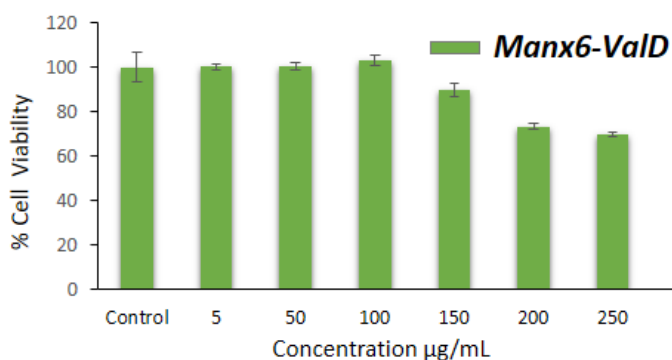


**Figure 4.22.** Cell viability of Manx6-ValD polymer in WT-MEF cell line.

#### 4.4. Conclusion

Using two abundant natural resources, a new synthetic methodology has been developed for the synthesis of completely biobased poly(ester urethane)s. The naturally abundant D-mannitol was converted into two bicyclic sugar diol by multistep synthesis. The secondary hydroxyl groups of D-mannitol were protected as an acetal linkage to get two different isomeric sugar diols. A detailed structural analysis for both the diol was performed and structure of diols was further confirmed by their single crystal structure. The second reacting partner was chosen from amino acid resources and converted into ester urethane monomer by suitable modifications. After confirming the thermal stability of both the reacting partner they were subjected for melt polymerisation reaction to synthesise renewable resource poly(ester urethane)s. Effect of two different sugar diol on thermal properties was studied in detail and it was found that the rigid structure of sugar diol was responsible for the high glass transition temperature of sugar based poly(ester urethane)s. Further the acetal Linkage was deprotected to get an amphiphilic amino acid sugar hybrid poly(ester urethane). The

amphiphilic polymer was in the polymer was deprotected to get amphiphilic amino acid sugar hybrid polyester(urethane)s which was forming  $200 \pm 10$  nm size nanoparticle in aqueous solvent. The cytotoxicity of these nanoparticles was tested in WT-MEF cell line, which confirmed the biocompatibility of these amino acid sugar hybrid polymers. In summary, the present study illustrates the first example of a polymer designed entirely from natural resources by using sugar and amino acids, and these polymers may provide an alternative to petroleum-based polymers in the future.

## References

- (1) Ghosh, K.; Jones, B. H. *ACS Sustainable Chem. Eng.* **2021**, *9*, 6170.
- (2) Filiciotto, L.; Rothenberg, G. *ChemSusChem* **2021**, *14*, 56.
- (3) Tokiwa, Y.; Calabia, B. P. *Appl. Microbiol. Biotechnol.* **2006**, *72*, 244.
- (4) Takayama, T.; Daigaku, Y.; Ito, H.; Takamori, H. *J. Mech. Sci. Technol.* **2014**, *28*, 4151.
- (5) Pappalardo, D.; Mathisen, T.; Finne-Wistrand, A. *Biomacromolecules* **2019**, *20*, 1465.
- (6) Bawa, K. K.; Oh, J. K. *Mol. Pharmaceutics* **2017**, *14*, 2460.
- (7) Tripathi, N.; Misra, M.; Mohanty, A. K. *ACS Eng. Au* **2021**, *1*, 7.
- (8) Anantharaj, S.; Jayakannan, M. *Biomacromolecules* **2012**, *13*, 2446.
- (9) Anantharaj, S.; Jayakannan, M. *Biomacromolecules* **2015**, *16*, 1009.
- (10) Stubbs, C. J.; Worch, J. C.; Prydderch, H.; Wang, Z.; Mathers, R. T.; Dobrynin, A. V.; Becker, M. L.; Dove, A. P. *Journal of the American Chemical Society* **2022**, *144*, 1243.
- (11) Bhaumik, A.; Peterson, G. I.; Kang, C.; Choi, T.-L. *J. Am. Chem. Soc.* **2019**, *141*, 12207.
- (12) Galbis, J. A.; García-Martín, M. d. G.; de Paz, M. V.; Galbis, E. *Chem. Rev.* **2016**, *116*, 1600.
- (13) Gandini, A.; Lacerda, T. M.; Carvalho, A. J. F.; Trovatti, E. *Chem. Rev.* **2016**, *116*, 1637.
- (14) Froidevaux, V.; Negrell, C.; Caillol, S.; Pascault, J.-P.; Boutevin, B. *Chem. Rev.* **2016**, *116*, 14181.
- (15) Feghali, E.; van de Pas, D. J.; Torr, K. M. *Biomacromolecules* **2020**, *21*, 1548.
- (16) Zhao, S.; Huang, X.; Whelton, A. J.; Abu-Omar, M. M. *ACS Sustainable Chem. Eng.* **2018**, *6*, 10628.

- (17) Lavilla, C.; de Ilarduya, A. M.; Alla, A.; García-Martín, M. G.; Galbis, J. A.; Muñoz-Guerra, S. *Macromolecules* **2012**, *45*, 8257.
- (18) Lavilla, C.; Alla, A.; Martínez de Ilarduya, A.; Muñoz-Guerra, S. *Biomacromolecules* **2013**, *14*, 781.
- (19) Hosseini, E. S.; Dervin, S.; Ganguly, P.; Dahiya, R. *ACS Applied Bio Materials* **2021**, *4*, 163.
- (20) Kirillova, A.; Yeazel, T. R.; Asheghali, D.; Petersen, S. R.; Dort, S.; Gall, K.; Becker, M. L. *Chemical Reviews* **2021**, *121*, 11238.
- (21) Albertsson, A.-C.; Varma, I. K. *Biomacromolecules* **2003**, *4*, 1466.
- (22) Tokiwa, Y.; Calabia, B. P. *J Polym Environ.* **2007**, *15*, 259.
- (23) Lavilla, C.; Alla, A.; Martínez de Ilarduya, A.; Benito, E.; García-Martín, M. G.; Galbis, J. A.; Muñoz-Guerra, S. *Biomacromolecules* **2011**, *12*, 2642.
- (24) Japu, C.; Martínez de Ilarduya, A.; Alla, A.; Jiang, Y.; Loos, K.; Muñoz-Guerra, S. *Biomacromolecules* **2015**, *16*, 868.
- (25) Fenouillot, F.; Rousseau, A.; Colomines, G.; Saint-Loup, R.; Pascault, J. P. *Prog. Polym. Sci.* **2010**, *35*, 578.
- (26) Saadaoui, A.; Medimagh, R.; Marque, S.; Prim, D.; Chatti, S.; Casabianca, H.; Said Zina, M. *Des. Monomers Polym.* **2017**, *20*, 221.
- (27) Gustini, L.; Lavilla, C.; de Ilarduya, A. M.; Muñoz-Guerra, S.; Koning, C. E. *Biomacromolecules* **2016**, *17*, 3404.
- (28) Zakharova, E.; Martínez de Ilarduya, A.; León, S.; Muñoz-Guerra, S. *Des. Monomers Polym.* **2017**, *20*, 157.
- (29) Japu, C.; Alla, A.; Martínez de Ilarduya, A.; García-Martín, M. G.; Benito, E.; Galbis, J. A.; Muñoz-Guerra, S. *Polym. Chem.* **2012**, *3*, 2092.
- (30) Lavilla, C.; Alla, A.; Martínez de Ilarduya, A.; Benito, E.; García-Martín, M. G.; Galbis, J. A.; Muñoz-Guerra, S. *J Polym. Sci A Polym. Chem.* **2012**, *50*, 3393.
- (31) Japu, C.; Martínez de Ilarduya, A.; Alla, A.; García-Martín, M. G.; Galbis, J. A.; Muñoz-Guerra, S. *Polym. Chem.* **2013**, *4*, 3524.
- (32) Lavilla, C.; Muñoz-Guerra, S. *Polymer Degradation and Stability* **2012**, *97*, 1762.
- (33) Japu, C.; Martínez de Ilarduya, A.; Alla, A.; García-Martín, M. G.; Galbis, J. A.; Muñoz-Guerra, S. *Polym. Chem.* **2014**, *5*, 3190.
- (34) Muñoz-Guerra, S.; Lavilla, C.; Japu, C.; Martínez de Ilarduya, A. *Green Chem.* **2014**, *16*, 1716.
- (35) Stebbins, N. D.; Yu, W.; Uhrich, K. E. *Biomacromolecules* **2015**, *16*, 3632.

- (36) Aluri, R.; Saxena, S.; Joshi, D. C.; Jayakannan, M. *Biomacromolecules* **2018**, *19*, 2166.
- (37) Aluri, R.; Jayakannan, M. *Polymer Chemistry* **2015**, *6*, 4641.
- (38) Saxena, S.; Jayakannan, M. *J Polym Sci A Polym Chem.* **2016**, *54*, 3279.
- (39) Aluri, R.; Jayakannan, M. *Biomacromolecules* **2017**, *18*, 189.
- (40) Joshi, D. C.; Saxena, S.; Jayakannan, M. *ACS Applied Polymer Materials* **2019**, *1*, 1866.
- (41) Saxena, S.; Pradeep, A.; Jayakannan, M. *ACS Appl. Bio Mater.* **2019**, *2*, 5245.

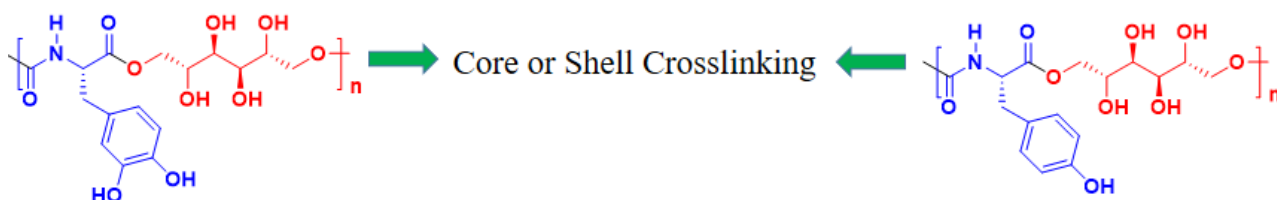
## Overall conclusion

In overall summery the thesis entitled as “**L-Amino Acid Based Amphiphilic Polymers for Drug Delivery Application.**” deals with synthesis of different amino acid based poly(esterurethane)s and polyurethanes for biomedical applications. L-Lysine was employed to synthesize new class of polyurethanes by solvent free and nonisocyanate route. The carboxylic acid functionality in the L-lysine was masked as an amide chemical linkage so that it does not interfere with the polymerization process and the diamine functionalities were readily converted into diurethanes for melt transurethane polycondensation with commercial diols to produce high molecular weight polyurethanes. Synthetic methodology was investigated in detail by optimizing different catalysts for trans urethane process. Unique thermoresponsive L-lysine based polyurethanes were developed for drug delivery applications. The thermoresponsive behavior of polymer was extensively studied by different techniques and it was found that the amphiphilic polymer was showing LCST temperature at 42 °C. Anticancer drug DOX was loaded in polyurethane nanocarriers and the thermoresponsive behavior of polymer was exploited for selective drug release at higher temperature. The polymer nanoparticles were stable at normal physiological conditions (37 °C, pH = 7.4 PBS) and able to release the loaded drug DOX at cancer tissue temperature (thermos responsive), or in the presence of lysosomal esterase enzymes (enzyme responsive). The cytotoxicity test was performed in different cell line and it was found that these L-lysine based nanocarriers were highly biocompatible and while drug loaded nanoparticles were showing excellent cell growth inhibition in cancer cells. Further efforts have made to synthesize phenol and catechol functionalized poly(ester-urethane)s. L-Tyrosine and L-DOPA resources were suitably modified with masked-monomer approach and subjected for melt polymerization to make new classes of enzyme-responsive phenol and catechol functionalized poly(ester-urethane)s. The electron rich aromatic nature of amino acids was explored for the encapsulation of Different electron deficient polyaromatic drugs like DOX and TPT inside the hydrophobic core. The aromatic electron rich nature of polymeric backbone promotes the encapsulation of electron deficient drug molecules by aromatic pi-pi stacking interactions. The aromatic interactions between L-DOPA and drug molecule was confirmed by decrease in the fluorescent intensity of drug and L-DOPA by fluorescence spectroscopy. The amphiphilic nature of polymer and hydrophobic interactions between aromatic unit facilitates the formation of core shell

type nanoparticle in aqueous medium having size around  $100\pm 10$  nm. The backbone of polymer contains the ester linkages which underwent enzymatic biodegradation in presence of lysosomal enzymes, resulting the disassembly of nanoparticle and release of loaded cargo. Further the petroleum based diols were replaced by sugar based diol to synthesise completely bio based amino acid–sugar hybrid poly(ester-urethane)s. The sugar based diols were synthesized from D-mannitol using multistep protection deprotection chemistry in which all the secondary hydroxyl groups was protected as acetal unit. These sugar based diols were well characterized by various spectroscopic techniques and finally, structure was confirmed from crystal structure. The sugar based diol and amino acid based ester(urethane) monomers was subjected for melt polymerization at  $150^{\circ}\text{C}$  in presence of catalyst to get completely bio based poly(ester-urethane) s. The glass transition temperature of sugar diol based polymers was found very high ( $85^{\circ}\text{C}$  - $90^{\circ}\text{C}$ ) compare to aliphatic diol based polymers The biocompatibility of these sugar based diols were checked in normal (WT-MEFs) cell line and it was found that polymers was highly biocompatible.

### Future direction

A new avenue for completely bio-based polymer synthesis has been opened up with the amino acid-sugar hybrid polymer synthesized in fourth chapter. The multifunctional amino acids like L-tyrosine and L-DOPA can be polymerized with these sugar diols to synthesize multifunctional poly(ester urethane)s. The functionality of amino acid and sugar can be used for various crosslinking reactions to increase the stability of nanocarriers. Further the phenolic and catechol unit can undergo crosslinking reactions under enzymatic conditions (HRP) which can be used to synthesize highly biocompatible hydrogels for various applications like tissue engineering, 3D cell culture etc.



## List of Publications

1. Joshi, D. C.; Saxena, S.; Jayakannan, M. *Development of L-Lysine Based Biodegradable Polyurethanes and Their Dual-Responsive Amphiphilic Nanocarriers for Drug Delivery to Cancer Cells*, *ACS Appl. Polym. Mater.* **2019**, *1*, 1866-1880.
2. Aluri, R.; Saxena, S.; Joshi, D. C.; Jayakannan, M. *Multistimuli-Responsive Amphiphilic Poly(ester-urethane) Nanoassemblies Based on L-Tyrosine for Intracellular Drug Delivery to Cancer Cells* *Biomacromolecules* **2018**, *19*, 2166-2181.
3. Joshi, D. C.; Akash, A. Jayakannan, M. *L-Amino acid Based Aromatic  $\pi$ - $\pi$  Interaction Driven Polymeric Drug Delivery System in Cancer Research*. *Manuscript under preparation*.
4. Joshi, D. C.; Jayakannan, M. *Development of Melt Polycondensation Strategy for L-Amino acids and Sugar Based Hybrid Polymers*. *Manuscript under preparation*.